



universität
wien

MASTERARBEIT / MASTER'S THESIS

Titel der Masterarbeit / Title of the Master's Thesis

„Experimental analysis of Time and Temperature
Dependent Clay-Calcite Reactions“

verfasst von / submitted by

Mag. Angelika Kern, Bakk.

angestrebter akademischer Grad / in partial fulfilment of the requirements for the degree of
Master of Science (M S.c.)

Wien, 2016 / Vienna 2016

Studienkennzahl lt. Studienblatt /
degree programme code as it appears on
the student record sheet:

A 066 815

Studienrichtung lt. Studienblatt /
degree programme as it appears on
the student record sheet:

Erdwissenschaften

Betreut von / Supervisor:

Ao. Univ. Prof. Dr. Theodoros Ntaflos

Eidesstattliche Erklärung

Ich erkläre an Eides statt, dass ich die vorliegende Arbeit selbstständig verfasst, andere als die angegebenen Quellen/Hilfsmittel nicht benutzt, und die den benutzten Quellen wörtlich und inhaltlich entnommene Stellen als solche kenntlich gemacht habe.

Statutory Declaration

I declare that I have authored this thesis independently, that I have not used other than the declared sources/resources, and that I have explicitly marked all material which has been quoted either literally or by content from the used sources.

Datum / date

(Unterschrift / signature)

Acknowledgements

Yet again I find myself in the position of having accomplished a tremendous task with the invaluable help of a lot of people – whom I now have the pleasure, privilege and honor to offer my most sincere and heartfelt thanks to.

First and foremost I want to thank my thesis advisor Theodoros Ntafflos, not only for his openmindedness concerning my thesis' topic but also for his open door whenever I approached him with new ideas, questions or yet another method I wanted to apply. You never fail to baffle me with your seemingly endless ability to both encourage my sometime overly enthusiastic ideas as well as keeping me firmly on track as to the means and limitations of my work.

My deepest gratitude also to Cornelius Tschegg who unwaveringly answered each of my inquiries with "Okay, let's do this and think it through!" and has always taken the time to advise me even after leaving the university. Between you two I can honestly and most gratefully say I have never before encountered such thorough and supporting supervision. I cannot express how much I appreciate your help and how much your enthusiasm for your work has been an inspiration to me.

Susanne Gier, Kurt Decker, Jürgen Reiter, Ben Huet and Rainer Abart are sincerely thanked for their help and advice with odd questions and spontaneous requests for help. Many thanks also go to Franz Kiraly, Peter Nagl, Werner Artner and Lutz Nasdala who provided invaluable help with all methods applied. ÖAI and especially Maria Trapichler are sincerely thanked for providing the archaeological samples for this thesis.

To all of my friends who helped, supported and suffered through my thesis with me: Wencke, Christa, Peter, Olesiya, Esther, Gregor, Kathl, Andrea S., Irene, Andrea F., Nathalie, Ronny, Alice, Michi, Iris, Flo, Dani, Tobi, Kathi, Martha, Astrid, Andi – you are the best! Thanks for keeping me on this side of sanity!

Finally, my family:

Daniel, how to express my gratitude to you and for you? Let me put it simply: you are an incredible friend and my mind's soulmate! You continue to make me better, both professionally and personally, and I am glad and honoured to call you my friend. (...and am – of course – bottomlessly thankful for all your neverending help!)

Philipp, you are my hero, my rock, my support, my pirate and so much more! I don't know, what I did to deserve you, but I'm not crazy enough to question you. Thank you for every day and every moment!

To my parents, siblings, siblings-in-law and my nephew, you are yet again the reason I could achieve what I set out to do! Talking, laughing, fighting, it does not matter, as long as you are behind me, around me and with me! Thank you for everything, I could not imagine my life without all of you!

THANK YOU!

Abstract

Commonly used determination of the firing temperature of ceramics based on temperature-dependent clay-calcite reactions is a well established method in archaeometry. While the effects of the firing temperatures have been carefully studied, little attention has been paid to the firing duration.

This thesis presents a thorough study of the impact of firing temperature and firing duration in ceramics with special focus on gehlenite. Experiments were set up using a mixture of calcite-free Stoobclay and pure Hierlatz calcite as raw materials. The homogenized clay-calcite mixture was fired at three different temperatures: 800° C, 900° C, and 1100° C. These temperatures represent the beginning of the clay-calcite to gehlenite reaction, the peak reaction temperature and the transgression of the established reaction temperature, respectively. Firing durations were set to three, five, seven, and nine hours for all samples in order to approximate realistic firing temperatures and durations. In addition, samples have been fired for eleven, 20, and 25 hours at 800° C in order to analyze the effect of the extended firing duration at low temperatures. All fired samples were analyzed using optical microscopy (OM), X-Ray Diffraction (XRD), Electron Probe Microanalysis (EPMA), and X-Ray Fluorescence (XRF). Samples of pure Stoob clay were fired under the same conditions to provide references and were analyzed by XRD. Furthermore, to study the applicability of the results, five archaeological sherds fired above 950° C and containing calcite, provided by ÖAI, were analyzed by optical microscopy, EPMA and Instrumental Neutron Activation Analysis (INAA).

XRD analyses of the experimental samples detected gehlenite only in specimen fired at 1100° C, independent of the soaking time. Mineral breakdown can be observed at 900° C. At nine hours soaking time at 900° C, the breakdown is most visible as most mineral peaks show a distinctive decline. Melting of the clay paste starts somewhere above 900° C and before 1100° C, which can be seen by the increase of amorphous phase in samples fired at 1100° C.

Microtextural in-situ analysis, using the microprobe, shows reaction rims in all samples, which indeed increase with increasing soaking time. Samples fired at 800° C have very narrow reaction rims that could only be measured with difficulties. Notably, gehlenite was detected in samples fired for 20 and 25 hours at 800° C, as well as all samples fired at both 900° C and 1100° C.

The analysis of the archaeological shards, which according to prior analysis, contain calcite showed them to be calcite free, which subsequently defied the purpose of the analysis. This can be seen as impressive proof that surface analysis or optical microscopy alone is very limited and can be misleading.

This thesis clearly indicates that the commonly employed method of inferring firing temperature of ceramics from clay-calcite reactions is susceptible to errors as it oversimplifies the effects of firing. Long firing durations at lower temperature can cause effects similar to those reached at shorter soaking time at high temperatures. It has to be kept in mind, that raw material holds the key to those observation, as the raw material used in this study did not behave as expected. While this does not invalidate the aforementioned method the thermal reactions depend strongly on the raw materials, especially the sintering temperature of the clay, and must not be over simplified. Furthermore, applying only XRD and optical microscopy as methods might be misleading, as gehlenite is not always detected by XRD, even if it can be found by EMPA. The analysis of the archaeological samples strengthens this conclusion, as it proved how easily bulk analysis can too unspecific.

Zusammenfassung

Die Bestimmung der Brenntemperatur von Keramiken beruhend auf temperaturabhängigen Ton-Kalzit-Reaktionen ist eine in der Archäometrie vielfach angewandte Methode. Während die von der Brenntemperatur abhängigen Prozesse gut bekannt sind, wurde dem Einfluss der Brenndauer bisher nur wenig Aufmerksamkeit geschenkt.

Diese Arbeit präsentiert eine grundlegende Studie über den Einfluss der Brenntemperatur und der Brenndauer in Keramiken mit besonderem Augenmerk auf die Entwicklung des Gehlenits. Für den experimentellen Ansatz wurde eine Mischung kalzitfreien Stoober Tons und reinen Hierlatzkalks als Rohmaterial gewählt. Diese homogenisierte Ton-Kalk-Mischung wurde anschließend bei drei verschiedenen Temperaturen gebrannt: 800° C, 900° C und 1100° C. Diese drei Temperaturstufen liegen zu Beginn, am Höhepunkt und über dem angenommenen Stabilitätsbereich des Gehlenit. Die Brenndauer wurde für alle Proben mit drei, fünf, sieben und neun Stunden festgesetzt. Darüber hinaus wurden die Proben bei 800° C für elf, 20 und 25 Stunden gebrannt, um die Auswirkungen einer längeren Brenndauer bei niedrigeren Temperaturen auf die unter diesen Bedingungen ablaufenden Reaktionen zu analysieren. Alle Proben wurden in Folge mittels Polarisationsmikrop (OM), Röntgendiffraktometrie (XRD), Elektronenstrahl Mikroanalyse (EMPA) und Röntgenfluoreszenz (XRF) untersucht. Proben reinen Stoober Tons wurden als Referenzmaterial unter denselben Bedingungen gebrannt und mittels XRD untersucht.

Weiters wurden, um die praktische Anwendbarkeit der Resultate zu überprüfen, fünf Scherben aus einem archäologischen Fundmaterial (vom ÖAI zur Verfügung gestellt) mit Polarisationsmikroskop, EPMA und Instrumenteller Neutronen Aktivierungsanalyse (INAA) untersucht, die als Grundbedingung kalkhältig und über 950° C gebrannt sein sollten.

Die XRD-Ergebnisse der Untersuchung der experimentellen Proben zeigen, dass Gehlenit nur in jenen Proben nachweisbar war, die mit 1100° C gebrannt wurden, unabhängig von der Brenndauer bei Maximaltemperatur. Weiters war der mineralische Breakdown bereits bei 900° C zu beobachten. Bei neun Stunden Brenndauer bei Maximaltemperatur ist der Kollaps der Tonminerale am besten erkennbar, da die Spitzenwerte der Minerale einen deutlichen Abfall zeigen. Das Schmelzen der Tonmasse beginnt bei einer Temperatur etwas oberhalb 900° C und unterhalb 1100° C. Mikrotexturelle in-situ-Analysen mittels Mikrosonde erbrachten Reaktionsränder in allen Proben, welche tatsächlich mit dem Anstieg der Brenndauer bei Maximaltemperatur zunahmen. Dennoch haben bei 800° C gebrannte Proben sehr schmale Reaktionsränder, die nur mit gewissen Schwierigkeiten gemessen werden können. Gehlenit konnte sowohl in Proben, die für 20 bzw. 25 Stunden bei 800° C gebrannt wurden, als auch in allen Proben, die bei 900° C und 1100° C gebrannt wurden, nachgewiesen werden.

Die genaue Analyse der als kalzithältig eingeschätzten, archäologischen Scherben wies auf, dass keine der Proben Kalzit enthält. Dies ist ein eindrucksvoller Hinweis auf die Bedeutung einer Untersuchung archäologischen Proben mit mehreren Methoden. Oberflächen- und Gesamtgesteinsanalysen alleine sind für umfassende Analysen stark fehleranfällig. Diese Untersuchungen zeigen, dass die Analyse von Ton-Kalzit-Reaktionen zwecks Bestimmung der Brenntemperatur von Keramiken weitaus komplizierter ist, als dies bisher angenommen wurde. Die thermischen Reaktionen hängen stark vom Rohmaterial ab, im Besonderen von der Sintertemperatur des Tons, und dürfen nicht zu stark vereinfacht werden. Außerdem kann die alleinige Anwendung von Gesamtgesteinsanalysen und optischer Mikroskopie leicht ein verzerrtes Bild wiedergeben, das in Folge zu Fehlschlüssen führt. Die Analyse der archäologischen Proben bestätigt diese Schlussfolgerungen, da sie zeigt, wie leicht eine Gesamtgesteinsanalyse zu ungenauen Ergebnissen führen kann.

Contents

1	Introduction	17
1.1	Archaeological background and scientific questions	17
1.2	Related work	18
1.3	Scope of this thesis	18
2	Gehlenite	21
3	Raw materials and sample preparation	23
3.1	Grey Stoob clay	23
3.2	Hierlatz calcite	25
3.3	Sample preparation	28
4	Experimental and analytical methods	31
4.1	Optical microscopy (OM)	31
4.2	Electron probe microanalysis (EPMA)	31
4.3	X-ray diffraction (XRD)	32
4.4	X-ray fluorescence analysis (XRF)	32
4.5	Instrumental Neutron Activation Analysis (INAA)	32
4.6	Raman spectroscopy (RS)	32
4.7	X-ray diffraction with high temperature chamber	32
5	Results	33
5.1	800°C	33
5.1.1	3 hours soaking time	34
5.1.2	5 hours soaking time	36
5.1.3	7 hours soaking time	38
5.1.4	9 hours soaking time	42
5.1.5	11 hours soaking time	48
5.1.6	20 hours soaking time	55
5.1.7	25 hours soaking time	59
5.2	900°C	63
5.2.1	3 hours soaking time	64
5.2.2	5 hours soaking time	69
5.2.3	7 hours soaking time	73
5.2.4	9 hours soaking time	78
5.3	1100°C	83
5.3.1	3 hours soaking time	84
5.3.2	5 hours soaking time	89
5.3.3	7 hours soaking time	95
5.3.4	9 hours soaking time	101
5.4	Archaeological samples	109
5.4.1	M2/104	110

5.4.2	M2/127	112
5.4.3	M2/138	114
5.4.4	M2/157	116
5.4.5	M2/161	118
6	Discussion	121
6.1	Experimental samples	121
6.2	Archaeological samples	126
7	Conclusio	129

List of Figures

2.1	Gehlenite stability field (white) in the ternary system $\text{CaO} - \text{SiO}_2 - \text{Al}_2\text{O}_3$ under dry conditions from Levin and Robbins (1964); if the system is SiO_2 saturated, gehlenite is not stable anymore and will be replaced by anorthite and/or wollastonite at temperatures above 1050°C	22
3.1	Geological map of Stooß, Burgenland; (Schönlaub, 2000)	24
3.2	XRD diagram showing the main minerals of Stooß clay; q: quartz, ill: illite, fs: feldspar, clch: clinocllore	25
3.3	Geological map of Kraushöhle, Northern Styria; the red dot marks the location of the cave; http://gis2.stmk.gv.at/atlas/	26
3.4	OM analysis of Hierlatz calcite from Kraushöhle, Styria	26
5.1	Samples fired at 800°C display a light ochre color.	34
5.2	Paste and a "healthy" appearing calcite grain in the sample fired at 800°C , 3 h	35
5.3	Combined XRD-diagrams of specimen soaked for 3 hours at 800°C with CaCO_3 (green) and without CaCO_3 (red); q: quartz, ill: illite, fs: feldspar	35
5.4	Paste and calcite grains of different sizes with very narrow reaction rims; 800°C , 3 h	36
5.5	Paste without phenocrysts and calcite grain with sign of breakdown in the middle in the sample fired at 800°C , 5 h	37
5.6	Combined XRD-diagrams of specimen soaked for 5 hours at 800°C with CaCO_3 (green) and without CaCO_3 (red); q: quartz, ill: illite, fs: feldspar	37
5.7	Paste and different calcite grains with very narrow reaction rims; 800°C , 5 h	38
5.8	Paste and calcite grain with no visible reaction rims in the sample fired at 800°C , 7 h	39
5.9	Combined XRD-diagrams of specimen soaked for 7 hours at 800°C with CaCO_3 (green) and without CaCO_3 (red); q: quartz, ill: illite, fs: feldspar	39
5.10	Paste and different calcite grains with reaction rims; ; (800°C , 7 h)	40
5.11	Ternary diagram with point analyses from the reaction rims that have a total higher than 95 % at 800°C and a soaking time of 7 h. No gehlenite could be detected in the rims.	41
5.12	Elemental distribution of Ca, Si and Al across a profile from calcite grains into the paste in the sample fired at 800°C , 9 h, moving from the edge of the calcite grain into the paste, see Fig. 5.15(d)	43
5.13	Paste and calcite grain with no visible reaction rims in the sample fired at 800°C , 9 h	44
5.14	Combined XRD-diagrams of specimen soaked for 9 hours at 800°C with CaCO_3 (green) and without CaCO_3 (red); q: quartz, ill: illite, fs: feldspar	44
5.15	Paste and different calcite grains with narrow reaction rims; 800°C , 9 h	45
5.16	Elemental mapping of a calcite showing in Fig. 5.15(c)	46
5.17	Ternary diagram with point analyses from the reaction rims that have a total higher than 95 % at 800°C and a soaking time of 9 h. Only three of the analyses could be plotted and non of them reaches the gehlenite stability field.	47
5.18	Paste and calcite grain with no visible reaction rims in the sample fired at 800°C , 11 h	48

5.19	Combined XRD-diagrams of specimen soaked for 11 hours at 800° C with $CaCO_3$ (green) and without $CaCO_3$ (red); q: quartz, ill: illite, fs: feldspar	49
5.20	Paste and different calcite grains with narrow reaction rims; (800° C, 11 h)	50
5.21	Elemental mapping of a calcite grain with a reaction rim (Fig. 5.20(c))	51
5.22	Ternary diagram with point analyses from the reaction rims that have a total higher than 95 % at 800° C and a soaking time of 11 h. No gehlenite could be detected.	52
5.23	Profiles analyzed in the sample fired at 800° C, 11 h, moving from the middle of the calcite grain to the rim, see Fig. 5.20(b)	53
5.24	EMPA profiles were performed to show the CA, Si and Al distribution from within the calcite grains into the paste in the sample fired at 800° C, 11 h; showing Ca diffuses varying distanced into the paste depending on the local mineralogy of the paste	54
5.25	Paste and calcite grain with no visible reaction rims in the sample fired at 800° C, 20 h	55
5.26	Combined XRD-diagrams of specimen soaked for 20 hours at 800° C with $CaCO_3$ (green) and without $CaCO_3$ (red); q: quartz, ill: illite, fs: feldspar	56
5.27	Paste and different calcite grains with signs of thermal breakdown; 800° C, 20 h	57
5.28	Ternary diagram with point analyses from the reaction rims that have a total higher than 95 % at 800° C and a soaking time of 20 h, for the first time, two points plot in the gehlenite stability field	58
5.29	Paste and calcite grain with no visible reaction rims in the sample fired at 800° C, 25 h	59
5.30	Combined XRD-diagrams of specimen soaked for 25 hours at 800° C with $CaCO_3$ (green) and without $CaCO_3$ (red); q: quartz, ill: illite, fs: feldspar	60
5.31	Paste and different calcite grains with reaction rims; 800° C, 25 hours	61
5.32	Ternary diagram with point analyses from the reaction rims that have a total higher than 95 % at 800° C and a soaking time of 20 h, two point analyses plot in the gehlenite stability field	62
5.33	Samples fired at 900° C display an ochre color, with the specimen containing no Ca being notably lighter.	63
5.34	Paste and calcite grain with no visible reaction rims in the sample fired at 900° C, 3 h	64
5.35	Combined XRD-diagrams of specimen soaked for 3 hours at 900° C with $CaCO_3$ (green) and without $CaCO_3$ (red); q: quartz, ill: illite, fs: feldspar	65
5.36	15 point analyses set in a line from within the calcite grain into the paste; Fig. 5.37(c). The distribution of Ca in the grain remains stable; Ca diffuses appr. 35 μ m into the paste. As can be seen in Fig. 5.37(c), while the paste is affected, there is no reaction rim yet; Si, Al and Fe move in direction to the calcite grain	65
5.37	Paste and different calcite grains: breakdown, with reaction rims and signs of shrinking; 900° C, 3 hours	66
5.38	Elemental mapping of a calcite grain with a reaction rim (Fig. 5.37(c)). The corresponding profile, Fig. 5.36, Ca moves at a faster rate into the paste than Al, Si and Fe into the grain	67
5.39	Ternary diagram with point analyses from the reaction rims that have a total higher than 95 % at 900° C and a soaking time of 3 h; three of which plot in the gehlenite stability field	68
5.40	Paste and calcite grain with no visible reaction rims in the sample fired at 900° C, 5 h	69
5.41	Combined XRD-diagrams of specimen soaked for 5 hours at 900° C with $CaCO_3$ (green) and without $CaCO_3$ (red); q: quartz, ill: illite, fs: feldspar	70

5.42	Paste and different calcite grains with with reaction rims of varying diameter; 900° C, 5 hours	71
5.43	EPMA profile from the reaction rim into the paste, Fig. 5.42(b); Ca diffuses appr. 12 µm into the paste; gehlenite was not detected	72
5.44	Ternary diagram with point analyses from the reaction rims that have a total higher than 95 % at 900° C and a soaking time of 5 h. None of the few analyses passing this threshold plots in the gehlenite stability field	72
5.45	Paste and calcite grain with no visible reaction rims in the sample fired at 900° C, 7 h	73
5.46	Combined XRD-diagrams of specimen soaked for 7 hours at 900° C with $CaCO_3$ (green) and without $CaCO_3$ (red); q: quartz, ill: illite, fs: feldspar	74
5.47	EPMA profile going from the calcite grain into the paste, see green line in Fig. 5.48(b). The distribution of Ca in the grain remains stable; Ca diffuses appr. 35 µm into the paste. As can be seen in Fig. 5.48(b), while the paste is affected, there is no reaction rim yet; Si, Al and Fe move in direction of the calcite grain at the same speed	74
5.48	Paste and different calcite grain; 900° C, 7 hours	75
5.49	Elemental mapping of a calcite grain (Cc) with a reaction rim (Fig. 5.48(c)) . . .	76
5.50	Ternary diagram with point analyses from the reaction rims that have a total higher than 95 % at 900° C and a soaking time of 7 h; five rim analyses analyses plot into the gehlenite stability field	77
5.51	Paste and calcite grain with no visible reaction rims in the sample fired at 900° C, 9 h	79
5.52	Combined XRD-diagrams of specimen soaked for 9 hours at 900° C with $CaCO_3$ (green) and without $CaCO_3$ (red); q: quartz, ill: illite, fs: feldspar	80
5.53	Ternary diagram with point analyses from the reaction rims that have a total higher than 95 % at 900° C and a soaking time of 9 h; three point analyses plot into the gehlenite stability field, while two plot into the anorthite stability field .	80
5.54	Paste and different calcite grains with varying states of breakdown and reaction rims; 900° C, 9 hours	81
5.55	Elemental mapping of two calcite grains (Cc) with reaction rims (Fig. 5.54(c)) .	82
5.56	All samples fired at 1100° C display a deep reddish-brown color.	83
5.57	Paste and calcite grain with visible reaction rims in the sample fired at 1100° C, 3 h	84
5.58	Combined XRD-diagrams of specimen soaked for 3 hours at 1100° C with $CaCO_3$ (green) and without $CaCO_3$ (red); q: quartz, mul: mullite, an: anorthite, geh: gehlenite, wo: (pseudo)wollastonite	85
5.59	Ternary diagram with point analyses from the reaction rims that have a total higher than 95 % at 1100° C and a soaking time of 3 h; six points plot into the gehlenite stability field and three into the anorthite stability field	85
5.60	Paste and different calcite grains; 1100° C, 3 hours	86
5.61	Elemental mapping of the close-up into a reaction rim; former grain boundaries cannot be identified anymore	87
5.62	Paste and calcite grain with visible reaction rim in the sample fired at 1100° C, 5 h	90
5.63	Combined XRD-diagrams of specimen soaked for 5 hours at 1100° C with $CaCO_3$ (green) and without $CaCO_3$ (red); q: quartz, mul: mullite, an: anorthite, geh: gehlenite, wo: (pseudo)wollastonite	90
5.64	Paste and different calcite grains or relicts thereof; 1100° C, 5 hours	91
5.65	Elemental mapping of a close-up into a reaction rim	92
5.66	Ternary diagram with point analyses from the reaction rims that have a total higher than 95 % at 1100° C and a soaking time of 5 h; 12 analyses plotting into the gehlenite stability field and two analyses plotting into the anorthite stability field	93
5.67	Paste and calcite grain with reaction rims in the sample fired at 1100° C, 7 h . . .	96

5.68	Combined XRD-diagrams of specimen soaked for 7 hours at 1100° C with $CaCO_3$ (green) and without $CaCO_3$ (red); q: quartz, mul: mullite, an: anorthite, geh: gehlenite, wo: (pseudo)wollastonite	96
5.69	Paste and reaction rims around relict/ former calcite grains; 1100° C, 7 hours . . .	97
5.70	Elemental mapping of a reaction rim (indicated by the red and dashed arrow), close-up, the grain boundaries cannot be determined anymore; (Fig. 5.69(c)) . . .	98
5.71	Ternary diagram with point analyses from the reaction rims that have a total higher than 95 % at 1100° C and a soaking time of 7 h; 14 analyses plotting into the gehlenite stability field and five analyses plotting into the anorthite stability field	99
5.72	Paste and calcite grain with visible reaction rims in the sample fired at 1100° C, 9 h	102
5.73	Combined XRD-diagrams of specimen soaked for 9 hours at 1100° C with $CaCO_3$ (green) and without $CaCO_3$ (red); q: quartz, mul: mullite, an: anorthite, geh: gehlenite, wo: (pseudo)wollastonite	102
5.74	Paste and different calcite grains with reaction rims; 1100° C, 9 hours	103
5.75	Elemental mapping of a reaction rim, indicated by the red and dashed arrow; the calcite grain (Cc) is completely decomposed	104
5.76	Ternary diagram with point analyses from the reaction rims that have a total higher than 95 % at 1100° C and a soaking time of 9 h; plotting into the stability fields of gehlenite (13 points) and anorthite (eight points)	105
5.77	Archaeological sherd M2/104	110
5.78	Archaeological sherd M2/127	112
5.79	Archaeological sherd M2/138	114
5.80	Archaeological sherd M2/157	116
5.81	Archaeological sherd M2/161	118
6.1	XRD diagram of samples containing calcite	124
6.2	Microprobe point analyses exceeding 95 % total	125
6.3	Statistical interpretation of all point analyses exceeding 95 % for all temperatures; circles stand for analysis, curves represent trends (2^{nd} order polynomials, least-squares fitting). While this shows an increasing trends for gehlenite for all temperatures, it must not be forgotten, that those analyses depend heavily on specifically selected points within each sample. This also explains why no gehlenite was detected in the sample fired for 5 h at 900° C	126
6.4	INAA analysis of all archaeological samples, plotted in against the primary mantle. The low Sr amount clearly shows the samples contain no calcite	127

1

Introduction

*"Look deeper into nature, and then you
will understand everything better"*
– Albert Einstein

This master thesis was initially intended as another, possibly more detailed, approach to the often researched topic of temperature determination in (ancient) ceramics (see section 1.2). After a closer look into the existing research, we decided to enhance the question at hand by concentrating specifically on the clay-calcite reactions and taking the firing time of the pottery into account, not only experimentally but also on archaeological samples. The archaeological samples were provided by the courtesy of the Austrian Archaeological Institute (Österreichisches Archologisches Institut - ÖAI) and consist of five sherds from an excavation in Velia, Italy. Hereafter, a detailed description of the preliminary work, experimental setup and final results, as well as the analyses of the aforementioned archaeological shards is given, before the results and applications are discussed.

The thesis is structured in six chapters of which the first is representing the archaeological background as well as the scientific questions and related work. Chapter 2 gives a short overview of the chosen raw material's geology. Chapter 3 presents the applied methods and the sample preparation, while chapter 4 describes the results of both the experimental and the archaeological samples. Chapter 5 discusses those results before chapter 6 finally represents the conclusion and future outlook of this research.

1.1 Archaeological background and scientific questions

As an archaeologist working with pottery, it is virtually impossible not to stumble upon questions which cannot be answered by purely archaeological or macroscopic methods. Those questions are concerning mainly three topics: the provenance of raw materials, dating of the sherds at hand (to a certain extent, although methods such as typology and dating through association with coins or other artefacts are currently used by archaeologists), and manufacturing techniques. Determination of the firing temperature falls under this last topic and its most important indicator are perhaps clay-carbonate reactions which form reaction rims around the former carbonate grain. Several analytical methods can be used to estimate the firing temperature, amongst which but not limited to are X-ray diffraction, X-ray fluorescence, Scanning Electron Microscope, Raman Spectroscopy, Optical Microscopy and Electron Probe Microanalysis, most of which have

been used in this thesis (see chapter 4).

While this is a well known and applied technique, there are still some ambiguities as to the minimum temperature the reaction needs to get started. In relation to this question, there is also the problem of the duration of firing or soaking time, which has so far been treated with a certain neglect. Considering, that the clay-carboate reaction is a thermal induced reaction, the firing temperature could and should be an important factor.

Hence, the scientific question investigated in this thesis is, whether or not the firing duration has an effect of the formation of clay-carbonate related minerals, specifically gehlenite.

To analyse the question, we set up experimental samples, consisting of calcite free Stoob clay with a controlled amount of pure calcite from Hierlatz Kalk (see chapter 3). Those samples were fired at temperatures of 800° C, 900° C and 1100° C for varying firing times and analysed with several geological methods (see chapter 4).

1.2 Related work

Analyzing ceramics is a very important field and a common task in archaeology. Firing temperature in particular have been of great interest, since it depends on several factors, such as type of kiln and firing techniques, and is thusly an indicator that allows archaeologists to draw conclusions regarding the firing process and the technological development of the potters. As a result, significant research has been done in this field. This section briefly lists relevant and related literature. Due to the diversity of the presented research, specific results will not be mentioned and compared here. Detail comparison of results to the listed literature will be done throughout the thesis in the relevant chapters.

The breakdown of clay minerals have been studied in detail by, e.g. Cultrone et al. (2001), Rathossi et al. (2004), Shoval (1988), Traoré et al. (2000), Aras (2004). Thermal behaviour of calcite and subsequent breakdown have been analysed in e.g. Trindade et al. (2009), Duminuco et al. (1998), Tschegg et al. (2009), Riccardi et al. (1999), Cogswell et al. (1996), Shoval et al. (1993), Maggetti et al. (1984). According to the aforementioned studies, clay minerals start breaking down at about 450° C, although illites can resist breakdown up until 900° C. Calcite is reported to decompose at 600° C and to have been completely transformed into Ca-mineral phases between 800° C and 900° C. Several studies have been experimenting with different firing temperatures; for example: Maritan et al. (2006), Maggetti et al. (2011), Aras (2004), Riccardi et al. (1999), Carretero et al. (2002), Cultrone et al. (2001), Duminuco et al. (1998). Notably, many studies focus on the firing temperature alone, since it will allow estimations of the potter's technological skills. Very specific breakdown temperature thresholds are assumed in this context. In light of this thesis and the broader literature, this is a potential oversimplification. It is well known in literature that the firing process is influenced by many factors, including raw and temper materials, kiln atmosphere, heating rate, soaking time¹ and cooling rate (Heimann and Maggetti (2014), Cantisani et al. (2012) and references therein), but so far little attention has been paid to the effect of different soaking time.

1.3 Scope of this thesis

This work tries to shed additional light on the breakdown of calcite over temperature. Given, that important conclusions are drawn based on this single observation of calcite breakdown, it is worth investigating if the temperature alone is the dominant factor or if time could be equally important.

¹ time during which the maximum temperature is maintained

While the author of course agrees that a complete and all-encompassing analysis of all factors that might impact the firing process would be of great interest, she also has to appreciate the fact that the complexity of such an undertaking grows exponentially with the factors under consideration. Investigating five temperature steps, for example, takes five samples. Five temperature steps with five different soaking times takes 25 samples. Adding five different types of clay into the equation would require 125 samples, and so on. Five steps each for all of the aforementioned (incomplete!) list of parameters would take a staggering 10 million samples. Notably, this is just the number of samples needed to be prepared and fired, and does not yet take any analysis into account.

Even with deliberately keeping the samples size small, with 15 experimental samples and five archaeological ones, analysis encompassed 30 XRD diagrams, about 1800 microprobe point analyses done by hand and as well as an uncounted number of Optical Microscopy (OM) and Back-scattered Electron (BSE) images, in addition to X-ray Fluorescence (XRF) and Instrumental Neutron Activation Analysis (INAA) data.

2

Gehlenite

*"The world is full of obvious things which
nobody by any chance ever observes."
– Arthur Conan Doyle*

Gehlenite ($Ca_2Al_2SiO_7$) is an end member of the melilite group and as such can be found in high temperature contact zones of calcareous rocks. Initially, mostly known for its presence in magmatic and metamorphic rocks (Hoschek, 1974), gehlenite can also form during ceramic firing, given enough Si and Al as well as an calcareous clay (Tschegg et al., 2009).

It mostly classifies as tetragonal, prismatic crystal with a transparent colour. Gehlenite can substitute Fe for Al, which decreases the stability of the mineral (Deer et al., 1986). The stability of gehlenite is further influenced by of H_2O . For temperature determination, gehlenite is a most important mineral, as it is the first Ca-alumo-silicate to form in calcareous clays during oxidizing firing. Due to its metastability, given enough SiO_2 , it transforms to anorthite ($CaAl_2Si_2O_8$) and wollastonite ($CaSiO_3$); see fig. 2.1. Therefore, gehlenite is stable between temperatures of approximately 800° C and 1050° C, with a maximum stability between 850° C and 950° C. This, in theory, allows for an estimation of the firing temperature and subsequently gives information of the technological skills of the potters (Heimann and Maggetti, 2014). However, even though most ancient ceramics usually were fired at temperatures below 1000° C, gehlenite is hard to detect, especially if the ceramic is found in humid climate (Heimann and Maggetti, 2014). This may be, because gehlenite will either dissolve in contact with solutions or transform to zeolites (Heimann and Maggetti, 2014). Gehlenite is best preserved in arid climate.

This makes temperature determination challenging, as the absence of gehlenite in ceramics formed of calcareous clay cannot necessarily be explained by lower firing temperatures. Furthermore, while specific temperature thresholds have defined, it is well known, that many factors such as grain sizes, raw materials, temper materials, firing time, heating rate, cooling rate and firing conditions influence the formation of new minerals. Hence, this thesis aims to study the influence of the soaking time of gehlenite formation at different temperatures.

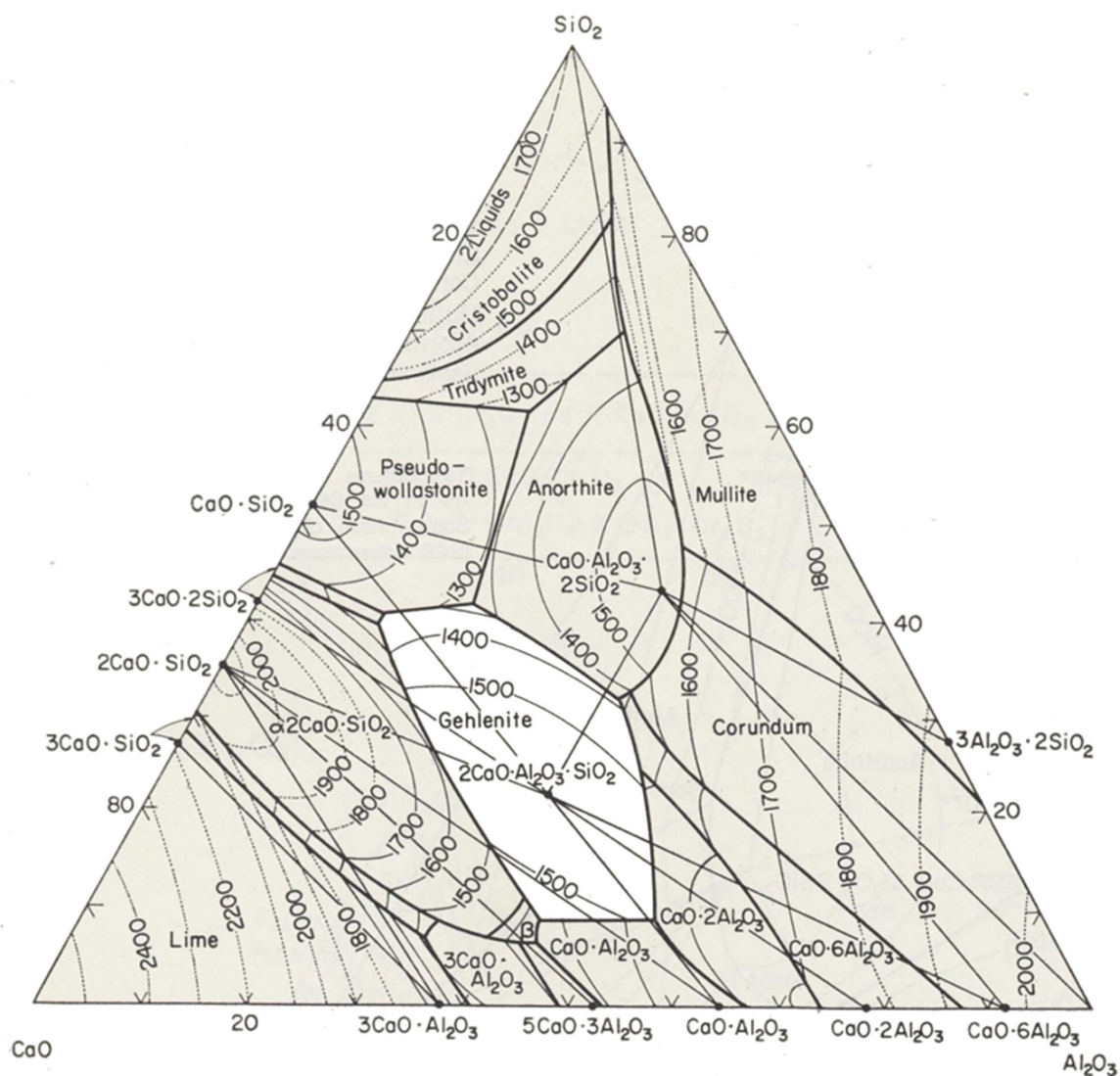
CaO–Al₂O₃–SiO₂ (cont.)

Figure 2.1: Gehlenite stability field (white) in the ternary system CaO – SiO₂ – Al₂O₃ under dry conditions from Levin and Robbins (1964); if the system is SiO₂ saturated, gehlenite is not stable anymore and will be replaced by anorthite and/or wollastonite at temperatures above 1050 °C

3

Raw materials and sample preparation

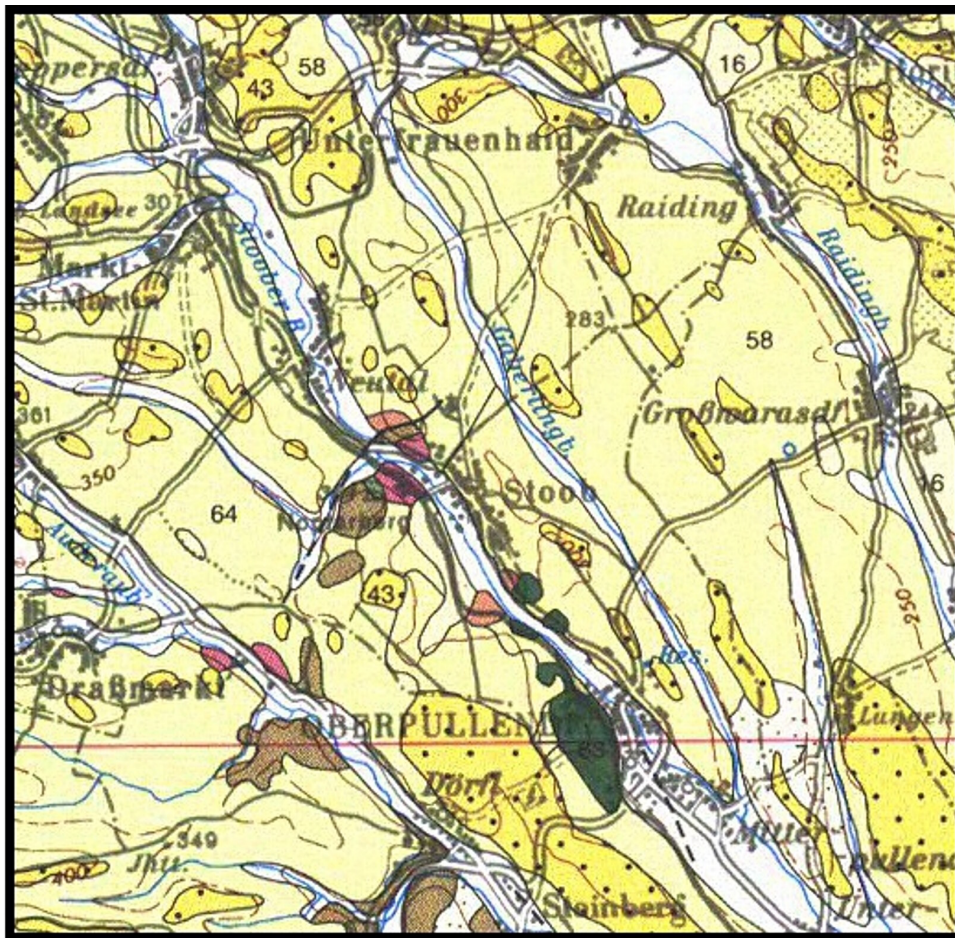
*"Geology gave us the immensity of time and taught us how
little of it our own species has occupied."
– Stephen Jay Gould*

This chapter presents the raw materials used for the experiments and give the background on their geology. Both the clay and the calcite have been chosen carefully for their specific properties as described below. The sample preparation is also described in this chapter.

3.1 Grey StooB clay

StooB lies in municipal Oberpullendorf, in western Burgenland, Austria. It has been famous for its ceramics industry since 1667 and still houses the technical college for pottery ("Fachschule für Keramik und Ofenbau"). This can be explained by the pliocen clay found in the vicinity of StooB, which very suitable for pottery. The clay can be differentiated by colour. First, so called "blue clay" builds the footwall and consists of organic-rich, very finely grained blue and homogenous clay with very good plasticity. Second, the so called "grey clay" can be found in the hanging wall. It is slightly less fine grained, but still very plastic (Vizenz, 1985). The clays are of pelitic origin and date to the upper Samartic and the Pannon (Schönlaub, 2000). The reason for choosing StooB clay as raw material lies not only in its obvious advantages for potters, but more importantly for this thesis, it contains only minimal traces of CaCO_3 and minor amounts of CaO (Götzinger et al., 2009). The clay chosen for this thesis belongs to the "grey clay" and was collected in Herrschaftswald on the boarder to Growarasdorf; see Fig. 3.1.

XRD analysis shows quartz, feldspar (albite and potassium-feldspar), clinocllore and illite (see figure 3.2).



1 : 200 000 (1cm = 2km)



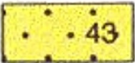
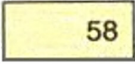

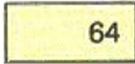

-  Older quarternary gravels; Upper Pleistocen - Lower Pleistocen
-  Pannonian sediments (clay, sand, gravel)
-  Oberpullendorf basalts
-  Samartian sediments (clay, sand, gravel)
-  Coarse gneiss

Figure 3.1: Geological map of Stöb, Burgenland; (Schönlaub, 2000)

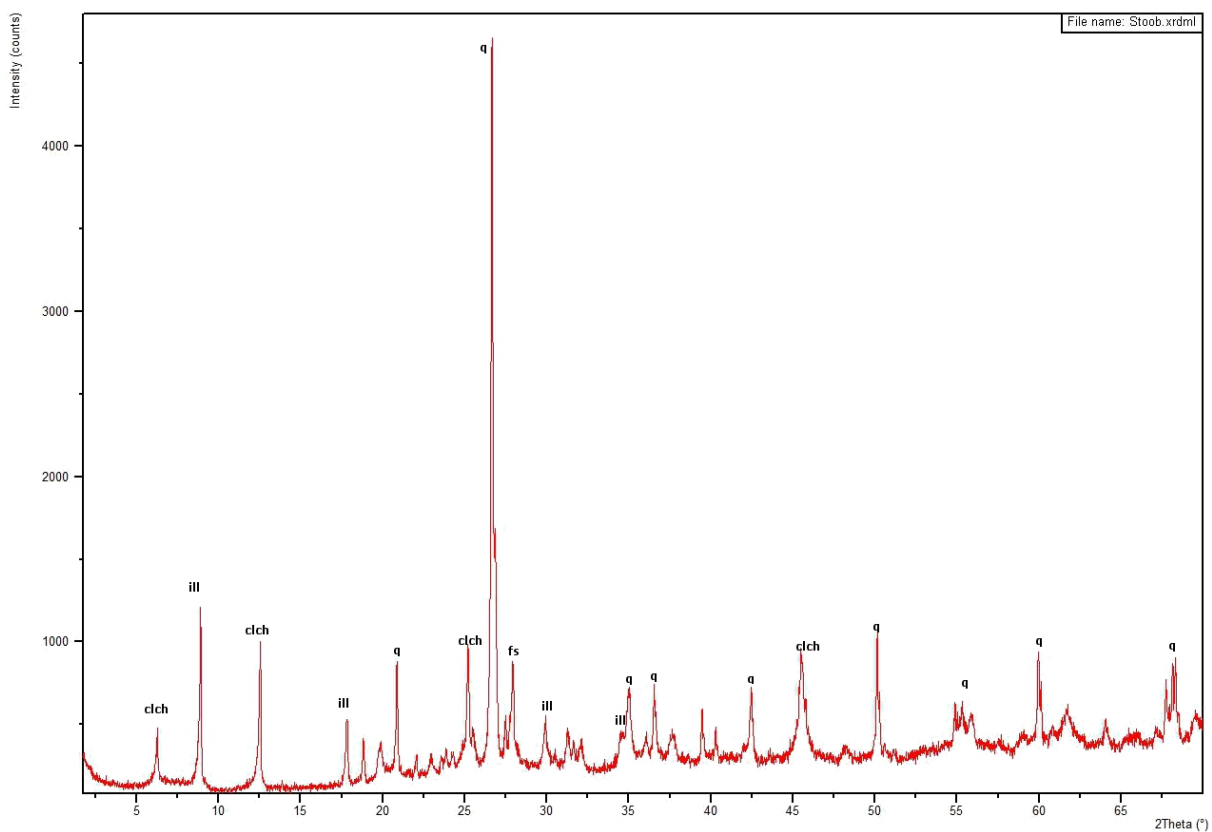


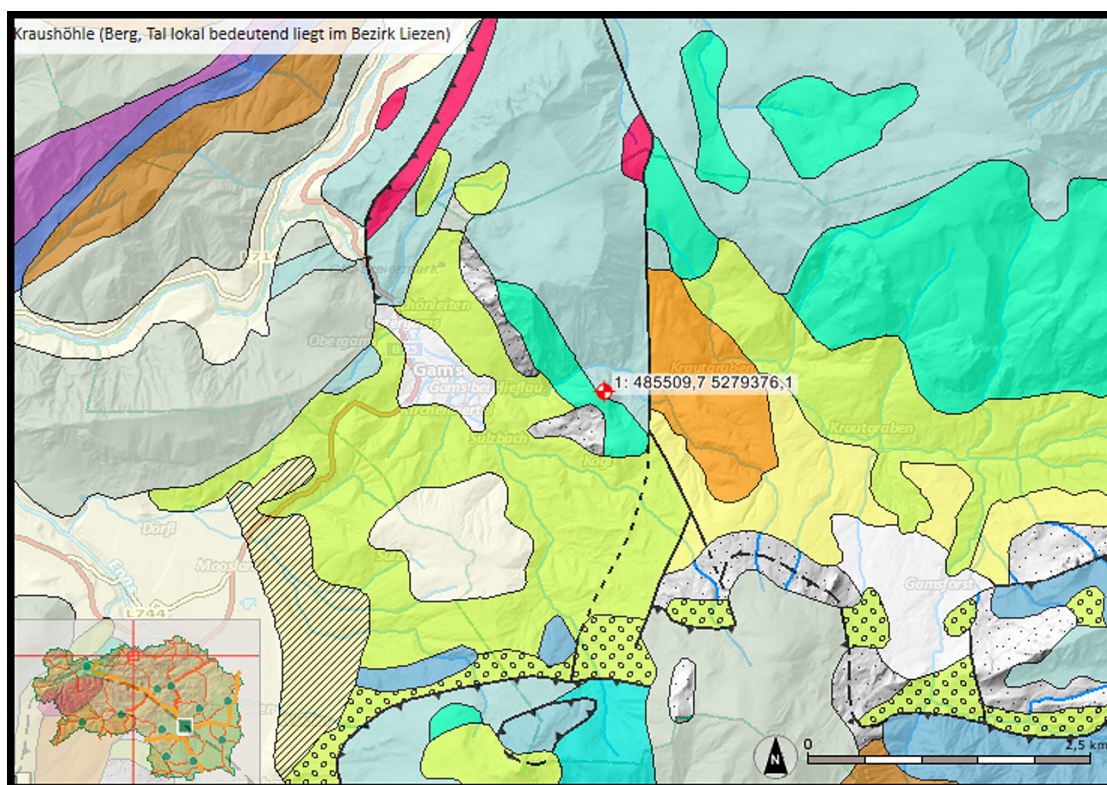
Figure 3.2: XRD diagram showing the main minerals of Stoob clay; q: quartz, ill: illite, fs: feldspar, clch: clinocllore

3.2 Hierlatz calcite

Hierlatz calcite was chosen as a raw material for our experiments due to its purity (see table 3.1), thus making calcite the main mineral producing reaction rims.

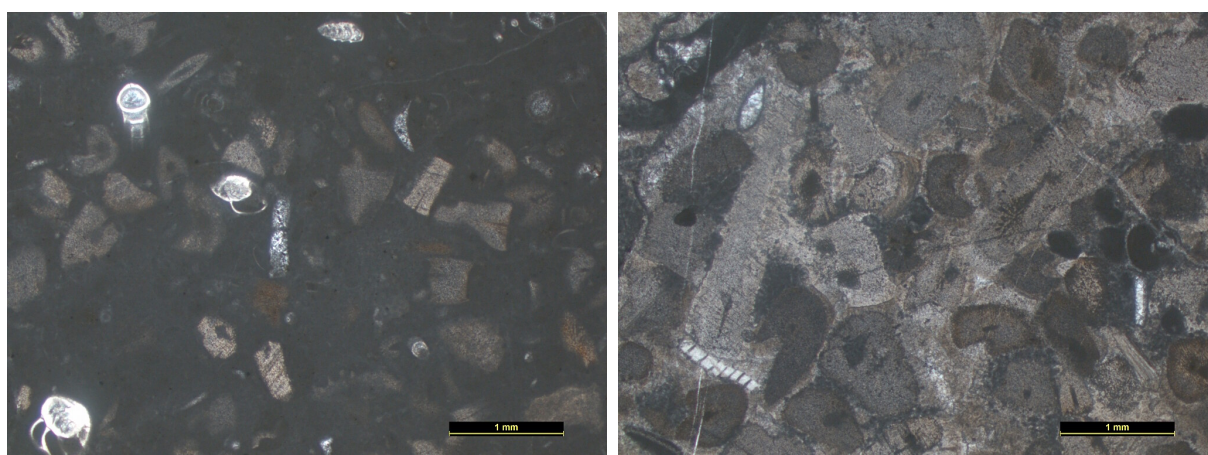
It was collected in Kraushöhle, a cave in northern Styria, Austria; see Fig. 3.3. The cave is part of the Hochschwab karst massiv, which is mainly built by Triassic carbonate rocks and belongs to the Northern Calcareous Alps (Plan et al., 2012).

The Hierlatz calcite itself is part of the Lower Jurassic Hierlatz Formation and consists mostly of crinoids, fragments of brachiopods and ammonites, as well as bivalves, gastropods and the occasional foraminifer all bound by biosparite or biomicrite (Vörös (1991), Flügel and Neubauer (1984) and Faupl (2003)).



- mostly carbonates; middle triassic - lower cretaceous
- mostly carbonates; middle triassic - jurassic
- mostly clastica
- carbonates; Grauwacken
- inneralpine basins; Neogen

Figure 3.3: Geological map of Kraushöhle, Northern Styria; the red dot marks the location of the cave;
<http://gis2.stmk.gv.at/atlas/>



(a) Hierlatz calcite; showing small foraminifers

(b) OM image of different fossils

Figure 3.4: OM analysis of Hierlatz calcite from Kraushöhle, Styria

SiO₂	0.02	5.94	0.11	0.04	0.26	0.04	0.08	0.12	bdl	0.61
TiO₂	bdl	0.03	bdl	bdl	bdl	bdl	bdl	bdl	bdl	bdl
Al₂O₃	bdl	1.78	0.05	0.02	0.12	0.02	0.03	bdl	bdl	0.29
FeO	bdl	45.84	0.05	bdl	0.07	0.02	0.09	0.03	0.03	0.07
CaO	55.48	18.69	55.09	54.71	54.57	59.55	54.47	48.66	54.76	54.22
MgO	0.41	0.42	0.46	0.84	0.48	0.48	0.61	0.06	0.56	0.45
MnO	bdl	0.19	bdl	0.04	bdl	bdl	0.02	bdl	bdl	0.03
K₂O	bdl	0.18	bdl	bdl	0.02	bdl	bdl	0.06	bdl	0.07
Na₂O	bdl	0.03	0.06	0.07	0.06	bdl	0.03	0.89	bdl	bdl
P₂O₅	bdl	0.26	bdl	bdl	bdl	0.05	bdl	31.85	bdl	bdl
Total	55.92	73.36	55.82	55.73	55.58	60.17	55.33	81.70	55.40	55.74

SiO₂	0.04	bdl	bdl	bdl	3.65	bdl	bdl	bdl	bdl	0.40
TiO₂	bdl	bdl	bdl	bdl	bdl	bdl	bdl	bdl	bdl	0.03
Al₂O₃	bdl	bdl	0.08	bdl	0.90	bdl	bdl	bdl	bdl	0.28
FeO	bdl	bdl	0.03	bdl	57.00	bdl	bdl	0.04	bdl	0.10
CaO	55.38	55.06	54.94	57.41	11.60	55.61	59.49	60.14	56.47	54.71
MgO	0.55	0.29	0.50	0.43	0.21	0.33	0.66	0.47	0.88	0.66
MnO	bdl	0.06	bdl	bdl	bdl	bdl	bdl	bdl	bdl	bdl
K₂O	bdl	bdl	bdl	bdl	0.12	bdl	bdl	bdl	bdl	0.04
Na₂O	0.08	bdl	0.07	bdl	bdl	0.05	bdl	0.04	bdl	bdl
P₂O₅	bdl	0.03	0.02	0.04	0.14	bdl	bdl	bdl	bdl	0.03
Total	56.07	55.48	55.64	57.92	73.63	56.02	60.19	60.73	57.39	56.24

SiO₂	bdl	2.08	0.06	0.02	0.04	0.07	1.19	5.85	0.67	0.90
TiO₂	bdl	0.05	bdl	bdl	bdl	bdl	bdl	bdl	bdl	0.03
Al₂O₃	0.03	0.23	bdl	0.06	bdl	0.06	0.44	1.31	0.30	0.13
FeO	bdl	68.02	0.02	0.03	0.03	0.11	0.29	64.33	0.12	0.05
CaO	53.76	1.73	62.27	56.28	56.28	56.20	60.63	3.10	54.66	56.97
MgO	0.93	0.12	0.33	0.99	0.61	0.51	0.28	0.20	0.64	0.55
MnO	bdl	bdl	0.06	bdl	0.05	0.05	bdl	0.17	bdl	0.03
K₂O	bdl	bdl	bdl	bdl	bdl	bdl	0.03	0.12	0.06	0.02
Na₂O	0.02	0.02	0.04	bdl	0.08	bdl	bdl	0.09	bdl	bdl
P₂O₅	bdl	0.04	bdl	0.02	0.03	bdl	bdl	0.33	0.06	bdl
Total	54.78	72.31	62.78	57.43	57.15	57.00	62.91	75.49	56.52	58.69

SiO₂	2.21	0.23	0.35	bdl	0.73	0.03	0.33
TiO₂	bdl	0.03	bdl	bdl	bdl	bdl	bdl
Al₂O₃	0.40	0.09	0.17	bdl	0.19	bdl	0.21
FeO	0.24	0.06	0.07	0.06	0.19	0.24	0.04
CaO	56.10	55.44	54.88	54.62	55.58	55.15	54.32
MgO	0.57	0.59	1.10	0.76	0.47	0.95	0.55
MnO	0.03	bdl	bdl	bdl	0.09	0.04	0.04
K₂O	0.19	0.02	0.05	0.02	0.04	bdl	0.04
Na₂O	bdl	bdl	bdl	bdl	0.02	0.03	0.02
P₂O₅	0.04	0.03	0.04	0.03	bdl	0.03	0.03
Total	59.81	56.49	56.68	55.52	57.32	56.47	55.59

Table 3.1: EPMA raw sample data in wt%, K41 sample. (bdl = below detection limit.)

3.3 Sample preparation

Sample sets were prepared for three different temperatures, each in double quantity containing calcite to have enough sample materials for all methods applied as well as a third set without any calcite as reference (see table 3.4).

The calcite was firstly crushed and pulverized using an agate mortar. The grain size varies between $2\mu\text{m}$ and 1mm to provide a range of different grain sizes. Previous literature (Heimann and Maggetti, 2014) suggests that the reaction rate is a function of the grain size, i.e. larger grains produce larger reaction rims (Maggetti and Küpfer, 1978). To get the best results possible, we chose to include a wide range of grain sizes. It was then mixed and homogenized with dried clay, in a mixture containing 90 % clay and 10 % calcite. Afterwards the mixture was rehydrated with 150 ml distilled water to 500 g of raw material and pressed into the burning form – a cylindrical form with a diameter of 1,5 cm and 2 cm height. Part of this prepared raw material mix was analysed by XRF (see tables 3.2 and 3.3). Firing temperatures were chosen to fit the production techniques used in ancient ceramics.

The samples were then air dried for a week and, additionally, for 3 hours in a kiln at 90°C . The firing was done in a single chambered kiln under oxidizing conditions, with a temperature increase of 100° per hour until the peak temperature was reached. Sample firing took place at 800°C , 900°C and 1100°C , with soaking times of 3 h, 5 h, 7 h and 9 h. A further set of samples was fired at 800° for 11 h, 20 h and 25 h. Full firing times/ time spent in the kiln compared to soaking time can be seen in table 3.4. The specimen were then taken out of the kiln directly and left to cool at room temperature (approximately 30°C for 2 hours). After cooling, all samples intended for thin sections were immediatly embedded in epoxy to avoid CaO reactions with humidity. The thin sections for samples fired at 900°C and 1100°C were regularly processed (cutting and grinding with water as support and cooling agent), while most of the 800°C samples underwent waterfree preparation (see chapter 5.1) with 98 % alcohol. This was done as a precaution since preliminary analysis of the specimen fired for 9 hours and 11 hours at 800°C showed very narrow and potentially fragile rims that might have been destroyed by regular thin section production ².

Specimen intended for XRD analysis were ground in an electric agate mill and pressed into powder pellets (see chapter 4).

SiO_2	TiO_2	Al_2O_3	Fe_2O_3	MnO	MgO	CaO	Na_2O	K_2O	P_2O_5	LOI	Sum
51.47	0.81	19.88	4.49	0.04	2.27	5.40	0.83	3.97	0.12	9.51	98.79

Table 3.2: Major element analysis in wt% of the mixed raw materials (90% clay, 10% calcite) used in the experiments; LOI = Loss on ignition

Sc	V	Cr	Co	Ni	Cu	Zn	As	Ga	Rb	Sr
14	167	138	24	84	48	141	15	26	184	86
Y	Zr	Nb	Ba	La	Ce	Hf	Ta	Pb	Th	U
34	130	17	634	46	79	1	1	34	1	16

Table 3.3: Trace element analysis in ppm of the mixed raw materials (90% clay, 10% calcite) used in the experiments

² In hindsight, we would now choose to prepare all samples waterfree, as CaO is the reactive phase and must be expected at to be still present in samples fired at higher temperatures

sample	clay:calcite (%)	total firing time	intended method	temperature (C)	soaking time (h)	heating rate (C/h)	containing calcite
800°C							
MaKern 3/800/A3	90:10	11	EMPA	800	3	100	yes
MaKern 3/800/B3	90:10	11	XRD	800	3	100	yes
MaKern 3/800/C3	100:0	11	XRD	800	3	100	no
MaKern 5/800/A4	90:10	13	EMPA	800	5	100	yes
MaKern 5/800/B4	90:10	13	XRD	800	5	100	yes
MaKern 5/800/C4	100:0	13	XRD	800	5	100	no
MaKern 7/800/A5	90:10	15	EMPA	800	7	100	yes
MaKern 7/800/B5	90:10	15	XRD	800	7	100	yes
MaKern 7/800/C5	100:0	15	XRD	800	7	100	no
MaKern 9/800/A1	90:10	17	EMPA	800	9	100	yes
MaKern 9/800/B1	90:10	17	XRD	800	9	100	yes
MaKern 9/800/C1	100:0	17	XRD	800	9	100	no
MaKern 11/800/A2	90:10	19	EMPA	800	11	100	yes
MaKern 11/800/B2	90:10	19	XRD	800	11	100	yes
MaKern 11/800/C2	100:0	19	XRD	800	11	100	no
MaKern 20/800/A2	90:10	28	EMPA	800	20	100	yes
MaKern 20/800/B2	90:10	28	XRD	800	20	100	yes
MaKern 20/800/C2	100:0	28	XRD	800	20	100	no
MaKern 25/800/A2	90:10	33	EMPA	800	25	100	yes
MaKern 25/800/B2	90:10	33	XRD	800	25	100	yes
MaKern 25/800/C2	100:0	33	XRD	800	25	100	no
900°C							
MaKern 3/900/A1	90:10	12	EMPA	900	3	100	yes
MaKern 3/900/B1	90:10	12	XRD	900	3	100	yes
MaKern 3/900/C1	100:0	12	XRD	900	3	100	no
MaKern 5/900/A2	90:10	14	EMPA	900	5	100	yes
MaKern 5/900/B2	90:10	14	XRD	900	5	100	yes
MaKern 5/900/C2	100:0	14	XRD	900	5	100	no
MaKern 7/900/A3	90:10	16	EMPA	900	7	100	yes

sample	clay:calcite (%)	total firing time	intended method	temperature (C°)	soaking time (h)	heating rate (C/h)	containing calcite
MaKern 7/900/B3	90:10	16	XRD	900	7	100	yes
MaKern 7/900/C3	100:0	16	XRD	900	7	100	no
MaKern 9/900/A4	90:10	18	EMPA	900	9	100	yes
MaKern 9/900/B4	90:10	18	XRD	900	9	100	yes
MaKern 9/900/C4	100:0	18	XRD	900	9	100	no
1100°C							
MaKern 3/1100/A1	90:10	14	EMPA	1100	3	100	yes
MaKern 3/1100/B1	90:10	14	XRD	1100	3	100	yes
MaKern 3/1100/C1	100:0	14	XRD	1100	3	100	no
MaKern 5/1100/A2	90:10	16	EMPA	1100	5	100	yes
MaKern 5/1100/B2	90:10	16	XRD	1100	5	100	yes
MaKern 5/1100/C2	100:0	16	XRD	1100	5	100	no
MaKern 7/1100/A3	90:10	18	EMPA	1100	7	100	yes
MaKern 7/1100/B3	90:10	18	XRD	1100	7	100	yes
MaKern 7/1100/C3	100:0	18	XRD	1100	7	100	no
MaKern 9/1100/A4	90:10	20	EMPA	1100	9	100	yes
MaKern 9/1100/B4	90:10	20	XRD	1100	9	100	yes
MaKern 9/1100/C4	100:0	20	XRD	1100	9	100	no

Table 3.4: Experimental setup for each sample; samples containing calcite were analyzed by OM, XRD and EPMA, samples without calcite were analyzed by EPMA as reference

4

Experimental and analytical methods

"It's still magic even if you know how it's done."
– Terry Pratchett

In order to fully address the scientific questions at hand and to ensure the most thorough analysis possible, several optical and chemical analytical methods were applied. Polished thin sections were produced for optical microscopy, electron probe microanalysis and Raman spectroscopy, while X-ray diffraction and X-ray fluorescence used powder pellets. In addition, a fused bead was produced for major element analysis with X-ray fluorescence. The performed Instrumental Neutron Activation Analysis also required pulverized samples of the archaeological sherds. Unless stated otherwise, all measurements were done at the Department of Lithospheric Research, University of Vienna.

4.1 Optical microscopy (OM)

This methods was used for a first overview of the paste and phase of the experimental sample set as well as morphological features in the archaeological samples.

4.2 Electron probe microanalysis (EPMA)

Electron probe microanalysis was used for in-situ analysis of small mineral phases such as can be expected in reaction rims. Polished and carbon-coated thin sections of all samples were analysed using a Cameca SX-100 electron microprobe against natural and synthetic standards with four wavelength-dispersive spectrometers. Operating conditions of 15 kV acceleration voltage and 20 nA beam current were set, standard correction was applied. Alumo-silicate reaction rims were studied and measured with a defocused beam with 5 μm diameter as to minimize the loss of Na and K.

In addition, specimen fired at 1100° C were further analysed with a Cameca SX FiveFe, with 15 kV acceleration voltage and 20 nA beam current, against natural and synthetic standards. PAP correction was applied.

Back-scattered electron (BSE) images were taken of all samples. The element distribution are represented by high resolution element mapping images.

4.3 X-ray diffraction (XRD)

Samples were analyzed by X-ray diffraction to gain the bulk mineralogical composition of the clay raw material, the experimental sample set as well as the calcite free reference samples. Powder pellets with preferred orientation were produced and measured with a PANalytical X'Pert Pro X-Ray Diffractometer using $\text{CuK}\alpha$ -radiation at 40 kV and 40 mA (step size 0.0167° , 5 s per step), scanning at an interval of $2-140^\circ 2\Theta$, at the Department for Geodynamics and Sedimentology, University of Vienna.

4.4 X-ray fluorescence analysis (XRF)

XRF was used to determine the bulk chemical major and trace elements of the raw material mixture of the experimental samples. The mixture was ground in an electric agate mill, homogenized and dried at 110°C and finally fired at 1050°C . Fused bead were used for major element analysis, consisting of 1:5 ratio diluted mixture of the sample material and $\text{Li}_6\text{B}_4\text{O}_7$ as flux. For trace analysis, crushed and milled sample material was mixed with polyvinyl alcohol as binding agent to form a pressed powder pellet. The analyses were performed on a sequential X-Ray spectrometer PHILIPS PW2404 with a Rh-excitation source.

4.5 Instrumental Neutron Activation Analysis (INAA)

This method was applied on the archaeological sherds only. As no calcite was found in any of the sherds (see chapters 5 and 6) this data could not be used further. Measurements were performed at Atominstitut, Technical University of Vienna.

4.6 Raman spectroscopy (RS)

Raman spectroscopy was applied to the sample set of 800°C . The intention was to assess the state of crystallinity of prospective gehlenite rims, but had to be given up since the rims proved too slim to be measured and because of high epoxy interference.

4.7 X-ray diffraction with high temperature chamber

This method was intended to monitor the breakdown of clay minerals and the exact timing of gehlenite formation at different temperatures in the heat chamber while measuring. It was performed at the X-ray center of Technical University Vienna. This experiment did not prove successful due to heavy textural interferences and had to be abandoned.

5

Results

*"Good books tell the truth, even when they're about
things that never have been and never will be.
They're truthful in a different way."
– Stanislaw Lem*

This chapter presents the results of both the experimental and archaeological samples analyzed. All experimental specimen containing calcite have been analyzed by OM, XRD and EMPA. Four specimen, the two fired at 800°C, nine and 11 hours soaking time, and two fired at 900°C, five and seven hours soaking time, were prepared as preliminary samples and differ slightly in the analytical approach, as will be explained in the text. In accordance to the difficulties of measuring the often very narrow reaction rims, a threshold of a total of 95 wt% for microprobe point analyses was chosen.

Samples containing no calcite were analyzed by XRD to provide reference diagrams. The calcite peak at $29,47^{\circ}2\Theta$ has an interference with illite at $29,49^{\circ}2\Theta$, which explains the small peak visible in the XRD graphs of samples containing no calcite.

Due to the small size of the provided archaeological sherds, XRD analysis was impossible; therefore they were analyzed by EPMA and INAA.

Microprobe point analyses surpassing the threshold of 95 wt% are presented in the appendix. Most images of samples are Back-scattered electron (BSE) images as they are more detailed than OM picture.

5.1 800°C

According to Cultrone et al. (2001), 800°C is the minimum temperature needed for gehlenite detection. Therefore, this temperature was studied very closely, with a wider range of soaking times than the other temperatures. Preliminary investigation by microprobe of the specimen soaked for 9 hours and 11 hours showed very narrow, potentially fragile reactions rims. To protect those rims as much as possible, all other samples for 800°C and their thin sections were produced water-free and with pure alcohol instead (see section 3.3). All samples present a light ochre color after firing, independent of the soaking time and the calcite content (see Fig. 5.1). Microtextural analysis of all samples via OM shows calcite grains with distinct grain boundaries and a clay paste where no minerals can be identified. BSE images show the paste to consist of

quartz, potassium-feldspar, albite and illite minerals embedded in clayey matrix. The minerals are unevenly distributed through the paste, showing clearly the heterogeneity of the clay. In areas consisting mostly of phyllosilicates, the paste appears to be more compressed. This observation is supported by XRD analysis. The clinocllore peak still visible in the XRD diagram of the clay raw material has disappeared completely (compare Fig. 3.2).



(a) Samples fired for 9 hours at peak temperature 800° C (b) Samples fired for 11 hours at peak temperature 800° C

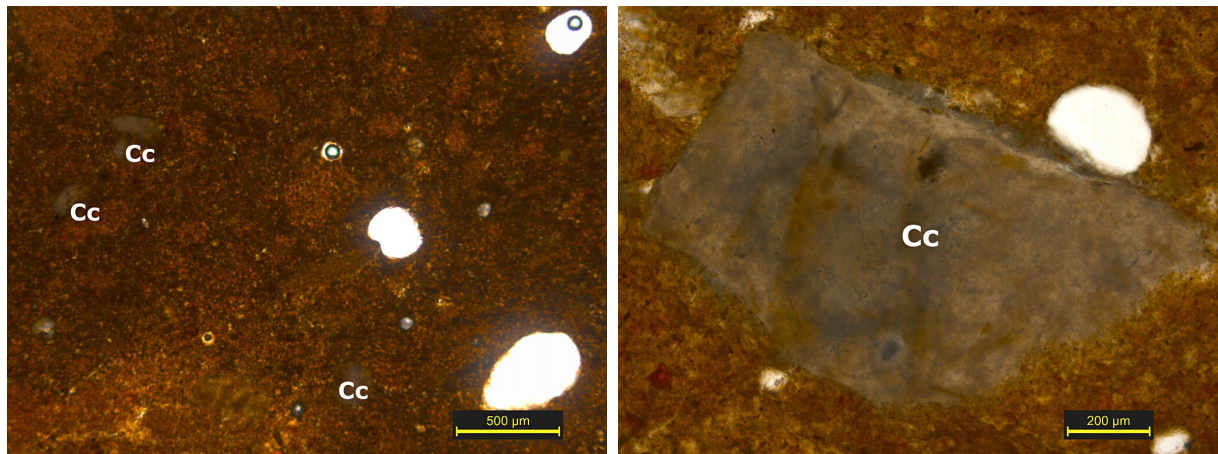
Figure 5.1: Samples fired at 800° C display a light ochre color.

5.1.1 3 hours soaking time

First general overview of the specimen with OM shows calcite grains with no visible signs of shrinking or reaction rims; Fig. 5.2(b). The paste shows a clay matrix which, apart from the calcite grains, is free of phenocrysts; Fig. 5.2(a). Upon closer look with BSE images, angular, medium-grained quartz, potassium-feldspar, albite and illite phenocrysts with very distinct grain boundaries embedded in the paste and no visible sintering effects on the paste can be seen. Most calcite grains display surface changes, that precede calcite breakdown, see Fig. 5.4(b) - (d). Small cracks can be detected within the grains, without signs of shrinking of the grain, Fig. 5.4(c). Around the calcite grains, apparently independent of the grain size, minuscule reaction rims of max. 2 μm can be observed (see Fig. 5.4(b) and (d)). Cracks start at some calcite grains and progress into the paste, Fig. 5.4(d).

In direct comparison of XRD diagram of the specimen containing calcite and the reference sample without calcite, the main difference lies within the calcite peak, Fig. 5.3. Furthermore, the diagrams show no crystallization or thermal breakdown of minerals. Gehlenite was not detected.

Point analyses within the reaction rims was unsuccessful due the narrow rim thickness, which was smaller than the defocused beam (see Section 4.2).



(a) Fine-grained clay paste; except for calcite (Cc), free of phenocrysts

(b) Calcite grain (Cc) with no visible reaction rim

Figure 5.2: Paste and a "healthy" appearing calcite grain in the sample fired at 800°C, 3 h

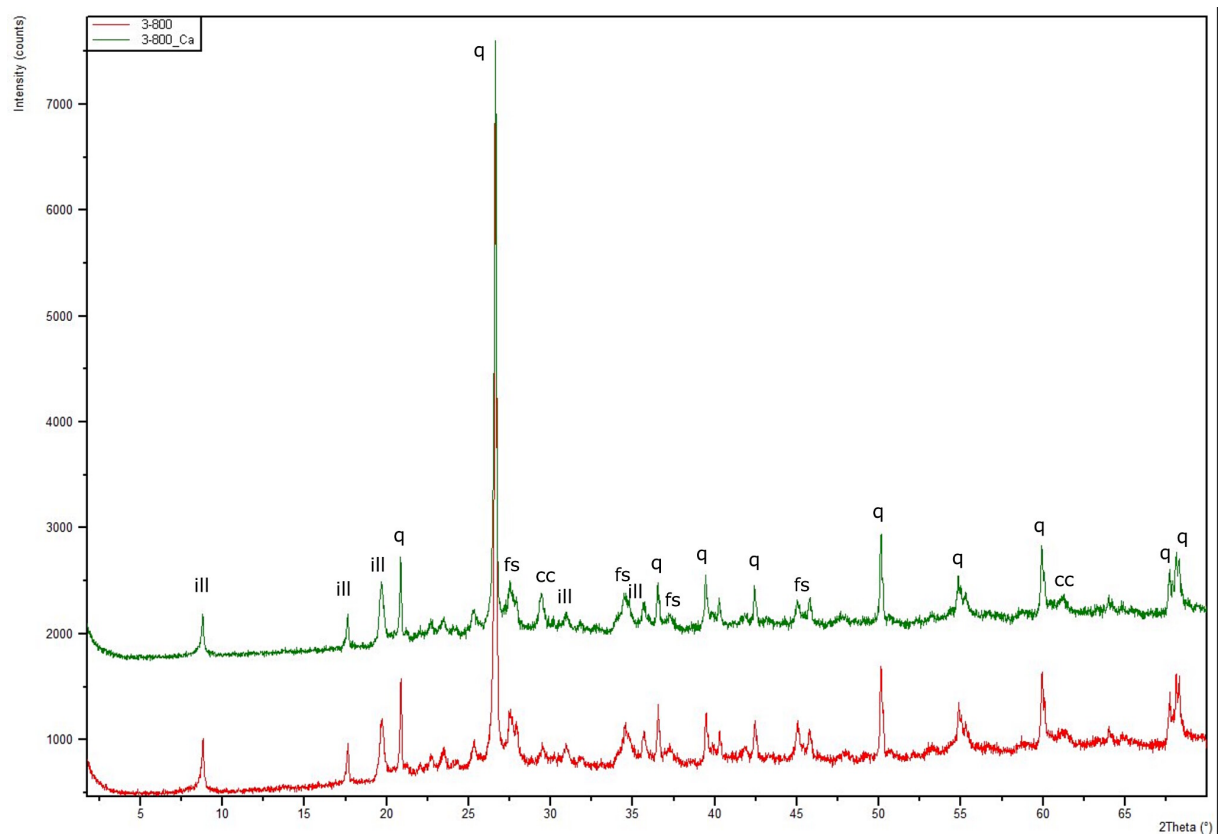


Figure 5.3: Combined XRD-diagrams of specimen soaked for 3 hours at 800°C with CaCO_3 (green) and without CaCO_3 (red); q: quartz, ill: illite, fs: feldspar

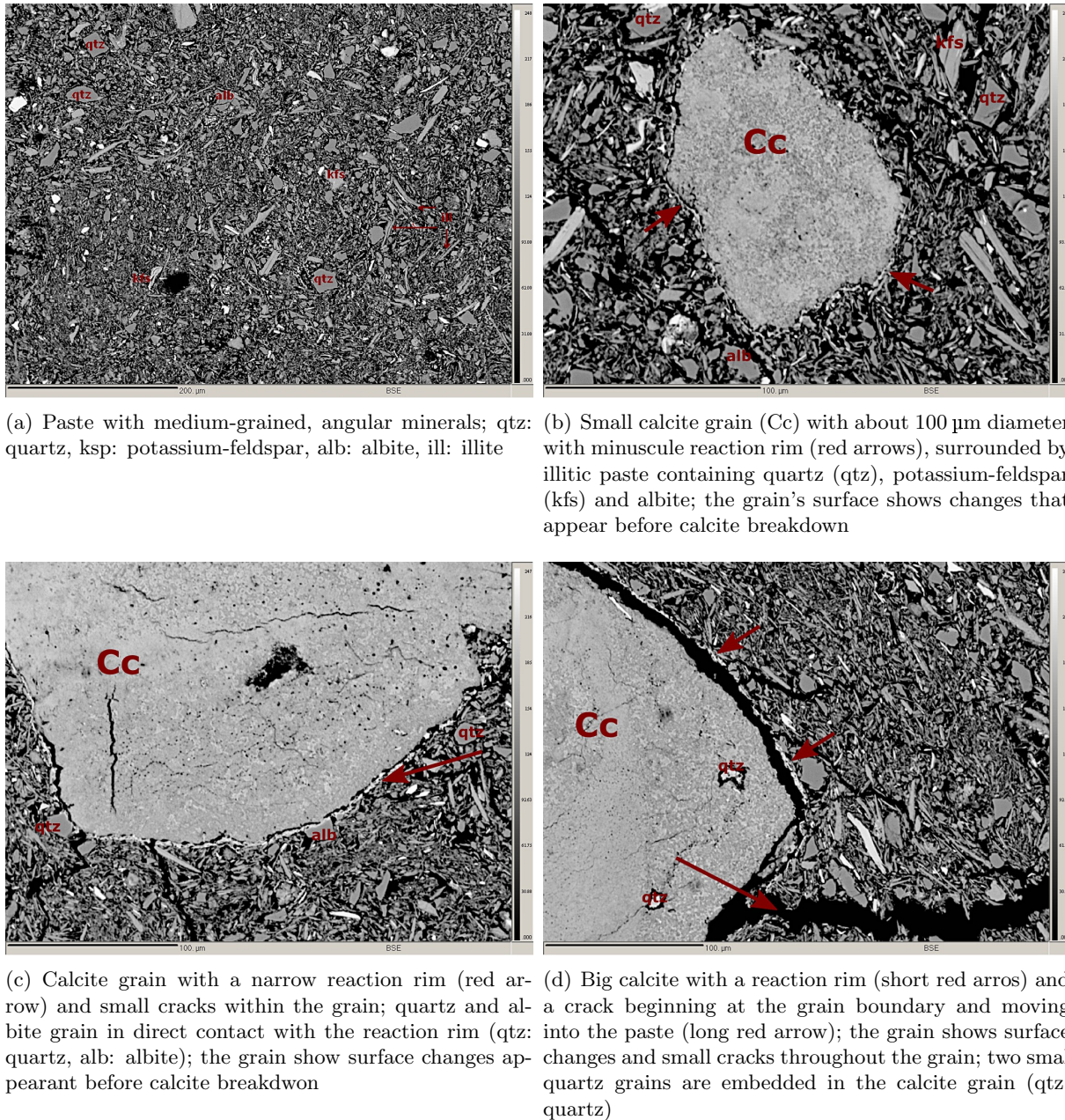


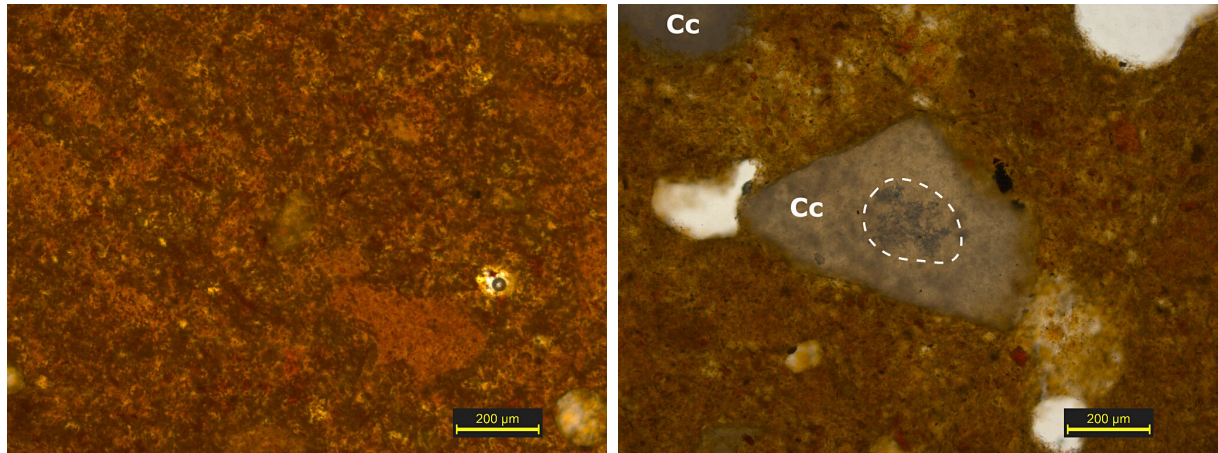
Figure 5.4: Paste and calcite grains of different sizes with very narrow reaction rims; 800° C, 3 h

5.1.2 5 hours soaking time

The first view with OM of the sample displays calcite grains without visible reaction rims. Some grains show signs of breakdown in the middle; Fig. 5.5(b). No other minerals can be identified in the paste; Fig. 5.5(a). BSE images show the paste to consist of quartz, potassium-feldspar, albite and illite. The phenocryst distribution throughout the sample is uneven, some areas consist solely of fine-grained clay paste. Most calcite grains show surface changes that precede calcite breakdown, but no breakdown yet. Some calcites that have small cracks starting within the grains and moving out into the paste (Fig. 5.7(b)), but no signs of shrinking. Narrow reaction rims can be found around some calcite grains, independent of their grain size, with about 2 μm in diameter; see Fig. 5.7(c) and (d).

XRD diagrams comparing the samples with and without calcite, show the main difference to be the calcite peak (Fig. 5.6), and neither mineral breakdown or crystallization. No gehlenite or another Ca-alumo-silicate phase was found.

Reaction rims were too small for point analysis. Point analysis in the calcite show no trend in the distribution of CaO throughout the grain (Fig. 5.7(b)).



(a) Fine-grained clay paste with free of phenocrysts

(b) Calcite grain (Cc) with signs of breakdown in the middle (dashed line), but without reaction rim

Figure 5.5: Paste without phenocrysts and calcite grain with sign of breakdown in the middle in the sample fired at 800°C, 5h

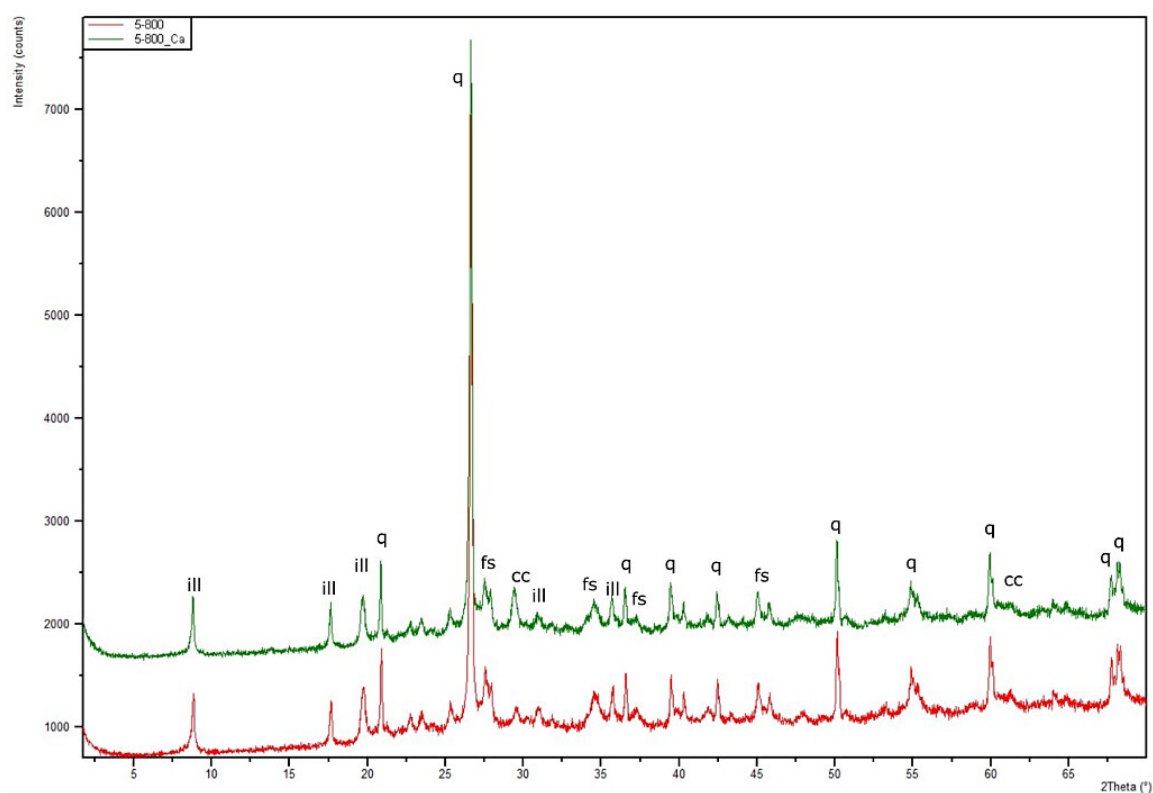
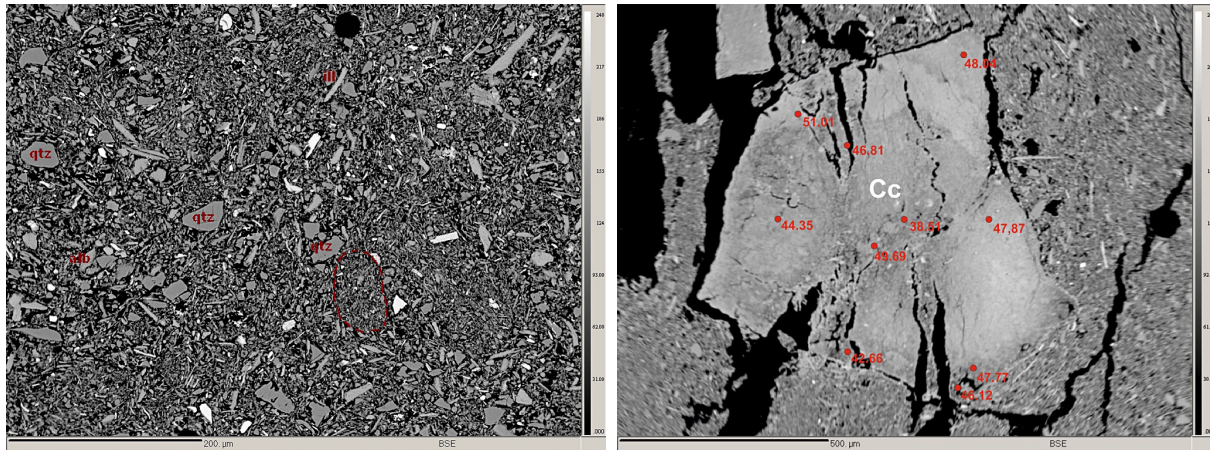
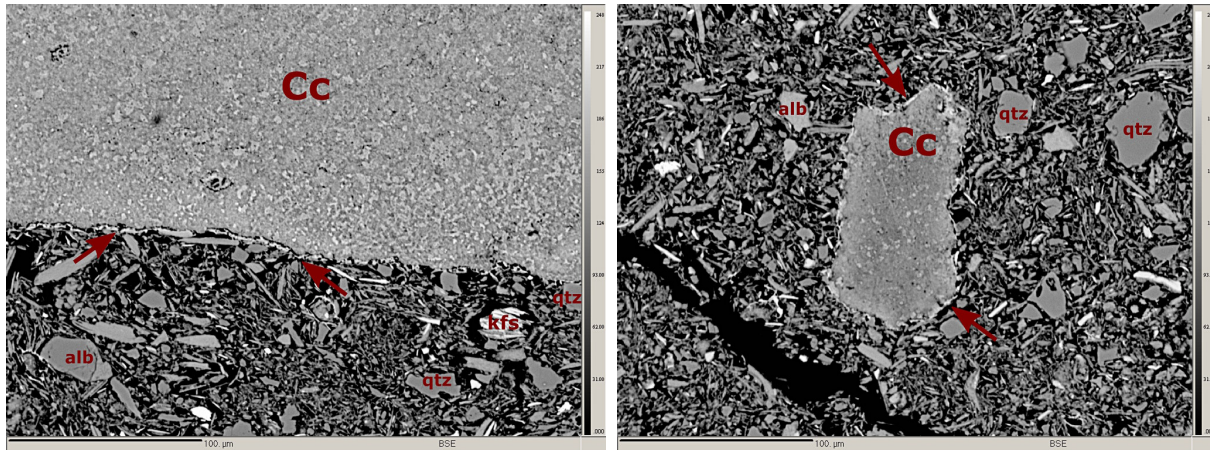


Figure 5.6: Combined XRD-diagrams of specimen soaked for 5 hours at 800°C with CaCO_3 (green) and without CaCO_3 (red); q: quartz, ill: illite, fs: feldspar



(a) Paste with well defined mineral boundaries; qtz: quartz, ksp: potassium-feldspar, alb: albite, ill: illite; dashed lines marks an area, where the paste is more compressed due to the absence of bigger mineral grains (b) Calcite (Cc) with cracks progressing from the grain into the matrix; numbers indicate EPMA point analyses: CaO distribution throughout the grain without a trend, in wt%



(c) Big calcite grain (Cc) with a narrow reaction rim (red arrows) of about 2 µm diameter and surface changes, without signs of breakdown and shrinking; the surrounding fine-grained clay paste contains quartz (qtz), albite (alb) and potassium-feldspar (ksp) phenocrysts (d) Small calcite (Cc) undisturbed by the crack in the paste, with few surface changes and a minuscule reaction rim (red arrows), no shrinking or breakdown visible

Figure 5.7: Paste and different calcite grains with very narrow reaction rims; 800 °C, 5 h

5.1.3 7 hours soaking time

First view with OM shows a paste with calcite grains with sharp grain boundaries embedded; Fig. 5.8. BSE images display the paste with no signs of sintering and distinct grain boundaries for all phenocrysts as well as areas of fine-grained clay paste, Fig. 5.10(a). With OM no reaction rims can be seen. With BSE images, rims with a diameter up to 4 µm can be found around some calcites of all sizes, see Fig. 5.10(b). Reaction rims are better developed when the grain is surrounded by quartz and feldspar grains than when embedded in clayey paste, compare Figs. 5.10(b) and (c) to (d). Small cracks within calcite grains can progress into the paste, Fig. 5.10(c). Most calcites still show no sign of shrinking, but very few can be detected where shrinking seems to start slowly, as can be seen in Fig. 5.10(b) and (d). The surface of all grains displays the changes connected to early breakdown.

Comparing the XRD diagrams of the specimen with and without calcite shows only the calcite

peak as main difference, without mineral crystallization or breakdown detectable (see Fig. 5.9). Therefore, gehlenite was not identified.

The reaction rims are still too narrow to be measured by EMPA. Point analysis within the calcites show notably low levels of CaO without concentration in either the middle of the grain or towards the rim; see Fig. 5.10(d). Points analyzed within reaction rims that reach more than 95 % total have been plotted in the CaO – SiO₂ – Al₂O₃ phase diagram in Fig. 5.11, but do not plot into the gehlenite stability field. All relevant point analyses are listed in table 5.1.

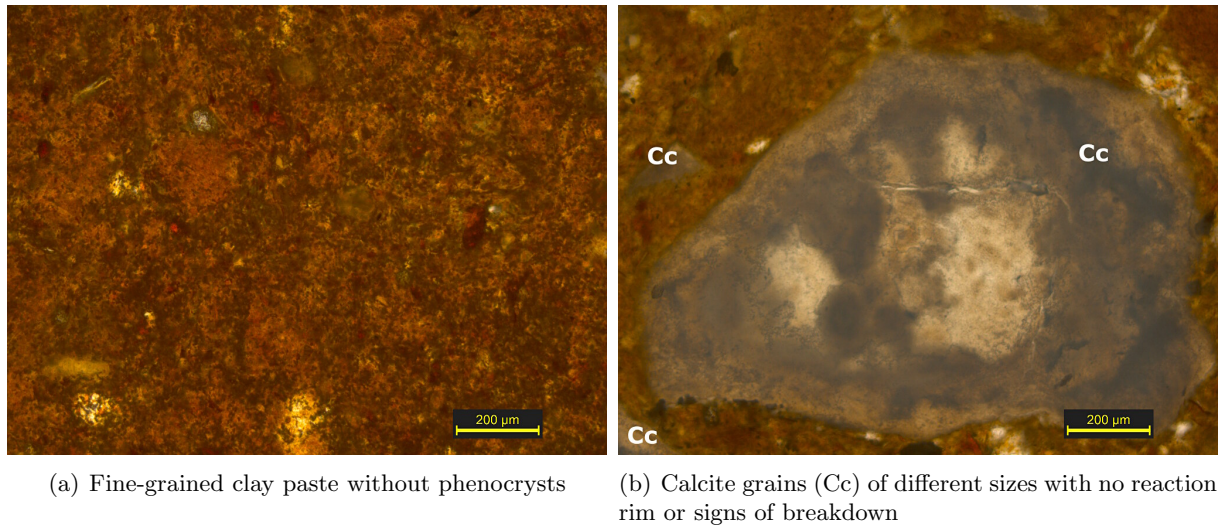


Figure 5.8: Paste and calcite grain with no visible reaction rims in the sample fired at 800°C, 7h

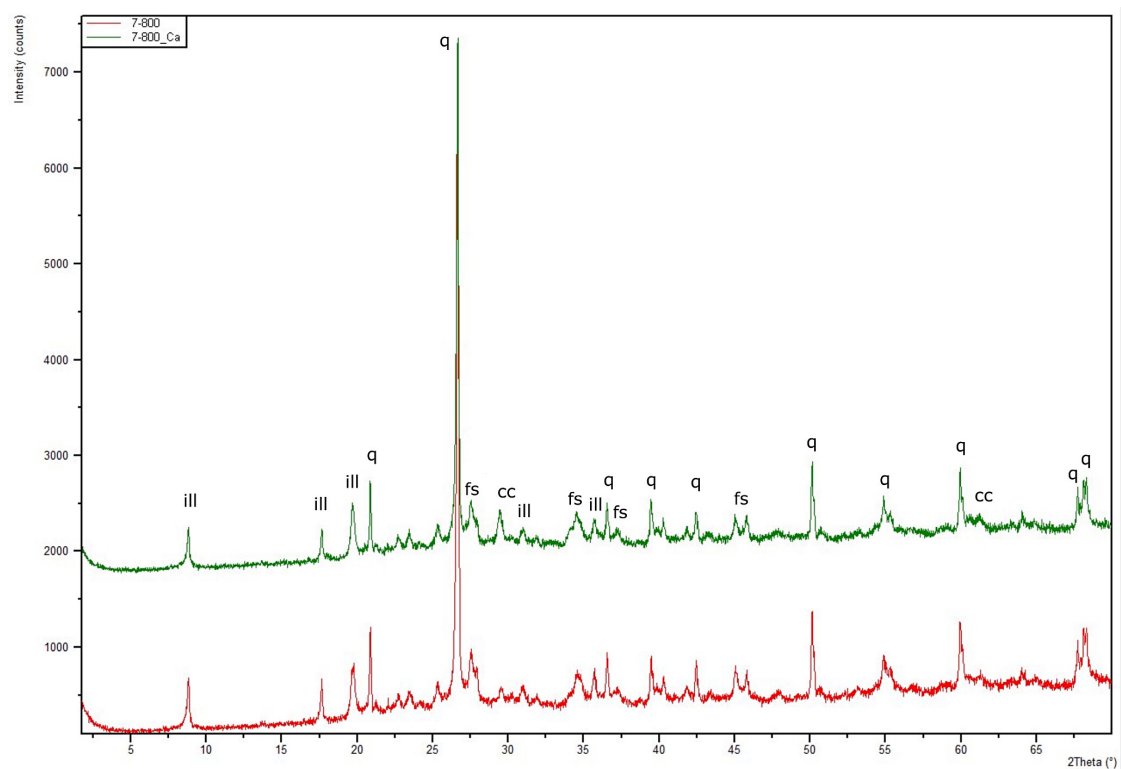
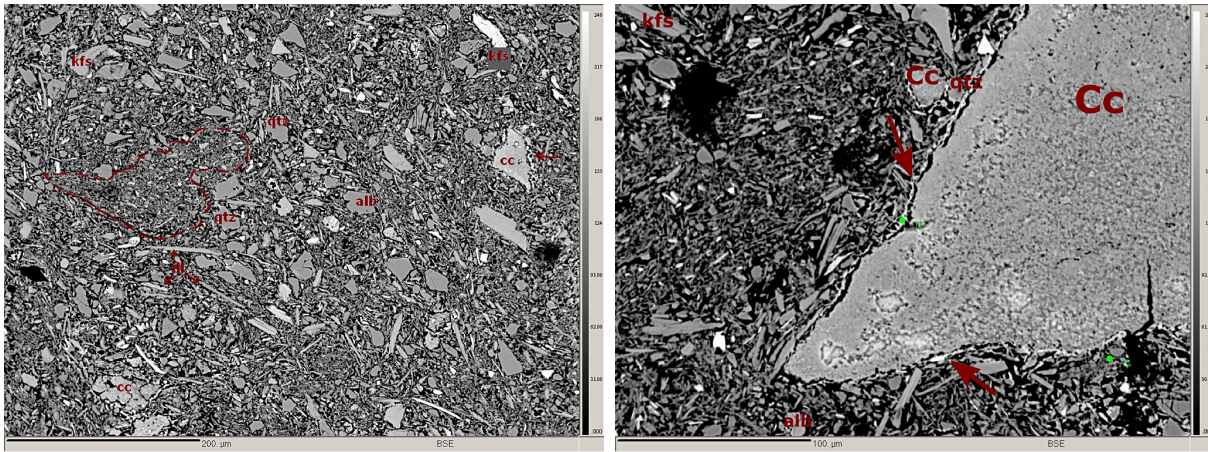
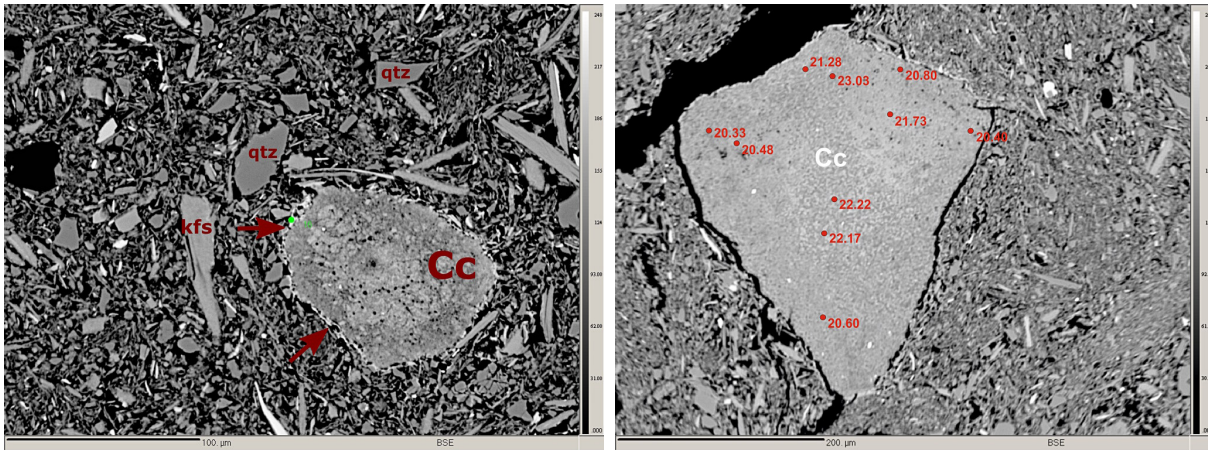


Figure 5.9: Combined XRD-diagrams of specimen soaked for 7 hours at 800°C with CaCO₃ (green) and without CaCO₃ (red); q: quartz, ill: illite, fs: feldspar



(a) Paste with medium-grained angular and elongated minerals; qtz: quartz, cc: calcite with small reaction rim (indicated by the white arrow), alb: albite, ill: illite; dashed lines indicate an area consisting of very fine grained clay minerals

(b) Calcite grain (Cc) with a minuscule reaction rim (red arrows) and a crack progressing into the paste; visible surface changes. The grain is connected to a smaller grain by a quartz grain (qtz)



(c) Small calcite grain with surface changes preceding breakdown and a narrow reaction rim; no sign of shrinking

(d) Calcite grain with a thin reaction rim and attempts of shrinking; CaO in wt% show an even distribution throughout the grain with low values; numbers indicated EPMA point analyses

Figure 5.10: Paste and different calcite grains with reaction rims; ; (800° C, 7h)

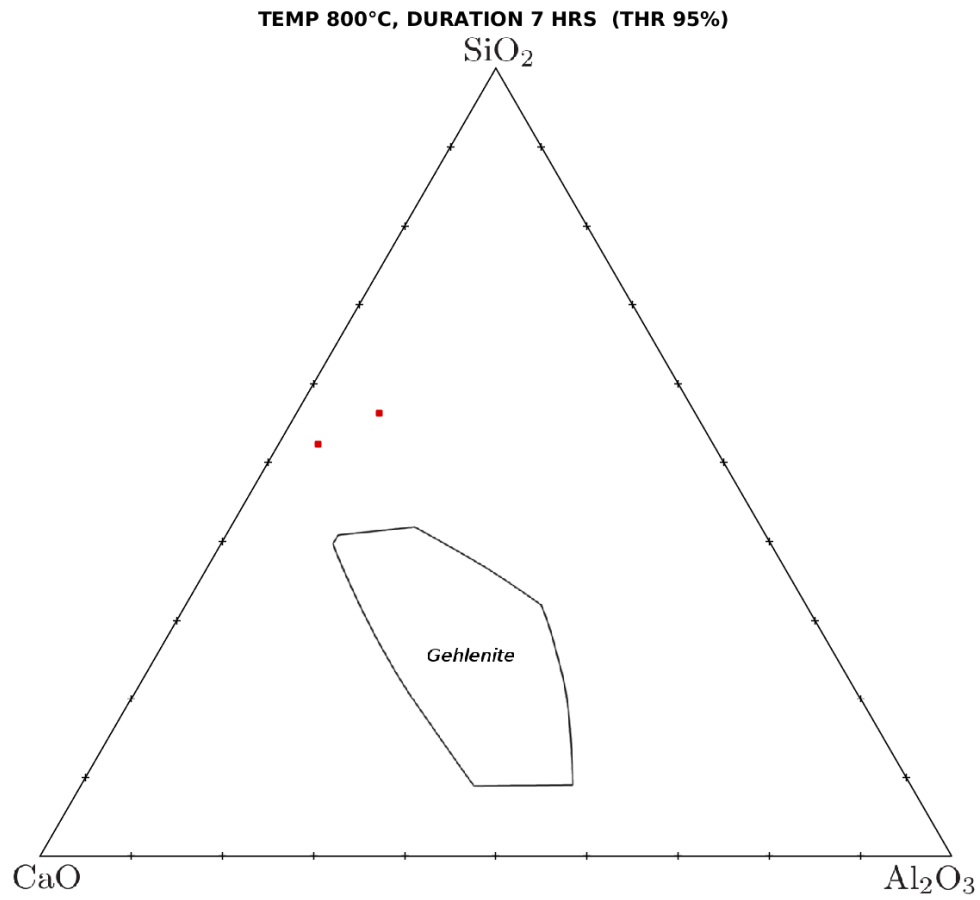


Figure 5.11: Ternary diagram with point analyses from the reaction rims that have a total higher than 95 % at 800°C and a soaking time of 7h. No gehlenite could be detected in the rims.

Set/Pt	4/1.	15/1.
SiO₂	49.05	49.19
TiO₂	0.50	0.09
Al₂O₃	7.96	4.10
FeO	4.29	0.87
CaO	30.22	40.73
MgO	2.95	0.63
K₂O	0.51	0.08
Na₂O	0.09	0.12
Total	95.57	95.81

Table 5.1: EPMA raw sample data in wt%, firing temperature 800°C, soaking time 7 hours. (bdl = below detection limit.)

5.1.4 9 hours soaking time

The specimen fired for 9 hours at 800°C is one of two 800°C samples that was prepared with water as cooling agent. As a part of the first sample set fired and analysed, microprobe analyses also included profiles, that were intended to measure the continuous decrease of Ca, when starting the profile within a calcite grain and moving outward into the paste, as well as the increase of other elements (most importantly Si and Al) in the other direction, especially for such narrow rims that did not allow defocused point analysis, with the intend of detecting gehlenite this way. While the decrease and increase of elements could be documented (Fig. 5.12), the rims were indiscernible and gehlenite was not detected. Therefore, one of the conclusions of those preliminary analysis was that hand selected, defocused point analyses provided better results, the difficulties notwithstanding.

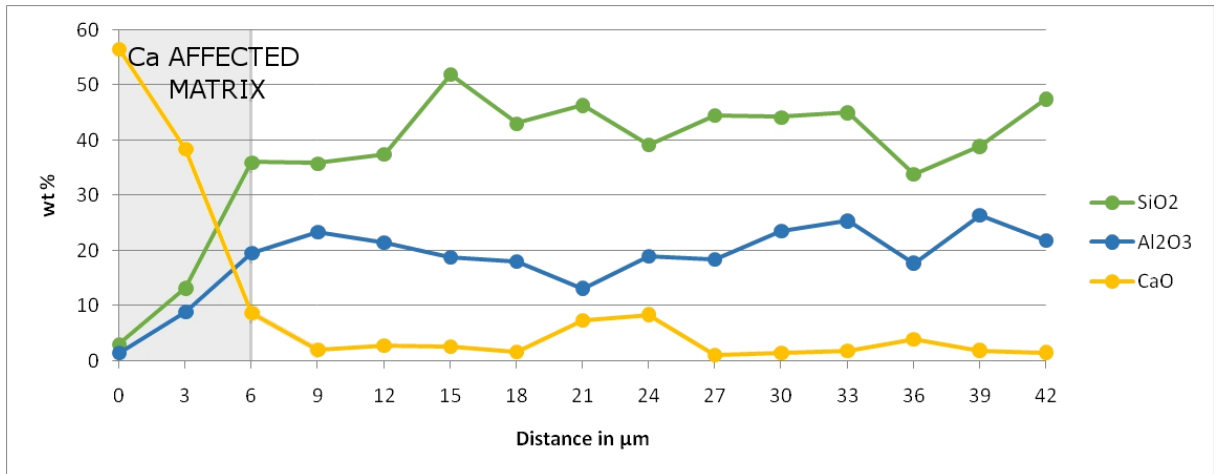
OM overview shows a paste free of phenocrysts and calcite grains with distinct grain boundaries and no sign of breakdown or reaction rims, see Fig. 5.13. BSE images of the paste show no sintering effects and for all minerals, as well as areas of concentrated phyllosilicates (Fig. 5.15(a)). BSE images show calcites of all sizes with narrow reaction rim of up to 3 µm diameter, see Fig. 5.15(c) and (d). Smaller calcite grain tend to show surface changes and produce broader reaction rims, Fig. 5.15(b). Elemental mapping was performed for the calcite grain in Fig. 5.15(c). As can be seen in Fig. 5.16, Ca is still very much confined within the grain boundaries, as well as Al, Si and Fe keeping to the paste.

XRD diagram comparison shows neither mineral breakdown nor formation in either the specimen containing calcite or the one without, as can be seen in Fig. 5.14. The distinct calcite peak remains the only difference, with no gehlenite detected.

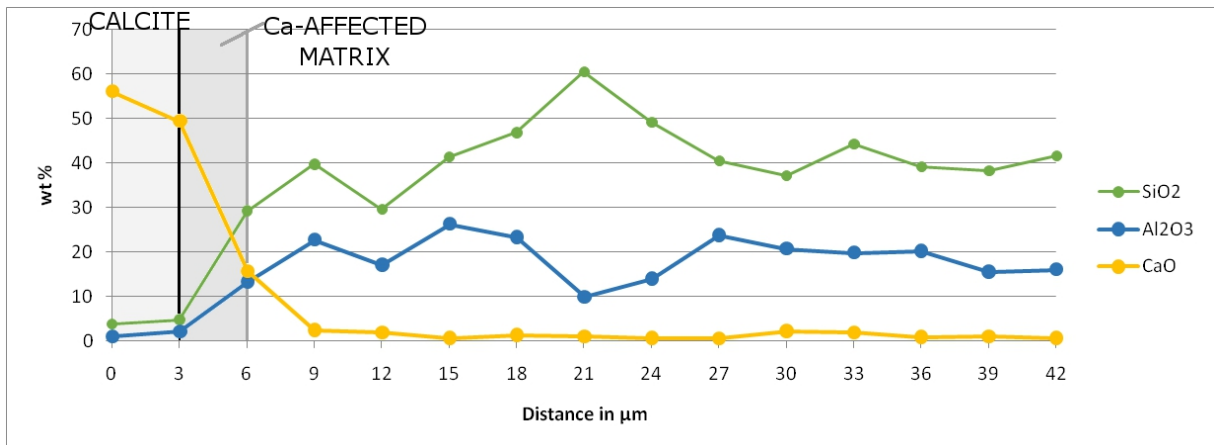
Point analyses surpassing 95 wt% total are plotted in Fig. 5.17, but are not plotting in the gehlenite stability field, for the corresponding point analyses see table reftab:rawdata-noco2-thr95-rot-800deg-9hrs. Results from within the calcite grain show a high variability of CaO values, that do not allow the assumption of a trend.

Set/Pt	1/9.	2/9.	10/1.
SiO₂	95.89	98.00	41.65
TiO₂	0.03	bdl	0.72
Al₂O₃	1.26	0.32	17.98
FeO	0.23	0.14	2.51
CaO	0.25	0.11	25.73
MgO	0.07	bdl	2.05
K₂O	0.24	0.14	6.51
Na₂O	bdl	bdl	0.03
Total	97.97	98.73	97.18

Table 5.2: EPMA raw sample data in wt%, firing temperature 800°C, soaking time 9 hours. (bdl = below detection limit.)



(a) EPMA profile from the calcite grain into the paste; red line in Fig. 5.15(d). Ca progresses about 6 μm into the paste



(b) Elemental distribution of Ca, Si and Al across a profile from the calcite into the paste; green line in Fig. 5.15(d). Ca progresses about 3 μm into the paste

Figure 5.12: Elemental distribution of Ca, Si and Al across a profile from calcite grains into the paste in the sample fired at 800°C, 9h, moving from the edge of the calcite grain into the paste, see Fig. 5.15(d)

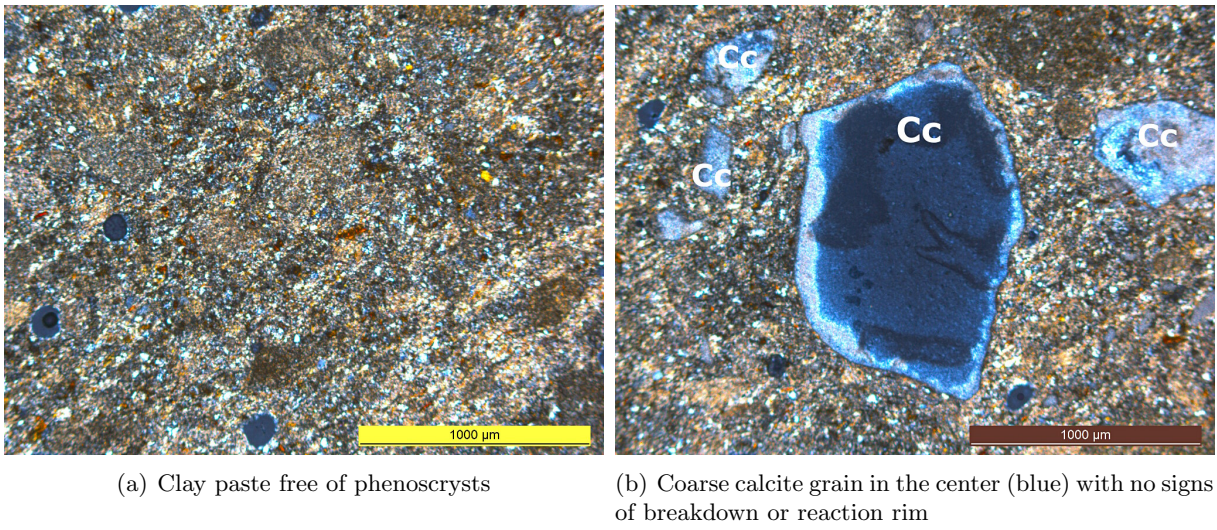


Figure 5.13: Paste and calcite grain with no visible reaction rims in the sample fired at 800° C, 9 h

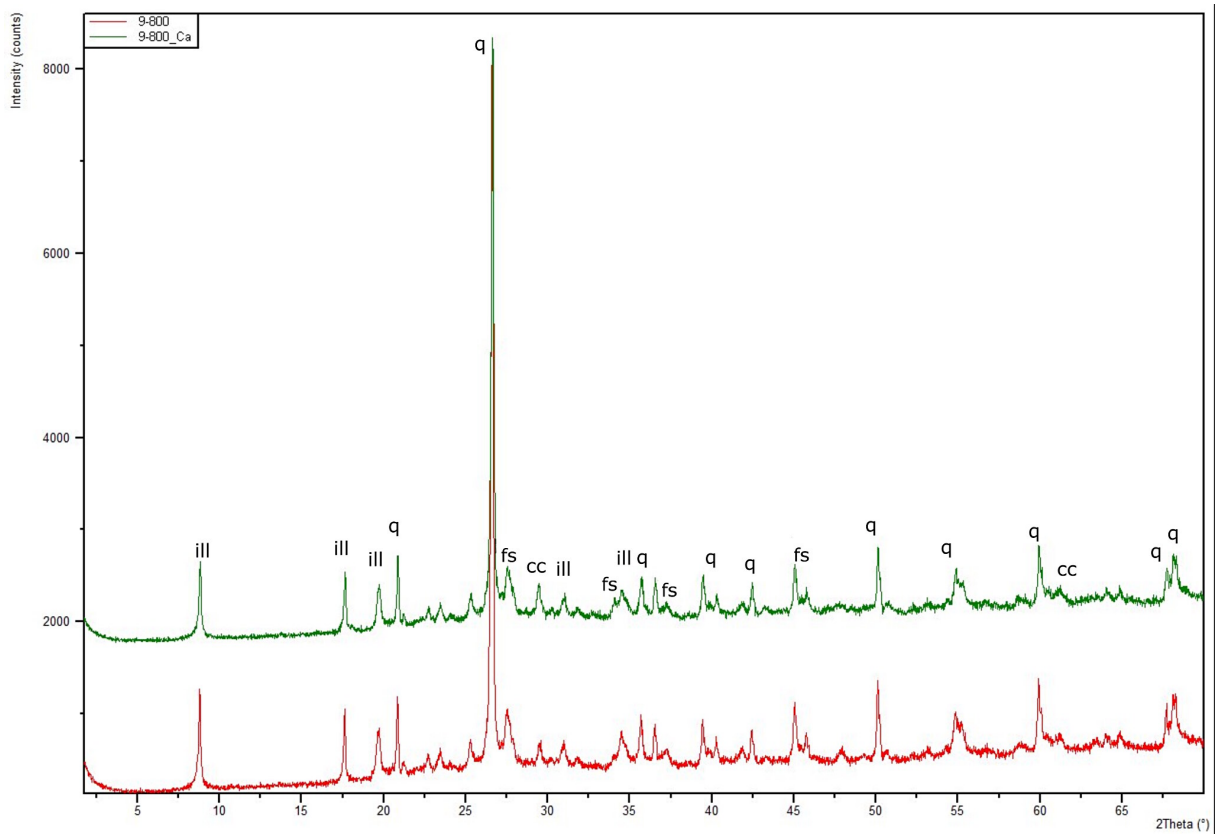
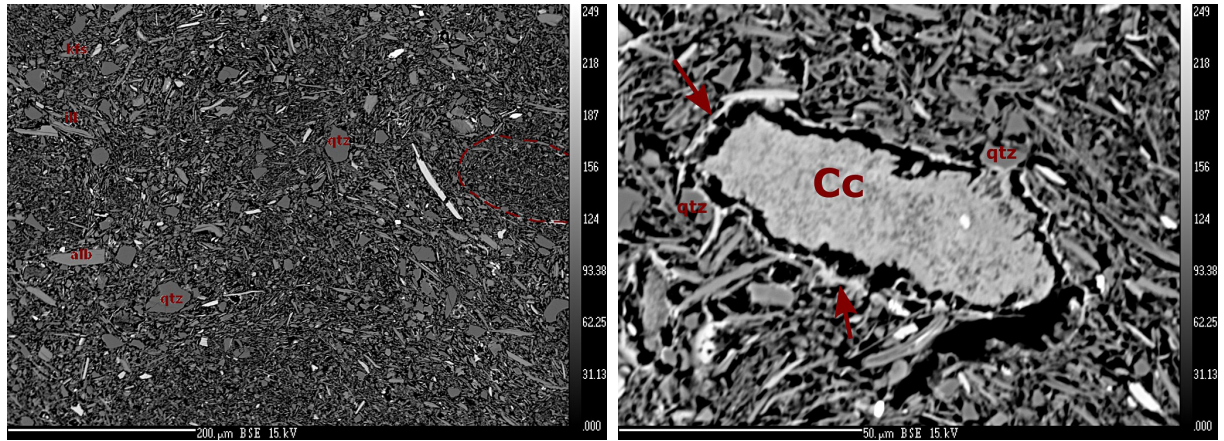
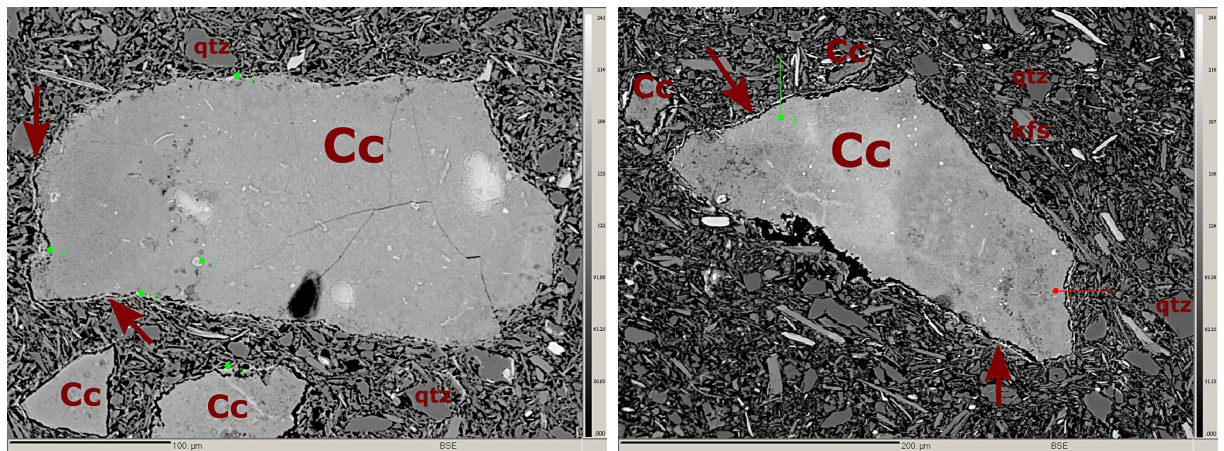


Figure 5.14: Combined XRD-diagrams of specimen soaked for 9 hours at 800° C with CaCO_3 (green) and without CaCO_3 (red); q: quartz, ill: illite, fs: feldspar

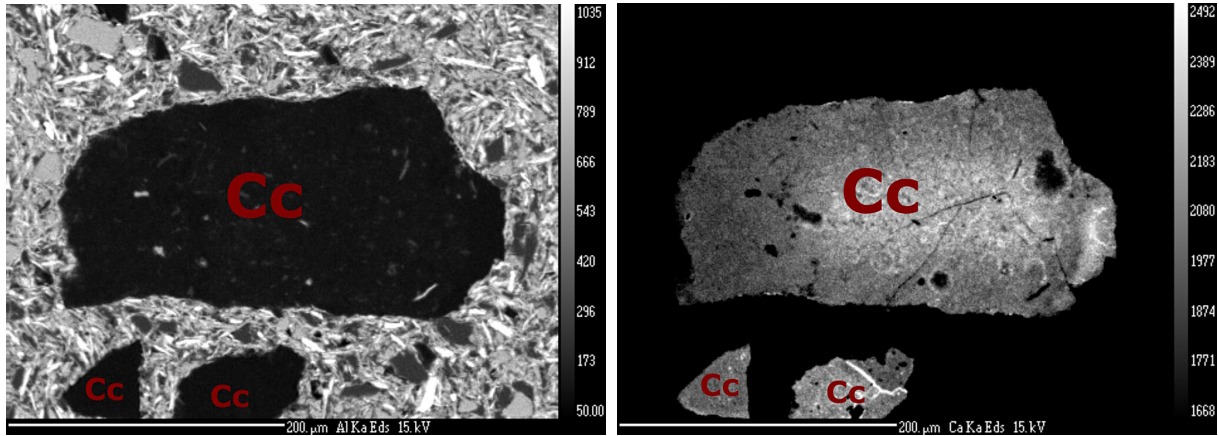


(a) Paste with discrete mineral angular grains; qtz: quartz, ksp: potassium-feldspar, alb: albite, ill: illite; dashed lines show an area of fine grained paste lacking phenocrysts (b) Small calcite grain surrounded by clayey paste with quartz; surface changes, minuscule reaction rim and signs of shrinking



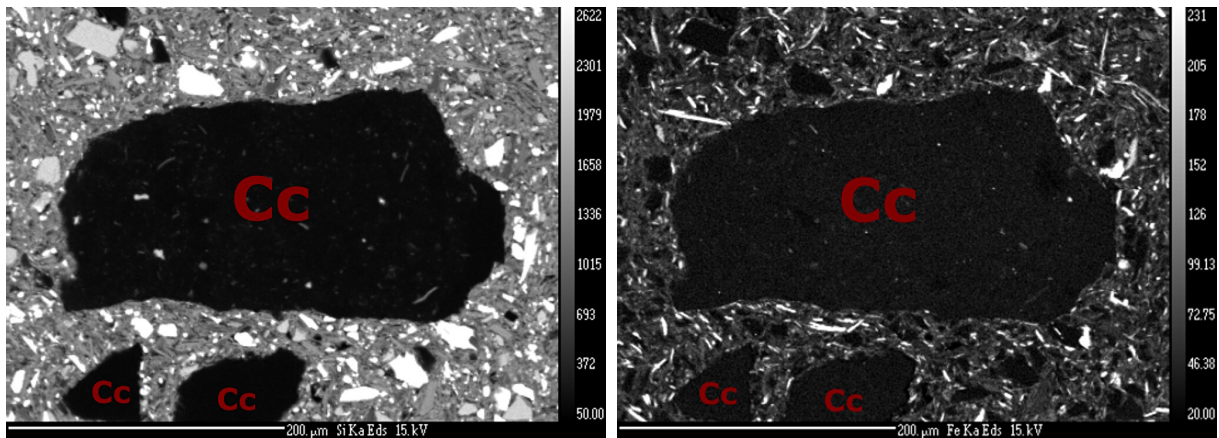
(c) Several calcite grains with a narrow reaction rim, no visible surface changes. The smaller grains show signs of shrinking, while the biggest appears unaffected; see Fig. 5.16 for elemental mapping (d) Calcite grain with narrow reaction rim, no visible surface change, possible beginning shrinking; profile are indicated by the red and the green line, showing the Ca, Si and Al distribution from the calcite grain into the paste (Fig. 5.12)

Figure 5.15: Paste and different calcite grains with narrow reaction rims; 800°C, 9h



(a) Elemental mapping for Al; Al keeps mostly to the paste and to illitic minerals surrounding the calcite grain. The Al visible within the grain appears only in concentrated small areas, presumably either because of small inclusions or contamination during thin section preparation

(b) Elemental mapping for Ca; Ca stays within the grain and appears to concentrate in the middle of the biggest grain (lighter area)



(c) Elemental mapping for Si; Si keeps to the paste, mostly concentrated in the quartz phenocrysts that are embedded in the paste. Quartz show no sign of decomposition. As with Al, Si is only found within the calcite grains in secluded areas, due either to tiny inclusions in the calcite or contamination

(d) Elemental mapping for Fe; Fe keeps to the paste, its distribution indicating the presence of Fe-oxides

Figure 5.16: Elemental mapping of a calcite showing in Fig. 5.15(c))

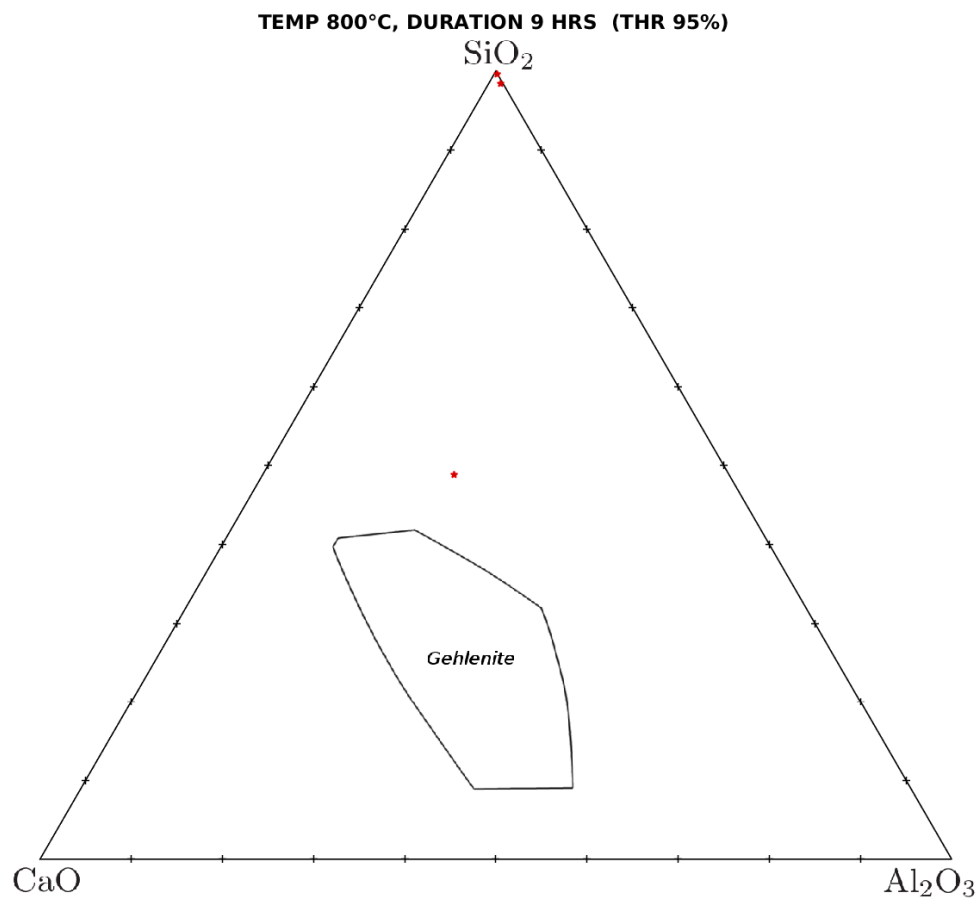


Figure 5.17: Ternary diagram with point analyses from the reaction rims that have a total higher than 95 % at 800°C and a soaking time of 9h. Only three of the analyses could be plotted and non of them reaches the gehlenite stability field.

5.1.5 11 hours soaking time

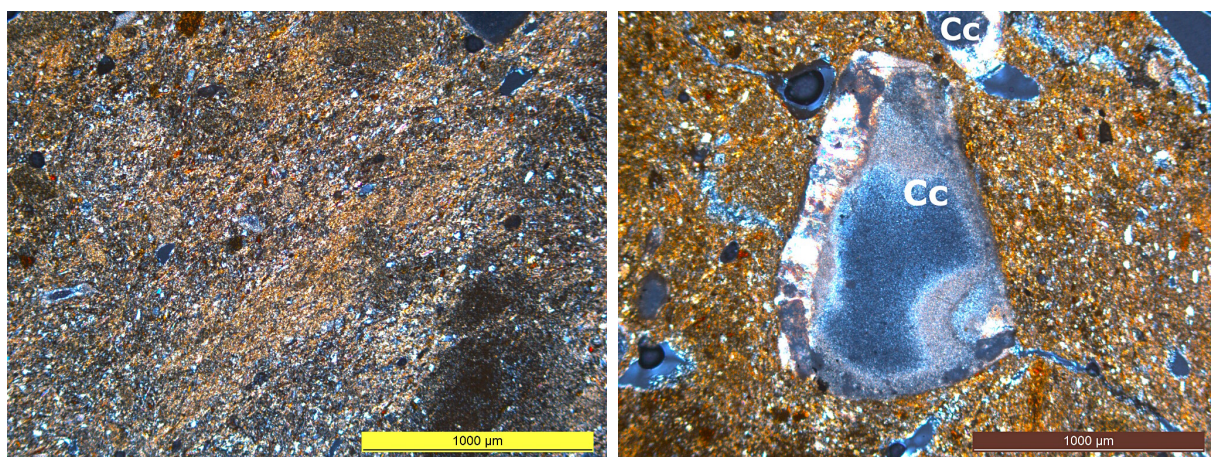
Just like the sample fired for 9 hours, this one was prepared as a preliminary sample and the thin section was produced with water as cooling agent. Since it was part of the first samples to be studied, analysis included microprobe profiles. The number of profiles measured increases the number of measurements done within this sample to a total of 339 points, which is the most of points analyzed in all of the samples.

OM analysis shows an indistinguishable paste and calcite grains without signs of breakdown or reaction rims, see Fig. 5.18. BSE image analysis (Fig. 5.20(a)) reveals the clayey paste to be unsintered and with sharp grain boundaries for all minerals. The calcite grains studied by BSE images show thin reaction rims of max. $3.5\text{ }\mu\text{m}$ diameter around calcite grains of all sizes. Especially small calcite grains also show signs of shrinking, see Fig. 5.20(b). All calcite grains display varying degrees of surface changes and, very occasionally, large calcite grains are starting to break down, usually combined with the beginning of shrinking, see Fig. 5.20(d).

Elemental mappings were performed in two calcites, with a thin reaction rim in close proximity to each other, still shows the elemental distribution to follow sharp grain boundaries, as can be seen in Fig. 5.21.

This calcite breakdown cannot yet be observed in the XRD analysis, even though the calcite peak is less pronounced than the one for lower soaking times at 800°C (Fig. 5.19). In comparison of the calcite containing specimen and the one without, the calcite peak remains the main difference, without gehlenite to be found.

As mentioned above, EPMA profiles were used to show the Ca, Si and Al distribution from within the calcite grain into the paste (Fig. 5.24). Ca diffusion for varying distances depending on the local paste composition surrounding the grain. Furthermore, profiles were also used to observe the Ca distribution within the grain, see Fig. 5.24. Profiles within the grains show a trend slight concentration of CaO in the fringe of the grain. Point analyses with a total higher than 95 wt%, see table 5.3, have been plotted in the phase diagram $\text{CaO} - \text{SiO}_2 - \text{Al}_2\text{O}_3$ (Fig. 5.22), but gehlenite was not detected.



(a) Heterogen fine-grained clay paste without visible minerals

(b) Calcite grain with no signs of breakdown or reaction rim and distinct grain boundaries

Figure 5.18: Paste and calcite grain with no visible reaction rims in the sample fired at 800°C , 11 h

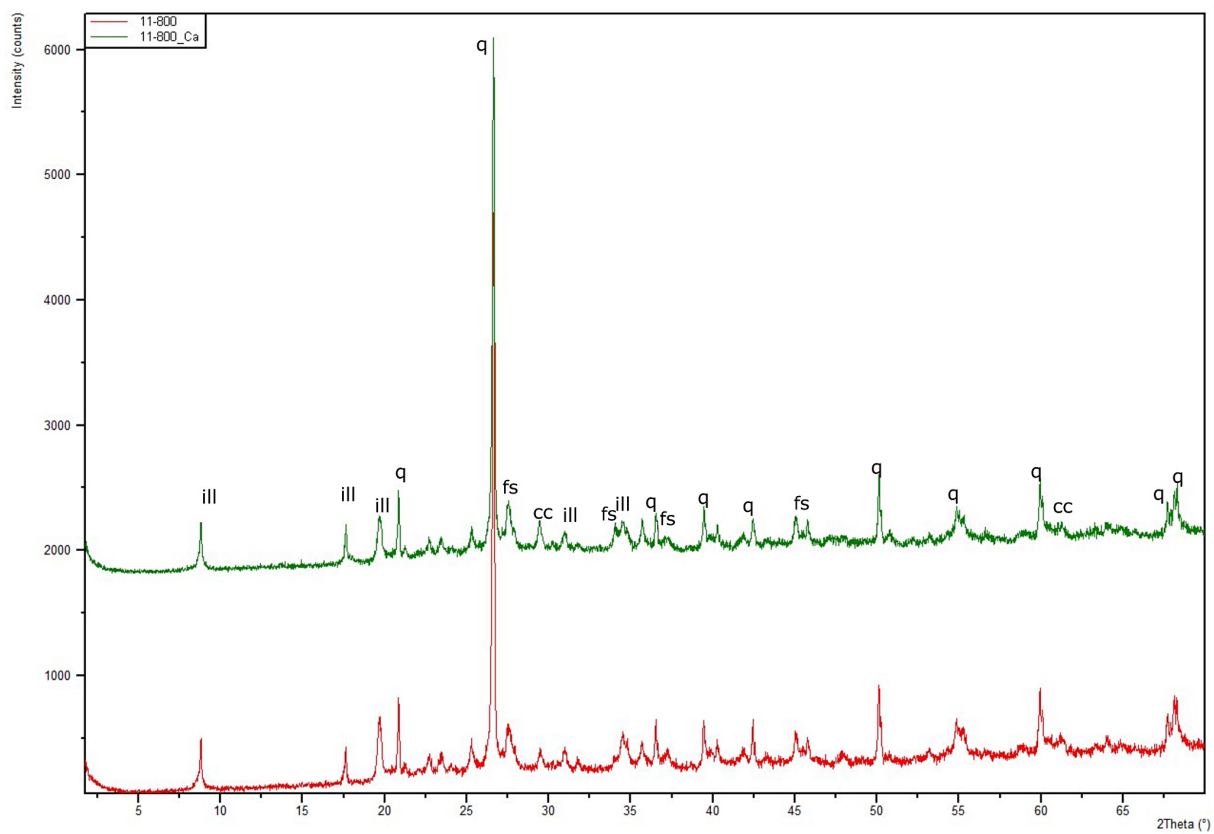
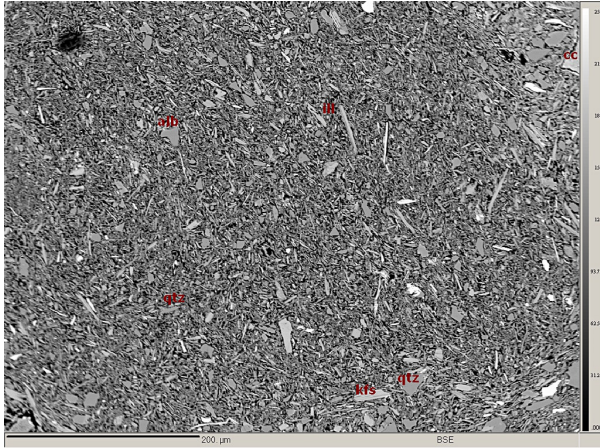


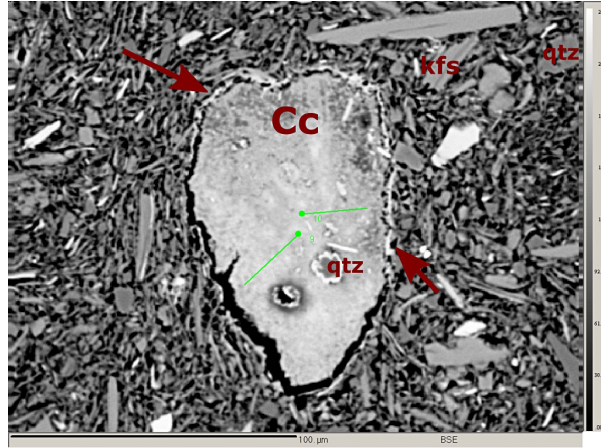
Figure 5.19: Combined XRD-diagrams of specimen soaked for 11 hours at 800°C with CaCO_3 (green) and without CaCO_3 (red); q: quartz, ill: illite, fs: feldspar

Set/Pt	9/2.	9/3.	10/2.	10/3.	14/11.	97/1.
SiO₂	65.75	93.44	74.56	94.50	94.90	98.67
TiO₂	0.14	0.03	0.10	bdl	0.07	bdl
Al₂O₃	5.83	1.25	3.12	0.98	1.81	0.14
FeO	1.16	0.23	0.51	0.12	0.20	0.02
CaO	21.31	0.78	17.21	0.48	0.09	0.76
MgO	0.70	0.12	0.41	0.07	0.24	bdl
MnO	bdl	bdl	bdl	bdl	bdl	bdl
K₂O	0.12	0.24	0.07	0.26	0.31	0.06
Na₂O	bdl	0.06	0.02	0.08	0.09	bdl
Total	95.02	96.15	96.01	96.48	97.71	99.62

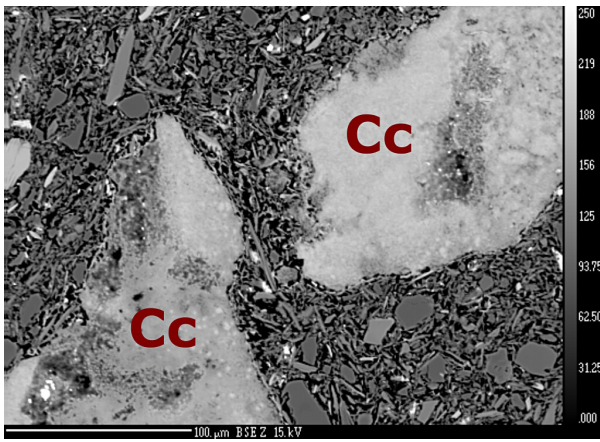
Table 5.3: EPMA raw sample data in wt%, firing temperature 800°C, soaking time 11 hours. (bdl = below detection limit.)



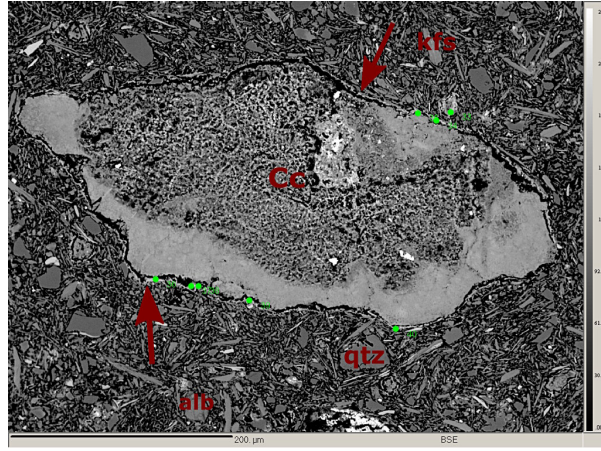
(a) Fine-grained paste with visible coarser angular and elongated mineral grains; qtz: quartz, ksp: potassium-feldspar, alb: albite, ill: illite



(b) Small calcite grain with signs of shrinking and reaction rim; EPMA profiles within the calcite grain are marked in green; the profiles showing the Ca distribution be seen in Fig. 5.23

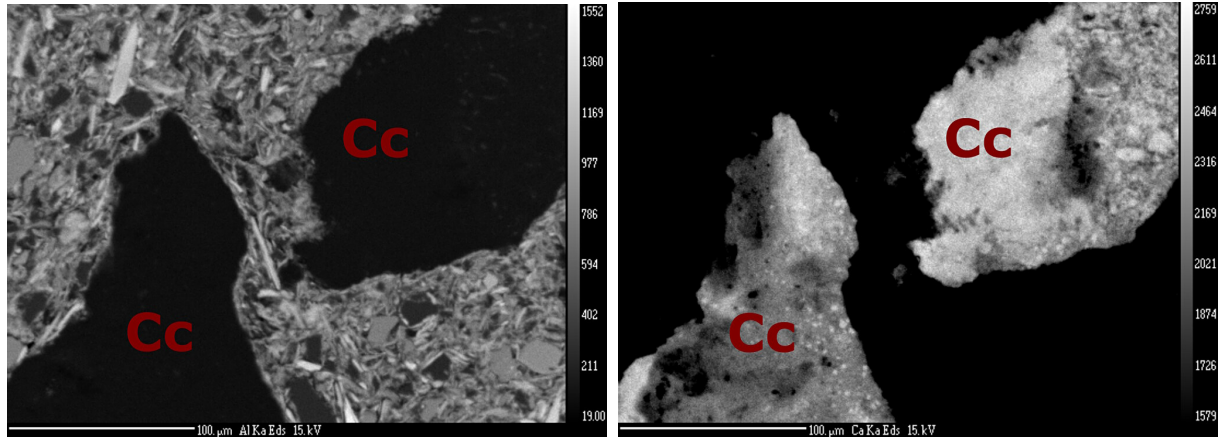


(c) Calcite grain with partial surface changes and a narrow reaction rim; see elemental mapping in Fig. 5.21



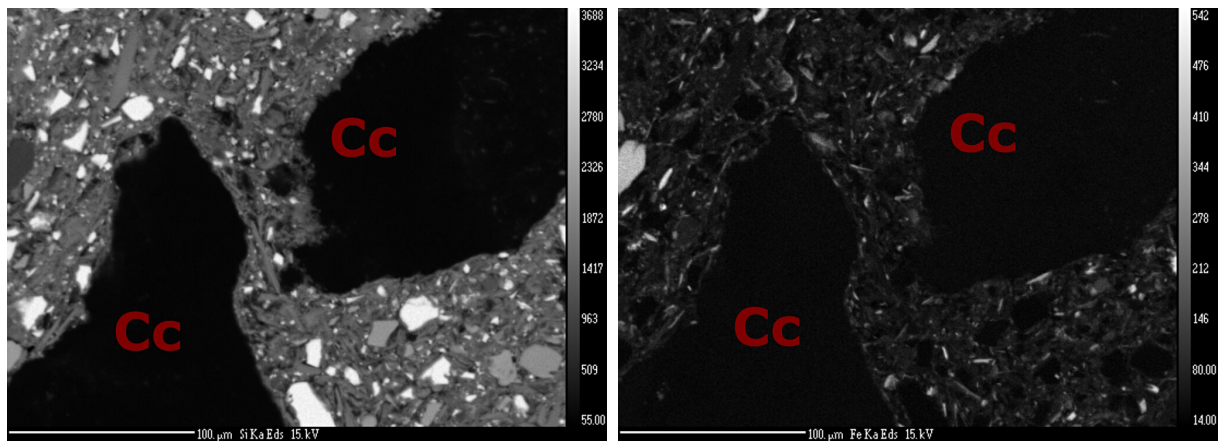
(d) Big calcite with thin reaction rim, signs of shrinking and breakdown showing in the middle of the grain; point analyses into the reaction rim do not point to gehlenite composition

Figure 5.20: Paste and different calcite grains with narrow reaction rims; (800°C, 11 h)



(a) Elemental mapping for Al; Al is confined into the paste and concentrated in illites

(b) Elemental mapping for Ca; Ca is concentrated only in the calcites and show an inhomogenous distribution within the two calcite grains in thos elemental X-Ray mapping



(c) Elemental mapping for Si; Si is concentrated in quartz phenocrysts embedded in the paste; quartz shows no sign of decomposition

(d) Elemental mapping for Fe; the paste is Fe-poor and only very few grains indicate the presence of Fe-oxides

Figure 5.21: Elemental mapping of a calcite grain with a reaction rim (Fig. 5.20(c))

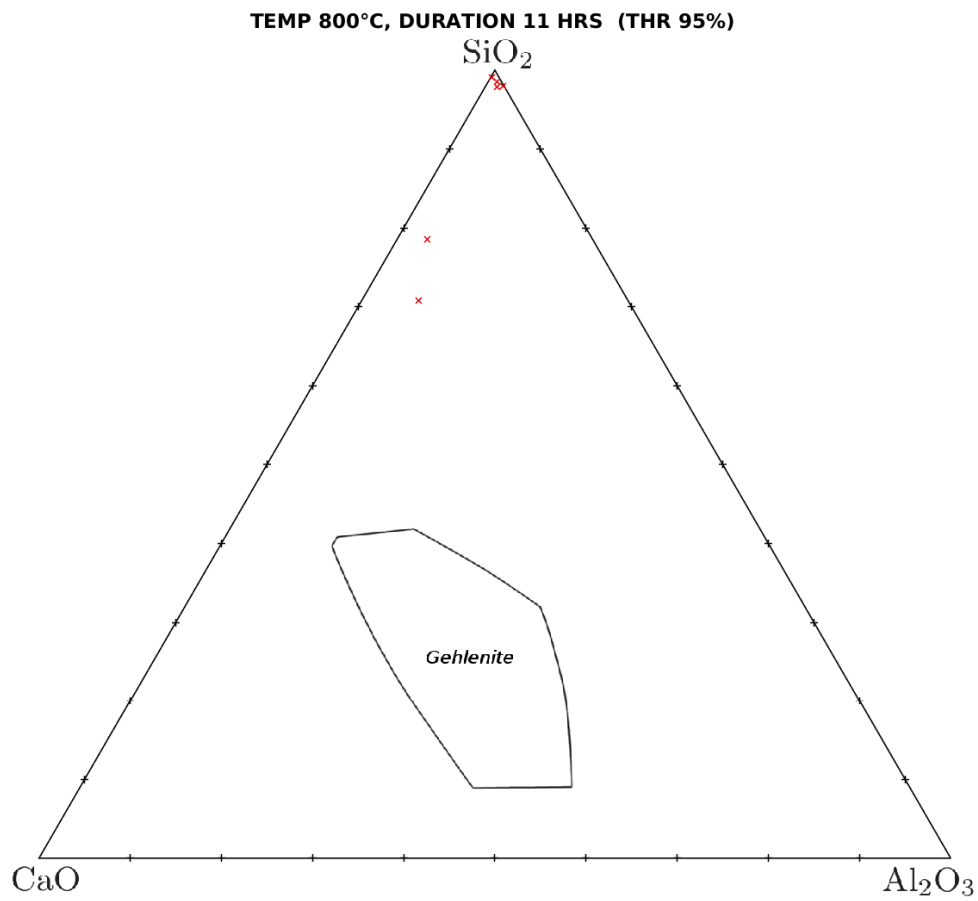
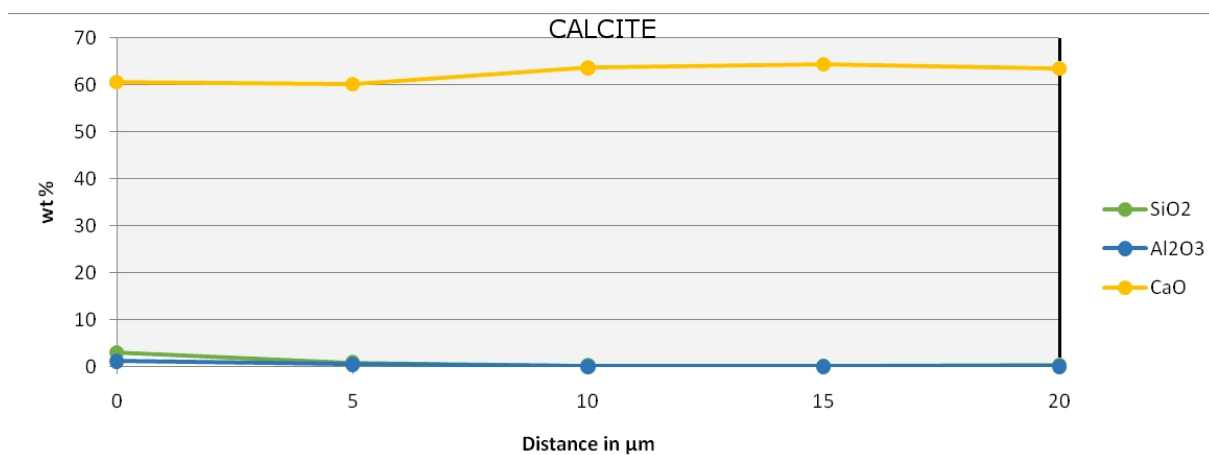
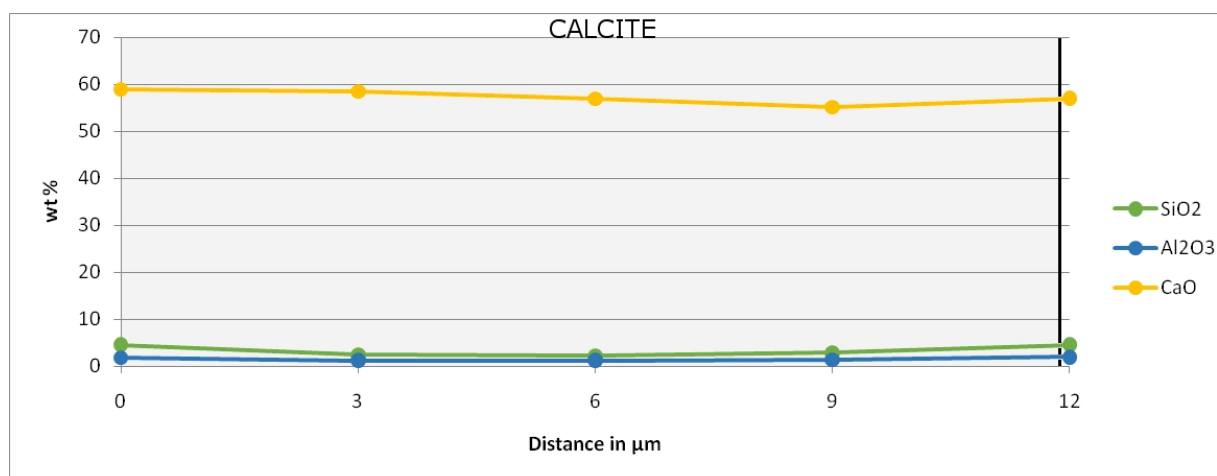


Figure 5.22: Ternary diagram with point analyses from the reaction rims that have a total higher than 95 % at 800° C and a soaking time of 11 h. No gehlenite could be detected.

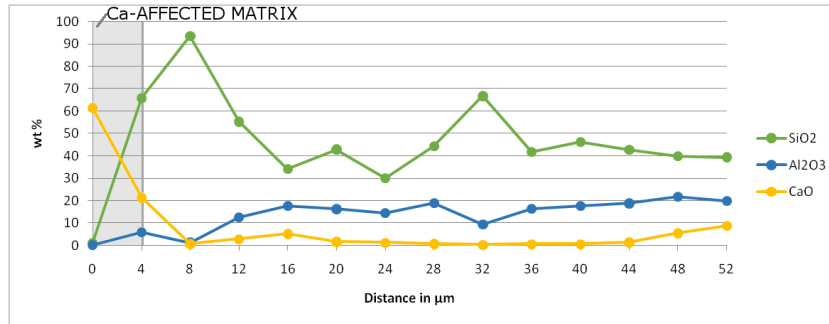


(a) EPMA profile crossing from the middle of the calcite grain to the rim; green line in Fig. 5.20(b) going from the middle to the lower left corner. Ca increases slightly from the middle outward

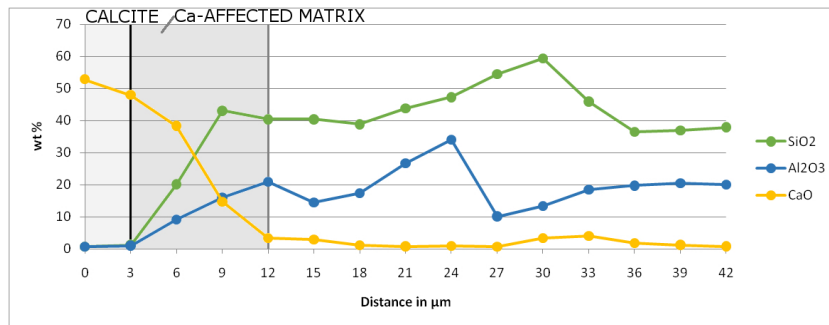


(b) EPMA profile crossing from the middle of the calcite grain to the rim; green line in Fig. 5.20(b) going from the middle to the right. Ca increases slightly from the middle outward

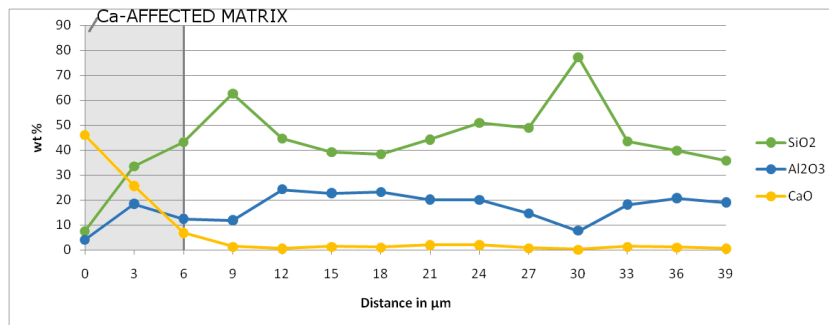
Figure 5.23: Profiles analyzed in the sample fired at 800°C, 11 h, moving from the middle of the calcite grain to the rim, see Fig. 5.20(b)



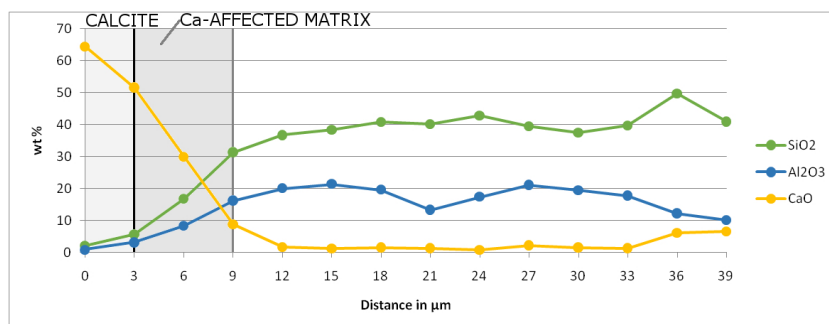
(a) EPMA profile from the calcite grain into the paste; Ca diffuses about 4 μm into the paste



(b) EPMA profile from the calcite grain into the paste; Ca diffuses about 9 μm into the paste



(c) EPMA profile from the calcite grain into the paste; Ca diffuses about 6 μm into the paste



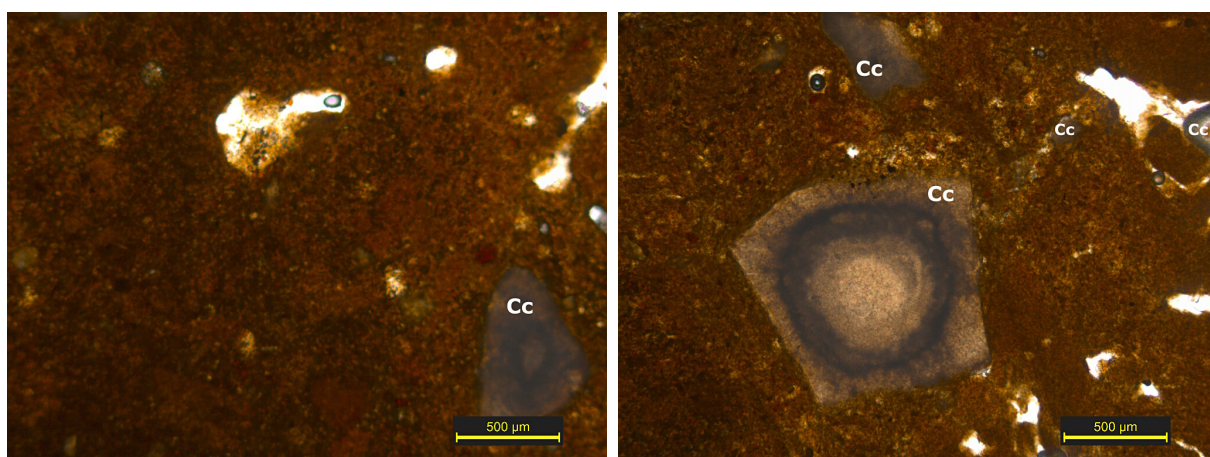
(d) EPMA profile from the calcite grain into the paste; Ca diffuses about 6 μm into the paste

Figure 5.24: EMPA profiles were performed to show the CA, Si and Al distribution from within the calcite grains into the paste in the sample fired at 800°C, 11 h; showing Ca diffuses varying distanced into the paste depending on the local mineralogy of the paste

5.1.6 20 hours soaking time

OM shows big calcites (up to 1.2 mm in diameter) for the specimen fired for 20 hours, that display the beginnings of breakdown and no reaction rims, see Fig. 5.25(b). No other minerals are discernible in the paste; Fig. 5.25(a). BSE images show the breakdown to start in the middle of the grain, while the grain boundaries are still stable, Fig. 5.27(b). The breakdown in the middle of the grain is preceded by overall changes in the calcite's surface (see Fig. 5.27(c)). The matrix remains unsintered, with all minerals retaining their distinct boundaries, see Fig. 5.27(a), and areas fine-grained clay minerals free of phenocrysts. Reaction rims are visible in BSE images. The rims have a diameter of max. 3.5 μm and appear to be more pronounced around smaller calcite grains, Fig. 5.27(d). Shrinking can be seen in calcite grains of all sizes, see Fig. 5.27(d). XRD analysis detects no gehlenite. Furthermore, in neither the diagram displaying the sample containing calcite nor the one without mineral breakdown or formation can be observed (Fig. 5.26). The calcite peak is again more distinct than in the samples fired for 11 h.

The rims are still too narrow for conclusive microprobe point analysis, so the chosen points focus on the calcite breakdown. Points analyzed within the calcite with changed surface structure show a slight trend within the CaO values, with CaO decreasing in the middle (see Fig. 5.27(c)). Calcites with breakdown starting in the middle of the grain (Fig. 5.27(b)), on the other hand, have a notable decrease of CaO going from the middle (appr. 66 weight%) to the grain's rims (appr. 47 weight%). All point analyses through the samples with a total of 95 % and more have been plotted in Fig. 5.28. This is the first time, that gehlenite is detected by microprobe analysis, see table 5.4.



(a) Fine-grained paste free of phenocrysts, surrounding a calcite grain (Cc) with no signs of breakdown or reaction rims
 (b) Coarse calcite grain (Cc) with distinct grain boundaries and signs of breakdown in the middle, reaction rims are not visible

Figure 5.25: Paste and calcite grain with no visible reaction rims in the sample fired at 800°C, 20 h

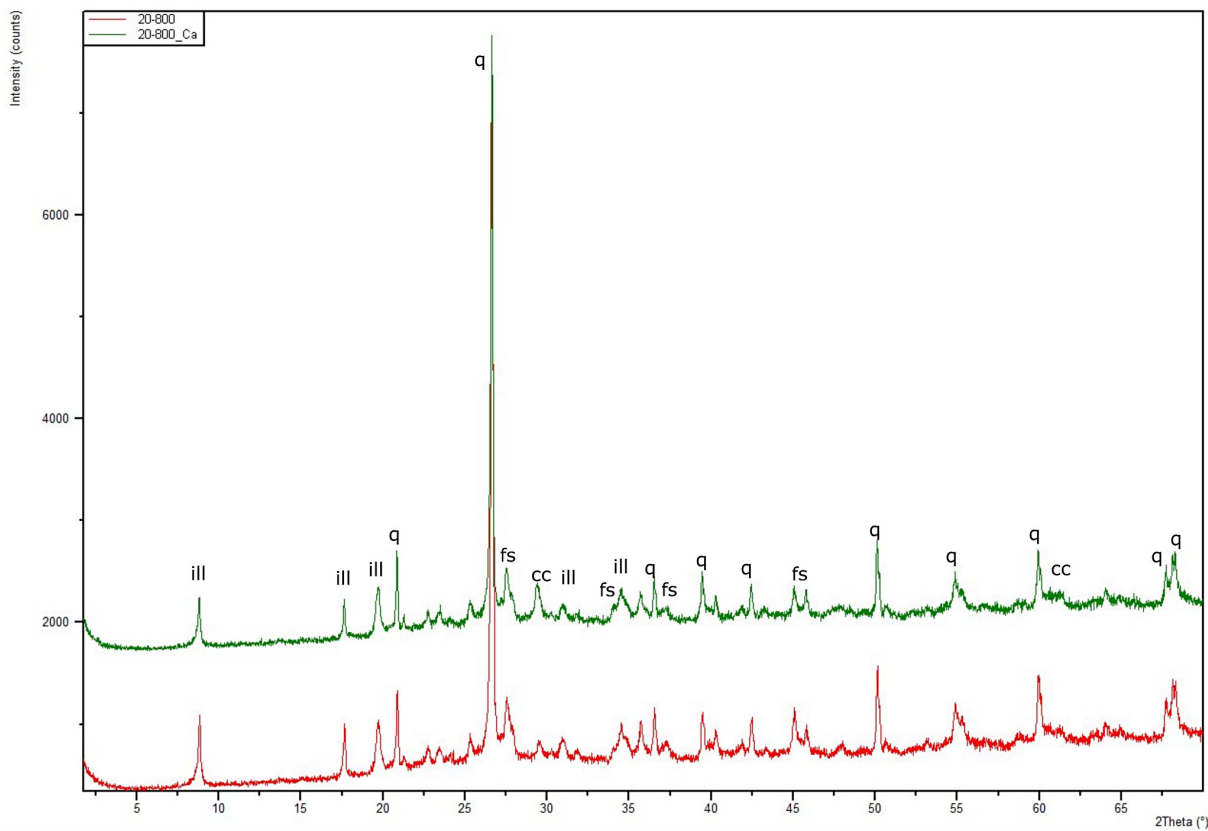
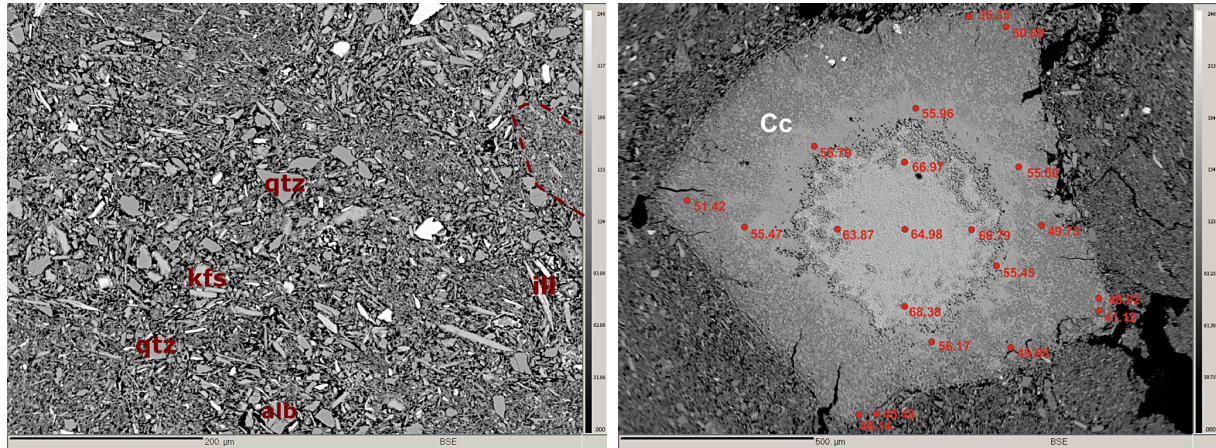


Figure 5.26: Combined XRD-diagrams of specimen soaked for 20 hours at 800°C with CaCO_3 (green) and without CaCO_3 (red); q: quartz, ill: illite, fs: feldspar

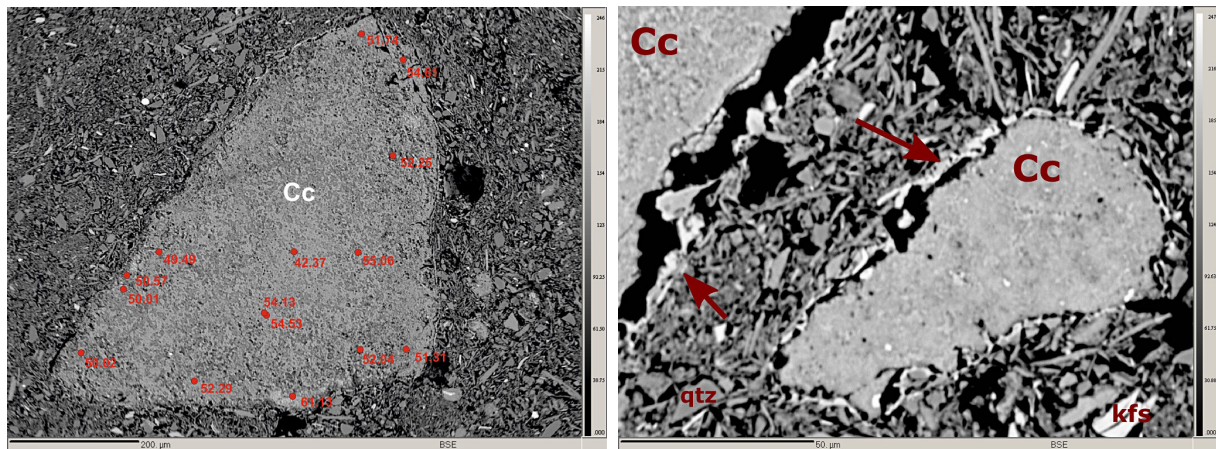
Set/Pt	6/1.	13/1.	14/1.	17/1.	18/1.	21/1.	23/1.
SiO₂	32.26	48.04	35.43	39.68	47.17	60.40	92.05
TiO₂	0.97	0.13	0.39	0.09	2.98	0.11	0.03
Al₂O₃	16.59	8.18	13.34	17.38	5.57	10.95	0.41
FeO	2.87	2.53	5.94	2.68	0.76	1.31	0.55
CaO	41.38	39.84	40.00	35.72	39.74	27.42	3.23
MgO	2.62	1.73	3.79	3.21	0.97	0.81	0.46
K₂O	0.32	0.33	0.74	0.35	0.81	0.60	0.15
Na₂O	0.06	0.17	0.05	0.05	0.05	0.09	0.16
Total	97.07	100.96	99.69	99.15	98.06	101.68	97.04

Table 5.4: EPMA raw sample data in wt%, firing temperature 800°C, soaking time 20 hours. (bdl = below detection limit.)



(a) Fine-grained paste with coarse angular and elongated mineral grains; qtz: quartz, ksp: potassium-feldspar, alb: albite, ill: illite, Cc: calcite; dashed lines show an area of fine grained paste lacking phenocrysts

(b) Big calcite grain (Cc) with about 1.2 mm diameter, starting to breakdown in the middle; with minuscule reaction rim; CaO in wt% shows a clear decrease in CaO from the middle of the grain to the rim; numbers indicate EPMA point analyses



(c) Big calcite grain (Cc) with surface changes before breakdown; CaO in wt% shows a slight trend in CaO distribution from the middle to the rim; numbers indicate EPMA point analyses

(d) Big calcite (Cc) and small calcite (Cc) with reaction rims, as indicated by the red arrows, and signs of shrinking; the big grain shows surface changes appearing before breakdown while the small grain shows an undisturbed surface

Figure 5.27: Paste and different calcite grains with signs of thermal breakdown; 800°C, 20 h

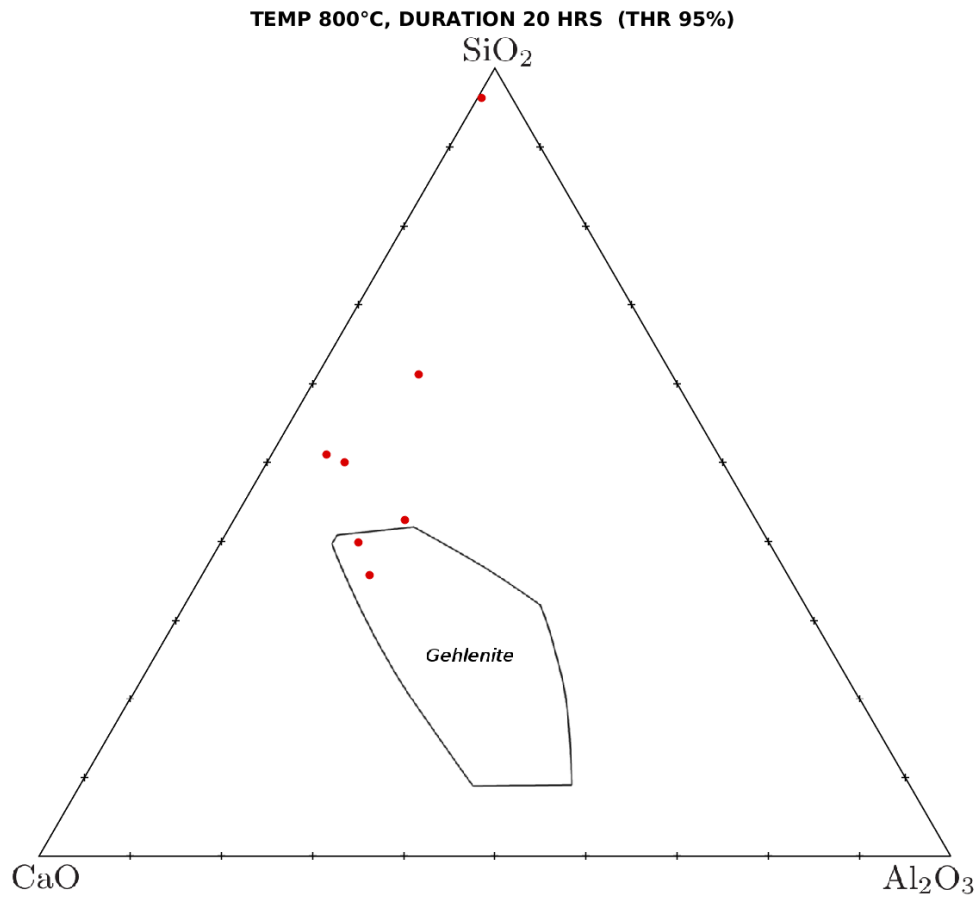


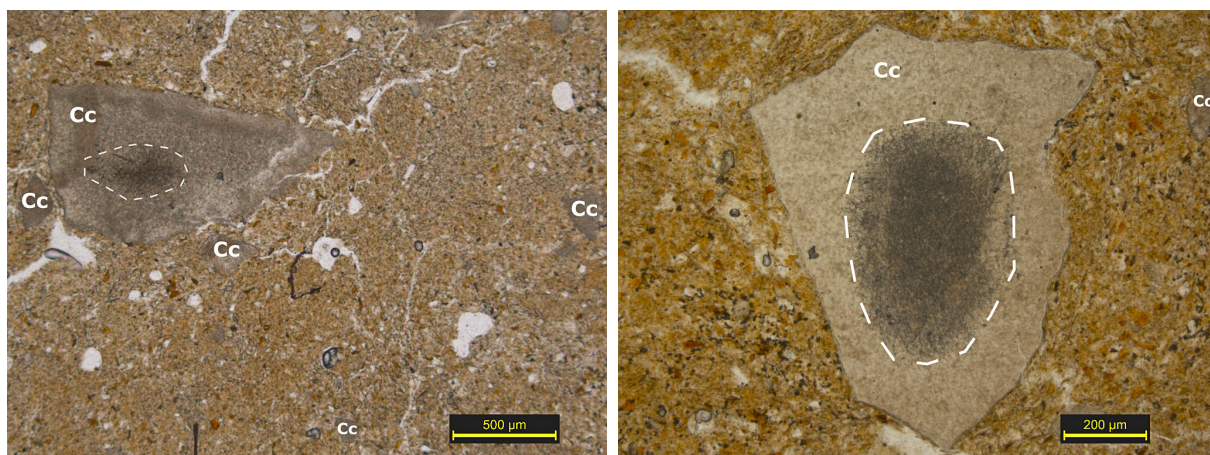
Figure 5.28: Ternary diagram with point analyses from the reaction rims that have a total higher than 95 % at 800° C and a soaking time of 20 h, for the first time, two points plot in the gehlenite stability field

5.1.7 25 hours soaking time

OM shows a fine-grained paste free of phenocrysts for the sample fired for 25 hours at 800°C; Fig. 5.29(a). The calcite grains visible with OM appear to be breaking up in the middle while retaining their grain boundaries. Reaction rims cannot be seen with; Fig. 5.29(b). Upon further investigation with BSE images, calcite grains look more "healthy" than expected after analysis of the sample fired for 20 h, even though some of the big calcites show signs of breakdown in the middle; Fig. 5.31(b). Calcites without thermal breakdown in their center often display surface changes that seem appear before breakdown. Most calcite grains have reaction rims, that reach up to 7 µm in diameter (Fig. 5.31(c)). The cracks, progressing from the calcite grains into the paste seem to be the reason for the distance of reaction rims to their respective grains, instead of shrinking of the grain; see Fig. 5.31(d).

XRD analysis comparing the two diagrams of the sample containing Ca and the one without Ca does not detect gehlenite, or any other phase breakdown or formation; Fig. 5.30.

Microprobe point analysis within the calcite grains finds no trend in the distribution of CaO throughout the grain. Point analyses in the reaction rims were still difficult, often resulting in a total much below 100 wt%. Analyses that exceed the threshold of 95 wt% total (see table 5.5) have been plotted in Fig. 5.32, plotting also in the gehlenite stability field.



(a) Fine-grained clay paste free of phenocrysts surrounding calcite grains (Cc) with signs of breakdown in the middle and no reaction rims (b) Calcite grain (Cc) with distinct grain boundaries and signs of breakdown but no visible reaction rims

Figure 5.29: Paste and calcite grain with no visible reaction rims in the sample fired at 800°C, 25 h

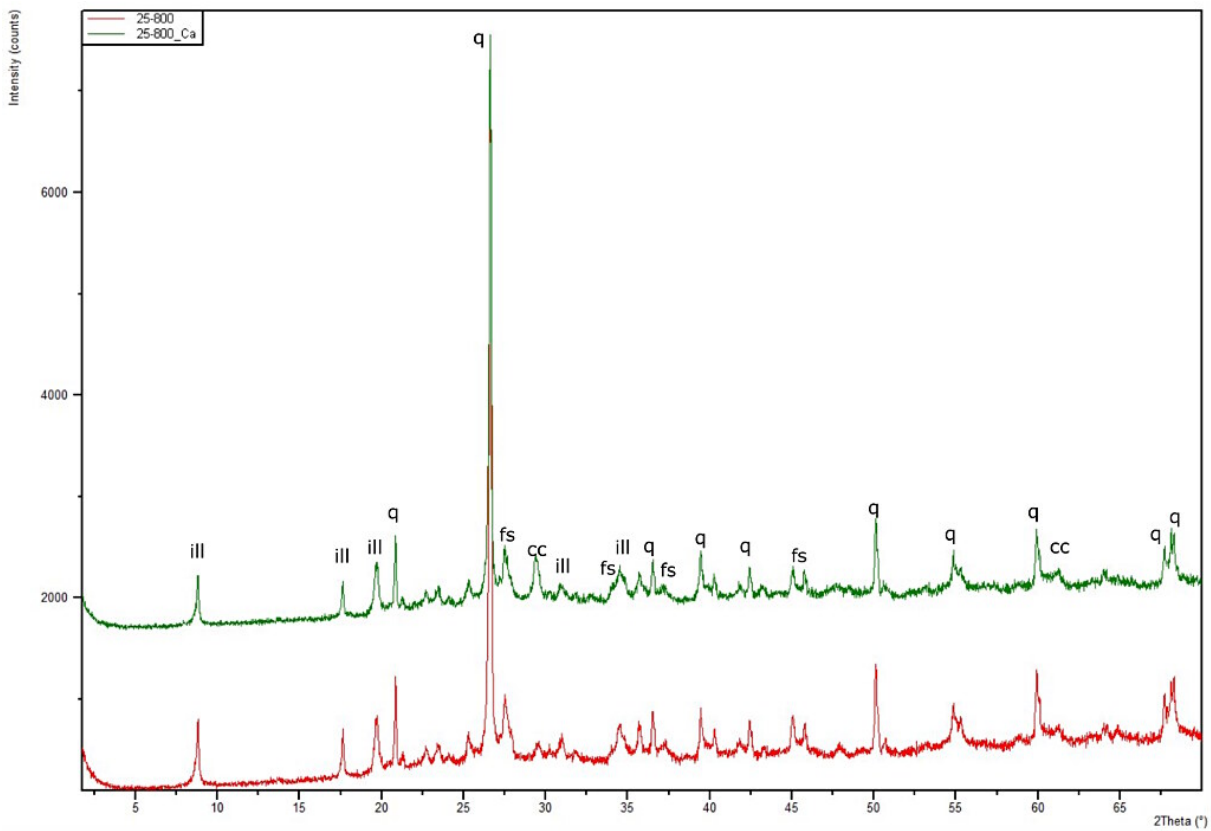
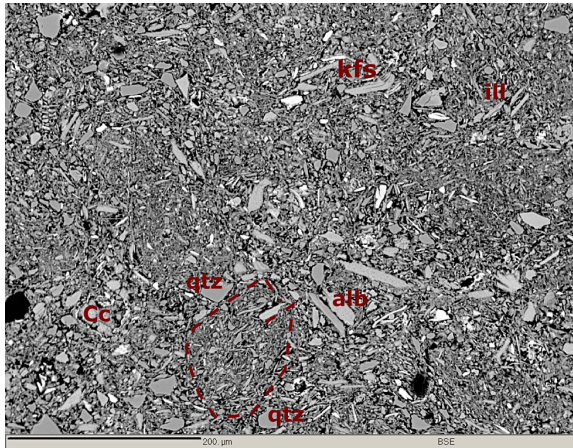


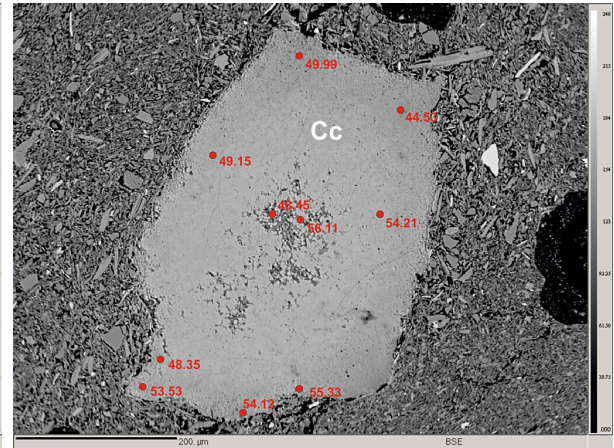
Figure 5.30: Combined XRD-diagrams of specimen soaked for 25 hours at 800°C with CaCO_3 (green) and without CaCO_3 (red); q: quartz, ill: illite, fs: feldspar

Set/Pt	27/1.	28/1.	34/1.	39/1.	43/1.	45/1.	54/1.	61/1.
SiO₂	29.96	38.38	41.17	44.25	53.19	32.56	44.88	29.11
TiO₂	bdl	0.29	bdl	0.06	0.05	0.30	0.28	0.23
Al₂O₃	23.23	23.43	0.09	15.65	15.58	19.09	26.23	15.83
FeO	0.08	2.83	0.06	1.68	0.27	2.26	1.62	2.46
CaO	39.62	28.87	57.01	31.94	26.26	40.14	20.98	47.15
MgO	0.61	1.43	0.11	0.94	0.36	2.18	1.53	1.71
K₂O	3.71	0.92	0.03	1.41	0.19	0.30	2.68	0.41
Na₂O	0.04	0.22	0.04	0.29	0.25	0.09	0.28	0.04
Total	97.25	96.36	98.50	96.22	96.15	96.93	98.47	96.95

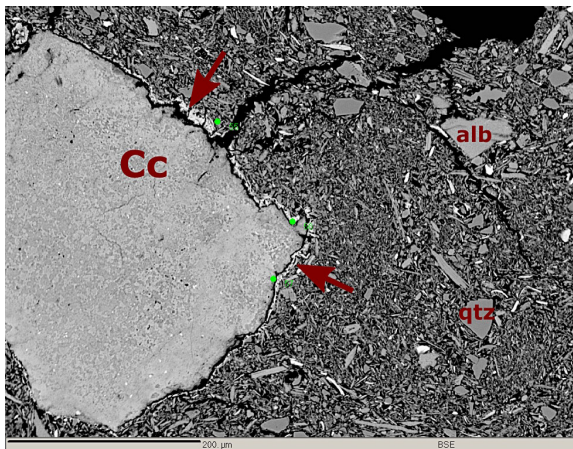
Table 5.5: EPMA raw sample data in wt%, firing temperature 800°C, soaking time 25 hours. (bdl = below detection limit.)



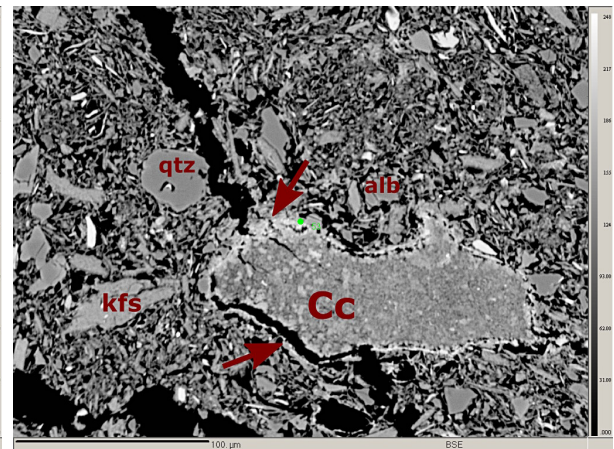
(a) Fine-grained clay paste with discrete mineral angular grains; qtz: quartz, ksp: potassium-feldspar, alb: albite, ill: illite; dashed lines indicate a fine-grained paste free of phenocrysts



(b) Big calcite grain with about 500 μm diameter, with signs of breakdown in the middle; CaO in wt% shows no trend in distribution; numbers indicate EPMA point analyses



(c) Calcite grain (Cc) with surface changes and partial reaction rim (red arrows), the crack moving from the paste to grain gives the impression of shrinking



(d) Small calcite (150 μm diameter) showing surface changes and a pronounced reaction rim (red arrows); the distance of the grain to paste/rim is connected to the cracks through the paste and not a sign of shrinking

Figure 5.31: Paste and different calcite grains with reaction rims; 800 °C, 25 hours

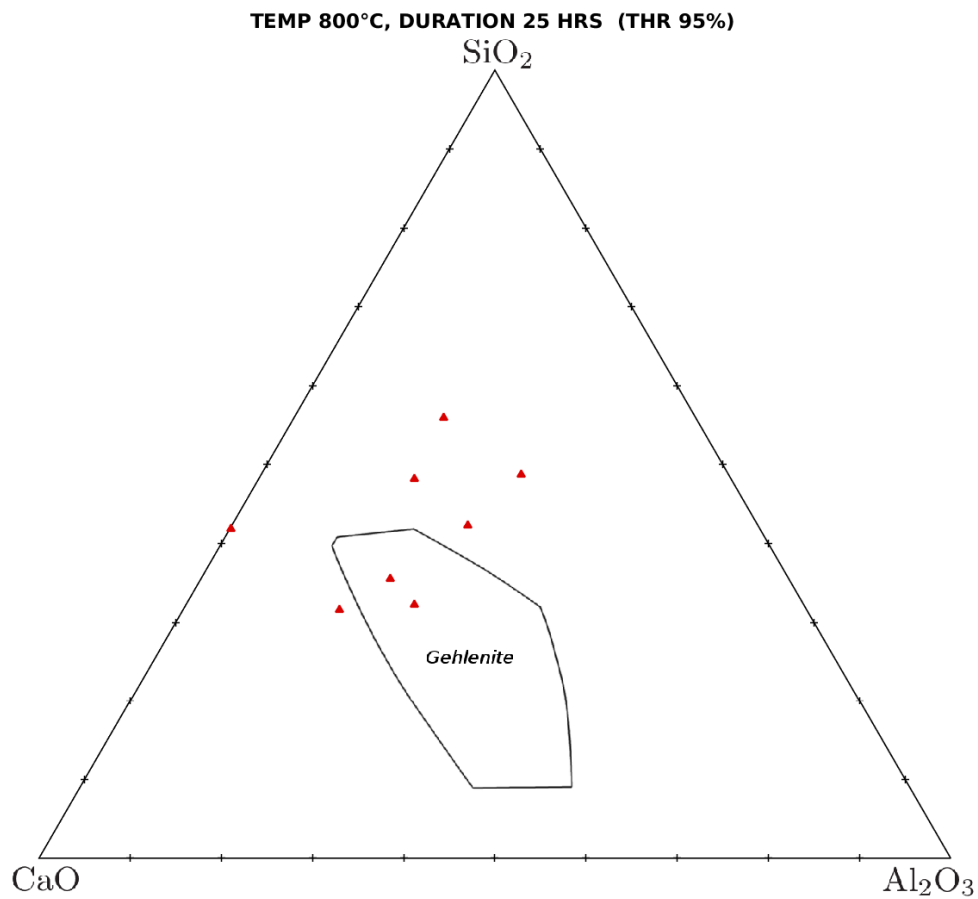


Figure 5.32: Ternary diagram with point analyses from the reaction rims that have a total higher than 95 % at 800° C and a soaking time of 20 h, two point analyses plot in the gehlenite stability field

5.2 900°C

The firing temperature of 900°C was chosen because Heimann and Maggetti (2014) states that "[...] such clays, when fired to 850°C–1050°C contain considerable amounts of gehlenite[...]" . It was therefore assumed, that in samples fired at 900°C enough gehlenite has formed to make it easy detectable. Soaking times for three, five, seven and nine hours were chosen. All thin sections were prepared with water as cooling agent. Samples fired for five and seven hours belong to the first set analyzed. Their analyses therefore include profiles, that were not continued in later samples. Additionally, a line of point analyses was measured in the sample fired for three hours.

The samples containing calcite show a dark ochre color after firing, while the ones without calcite have a visibly lighter ochre appearance and more closely resemble the samples fired at 800°C; Fig. 5.33.

Microtextural analysis with BSE images show no sintering effects on the paste and sharp grain boundaries. Quartz, calcite, plagioclase and illite can be identified by XRD. Point analysis confirms all aforementioned minerals.



(a) Samples fired for 3 hours at peak temperature 900°C



(b) Samples fired for 5 hours at peak temperature 900°C



(c) Samples fired for 7 hours at peak temperature 900°C



(d) Samples fired for 9 hours at peak temperature 900°C

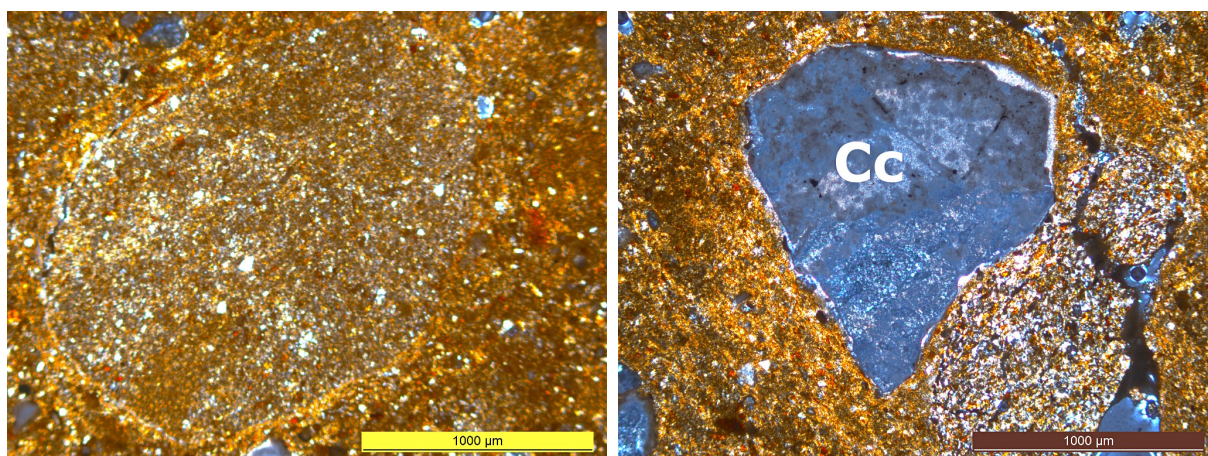
Figure 5.33: Samples fired at 900°C display an ochre color, with the specimen containing no Ca being notably lighter.

5.2.1 3 hours soaking time

First overview of the sample fired for 3 hours at 900°C with OM shows the paste free of phenocrysts other than calcite (Fig. 5.34(a)). Calcite grains show partial breakdown, but no reaction rims, see Fig. 5.34(b). BSE image analysis confirms the calcite breakdown and also detects shrinking of calcite grains and reaction rims, see Fig. 5.37(b). Reaction rims reach up to 5 µm in diameter. Breakdown within calcites starts at one or more points in the grain and progresses to the rim, while maintaining the grain boundaries, see Fig. 5.37(c) and (d). Calcite grains of a max. 50 µm can decompose completely leaving only, as can be seen in Fig. 5.37(a). BSE image analysis of the paste shows all other minerals with distinct grain boundaries as well as areas of compressed phyllosilicates, see Fig. 5.37(a)

XRD analysis comparing the two graphs of the sample containing Ca and the one without Ca does not detect gehlenite, but all peaks reach less counts than XRD analysis of samples fired at 800°C; Fig. 5.35. Especially the calcite peak is effected and hard to distinguish from the interfering illite peak in the sample containing no calcite.

Microprobe point analysis, set in a line from within the grain to the paste (Fig. 5.37(c)), show higher concentrations of CaO within the grain (appr. 60 wt%) than expected in CaCO_3 , indicating the breakdown to pure CaO. Analyses from within reaction rims can range from a gehlenite incipient stage (Fig. 5.37(d)) to crystallized gehlenite; Fig. 5.37(b). All analyses surpassing a total of 95 wt% (see table 5.6) were plotted in Fig. 5.39. Elemental mapping, as can be seen in Fig. 5.38, shows Ca partially extending beyond the grain's boundaries, as well as Si, Al and Fe progressing into the grain but at a slower rate.



(a) Clay paste free of phenocrysts

(b) Calcite grain (Cc, blue) with distinct grain boundaries and signs of breakdown, but no visible reaction rims

Figure 5.34: Paste and calcite grain with no visible reaction rims in the sample fired at 900°C, 3h

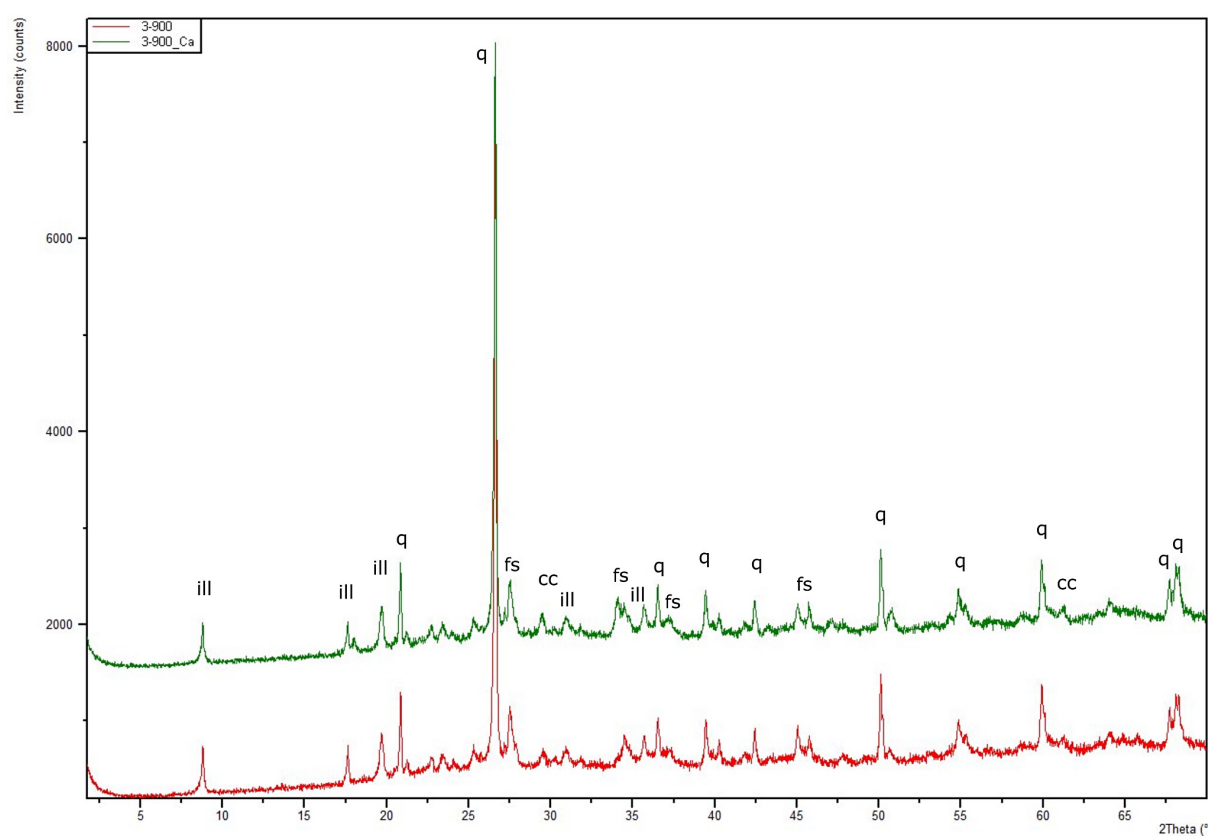


Figure 5.35: Combined XRD-diagrams of specimen soaked for 3 hours at 900°C with CaCO_3 (green) and without CaCO_3 (red); q: quartz, ill: illite, fs: feldspar

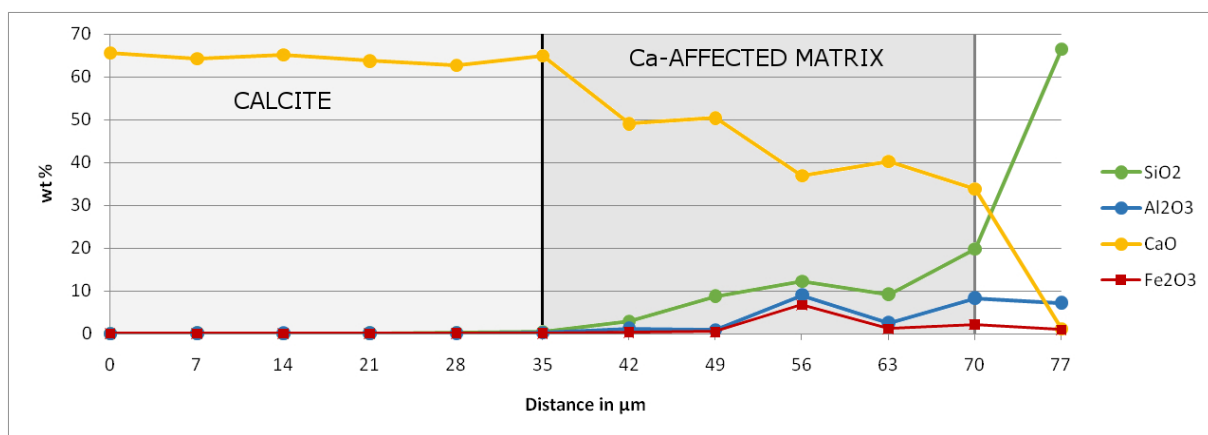
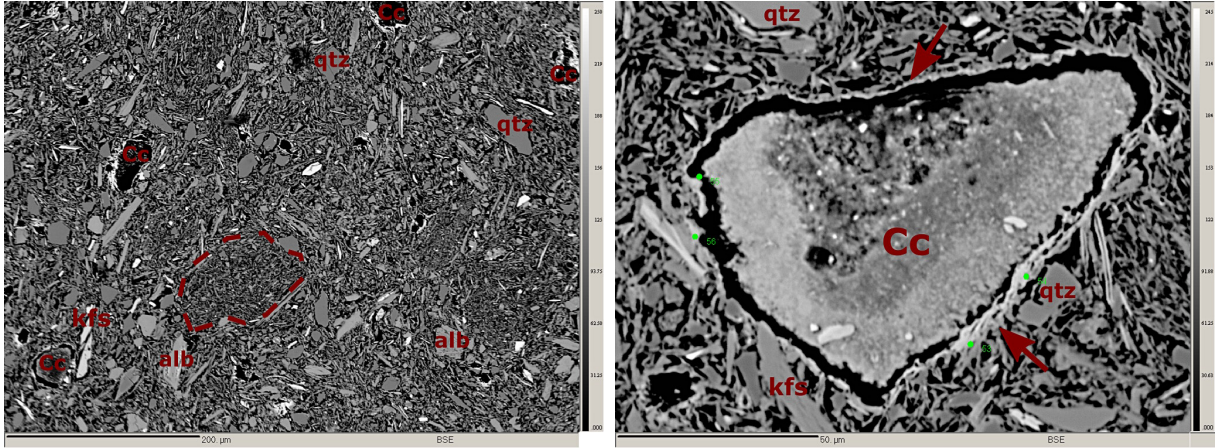
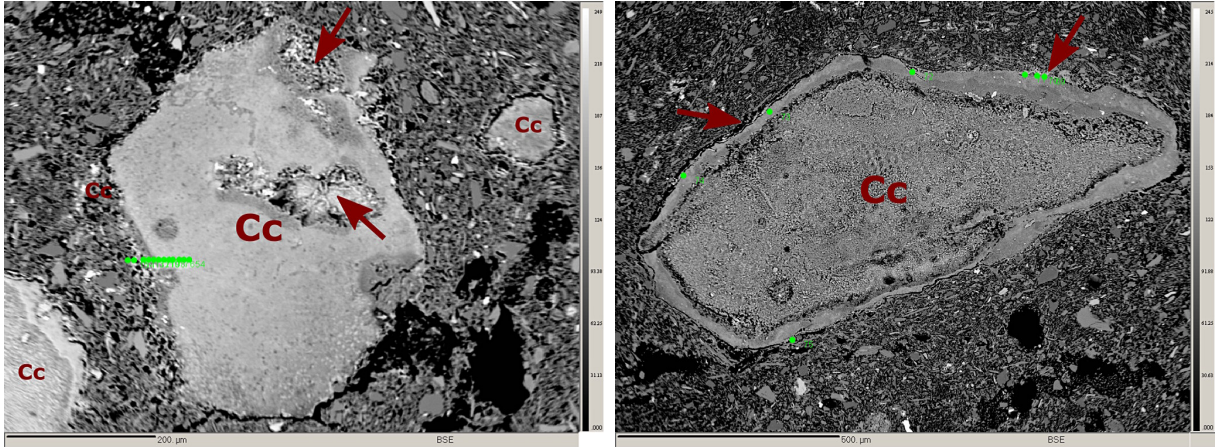


Figure 5.36: 15 point analyses set in a line from within the calcite grain into the paste; Fig. 5.37(c). The distribution of Ca in the grain remains stable; Ca diffuses appr. 35 μm into the paste. As can be seen in Fig. 5.37(c), while the paste is affected, there is no reaction rim yet; Si, Al and Fe move in direction to the calcite grain



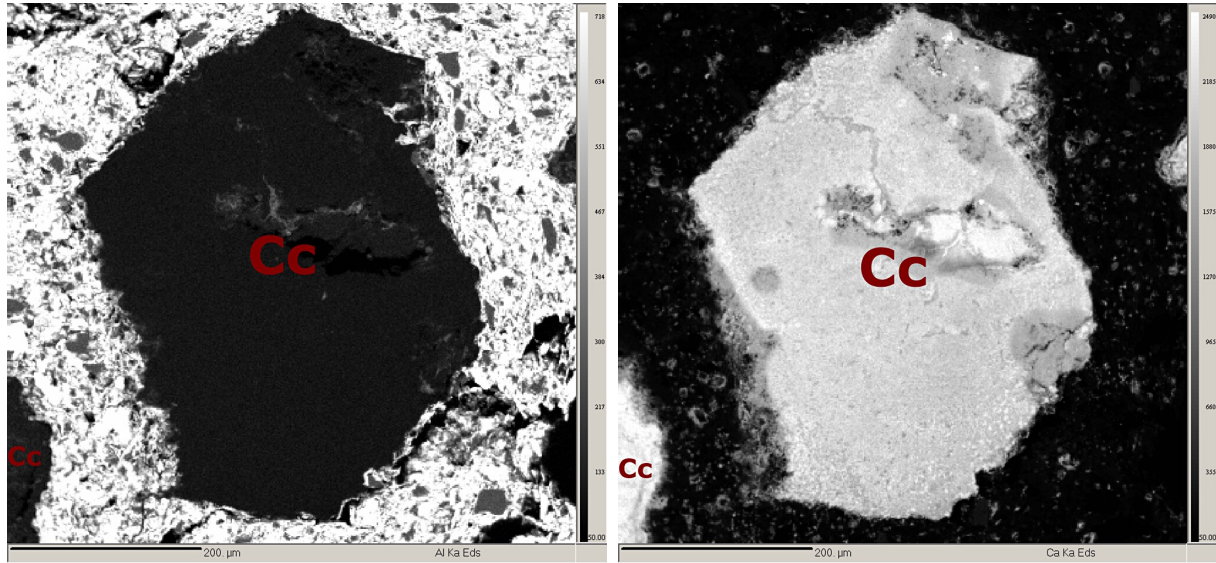
(a) Fine-grained paste with visible coarser angular and elongated mineral grains; qtz: quartz, kfs: potassium-feldspar, alb: albite, ill: illite, cc: calcite; dashed lines indicates fine-grained paste free of phenocrysts



(c) Calcite grain with breakdown (red arrows) starting in several places and Ca diffusing into the paste; points analyzed (green dots) in a line going from the calcite grain into the paste (Fig. 5.36); elemental mapping can be seen in Fig. 5.38

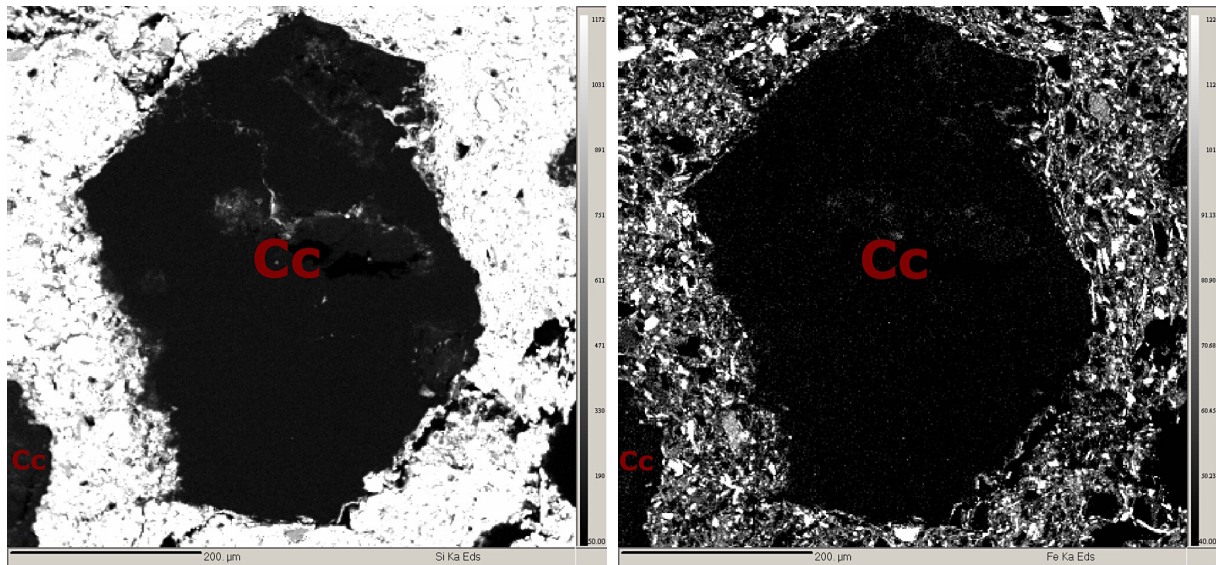
(d) Calcite (Cc) breaking down in the middle, leaving only the boundaries intact; narrow reaction rims indicated by red arrows

Figure 5.37: Paste and different calcite grains: breakdown, with reaction rims and signs of shrinking; 900°C, 3 hours



(a) Elemental mapping for Al; Al starts diffusing into the calcite grain around its boundaries (lower right corner of the calcite grain), but is mostly concentrated in the paste

(b) Elemental mapping for Ca; Ca diffuses into the paste for appr. 35 µm (Fig. 5.36); inhomogeneous Ca distribution, Ca is concentrated in areas, where the calcite starts to breakdown



(c) Elemental mapping for Si; Si diffuses towards the calcite grain's boundaries faster than Al and Fe

(d) Elemental mapping for Fe; paste containing high amount of Fe, indicating the presence of Fe-oxides, Fe does not diffuse into the calcite grain

Figure 5.38: Elemental mapping of a calcite grain with a reaction rim (Fig. 5.37(c)). The corresponding profile, Fig. 5.36, Ca moves at a faster rate into the paste than Al, Si and Fe into the grain

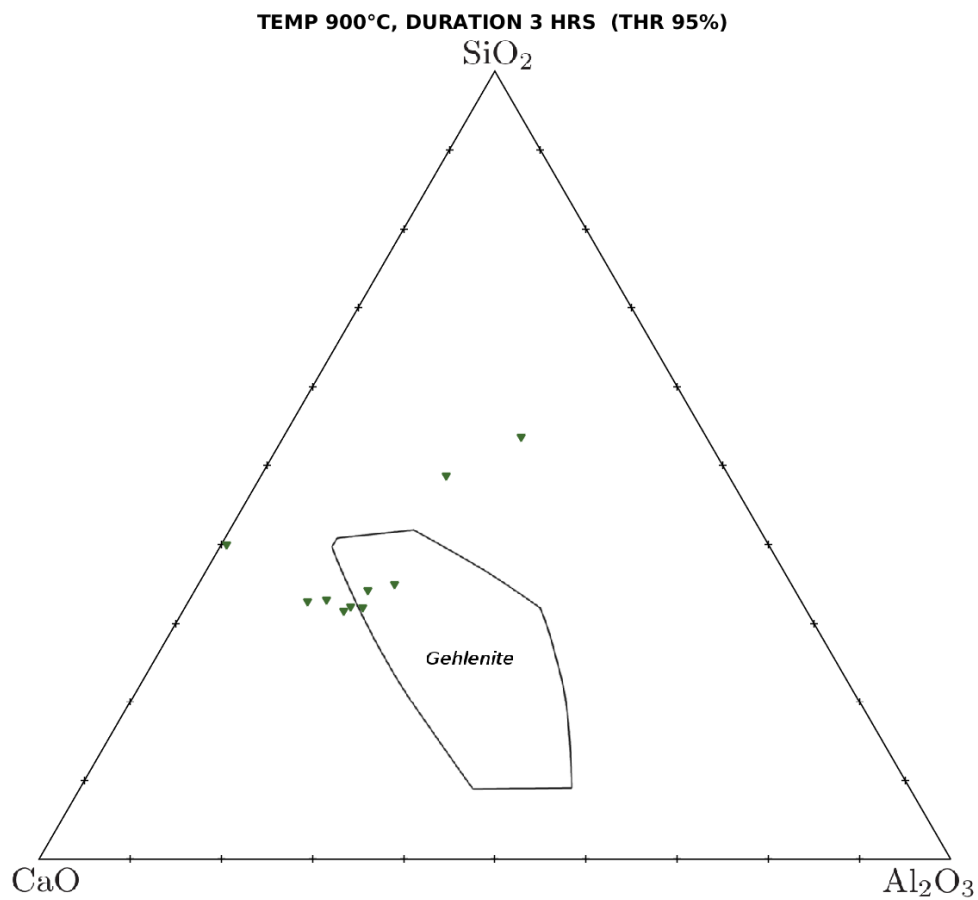


Figure 5.39: Ternary diagram with point analyses from the reaction rims that have a total higher than 95 % at 900° C and a soaking time of 3 h; three of which plot in the gehlenite stability field

Set/Pt	54/1.	60/1.	61/1.	62/1.	65/1.	66/1.	67/1.	71/1.	76/1.
SiO ₂	29.82	29.85	28.82	31.15	49.18	44.85	29.27	31.61	33.20
TiO ₂	0.07	0.32	0.07	0.05	0.72	0.21	4.46	0.45	0.31
Al ₂ O ₃	16.76	18.18	16.14	12.40	23.91	18.76	13.30	17.53	20.41
FeO	1.67	2.04	1.73	1.02	2.26	3.55	1.70	2.37	1.83
CaO	46.09	45.26	46.44	51.42	18.61	28.52	46.05	43.27	41.20
MgO	1.12	1.31	1.95	1.20	2.22	2.17	1.33	2.08	1.53
K ₂ O	0.13	0.23	0.24	0.41	0.80	0.43	0.50	0.30	0.28
Na ₂ O	bdl	0.02	0.06	bdl	1.18	0.55	0.16	bdl	0.03
Total	95.66	97.22	95.45	97.65	98.87	99.06	96.78	97.62	98.79

Table 5.6: EPMA raw sample data in wt%, firing temperature 900°C, soaking time 3 hours. (bdl = below detection limit.)

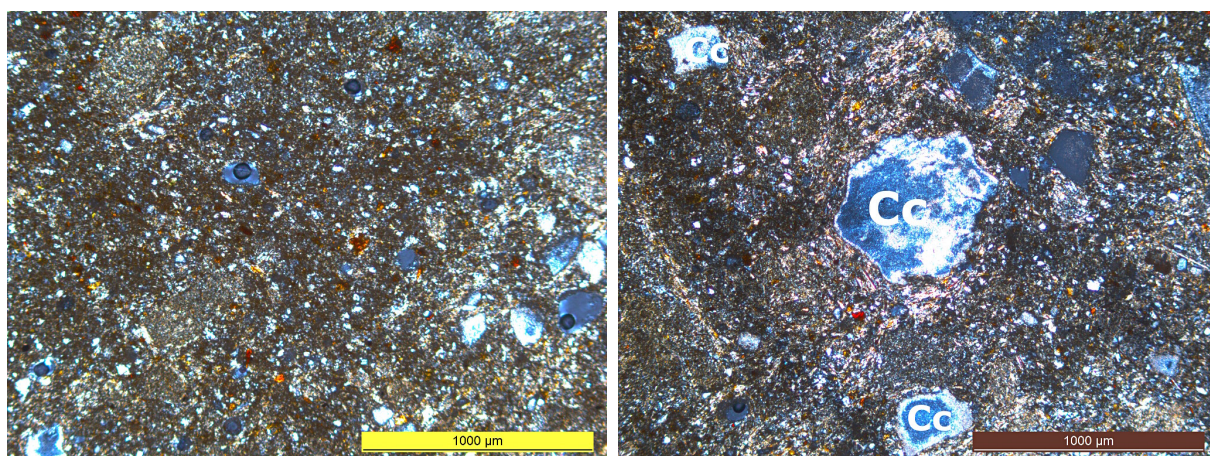
5.2.2 5 hours soaking time

The specimen soaked for 5 hours at peak temperature was another one of the preliminary samples. EPMA analysis include profiles.

Calcite breakdown is visible by OM, the paste flows around the calcite grains; Fig. 5.40(b). Reaction rims or shrinking cannot be seen by OM. Minerals embedded in the fine-grained clase paste are quartz phenocrysts, see Fig. 5.40(b). Reaction rims of up to 10 μm can only be seen in BSE images and are found around calcites of all grain sizes. Calcites shrinking is also evident in many grains, independent of the grain size, even though some small grains have decomposed completely, leaving only the reaction rim; Fig. 5.42(b) – (d). Calcite breakdown is irregular, having some calcites almost completely decomposed (Fig. 5.42(b)), while others seem almost unaffected, see Fig. 5.42(c), and every state in between (Fig. 5.42(d).)

XRD diagram comparison shows no mineral breakdown or formation. Gehlenite was not detected, the calcite peak presents the main difference between the sample containing calcite and the one without; Fig. 5.41.

EPMA profiles cross from the rim into the paste (Fig. 5.42(b)). The results show an incipient gehlenite crystallization state to rapidly decreasing CaO the further the analysis progresses into the paste. Point analyses within calcite grains, even if they are not decomposed, show a high concentration of CaO, especially in the middle of the grain with a decreasing trend to the rim. All point analyses surpassing a total of 95 wt% are plotted in the $\text{CaO} - \text{SiO}_2 - \text{Al}_2\text{O}_3$ phase diagram; Fig. 5.44. All corresponding analyses are listed in table 5.7. Very few analyses cross this threshold, none of which plot in the gehlenite stability field.



(a) Fine-grained clay paste surrounding calcite grains (b) Calcite grain (Cc, blue) with distinct grain boundaries and signs of breakdown but no visible reaction rims (white)

Figure 5.40: Paste and calcite grain with no visible reaction rims in the sample fired at 900°C, 5 h

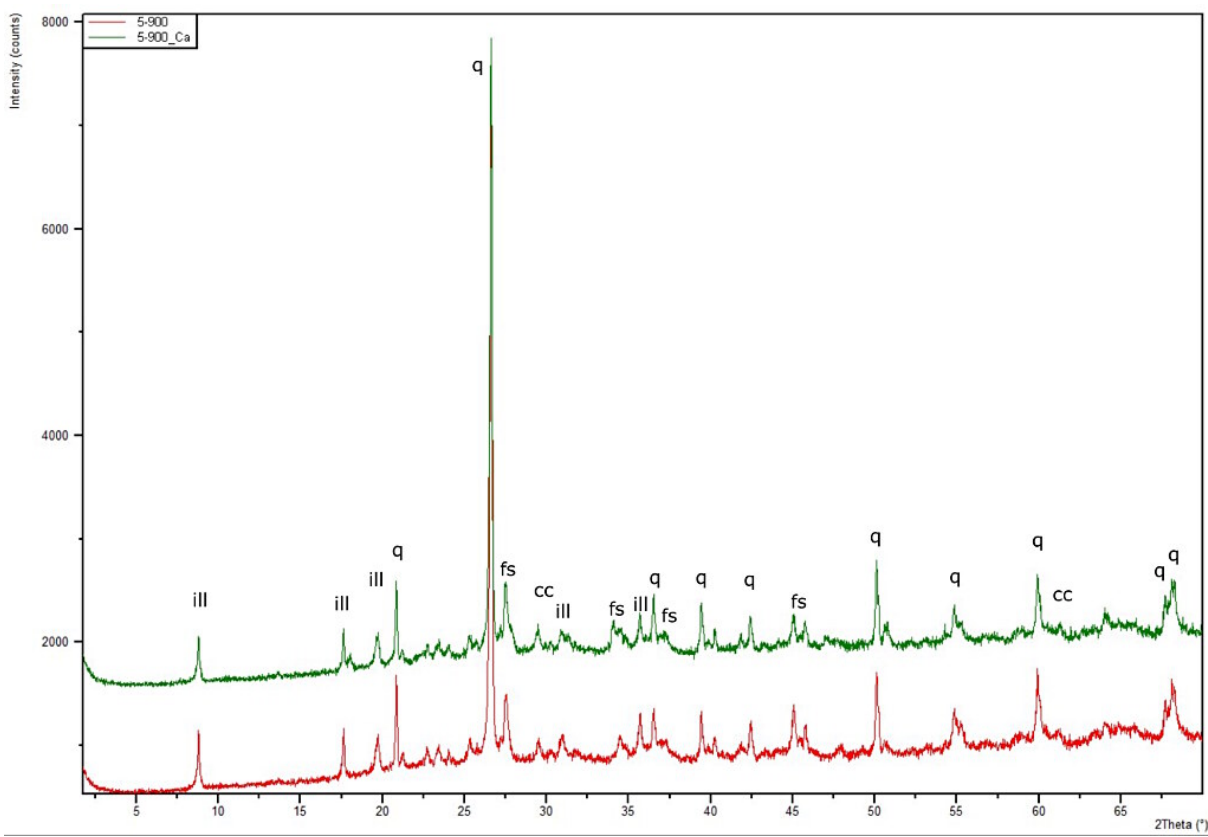
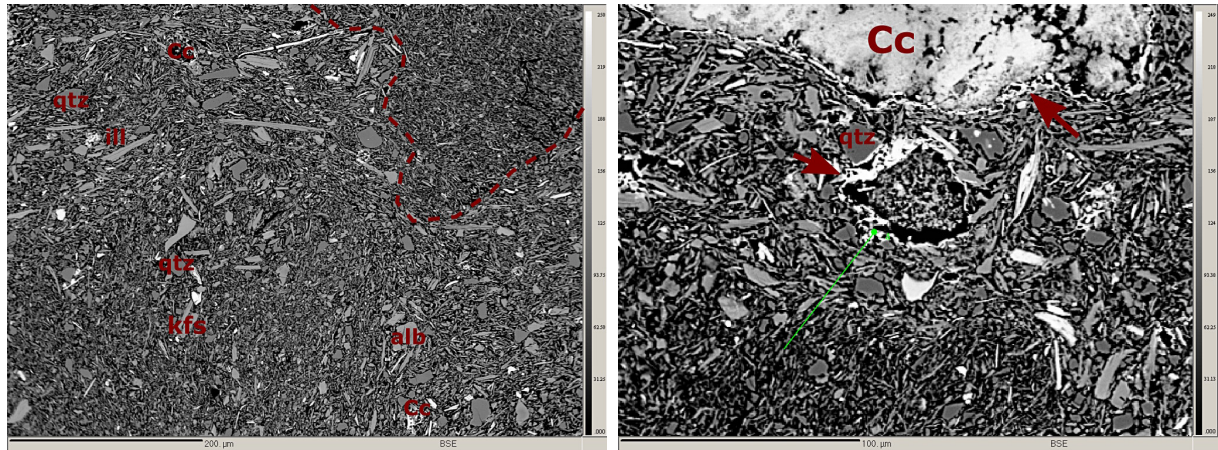


Figure 5.41: Combined XRD-diagrams of specimen soaked for 5 hours at 900°C with CaCO_3 (green) and without CaCO_3 (red); q: quartz, ill: illite, fs: feldspar

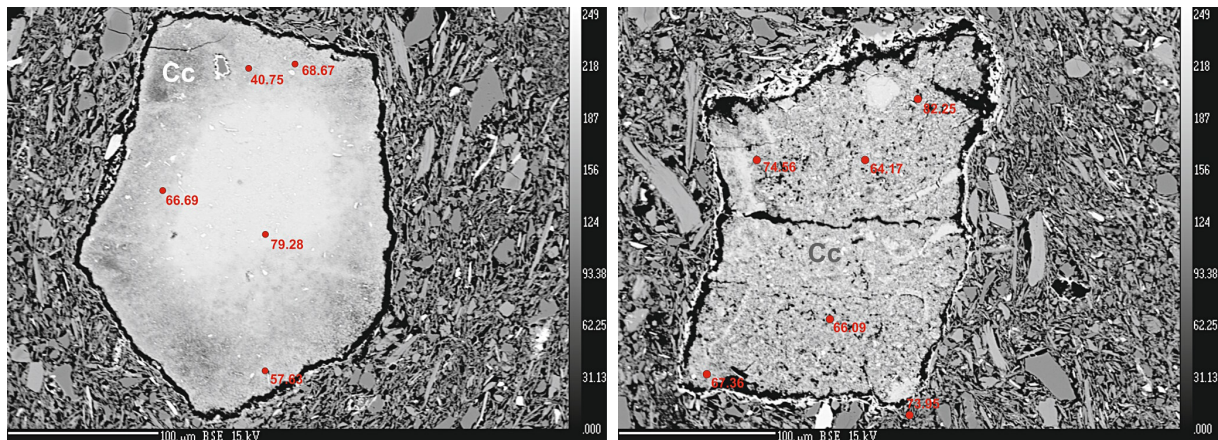
Set/Pt	2/33.	2/35.	2/51.	2/59.	4/3.
SiO₂	62.47	94.49	99.17	54.10	48.12
TiO₂	0.23	0.04	0.04	0.11	0.13
Al₂O₃	26.71	2.01	0.77	31.34	13.84
FeO	1.69	0.20	0.10	2.64	0.55
CaO	0.89	0.07	0.05	1.06	31.74
MgO	1.12	0.20	0.06	3.16	0.41
MnO	bdl	bdl	bdl	0.04	bdl
K₂O	3.30	0.28	0.09	5.14	0.45
Na₂O	1.11	0.08	0.03	1.12	0.34
Total	97.52	97.36	100.31	98.73	95.57

Table 5.7: EPMA raw sample data in wt%, firing temperature 900°C, soaking time 5 hours. (bdl = below detection limit.)



(a) Fine-grained paste with no visible sintering and discrete angular and elongated minerals; qtz: quartz, kfs: potassium-feldspar, alb: albite, ill: illite, cc: calcite; dashed lines indicates a fine-grained paste free of phenocrysts

(b) Small calcite grain almost completely decomposed with explicit reaction rim (ref arrow). The bigger grain above the small grain displays surface changes and also has a reaction rim (red arrow) which is much narrower than the one of the smaller grain; the green line represents the EPMA profile from the reaction rim into the Ca-affected paste



(c) Seemingly "healthy" calcite grain (Cc) with signs of shrinking and narrow reaction rim; CaO distribution in wt% shows a high amount of CaO in the middle of the grain and an uneven distribution closer to the grains boundary; numbers indicate EPMA point analyses

(d) Calcite grain (Cc), partially breaking down with signs of shrinking and considerable reaction rim; inhomogeneous CaO distribution (in wt%), numbers indicate EPMA point analyses

Figure 5.42: Paste and different calcite grains with reaction rims of varying diameter; 900°C, 5 hours

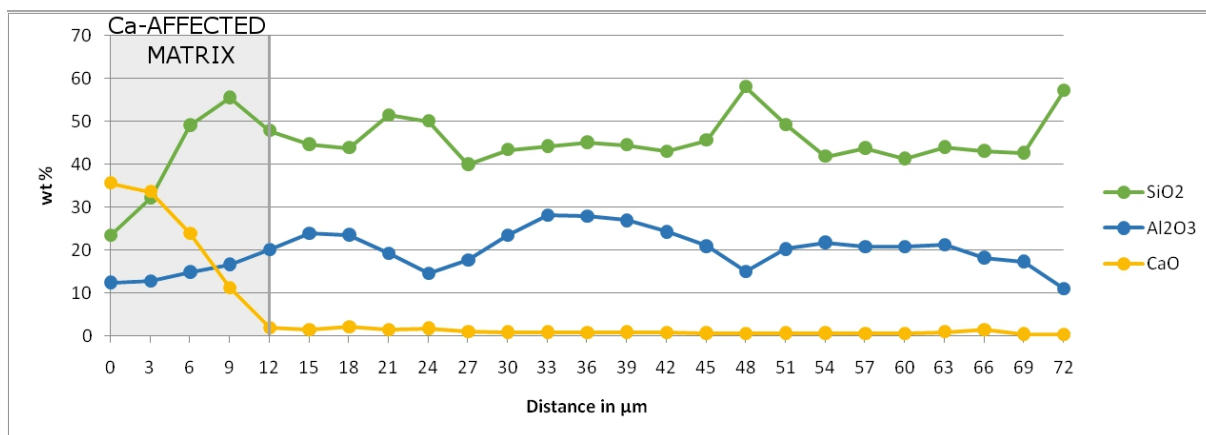


Figure 5.43: EPMA profile from the reaction rim into the paste, Fig. 5.42(b); Ca diffuses appr. 12 μm into the paste; gehlenite was not detected

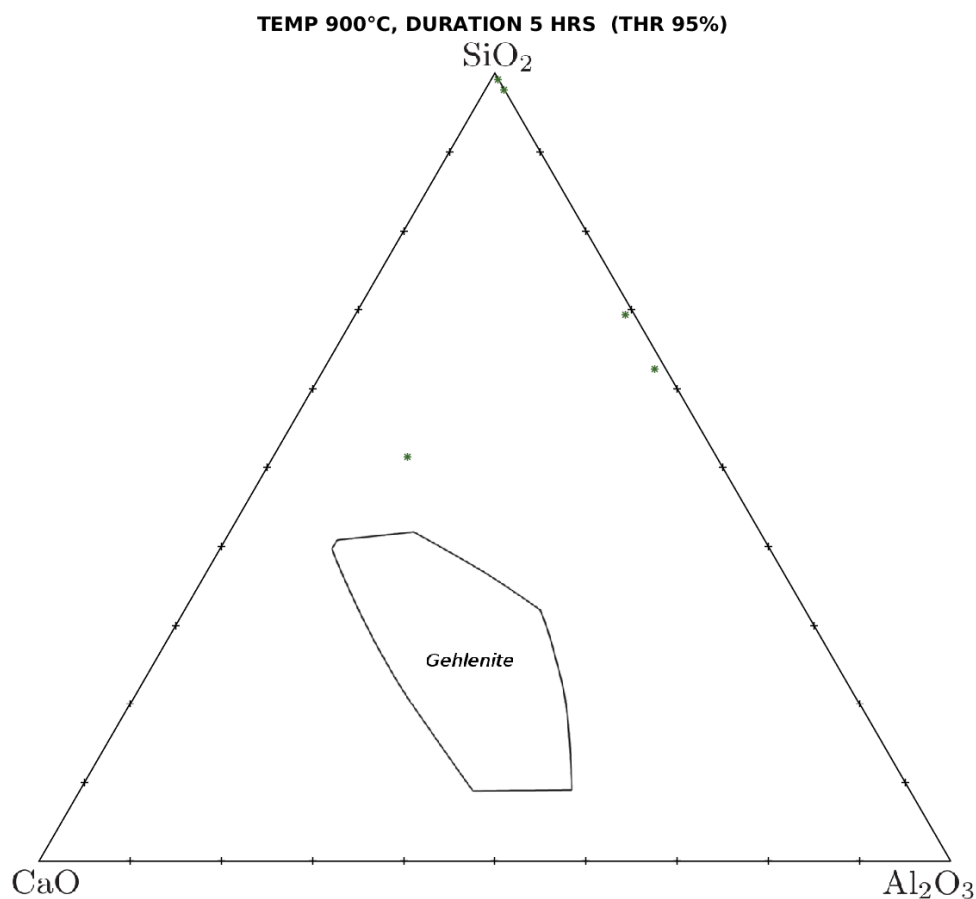


Figure 5.44: Ternary diagram with point analyses from the reaction rims that have a total higher than 95 % at 900°C and a soaking time of 5 h. None of the few analyses passing this threshold plots in the gehlenite stability field

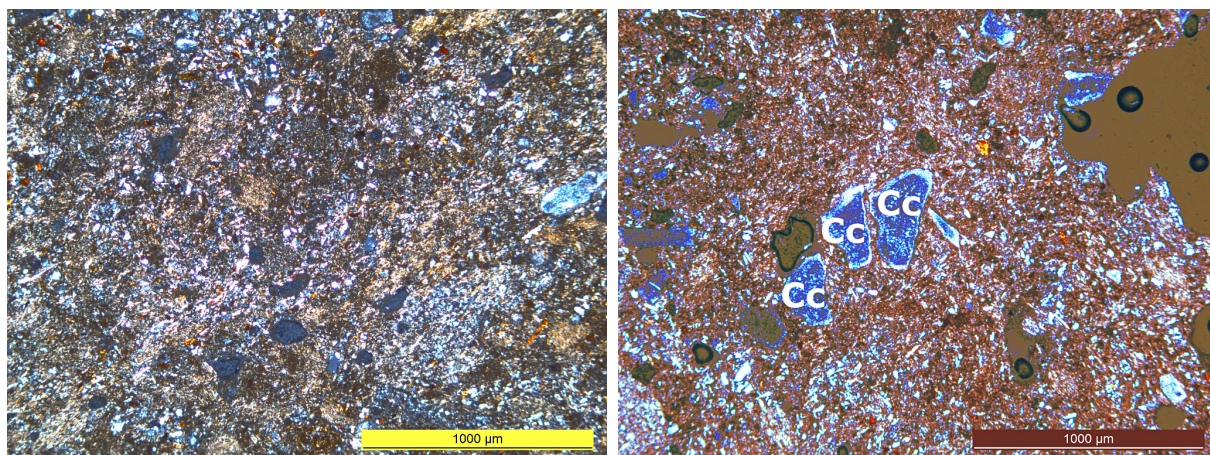
5.2.3 7 hours soaking time

This is the last sample of the first sample set analyzed. The analyses again include microprobe profiles.

OM shows a finely grained paste free of phenocrysts, see Fig. 5.45(a). Calcite grains show signs of breakdown, but no reaction rims can be seen; Fig. 5.45(b). BSE image analysis show the beginning of sintering in the paste. All phenocrysts embedded in the paste still have pronounced grain boundaries; see Fig. 5.48(a). Reaction rims reach up to 15 μm , but can still only be seen with BSE images. Shrinking can be observed in some calcites, independent of the grain size, but it is not constant during the sample. Some calcites appear "healthy" with very narrow reaction rims and no signs of shrinking or breakdown, as can be seen in Fig. 5.48(c) and (d), where all stages of calcite breakdown and/or shrinking are present. Reaction rims tend to grow irregularly around the grains, with one side of the grain showing no rim at all while on the other side the rim is more pronounced; Fig. 5.48(b).

The XRD analysis does not reflect the beginning sintering of the paste yet, neither mineral formation nor breakdown can be observed. The distinct calcite peak remains the most important difference between the graph of the sample containing calcite and the one containing no calcite as gehlenite was not detected; Fig. 5.46.

Microprobe point analyses have been plotted in the ternary plot in Fig. 5.50, some of which are plotting into the gehlenite stability field, see corresponding point analyses in table 5.8. Profiles started in the reaction rim and went into the paste (Fig. 5.48(b)). Incipient gehlenite crystallization stages could be detected. Better results could be obtained by measuring directly into the rim with point analyses; compare Fig. 5.48(b) and (d). Elemental mapping on a calcite grain with signs of shrinking and breakdown as well as a reaction rim show the progression of Ca into the rim and the distinct fissure between rim and grain. Al and Si move into the grain boundaries, therefore the former grain boundaries cannot be identified anymore (Fig. 5.49).



(a) Heterogen fine-grained clay paste free of phenocrysts (b) Calcite grain (Cc, blue) with distinct grain boundaries, no visible reaction rims, the paste flows around the grains

Figure 5.45: Paste and calcite grain with no visible reaction rims in the sample fired at 900°C, 7h

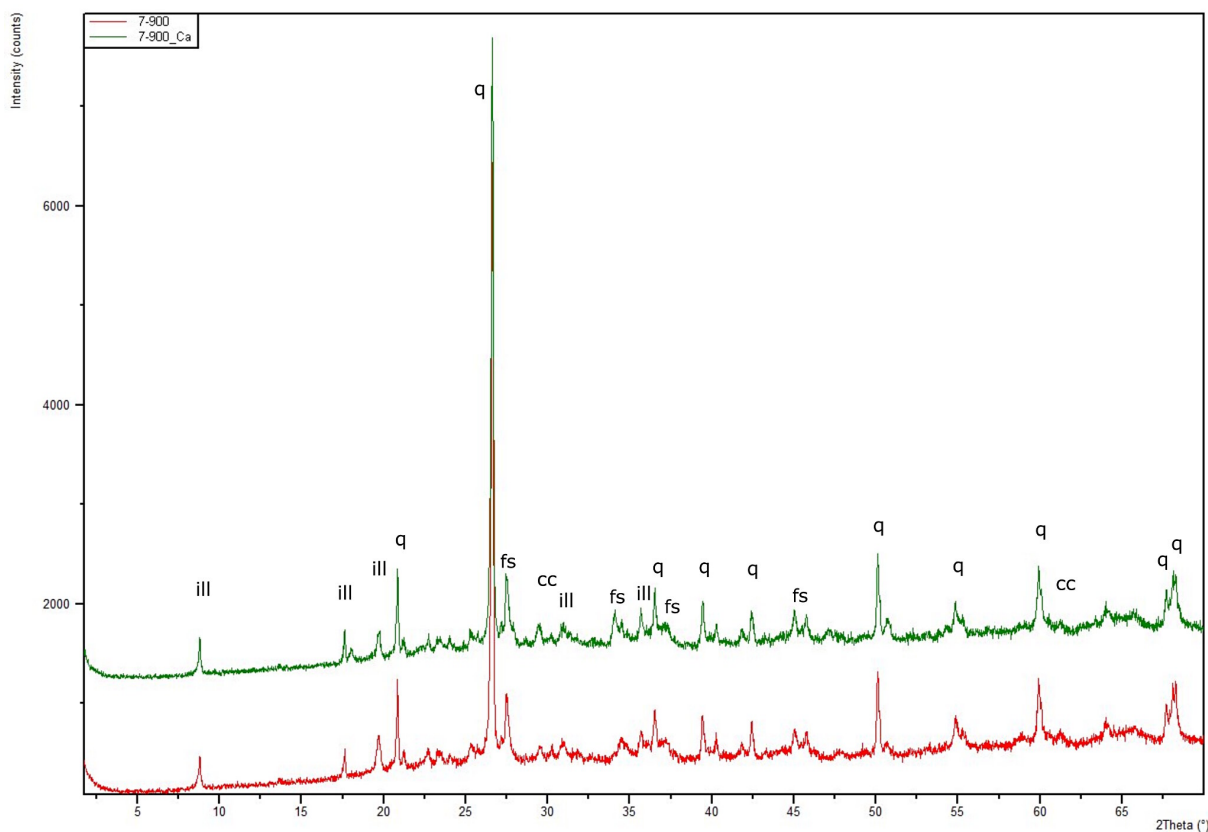


Figure 5.46: Combined XRD-diagrams of specimen soaked for 7 hours at 900°C with CaCO_3 (green) and without CaCO_3 (red); q: quartz, ill: illite, fs: feldspar

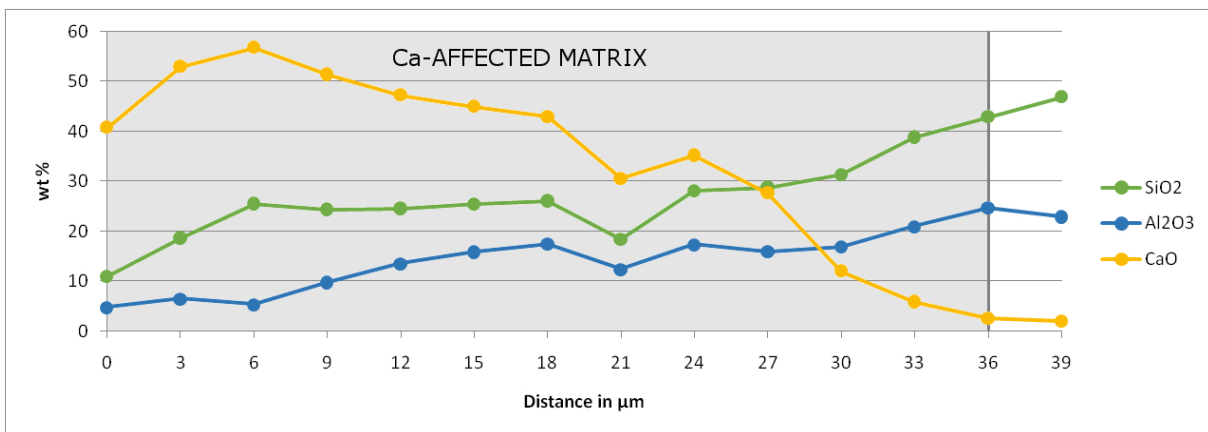
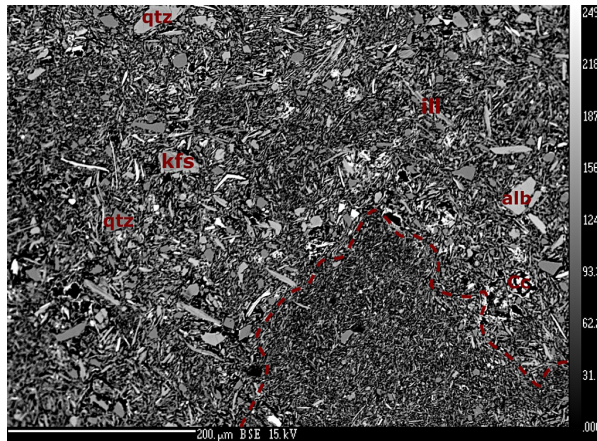
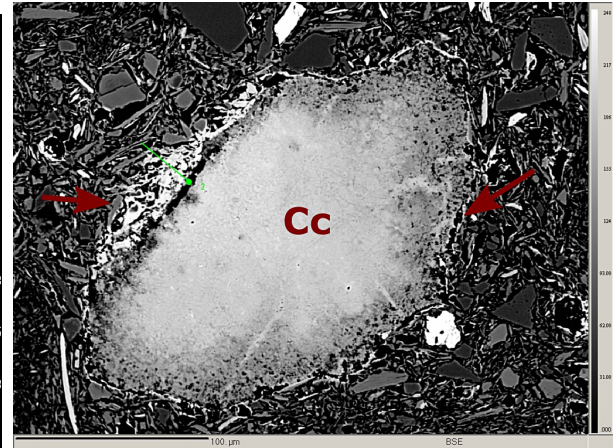


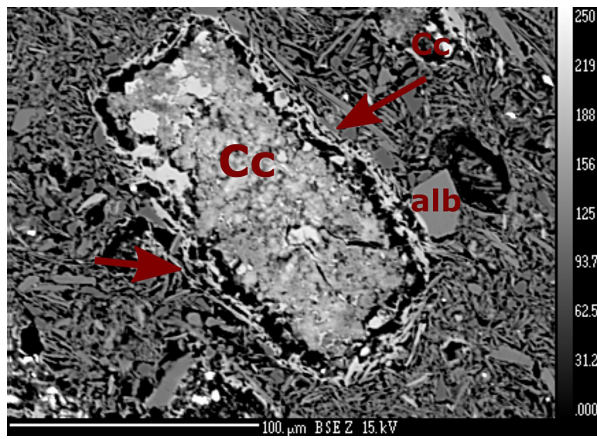
Figure 5.47: EPMA profile going from the calcite grain into the paste, see green line in Fig. 5.48(b). The distribution of Ca in the grain remains stable; Ca diffuses appr. 35 µm into the paste. As can be seen in Fig. 5.48(b), while the paste is affected, there is no reaction rim yet; Si, Al and Fe move in direction of the calcite grain at the same speed



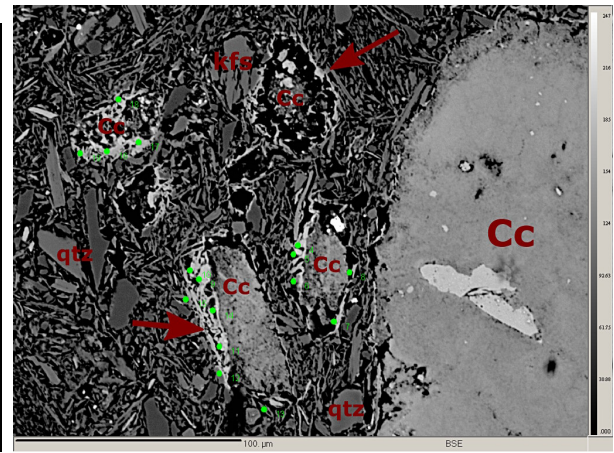
(a) Paste with partially defined mineral grain boundaries and beginning of sintering; qtz: quartz, ksp: potassium-feldspar, alb: albite, ill: illite, cc: calcite; dashed lines indicates a fine-grained clay paste free of phenocrysts



(b) Calcite grain (Cc) with irregular reaction rim (red arrows), profile (green line) crossing from the grain through the rim into the paste; Fig. 5.47

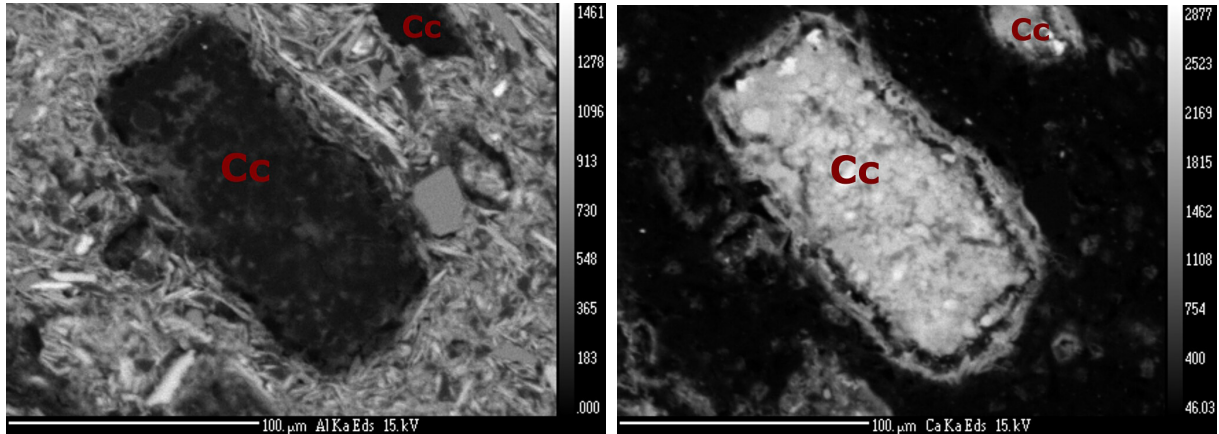


(c) Calcite grain (Cc) with signs of breakdown, shrinking and a uniformly reaction rim (indicated by the red arrows); elemental mapping see Fig. 5.49



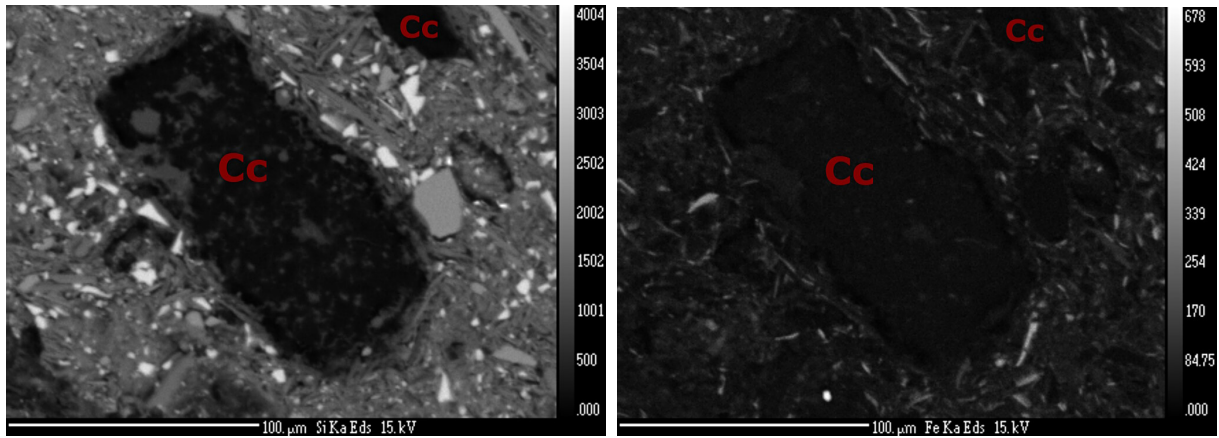
(d) Different calcite grains (Cc) showing various stages of breakdown and reaction rim formation (red arrows); the smaller grains are mostly decomposing, while the big calcite grain appears "healthy"

Figure 5.48: Paste and different calcite grain; 900°C, 7 hours



(a) Elemental mapping for Al; Al is mostly distributed, but diffuses also into the reaction rim

(b) Elemental mapping for Ca; both the reaction rim and calcite shrinking can be clearly seen; in the upper right corner, a second, smaller calcite grain without reaction rim can be seen



(c) Elemental mapping for Si; Si is mostly confined to the paste and the quartz phenocrysts, but can also be seen to accumulate in the rim; quartz (lighter areas) shows presents small grained, angular minerals

(d) Elemental mapping for Fe; Fe content in the paste is very low, very few areas indicate the presence of Fe-oxides

Figure 5.49: Elemental mapping of a calcite grain (Cc) with a reaction rim (Fig. 5.48(c))

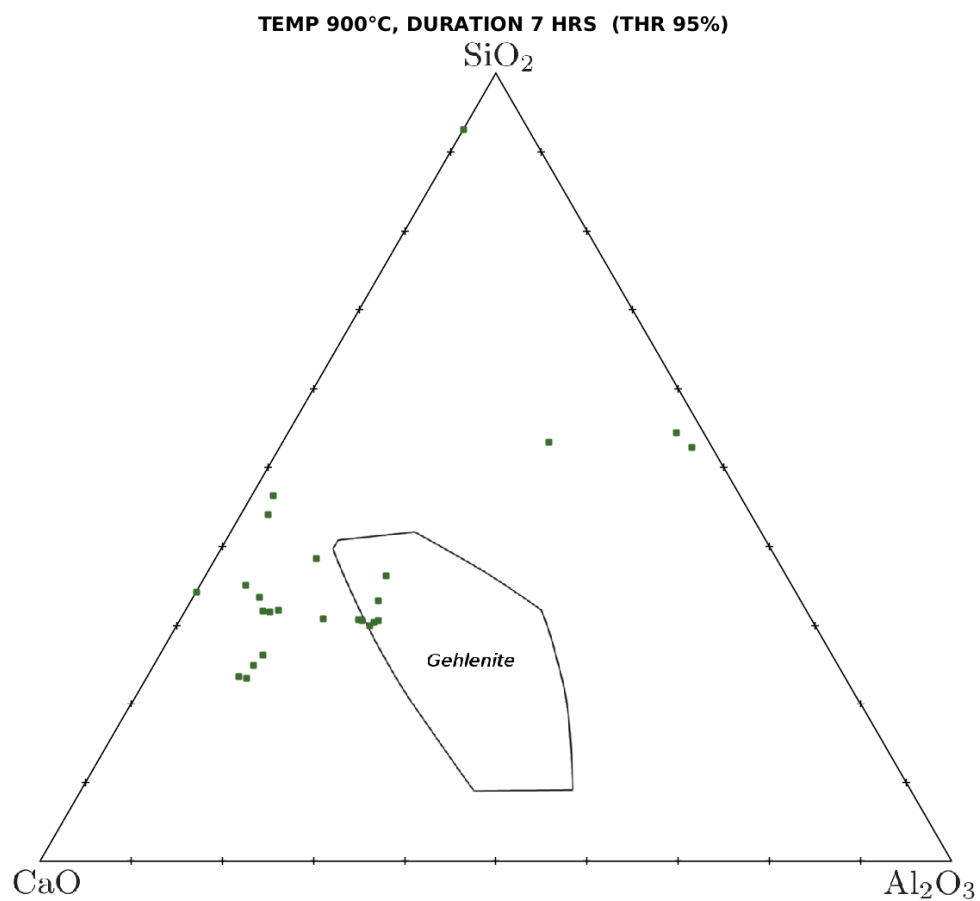


Figure 5.50: Ternary diagram with point analyses from the reaction rims that have a total higher than 95 % at 900°C and a soaking time of 7h; five rim analyses analyses plot into the gehlenite stability field

Set/Pt	3/1.	5/1.	6/1.	7/1.	8/1.	9/1.	10/1.	12/1.	13/1.	15/1.
SiO₂	35.83	31.05	41.68	29.56	34.23	24.94	28.88	33.43	28.90	28.91
TiO₂	0.70	bdl	0.13	0.30	0.48	0.15	0.28	0.13	0.07	0.29
Al₂O₃	10.31	9.17	2.88	18.34	18.81	10.83	14.67	4.77	22.60	18.46
FeO	0.50	0.22	1.31	4.42	15.29	1.49	0.97	0.87	27.31	1.91
CaO	47.06	57.91	50.15	41.33	11.34	59.36	50.20	57.10	1.60	46.84
MgO	0.59	0.39	1.10	1.69	19.14	0.31	0.76	0.41	13.73	0.98
MnO	bdl	bdl	bdl	bdl	bdl	bdl	bdl	bdl	bdl	bdl
K₂O	0.21	0.09	0.06	0.15	0.66	0.06	0.13	0.09	1.34	0.20
Na₂O	0.07	bdl	0.02	0.02	0.18	bdl	0.03	0.04	0.51	0.05
Total	95.26	98.84	97.34	95.81	100.13	97.15	95.90	96.83	96.08	97.63

Set/Pt	16/1.	18/1.	19/1.	21/1.	23/1.	27/1.	29/1.	32/1.	33/1.	37/1.
SiO₂	29.17	31.08	33.55	22.00	22.21	30.72	28.62	28.68	30.63	28.19
TiO₂	0.14	0.74	0.80	0.04	0.10	0.07	0.15	0.32	0.04	0.10
Al₂O₃	20.72	6.76	18.36	10.40	9.49	9.80	20.30	18.78	8.24	24.27
FeO	1.55	0.97	1.48	0.51	0.48	0.96	1.21	1.38	0.46	26.97
CaO	45.37	54.81	40.65	62.18	62.75	55.74	46.71	46.27	57.52	1.22
MgO	0.91	0.71	1.01	0.05	0.18	0.69	0.84	1.29	0.56	13.03
MnO	bdl	bdl	bdl	bdl	bdl	bdl	bdl	bdl	bdl	bdl
K₂O	0.34	0.09	0.21	bdl	bdl	0.15	0.62	0.23	0.09	1.61
Na₂O	0.04	bdl	bdl	0.05	0.07	bdl	bdl	0.03	bdl	0.50
Total	98.23	95.17	96.05	95.23	95.27	98.13	98.46	96.97	97.54	95.91

Set/Pt	41/1.	42/1.	22/1.	33/1.
SiO₂	33.60	45.26	93.45	23.33
TiO₂	0.05	0.03	bdl	bdl
Al₂O₃	0.10	2.29	0.03	10.20
FeO	0.11	0.19	0.04	1.71
CaO	64.65	50.01	7.19	60.00
MgO	bdl	0.18	bdl	1.11
MnO	bdl	bdl	bdl	bdl
K₂O	0.05	0.06	0.04	0.10
Na₂O	bdl	bdl	bdl	0.09
Total	98.56	98.02	100.76	96.54

Table 5.8: EPMA raw sample data in wt%, firing temperature 900°C, soaking time 7 hours. (bdl = below detection limit.)

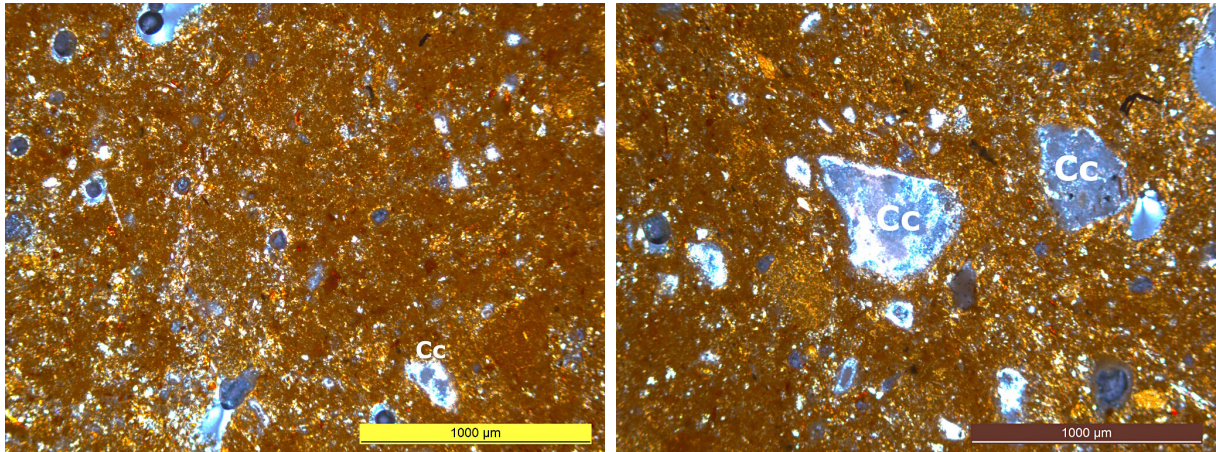
5.2.4 9 hours soaking time

Calcite breakdown can be observed with OM in big calcite grains ($>400\mu\text{m}$), while reaction rims cannot be seen; Fig. 5.51(b). The paste is finely grained, minerals embedded other than calcite into the paste are unidentifiable; Fig. 5.51(a). BSE images show the paste with signs of sintering and all minerals still presenting their well defined grain boundaries; Fig. 5.54(a). Both the breakdown and reaction rims are visible in BSE images, with rim reaching a diameter of max. $7\mu\text{m}$. Calcite breakdown can be found in all forms, ranging from appearing almost healthy to having decomposed completely; Fig. 5.54(b) to (d). Shrinking can particularly be seen in smaller grains of up to $120\mu\text{m}$ diameter, see Fig. 5.54(d).

Comparative XRD analysis of the specimen with and without calcite shows a distinct breakdown

of most phases in the sample with calcite. The calcite peak is nearly gone, as are the feldspar and illite peaks. Phase formation cannot be observed; Fig. 5.52.

Point analyses into reaction rims provided results from incipient gehlenite crystallization stages to phases resembling anorthite. Analyses within calcite grains do not allow the assumption of a general trend. All point analyses surpassing a total of 95 wt% have been plotted in the phase diagram in Fig. 5.53 and listed in table 5.9. Elemental mapping shows the migration of Ca into the paste in the top area of the image, where the most pronounced reaction of this grain can be found. In the bottom left area of the image, Ca can be observed concentrating into the rim. The migration of both Si and Al can also best be seen in the part of the image; Fig. 5.55.



(a) Fine-grained clay paste surrounding calcite grains with no signs of reaction rims

(b) Calcite grain (Cc, blue) with distinct grain boundaries and signs of breakdown but no visible reaction rims

Figure 5.51: Paste and calcite grain with no visible reaction rims in the sample fired at 900°C, 9h

Set/Pt	47/1.	49/1.	50/1.	53/1.	54/1.	70/1.	72/1.	75/1.	80/1.
SiO ₂	35.73	29.08	49.06	31.30	36.06	58.65	30.53	29.93	30.67
TiO ₂	0.08	0.30	0.66	0.68	0.03	bdl	0.30	0.13	0.13
Al ₂ O ₃	5.25	11.72	22.64	19.16	11.21	17.89	16.77	16.46	10.36
FeO	3.00	1.79	3.31	3.56	0.45	0.41	2.61	1.30	1.11
CaO	39.99	51.87	17.51	37.95	42.68	15.47	43.27	49.07	55.38
MgO	12.81	0.71	2.47	2.36	1.02	0.25	1.83	0.88	0.84
K ₂ O	0.13	1.20	1.42	0.25	3.74	1.62	0.11	0.41	0.25
Na ₂ O	bdl	0.11	0.56	bdl	0.03	1.49	0.05	bdl	bdl
Total	96.99	96.78	97.62	95.27	95.22	95.78	95.47	98.18	98.74

Table 5.9: EPMA raw sample data in wt%, firing temperature 900°C, soaking time 9 hours. (bdl = below detection limit.)

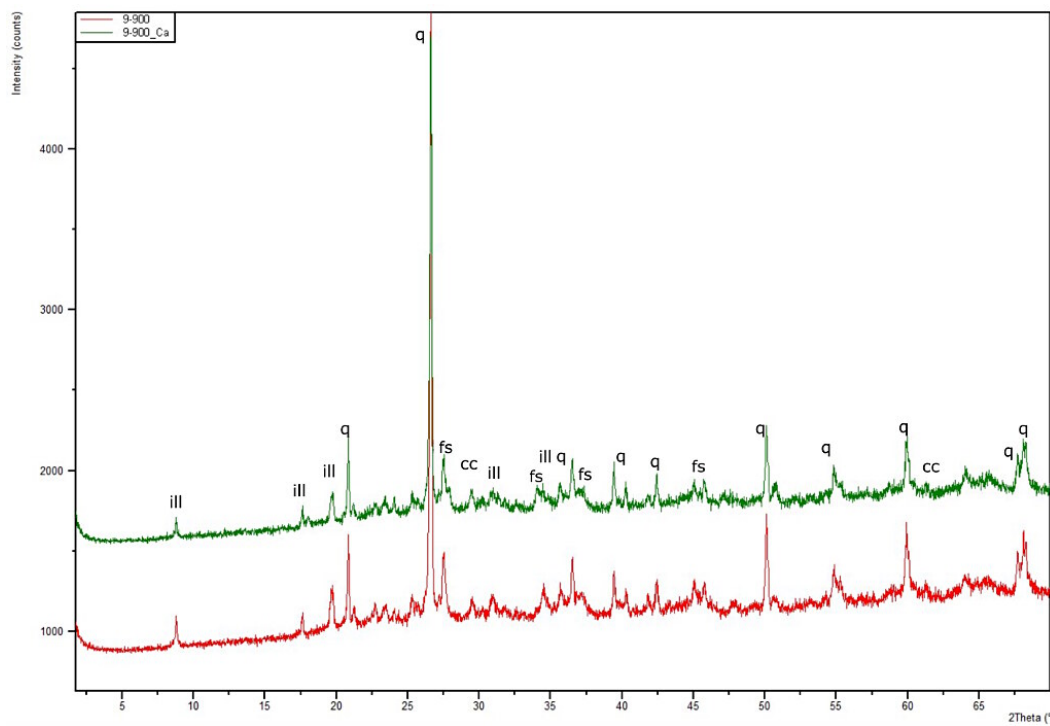


Figure 5.52: Combined XRD-diagrams of specimen soaked for 9 hours at 900°C with CaCO_3 (green) and without CaCO_3 (red); q: quartz, ill: illite, fs: feldspar

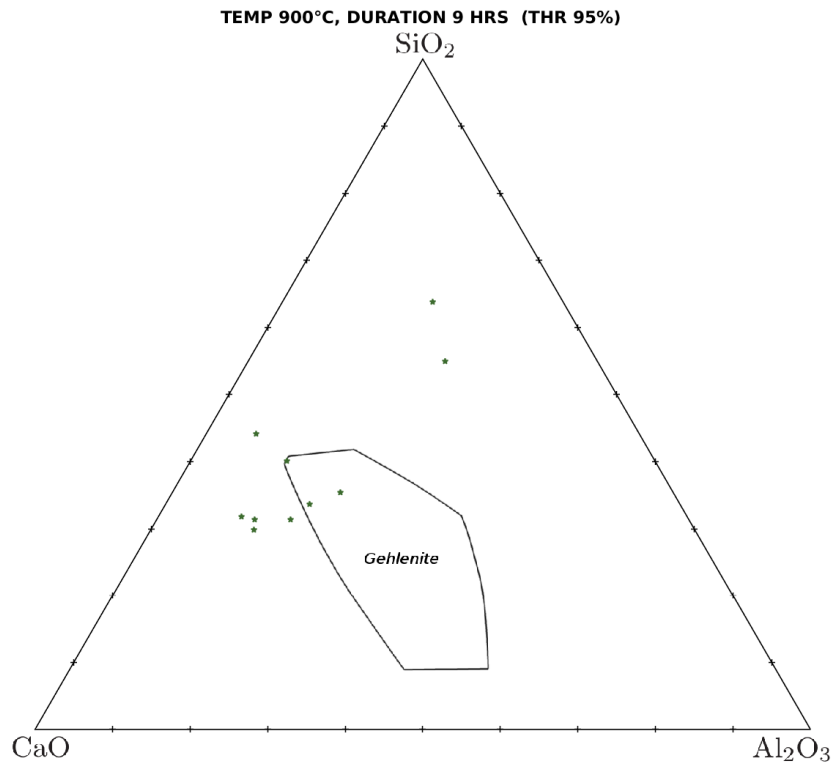
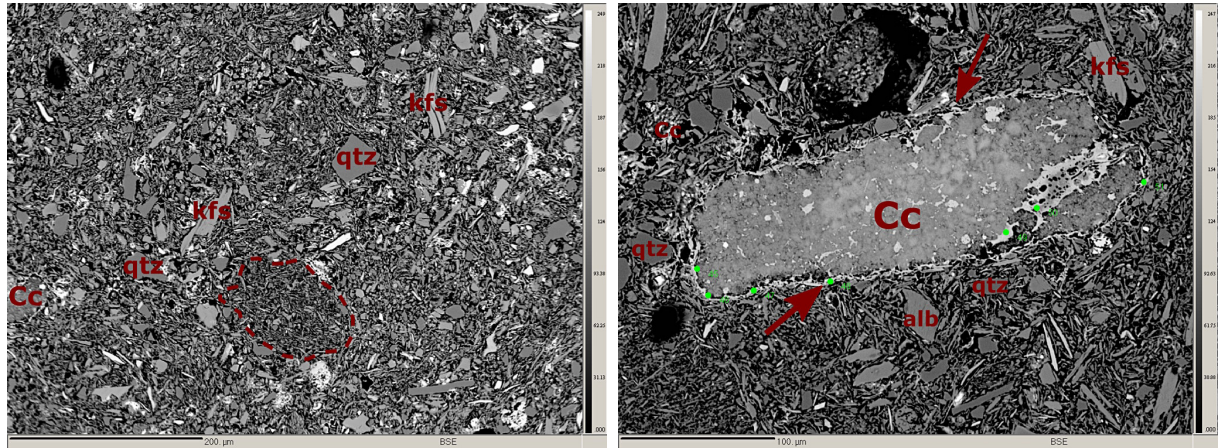
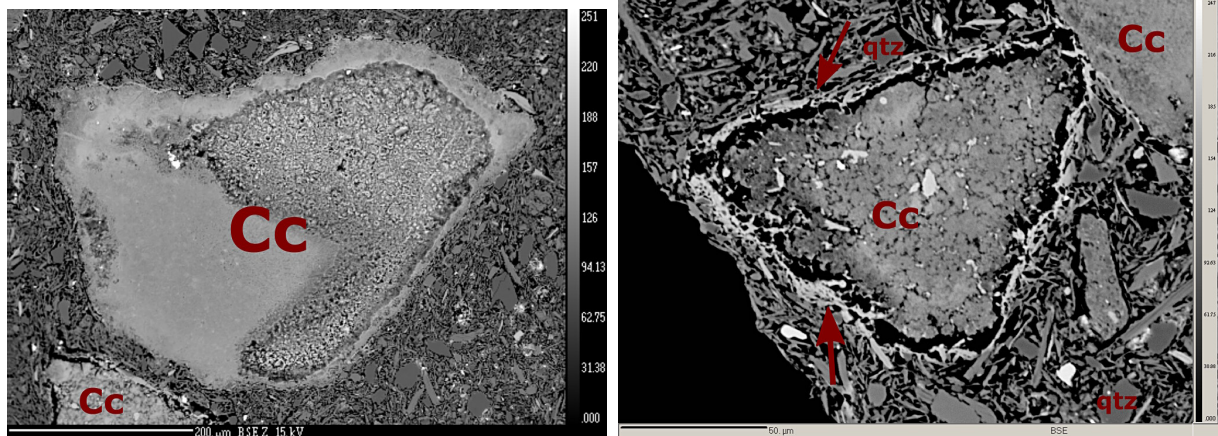


Figure 5.53: Ternary diagram with point analyses from the reaction rims that have a total higher than 95% at 900°C and a soaking time of 9 h; three point analyses plot into the gehlenite stability field, while two plot into the anorthite stability field



(a) Fine-grained paste with medium-grained angular and elongated minerals; qtz: quartz, kfs: potassium-feldspar, alb: albite, ill: illite, cc: calcite; dashed indicates an area of very fine-grained clay paste

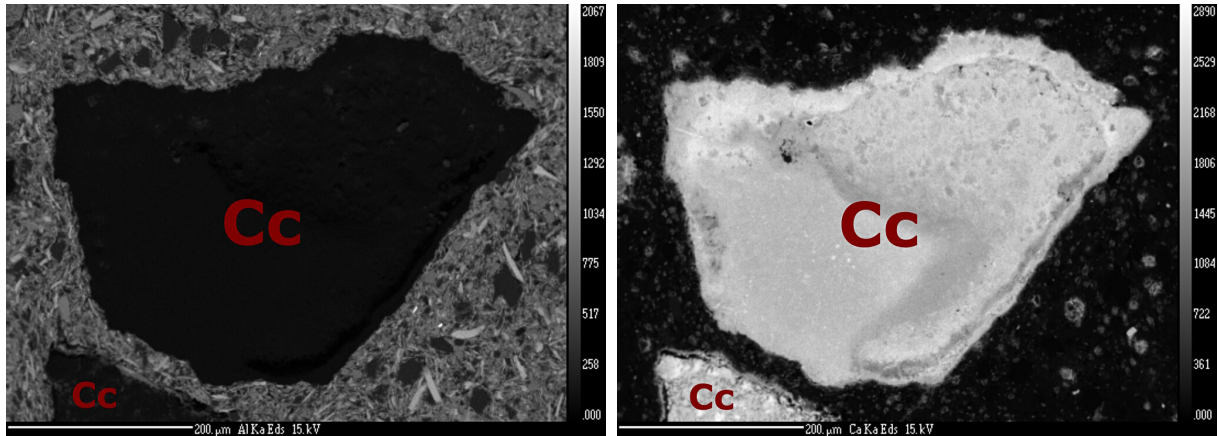
(b) Calcite grain (Cc) with surface changes, the reaction rim (red arrow) growing into the grain, no sign of shrinking



(c) Calcite partially breaking down, with a very thin reaction rim on the top of the grain; calcite grain with signs of shrinking and a much more pronounced reaction rim in the bottom left corner of the picture; Elemental mapping of the grain can be seen in Fig. 5.55

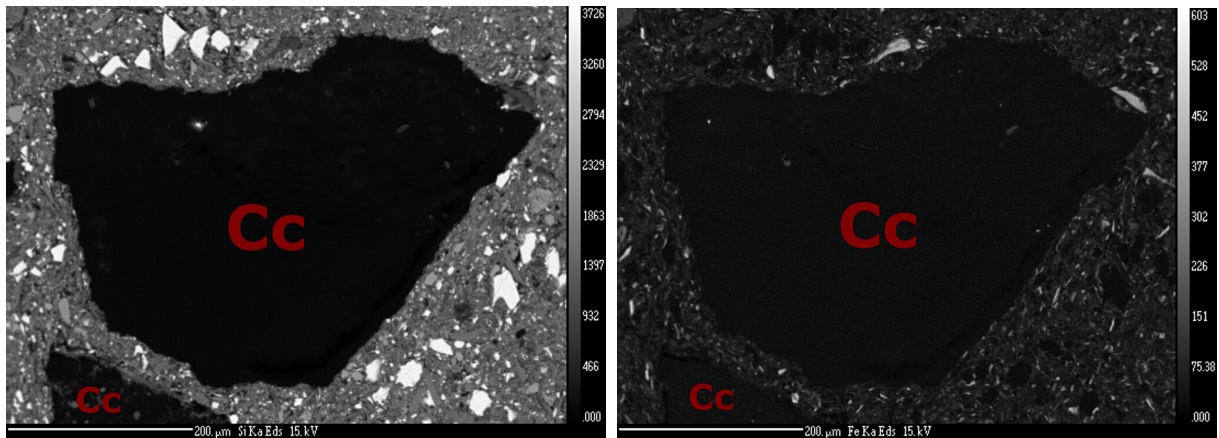
(d) Small calcite grain with signs of shrinking, breakdown and a reaction rim (red arrows). The bigger grain in the upper right corner shows no surface change and a much smaller reaction rim than the small grain

Figure 5.54: Paste and different calcite grains with varying states of breakdown and reaction rims; 900°C, 9 hours



(a) Elemental mapping for Al; Al keeps to the paste around the big calcite grain, but can be seen to diffuse into the reaction rim of the smaller grain

(b) Elemental mapping for Ca; Ca remains constraint within the grain boundaries of the big calcite grain; Ca diffuses into the reaction rim of the small calcite grain; the distribution in both grains is inhomogeneous



(c) Elemental mapping for Si; Si diffuses into the reaction rim of the small calcite grain, but does not cross the grain boundaries of the big grain; Si in the paste is concentrated in quartz minerals, which are medium-grained and angular

(d) Elemental mapping for Fe; Fe diffuses into neither the big nor the small calcite grain; Fe is also very low in the paste, with very few signs for the presence of Fe-oxides

Figure 5.55: Elemental mapping of two calcite grains (Cc) with reaction rims (Fig. 5.54(c))

5.3 1100°C

The firing temperature of 1100°C was chosen as a temperature where gehlenite was expected to transform into anorthite (Tschegg et al., 2009). The expectation was therefore to find relicts of gehlenite and newly formed anorthite feeding from it. Four samples were prepared and fired for three, five, seven, and nine hours, respectively. All thin sections were prepared with water as cooling agent. All samples are of a deep reddish-brown color, independent of calcite content; Fig. 5.56.

XRD show a strong incline of the graph, which indicates the presence of amorphous phases (Cultrone et al., 2001) and decomposed minerals. Breakdown of mineral phases can also be observed. In addition, new phases, which have been detected at neither 800°C nor 900°C can be found. Those phases include mullite, anorthite and spinel. The illite peak still visible in the samples fired at 900°C has disappeared completely.

Samples fired at 1100°C have been analyzed both by a Cameca SX-100 electron microprobe and a Cameca SX FiveFe electron microprobe. Microtextural analysis with OM and BSE images show the paste completely sintered with only quartz retain some grain boundaries. Reaction rims forming around most calcites are pronounced and can be seen by OM.



(a) Samples fired for 3 hours at peak temperature 1100°C



(b) Samples fired for 5 hours at peak temperature 1100°C



(c) Samples fired for 7 hours at peak temperature 1100°C



(d) Samples fired for 9 hours at peak temperature 1100°C

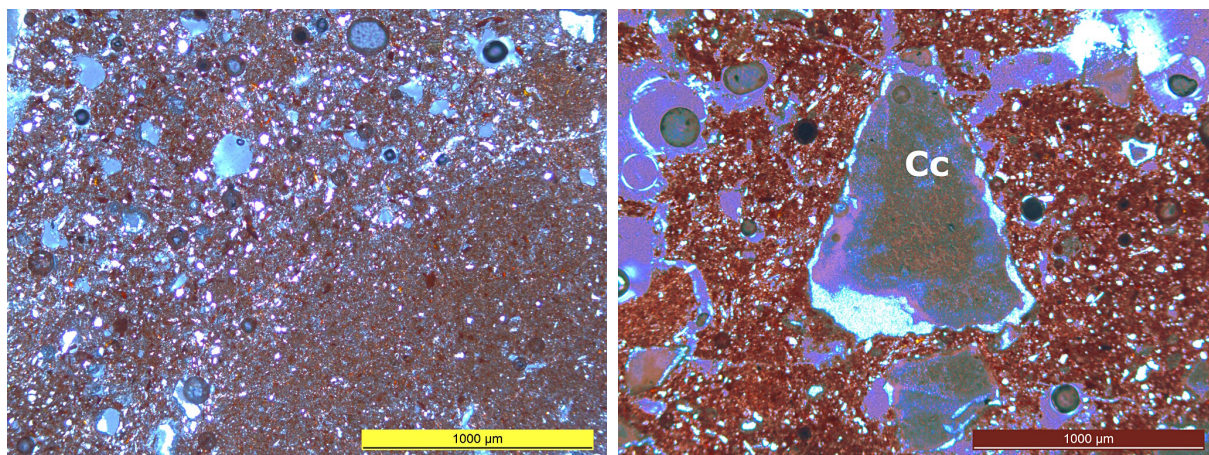
Figure 5.56: All samples fired at 1100°C display a deep reddish-brown color.

5.3.1 3 hours soaking time

Using OM, the paste shows to be sintered and poros, with only some of the calcite grains still retaining their grain boundaries; Fig. 5.57. Upon closer look with BSE images, it can be seen that quartz phenocrysts also retain their form, even though the boundaries are not as clearly defined as at lower temperatures, see Fig. 5.60(a). Calcites are mostly decomposed, even though some relicts remain. Rims form irregularly and tend to not completely surround the calcite grains, independent of the grain size (see Fig. 5.60(b) and (d)). A close-up into the rims reveals them to be inhomogeneous, by forming zones of varying Ca concentration, depending on the elements at disposal; Fig. 5.60(c). Rims can reach a diameter of 35 μm .

Comparing the XRD diagrams of the sample containing calcite and the one without calcite, significant differences can be seen. While both show an increase of background noise as a result of amorphous phases and mineral breakdown, the sample with calcite has more new phases, such as gehlenite and anorthite, than the other one. Most prominently, the feldspar peak is completely gone in the red graph, while in its place the anorthite peak can be seen in the green graph; Fig. 5.58.

Microprobe analyses into calcite grains show a decrease of Ca in the middle as well as an increase closer to the rims. In few cases, wollastonite or wollastonite-resembling phases can be found embedded into former calcite grains. A close-up into the rims show them to inhomogen and display both zoning and spongy structures; Fig. 5.60(c). All points analyzed with a total of 95 wt% or more have been plotted in Fig. 5.59 and are listed in table 5.10. Analyses plot both into the gehlenite and the anorthite stability field. Elemental mapping in false colors shows the migration of Ca into the paste with an inhomogeneous distribution as well as the progress of Al and Si into the calcite grain. The former grain boundaries cannot be identified anymore (see Fig. 5.61).



(a) Sintered paste with high porosity

(b) Relicts of a coarse calcite grain (Cc) in the middle with visible reaction rims

Figure 5.57: Paste and calcite grain with visible reaction rims in the sample fired at 1100°C, 3 h

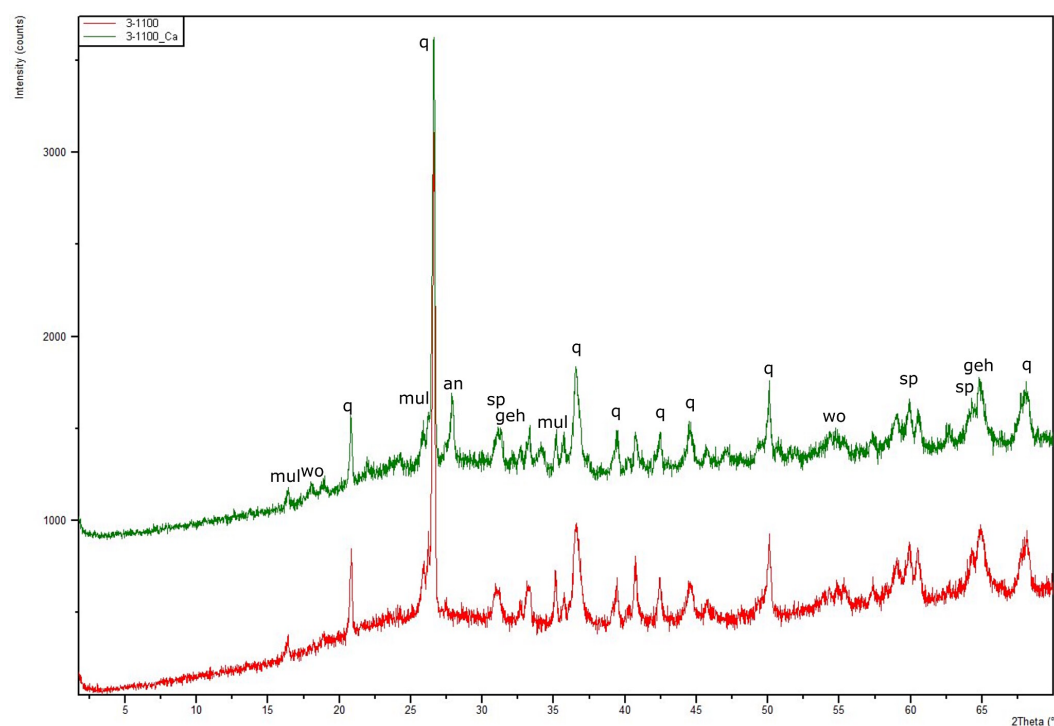


Figure 5.58: Combined XRD-diagrams of specimen soaked for 3 hours at 1100°C with CaCO_3 (green) and without CaCO_3 (red); q: quartz, mul: mullite, an: anorthite, geh: gehlenite, wo: (pseudo)wollastonite

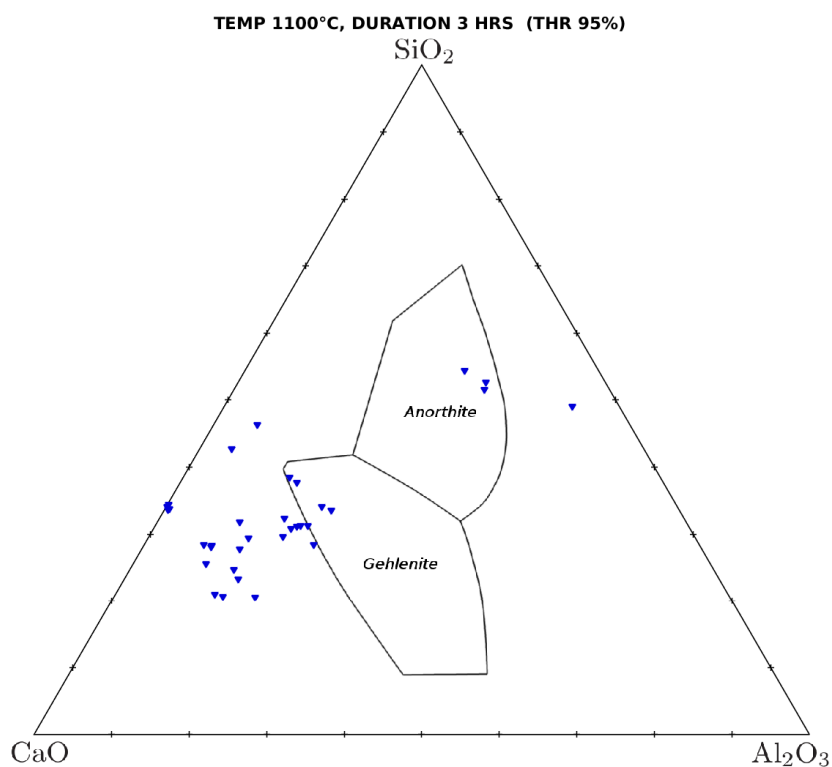
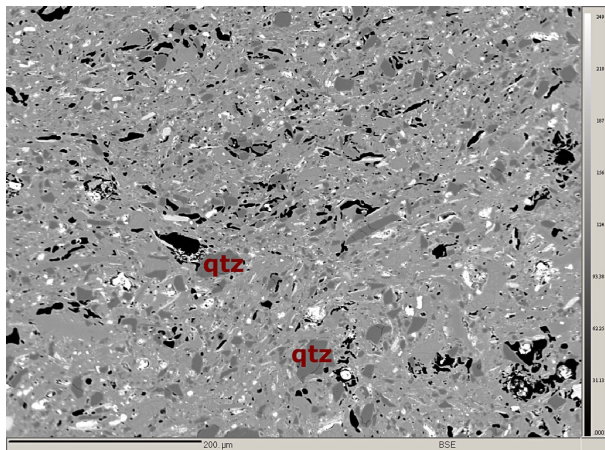
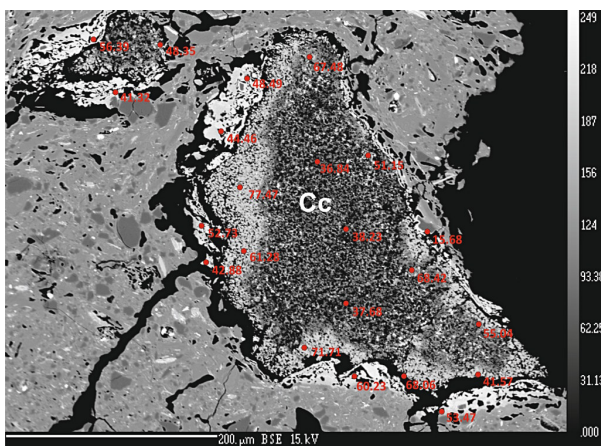


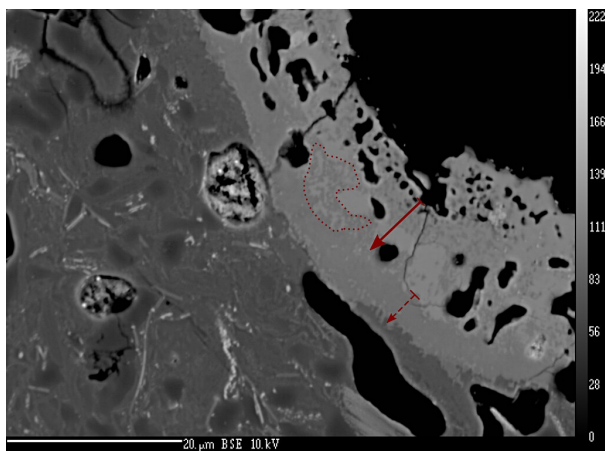
Figure 5.59: Ternary diagram with point analyses from the reaction rims that have a total higher than 95% at 1100°C and a soaking time of 3h; six points plot into the gehlenite stability field and three into the anorthite stability field



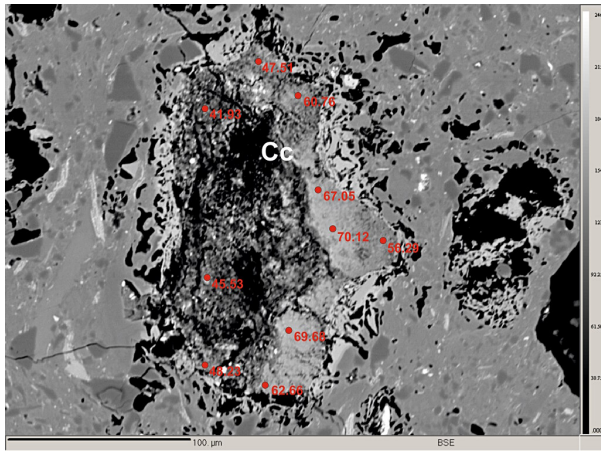
(a) Sintered, porous paste with still recognizable quartz grains



(b) Mostly decomposed calcite grain with obvious reaction rim, embedded in sintered paste; Ca shows an increasing trend in its distribution from the decomposed parts of the calcite grain to parts not yet decomposed completely; numbers indicate EPMA point analyses

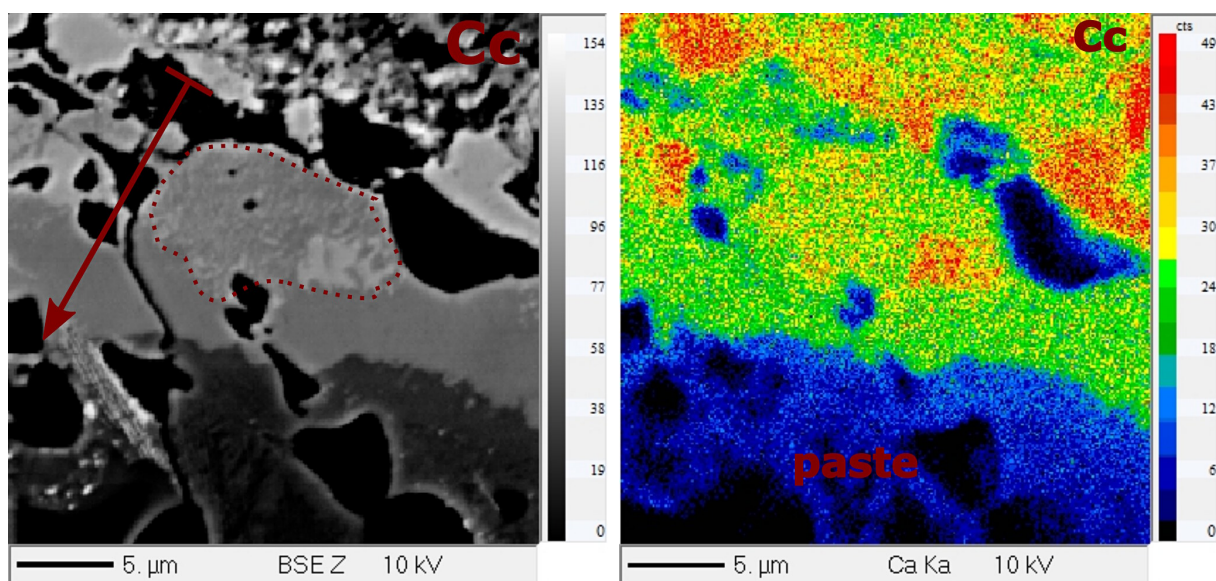


(c) Close-up of a reaction rim, showing zoning and a spongy structure, the red arrow indicates the zone with more Ca, the dashed arrow indicating the zone with lesser Ca, the dotted line indicates a spongy area



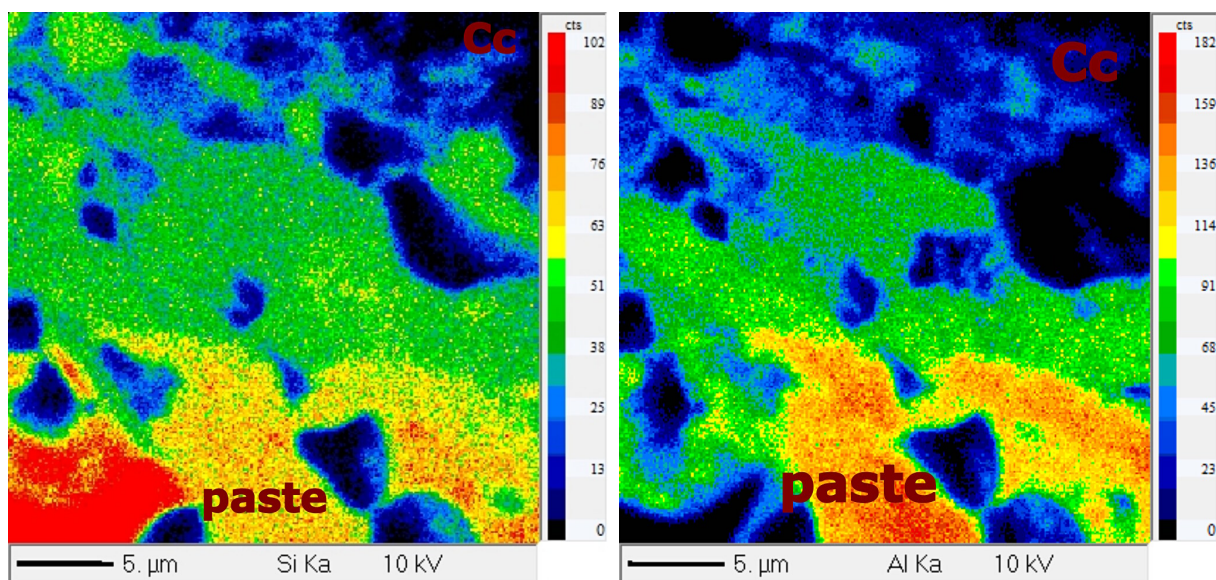
(d) Partially decomposed calcite grain with relict calcite and distinct reaction rims next to a smaller, completely decomposed calcite grain with a partial reaction rim; Ca shows higher concentrations in those parts of the grain that are not yet decomposed; numbers indicate EMPA point analyses

Figure 5.60: Paste and different calcite grains; 1100° C, 3 hours



(a) Elemental mapping BSE, reaction rim; Ca diffuses from the decomposed calcite grain (Cc) into the paste; the red arrow indicates the reaction rim, the dotted line highlights a spongy area

(b) Elemental mapping for Ca; Ca diffuses continuously from the decomposed calcite grain (Cc) into the paste. The spongy area (see Fig. 5.60(a)) shows an uneven distribution of Ca



(c) Elemental mapping for Si; Si diffuses into the reaction rim, the concentration of Si in the lower left corner indicates the remains of a quartz grain

(d) Elemental mapping for Al; Al also diffuses into the reaction rim, approximately the same distance as Si

Figure 5.61: Elemental mapping of the close-up into a reaction rim; former grain boundaries cannot be identified anymore

— EPMA raw sample data, 1100°C, 3 hours —

Set/Pt	24/1.	25/1.	29/1.	31/1.	37/1.	38/1.	43/1.	52/1.	54/1.	57/1.
SiO₂	27.26	22.66	49.47	30.40	27.78	30.42	17.89	44.09	25.73	28.28
TiO₂	0.57	0.16	0.69	0.10	0.36	0.10	0.54	0.13	0.37	0.09
Al₂O₃	11.97	14.28	25.72	10.10	16.69	15.23	12.14	5.40	11.68	16.43
FeO	3.28	0.93	4.81	0.97	2.55	1.92	6.93	0.85	2.03	1.18
CaO	53.47	60.23	15.68	55.03	44.46	48.49	56.38	45.72	55.24	50.62
MgO	1.19	0.10	0.79	1.28	3.22	2.60	1.35	1.91	0.80	1.46
MnO	bdl	bdl	0.02	bdl	bdl	bdl	0.11	0.04	0.06	0.03
K₂O	0.02	bdl	0.90	bdl	0.02	bdl	bdl	0.36	bdl	0.03
Na₂O	bdl	bdl	1.05	bdl	bdl	bdl	bdl	0.05	bdl	bdl
P₂O₅	bdl	bdl	bdl	bdl	bdl	bdl	bdl	bdl	bdl	bdl
SO₂	bdl	0.12	bdl	bdl	bdl	bdl	0.08	bdl	0.81	0.04
Total	97.79	98.51	99.13	97.94	95.08	98.78	95.41	98.55	96.74	98.16

Set/Pt	1/1.	2/1.	3/1.	4/1.	8/1.	9/1.	11/1.	16/1.	17/1.	18/1.
SiO₂	27.81	37.80	26.02	35.60	33.09	29.08	29.27	33.66	33.23	23.97
TiO₂	0.04	0.12	0.23	0.25	0.53	0.07	0.10	0.10	0.09	0.19
Al₂O₃	21.44	3.67	23.80	12.69	13.21	16.80	17.28	0.09	0.49	12.95
FeO	0.45	2.30	27.77	1.71	4.53	2.87	1.67	0.13	0.10	1.25
CaO	48.66	46.97	3.24	44.34	41.45	48.55	47.47	64.85	64.71	59.93
MgO	0.99	8.28	12.04	4.62	5.27	1.85	1.98	0.02	0.04	0.08
MnO	bdl	0.05	0.15	0.02	0.05	bdl	bdl	bdl	bdl	bdl
K₂O	0.11	bdl	2.12	0.05	0.03	0.02	0.04	0.02	bdl	bdl
Na₂O	bdl	bdl	0.78	bdl	bdl	bdl	0.03	bdl	bdl	bdl
P₂O₅	bdl	0.07	0.04	bdl	0.70	0.04	bdl	0.14	0.11	0.12
SO₂	bdl	bdl	bdl	bdl	bdl	bdl	bdl	bdl	bdl	bdl
Total	99.50	99.27	96.18	99.27	98.87	99.28	97.84	99.01	98.81	98.51

Set/Pt	19/1.	20/1.	21/1.	22/1.	23/1.	26/1.	27/1.	29/1.	30/1.	2/1.
SiO₂	29.48	23.84	33.51	27.46	32.45	27.64	19.65	17.83	27.68	31.61
TiO₂	0.21	0.41	0.07	0.06	0.06	0.02	0.06	1.22	0.06	0.36
Al₂O₃	18.56	8.80	0.08	8.62	0.46	8.59	17.51	10.88	7.48	20.38
FeO	2.47	2.04	0.12	0.81	0.23	0.80	1.26	10.65	0.49	1.59
CaO	46.36	60.63	63.62	61.58	63.48	61.38	58.59	56.08	62.22	42.31
MgO	1.24	0.23	0.03	0.08	0.23	0.09	0.07	0.60	0.08	1.77
MnO	0.04	bdl	bdl	bdl	0.02	0.02	0.04	0.40	0.03	bdl
K₂O	0.03	bdl	bdl	bdl	bdl	0.03	bdl	bdl	bdl	0.04
Na₂O	0.03	bdl	0.04	bdl	0.04	bdl	bdl	bdl	bdl	0.06
P₂O₅	0.11	0.13	bdl	bdl	0.10	0.04	bdl	0.05	bdl	bdl
SO₂	bdl	bdl	bdl	bdl	bdl	bdl	bdl	bdl	bdl	bdl
Total	98.52	96.09	97.48	98.61	97.08	98.63	97.22	97.72	98.07	98.13

continued on next page...

— EPMA raw sample data, 1100°C, 3 hours —

Set/Pt	3/1.	4/1.	5/1.	6/1.
SiO₂	49.41	33.03	30.40	48.79
TiO₂	0.36	0.09	0.27	0.36
Al₂O₃	30.91	0.58	17.92	29.59
FeO	1.51	0.27	4.47	2.51
CaO	15.40	64.14	40.85	14.20
MgO	0.63	0.16	3.67	0.77
MnO	bdl	0.04	0.05	0.03
K₂O	0.75	0.05	0.08	0.85
Na₂O	1.30	bdl	0.04	1.22
P₂O₅	bdl	bdl	bdl	bdl
SO₂	bdl	bdl	bdl	bdl
Total	100.30	98.36	97.75	98.31

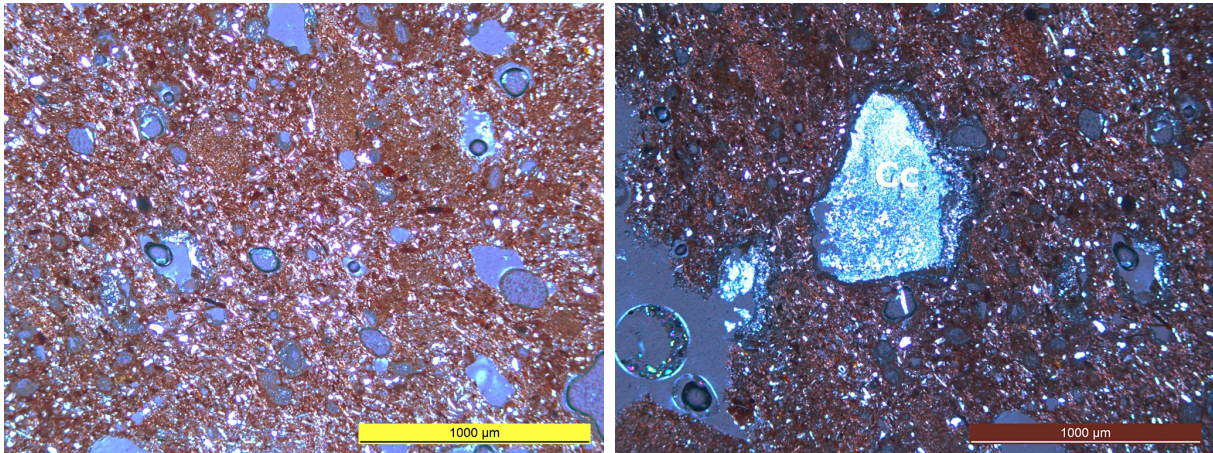
Table 5.10: EPMA raw sample data in wt%, firing temperature 1100°C, soaking time 3 hours. (bdl = below detection limit.)

5.3.2 5 hours soaking time

First optical analysis with OM show high porosity in the paste and no identifiable minerals; Fig. 5.62(a). Calcite grains and their reaction rims can also be seen; Fig. 5.62(b). BSE images reveals the paste sintered with quartz grains still recognizable but smaller; Fig. 5.64(a). Most calcite grains are decomposed with some relict calcite in their middle, and display reaction rims that form irregularly around the grains, see Fig. 5.64(d). Those rims can reach up to 110 µm. Very few big calcite grains of at least 400 µm in diameter appear almost healthy, with only minimal signs of decomposing. Reaction rims near such grains are much thinner and not as wide-spread around the grain; Fig. 5.64(b).

XRD analysis of both the specimen with and without calcite show increased amorphous phases. The sample containing calcite contains gehlenite and anorthite, while the sample without calcite shows less variability in the new phases, see Fig. 5.63.

Point analyses into calcite grains display a trend of decreasing CaO from the middle of the grain to the rims. However, analyses done in the grains that are not yet decomposed provide no clear trend. Point analyses of the rims detect incipient gehlenite stages to gehlenite. All point analyses surpassing the threshold of 95 wt% total or more have been plotted in Fig. 5.66, some plotting in the gehlenite stability field as well in the anorthite stability field. All corresponding point analyses are listed in table 5.11 Close-up elemental mapping of a rim shows the migration of Ca into the paste in zones, while both Al and Si move into the former grain. Grain boundaries are not to be determined anymore; Fig. 5.65.



(a) Sintered paste, showing higher porosity than samples fired at lower temperatures (blue areas) (b) Calcite grain (Cc) in the middle with visible reaction rims

Figure 5.62: Paste and calcite grain with visible reaction rim in the sample fired at 1100°C, 5 h

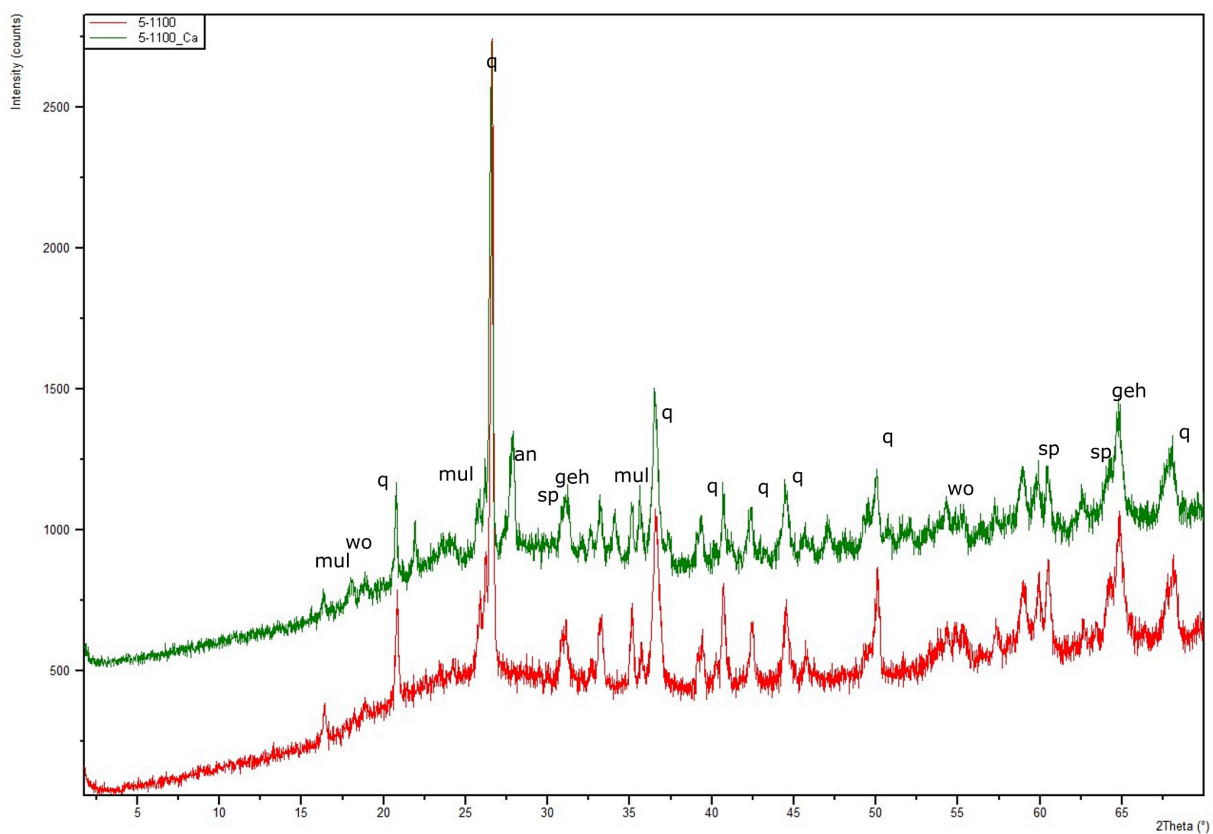
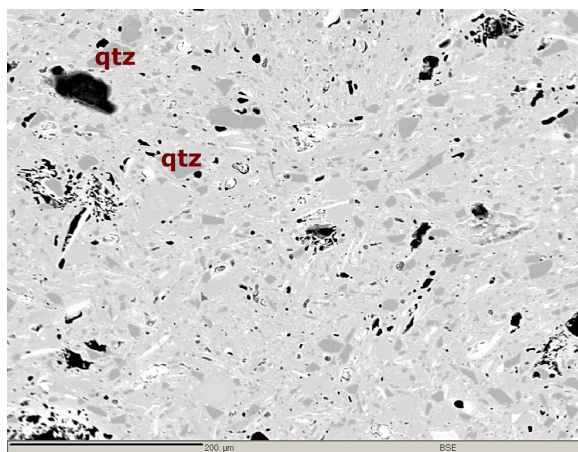
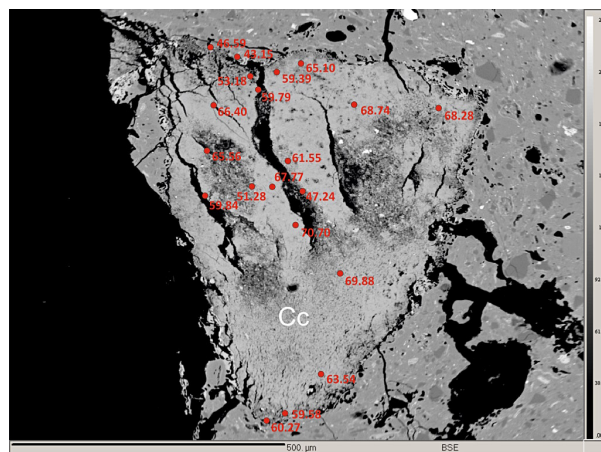


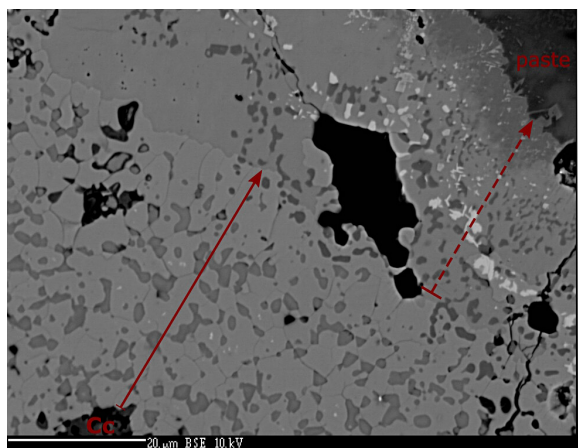
Figure 5.63: Combined XRD-diagrams of specimen soaked for 5 hours at 1100°C with CaCO_3 (green) and without CaCO_3 (red); q: quartz, mul: mullite, an: anorthite, geh: gehlenite, wo: (pseudo)wollastonite



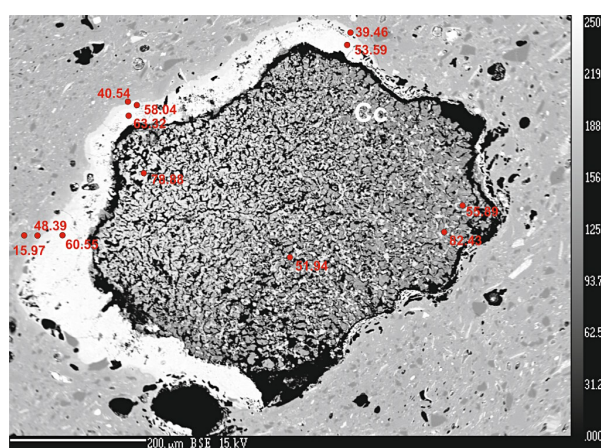
(a) Sintered paste with quartz phenocrysts retaining their grain boundaries; qtz: quartz



(b) Coarse calcite grain with signs of breakdown, narrow reaction rim growing in the upper part of the grain and cracks in the middle of the grain; point analysis into the grain shows no trend for the distribution of Ca; numbers indicate EPMA point analyses



(c) Close-up of reaction rim with zoning, the red arrow indicates the movement of Ca from the grain into the paste and the zone with higher Ca; the dashed arrow represents the zone with less Ca; the inhomogeneous Ca distribution is visible in the spongy areas



(d) Decomposed calcite grain with calcite relicts in the middle and a pronounced reaction rim; point analysis into the grain shows no trend within the grain; analyses in the rim show a decrease of Ca the further into the paste it progresses; numbers indicate EPMA point analyses

Figure 5.64: Paste and different calcite grains or relicts thereof; 1100°C, 5 hours

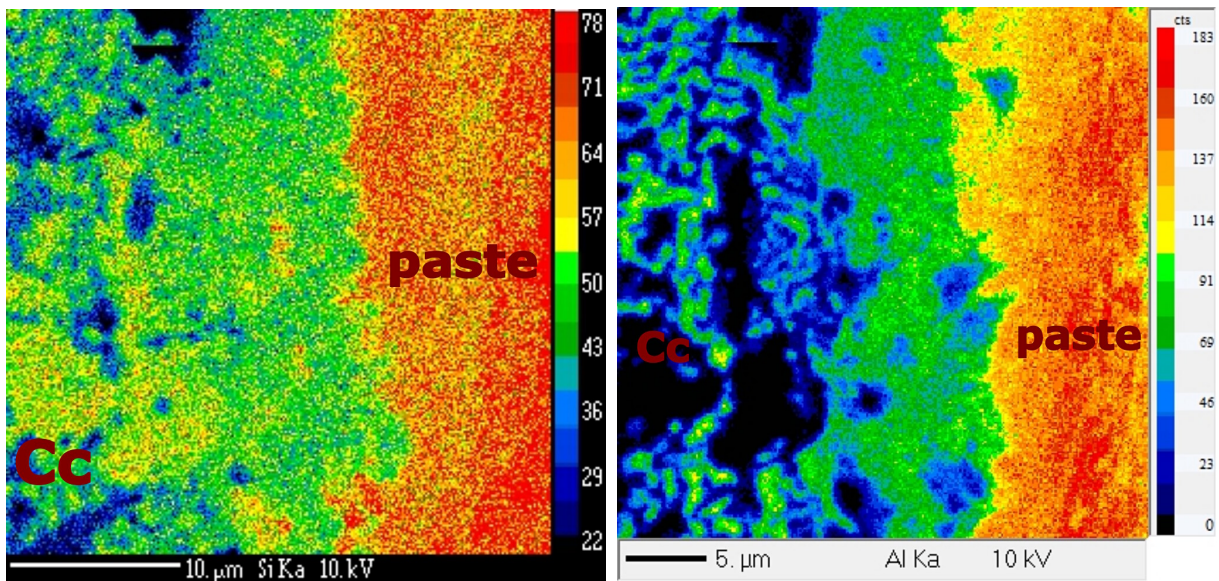
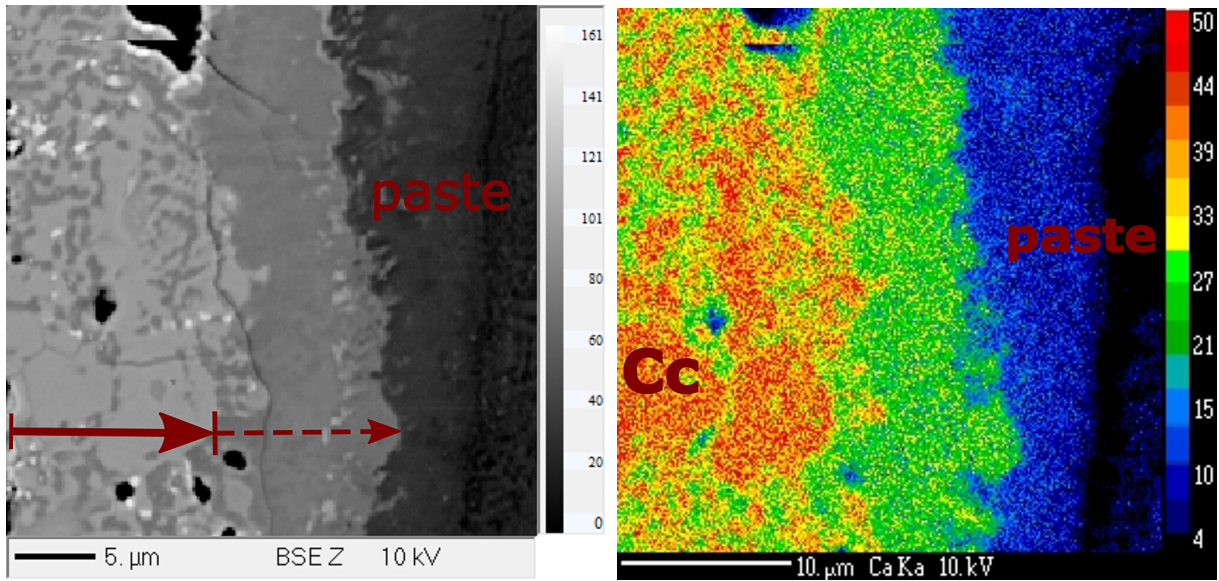


Figure 5.65: Elemental mapping of a close-up into a reaction rim

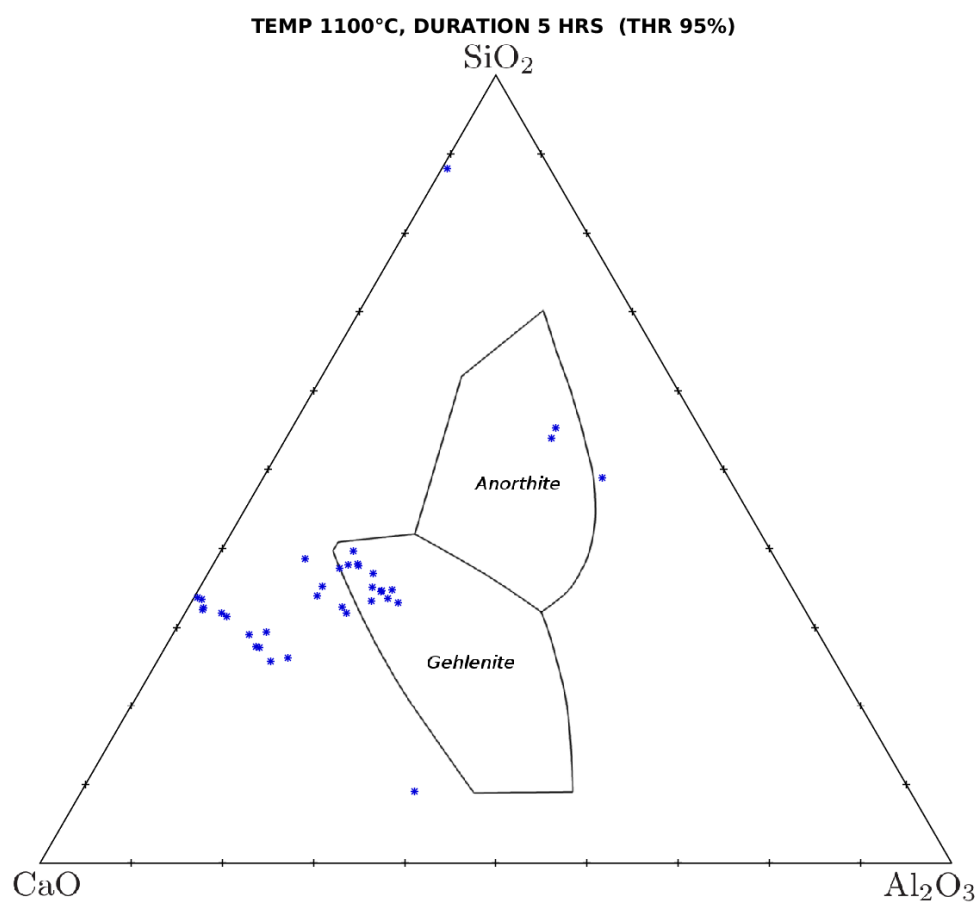


Figure 5.66: Ternary diagram with point analyses from the reaction rims that have a total higher than 95 % at 1100° C and a soaking time of 5 h; 12 analyses plotting into the gehlenite stability field and two analyses plotting into the anorthite stability field

— EPMA raw sample data, 1100°C, 5 hours —

Set/Pt	67/1.	68/1.	69/1.	71/1.	72/1.	73/1.	74/1.	77/1.	79/1.	80/1.
SiO₂	26.02	31.68	30.92	33.34	26.75	31.29	50.92	75.46	26.66	32.32
TiO₂	2.05	0.95	0.37	0.12	0.09	0.71	0.33	0.03	0.13	0.19
Al₂O₃	8.98	12.38	1.68	13.91	10.09	12.31	27.54	0.50	9.61	18.79
FeO	6.79	4.40	1.94	4.38	0.95	2.17	1.83	0.10	1.01	2.52
CaO	53.59	39.46	63.32	40.54	60.55	48.39	15.97	9.60	60.67	42.08
MgO	1.03	6.35	0.21	6.64	0.04	4.17	0.51	4.97	0.04	3.19
MnO	0.09	0.08	0.04	0.09	bdl	0.03	0.05	bdl	0.03	0.05
K₂O	bdl	0.03	bdl	0.03	bdl	bdl	1.10	0.27	bdl	0.04
Na₂O	bdl	0.20	bdl	0.16	0.08	0.05	1.39	10.72	bdl	0.17
P₂O₅	bdl	bdl	bdl	bdl	bdl	bdl	bdl	bdl	bdl	bdl
SO₂	0.05	bdl	0.07	bdl	bdl	bdl	bdl	0.22	0.02	bdl
Total	98.61	95.53	98.59	99.24	98.58	99.14	99.63	101.89	98.17	99.36

Set/Pt	81/1.	82/1.	83/1.	84/1.	85/1.	86/1.	31/1.	32/1.	34/1.	35/1.
SiO₂	31.36	33.51	28.85	29.05	30.87	31.47	30.75	8.62	24.49	33.22
TiO₂	0.08	0.19	0.05	0.26	0.16	0.24	0.15	0.06	0.21	0.14
Al₂O₃	3.94	12.60	8.28	16.20	4.70	21.57	17.95	34.79	13.23	0.41
FeO	0.31	3.13	0.63	2.53	0.77	1.90	4.75	2.85	1.80	0.19
CaO	63.37	43.34	61.96	46.21	62.71	41.93	40.44	51.79	55.87	64.87
MgO	0.04	5.65	0.04	2.75	0.08	2.17	5.02	0.12	0.10	0.11
MnO	bdl	0.05	bdl	bdl	0.03	0.03	0.03	bdl	bdl	bdl
K₂O	bdl	0.05	bdl	0.02	bdl	0.05	0.03	bdl	0.02	bdl
Na₂O	bdl	0.03	0.04	0.13	0.06	0.19	0.04	0.02	0.09	bdl
P₂O₅	bdl	bdl	bdl	bdl	bdl	bdl	0.04	0.03	0.04	0.24
SO₂	0.60	bdl	0.06	0.35	0.04	bdl	bdl	bdl	bdl	bdl
Total	99.73	98.57	99.92	97.49	99.42	99.55	99.19	98.31	95.88	99.19

Set/Pt	36/1.	37/1.	42/1.	43/1.	44/1.	45/1.	47/1.	49/1.	50/1.	118/1.
SiO₂	32.03	31.08	35.42	29.83	25.20	29.65	30.89	33.72	32.05	35.38
TiO₂	0.36	0.18	0.14	0.08	0.13	0.58	0.12	0.15	0.09	bdl
Al₂O₃	17.27	1.64	13.04	17.55	12.19	15.30	19.53	14.29	12.16	8.92
FeO	3.10	1.07	3.70	2.91	0.77	3.45	3.29	3.78	2.16	1.93
CaO	42.11	63.01	40.92	42.02	60.64	46.00	41.35	41.10	46.94	47.19
MgO	2.98	1.64	5.99	4.73	0.07	3.34	3.19	5.96	3.89	3.16
MnO	bdl	0.03	0.06	bdl	bdl	bdl	0.03	0.05	0.04	0.06
K₂O	0.05	bdl	0.02	bdl	bdl	0.04	0.07	0.05	0.03	0.04
Na₂O	0.07	bdl	bdl	bdl	bdl	bdl	0.07	0.04	bdl	0.18
P₂O₅	bdl	bdl	bdl	0.06	0.07	0.13	bdl	bdl	bdl	bdl
SO₂	bdl	bdl	bdl	bdl	bdl	bdl	bdl	bdl	bdl	bdl
Total	97.99	98.67	99.30	97.21	99.06	98.49	98.54	99.14	97.37	96.86

continued on next page...

— EPMA raw sample data, 1100°C, 5 hours —

Set/Pt	8/1.	9/1.	10/1.	12/1.	13/1.
SiO₂	32.87	31.51	45.70	33.16	52.09
TiO₂	0.07	0.40	0.26	0.15	0.25
Al₂O₃	1.00	15.51	34.77	20.23	27.30
FeO	0.22	5.83	1.76	1.66	2.02
CaO	64.17	38.47	12.97	42.01	14.91
MgO	0.08	5.26	0.44	1.88	0.49
MnO	bdl	0.07	0.03	0.04	0.03
K₂O	bdl	0.04	1.05	0.09	1.20
Na₂O	bdl	0.12	1.30	0.10	1.30
P₂O₅	bdl	bdl	bdl	bdl	bdl
SO₂	bdl	bdl	bdl	bdl	bdl
Total	98.41	97.20	98.27	99.33	99.60

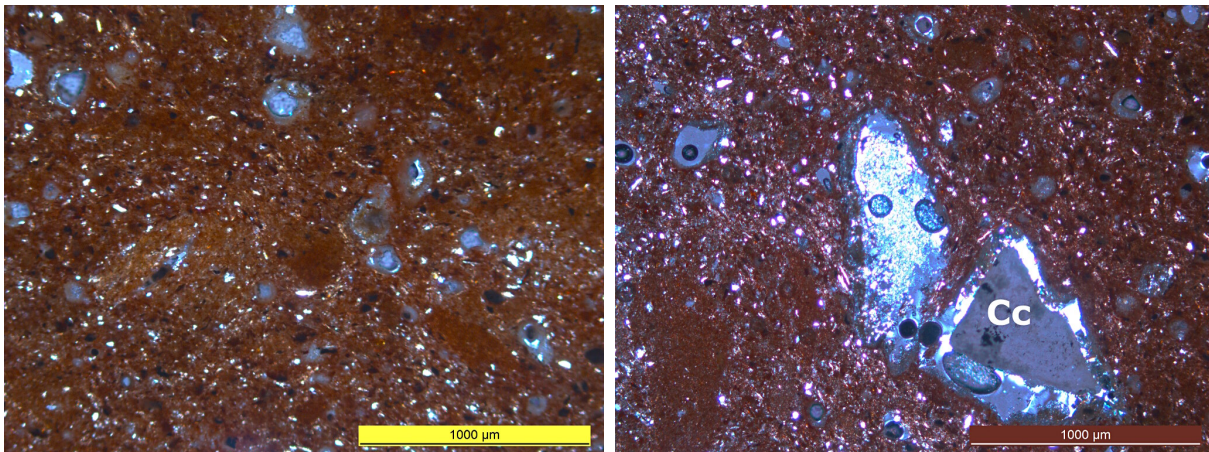
Table 5.11: EPMA raw sample data in wt%, firing temperature 1100°C, soaking time 5 hours. (bdl = below detection limit.)

5.3.3 7 hours soaking time

OM shows decomposed calcite grains with partial reaction rims embedded in sintered paste, Fig. 5.67(a). This is mostly confirmed (Fig. 5.69(a)) by BSE image analysis, but although quartz keeps to its grain boundaries, they are not as distinct anymore and smaller than in the samples fired for 3 h and 5 h. Calcite grains show a variety of decomposition stages. It can range from calcites appearing almost "healthy" with thin reaction areas (see Fig. 5.69(d)) to completely decomposed with reaction rims around the former grain (see Fig. 5.69(b)). Reaction rims are up to 80 µm thick, but are usually formed irregularly around the grains. Within the rim Ca zoning is visible, with spongy areas and Fe-enriched phases (see Fig. 5.69(c)). Given a sufficient Si saturation, wollastonite can form.

Comparing the XRD diagrams of the sample with calcite and the one without, both have a similarly increased background noise, indicating amorphous phases. Both samples show the formation of new phases, but the samples containing calcite has a bigger variability such as gehlenite, anorthite and wollastonite; Fig. 5.68.

Point analyses into the calcite grain in Fig. 5.69(d) show no clear trend in the Ca distribution, except for a reduced amount of Ca at points 14, 15 and 17 at the closest contact to the reaction rims. Rims have overall developed well enough to get good analyses, with some of the point analyses detecting gehlenite. Those analyses surpassing threshold of 95 wt% total have been listed in table 5.12 and plotted in the phase diagram in Fig. 5.71, nine of the analyses plotting into the gehlenite stability field and five into the anorthite stability field. Close-up elemental mapping of a rim in false colors shows the migration of Ca into the paste, while both Al and Si move into the former grain boundaries with especially Al being concentrated in closed spots. Fe is concentrated in the needle-like structures within the rim. Grain boundaries cannot be determined; Fig. 5.70.



(a) Sintered paste with no visible phenocrysts and high porosity (blue areas) (b) Calcite grain (Cc) breaking down with visible reaction rims

Figure 5.67: Paste and calcite grain with reaction rims in the sample fired at 1100°C, 7h

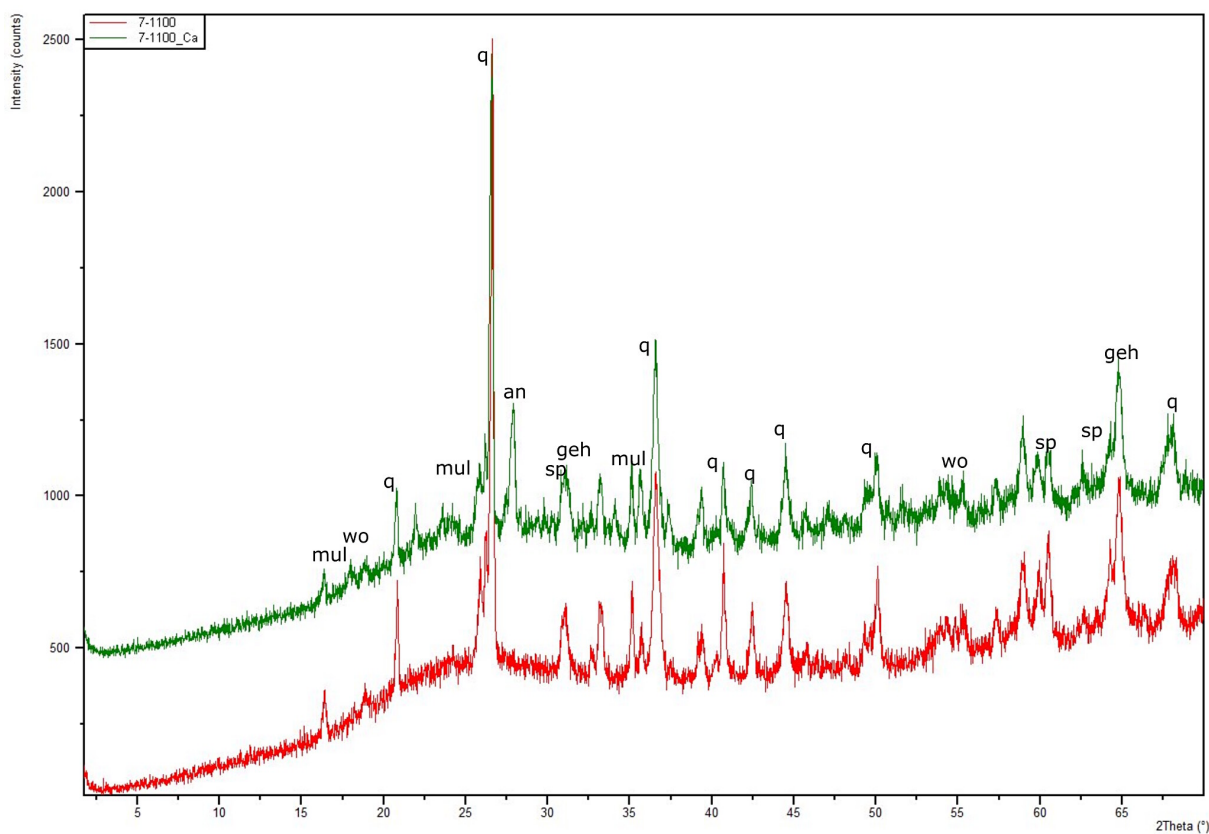


Figure 5.68: Combined XRD-diagrams of specimen soaked for 7 hours at 1100°C with CaCO_3 (green) and without CaCO_3 (red); q: quartz, mul: mullite, an: anorthite, geh: gehlenite, wo: (pseudo)wollastonite

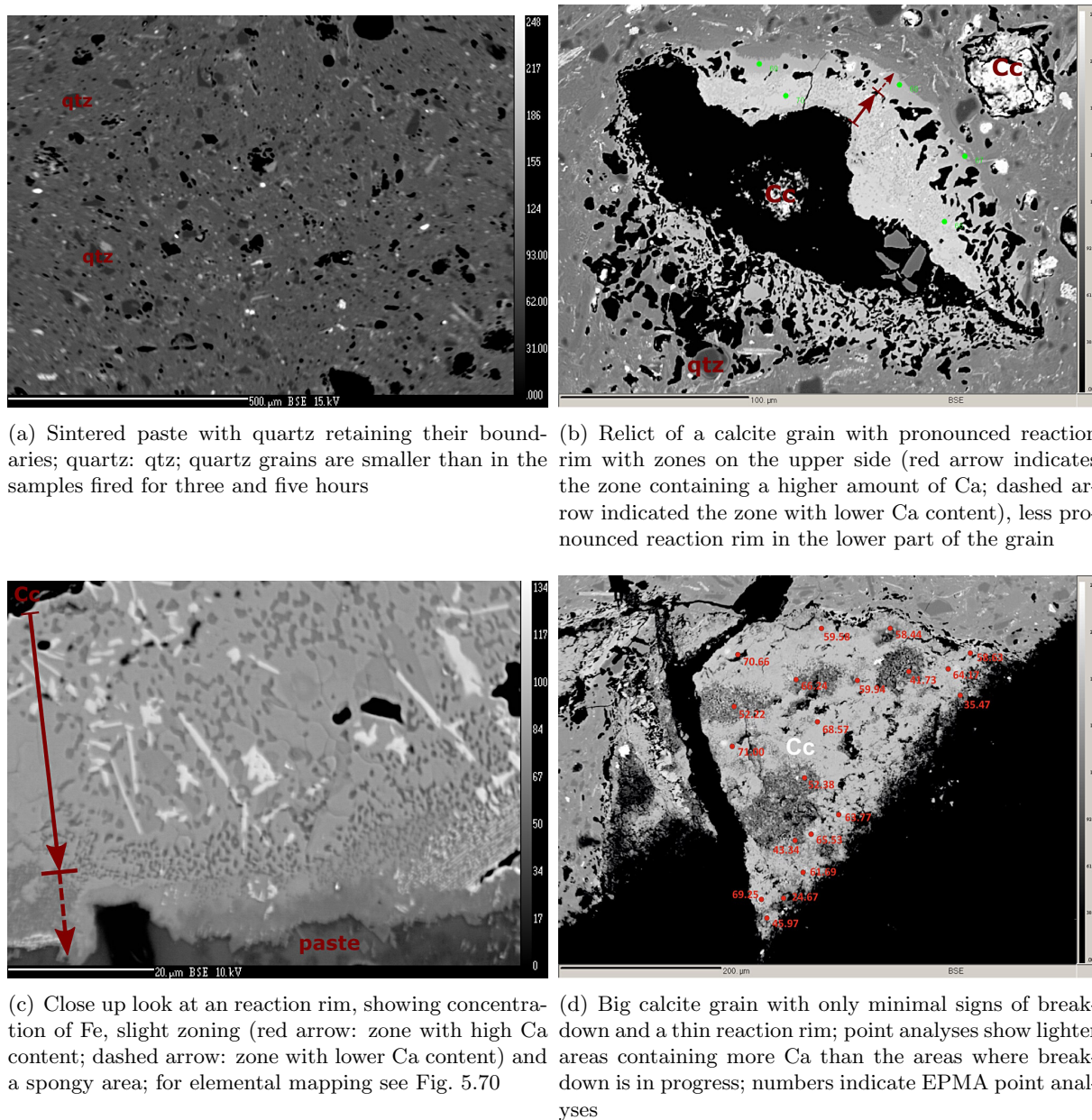
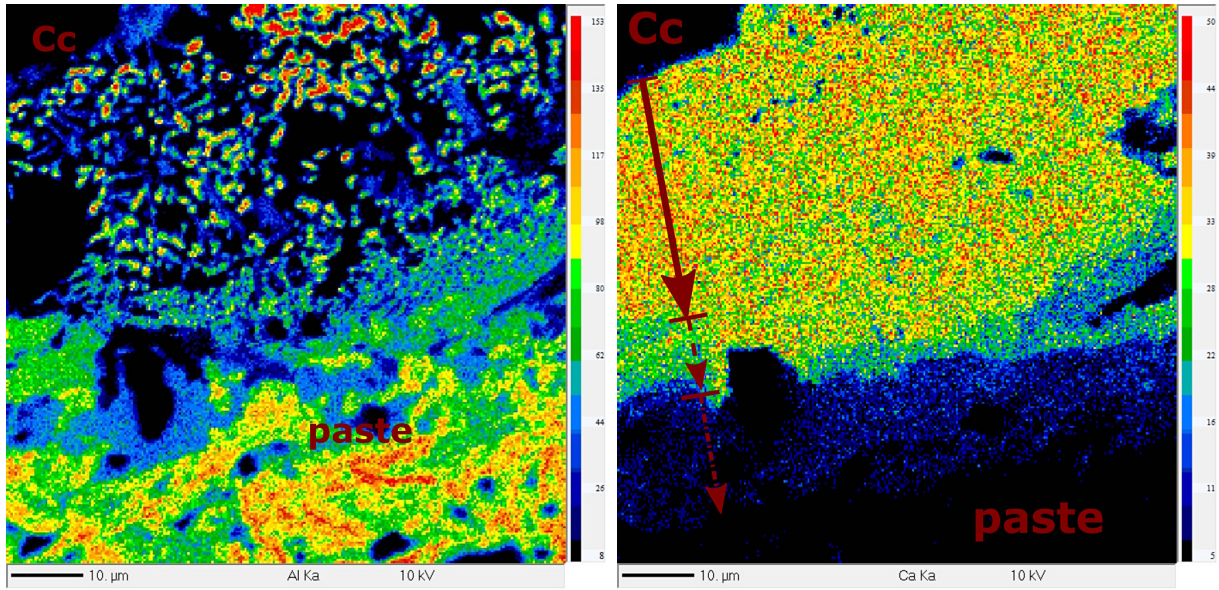
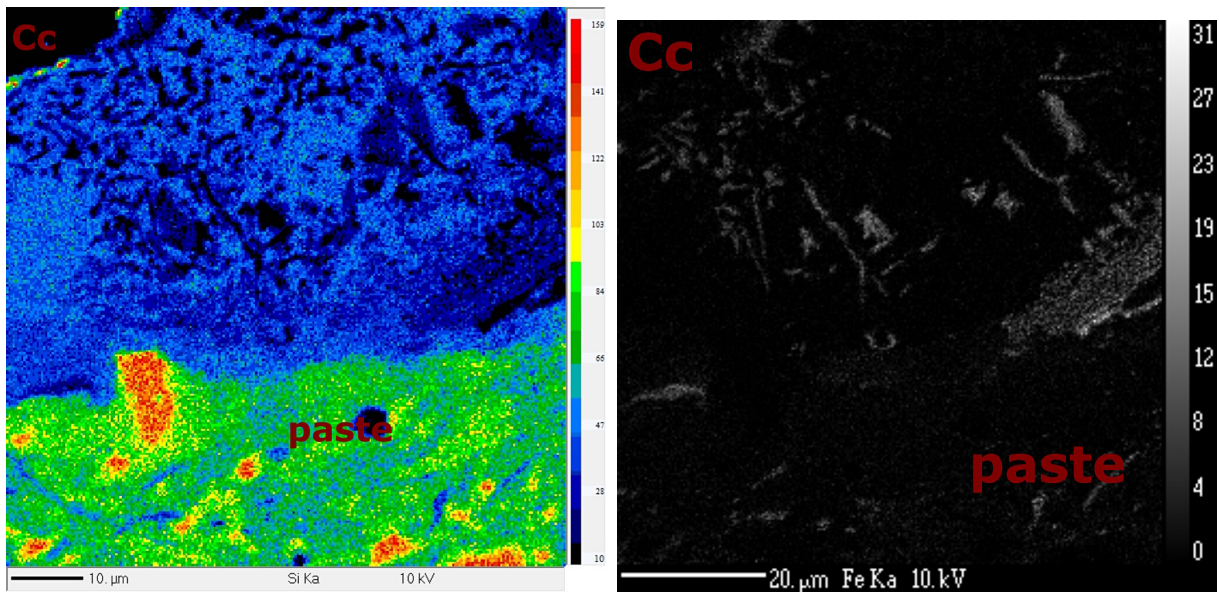


Figure 5.69: Paste and reaction rims around relict/ former calcite grains; 1100°C, 7 hours



(a) Elemental mapping for Al; Al diffuses into the grain from the paste, showing zoning and a spongy area close to the grain

(b) Elemental mapping for Ca; Ca diffuses mostly evenly into the paste for about 40 μm , before the diffusion slows down to a considerably lower rate for another 20 μm



(c) Elemental mapping for Si; Si diffuses towards the grain, but slower than Al

(d) Elemental mapping for Fe; Fe is concentrated in the rim in elongated structures

Figure 5.70: Elemental mapping of a reaction rim (indicated by the red and dashed arrow), close-up, the grain boundaries cannot be determined anymore; (Fig. 5.69(c))

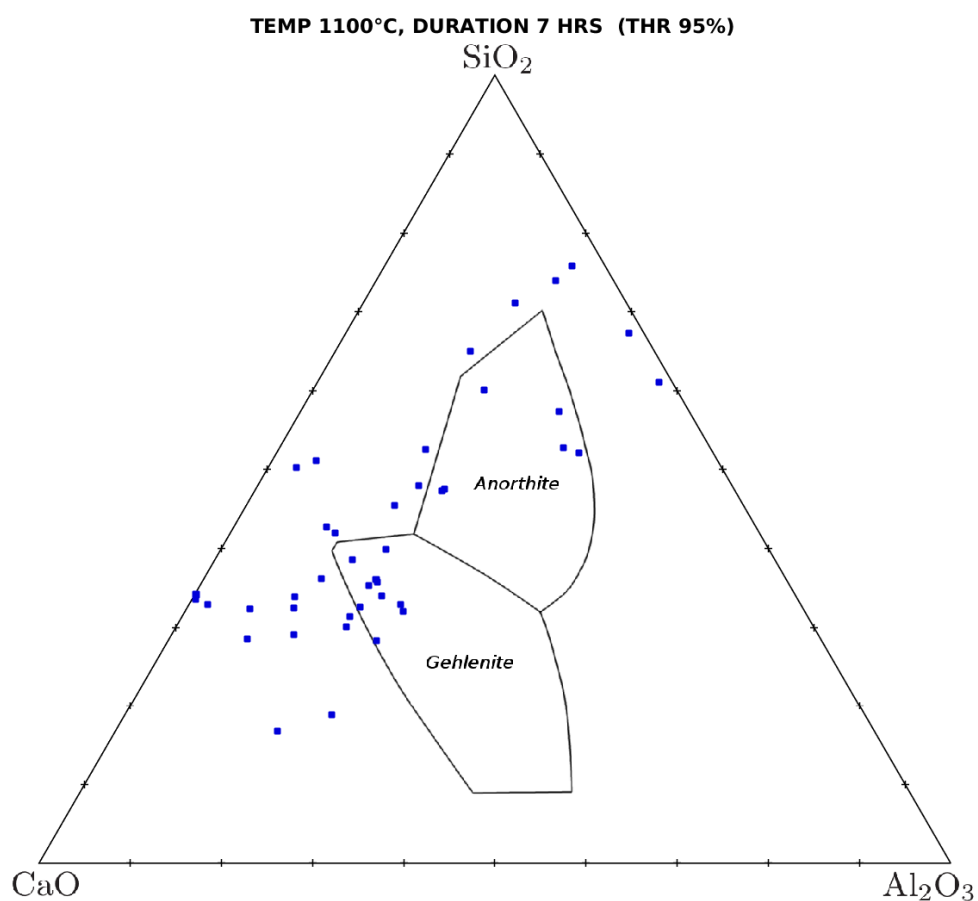


Figure 5.71: Ternary diagram with point analyses from the reaction rims that have a total higher than 95 % at 1100° C and a soaking time of 7h; 14 analyses plotting into the gehlenite stability field and five analyses plotting into the anorthite stability field

— EPMA raw sample data, 1100°C, 7 hours —

Set/Pt	1/1.	2/1.	3/1.	4/1.	5/1.	6/1.	7/1.	8/1.	9/1.	10/1.
SiO₂	46.60	46.49	46.33	43.34	48.55	52.45	53.70	53.47	33.10	18.18
TiO₂	0.14	0.13	0.16	1.54	0.53	0.31	0.47	0.47	0.05	0.08
Al₂O₃	17.10	20.25	20.11	13.32	4.60	25.93	24.84	32.76	0.39	21.95
Cr₂O₃	bdl	0.04	bdl	0.05	bdl	0.02	bdl	bdl	0.04	bdl
FeO	0.95	1.05	0.92	8.94	1.06	2.46	5.15	3.45	0.17	1.40
CaO	33.37	31.09	31.39	25.86	41.83	13.03	1.32	1.32	65.24	56.70
MgO	0.45	0.36	0.33	6.91	1.00	0.93	4.31	3.18	0.03	0.05
MnO	0.05	0.02	0.04	0.11	0.08	bdl	0.04	0.02	bdl	bdl
K₂O	0.03	0.02	bdl	0.13	0.10	1.59	5.43	4.74	bdl	bdl
Na₂O	0.08	bdl	bdl	0.03	0.05	1.61	0.92	0.88	0.04	bdl
P₂O₅	bdl	bdl	bdl	bdl	bdl	bdl	bdl	bdl	bdl	bdl
Total	98.77	99.45	99.30	100.23	97.80	98.35	96.19	100.30	99.08	98.38

Set/Pt	11/1.	12/1.	13/1.	14/1.	15/1.	17/1.	18/1.	19/1.	51/1.	52/1.
SiO₂	13.44	27.01	66.69	66.95	28.04	54.19	31.20	28.56	31.18	35.50
TiO₂	1.64	0.03	bdl	bdl	0.08	1.51	0.25	0.05	0.20	0.24
Al₂O₃	14.27	21.82	17.70	18.14	8.43	16.95	10.20	17.74	6.76	13.86
Cr₂O₃	0.02	bdl	bdl	bdl	bdl	bdl	0.03	bdl	bdl	bdl
FeO	16.33	1.39	0.89	1.01	0.48	3.90	3.23	1.87	1.88	3.08
CaO	52.62	46.53	5.76	3.21	61.63	19.04	50.73	48.62	58.52	42.56
MgO	0.69	1.60	0.39	0.65	0.11	1.33	3.16	2.01	0.55	3.73
MnO	0.45	bdl	bdl	0.02	bdl	0.06	0.03	bdl	bdl	0.06
K₂O	bdl	0.05	5.20	6.65	0.02	0.94	0.03	bdl	bdl	0.03
Na₂O	bdl	0.02	1.56	1.45	0.04	0.49	bdl	0.03	0.03	bdl
P₂O₅	bdl	bdl	bdl	bdl	bdl	bdl	bdl	bdl	0.04	bdl
Total	99.46	98.47	98.20	98.08	98.84	98.42	98.85	98.90	99.17	99.06

Set/Pt	53/1.	54/1.	55/1.	56/1.	57/1.	58/1.	59/1.	60/1.	61/1.	62/1.
SiO₂	40.12	44.01	35.54	29.70	31.17	30.62	31.17	33.69	34.30	33.89
TiO₂	0.52	0.32	0.39	0.20	0.39	0.13	0.06	0.06	0.08	0.23
Al₂O₃	9.49	15.67	16.11	17.49	16.31	22.86	11.21	0.10	12.23	18.29
Cr₂O₃	bdl	bdl	bdl	bdl	bdl	bdl	bdl	bdl	bdl	bdl
FeO	2.17	1.35	5.31	1.94	4.47	1.82	1.07	0.13	0.77	2.18
CaO	44.21	37.04	37.37	47.65	40.74	42.12	53.50	64.84	48.33	42.66
MgO	2.36	1.42	5.50	2.46	5.51	1.72	1.64	0.09	3.68	2.04
MnO	0.04	0.02	0.08	bdl	0.02	bdl	bdl	0.02	bdl	bdl
K₂O	bdl	0.04	0.03	0.05	0.05	0.05	0.03	bdl	0.04	0.07
Na₂O	bdl	bdl	bdl	bdl	bdl	bdl	bdl	bdl	bdl	bdl
P₂O₅	bdl	0.02	bdl	bdl	0.02	bdl	bdl	0.02	bdl	bdl
Total	98.92	99.89	100.34	99.50	98.70	99.35	98.71	98.95	99.43	99.38

continued on next page...

— EPMA raw sample data, 1100°C, 7 hours —

Set/Pt	63/1.	64/1.	65/1.	66/1.	67/1.	68/1.	69/1.	70/1.	14/1.	15/1.
SiO₂	33.81	30.67	30.23	27.69	47.15	33.22	39.93	33.99	33.58	30.95
TiO₂	0.05	0.14	0.07	0.07	0.26	0.16	0.10	bdl	0.10	0.17
Al₂O₃	0.18	18.50	17.56	12.71	2.94	17.52	10.92	0.11	0.13	21.86
Cr₂O₃	bdl	bdl	bdl	bdl	bdl	bdl	bdl	bdl	bdl	bdl
FeO	0.12	3.58	2.31	1.95	1.69	3.20	1.47	0.17	0.12	2.12
CaO	65.07	40.93	44.96	54.72	43.74	41.36	44.27	65.11	64.49	41.25
MgO	0.04	4.25	3.71	0.36	1.87	3.75	2.38	0.11	0.03	1.67
MnO	0.02	0.03	0.03	bdl	0.11	0.05	0.04	0.05	bdl	0.05
K₂O	bdl	0.03	0.03	bdl	0.15	0.03	0.02	bdl	bdl	0.12
Na₂O	bdl	bdl	0.05	bdl	0.12	0.04	0.02	bdl	bdl	0.13
P₂O₅	0.07	bdl	bdl	0.06	0.08	0.04	bdl	0.08	bdl	bdl
Total	99.39	98.14	98.94	97.56	98.11	99.37	99.17	99.66	98.46	98.31

Set/Pt	16/1.	17/1.	18/1.	19/1.	20/1.	21/1.
SiO₂	63.35	57.61	32.04	34.03	49.07	48.67
TiO₂	0.68	1.25	0.08	0.12	0.26	0.21
Al₂O₃	14.85	13.17	2.00	17.82	31.19	28.71
Cr₂O₃	bdl	bdl	bdl	bdl	bdl	bdl
FeO	2.31	3.76	0.55	1.98	2.51	2.07
CaO	10.82	17.86	63.48	42.61	13.84	14.83
MgO	0.86	2.01	0.20	2.30	0.27	0.55
MnO	0.04	0.06	0.04	0.02	bdl	0.04
K₂O	3.54	1.94	bdl	0.03	1.00	0.74
Na₂O	0.89	0.57	0.02	0.04	1.68	1.19
P₂O₅	bdl	bdl	bdl	bdl	bdl	bdl
Total	97.33	98.22	98.41	98.94	99.82	97.00

Table 5.12: EPMA raw sample data in wt%, firing temperature 1100°C, soaking time 7 hours. (bdl = below detection limit.)

5.3.4 9 hours soaking time

The sample fired for 9 hours at peak temperature shows sintered paste with calcite relicts surrounded by reaction rim with OM; Fig. 5.72. Upon closer look with BSE images completely sintered paste flowing around quartz grains with blurry boundaries can be seen; Fig. 5.74(a). Calcite grains have mostly decomposed with either relicts of calcite or a hole flanked by reactions rims remaining; Fig. 5.74(b). Very few big calcites of about 600 µm diameter appear healthy with almost no signs of decomposition. They show small reaction rims and signs of shrinking, see Fig. 5.74(d). Reaction rims form irregularly around all grains, reaching a diameter of max. 120 µm. The close-up into a reaction rim shows both zoning and spongy areas, displaying an inhomogeneous distribution of Ca; Fig. 5.74(c).

XRD analysis of both the sample containing calcite as well as the one without, increased amounts of amorphous phases can be seen in the rising background noise. Formation of new phases can be seen in both specimen, but are more abundant in the calcite containing one. Both gehlenite and anorthite could be identified; Fig. 5.73.

Point analyses into the calcite with signs of breakdown (Fig. 5.74(d)) show an overall increased amount of CaO, but no trend of the CaO distribution within the grain. Analyses into the re-

action rims found both gehlenite and possible anorthite (Fig. 5.74(b)). Further points analyzed that surpassed the threshold of 95 wt% total were listed in table reftab:rawdata-noco2-thr95-rot-1100deg-9hrs and plotted in the $\text{CaO} - \text{SiO}_2 - \text{Al}_2\text{O}_3$ phase diagram, plotting both in the gehlenite and anorthite stability field; Fig. 5.76. Elemental mapping in false color into one of the reaction rims can be seen in Fig. 5.75. Ca shows distinct zoning, as it migrates into the paste. Si and Al progress into the grain, with Al having more advanced than Si. The former grain boundaries cannot be identified anymore.

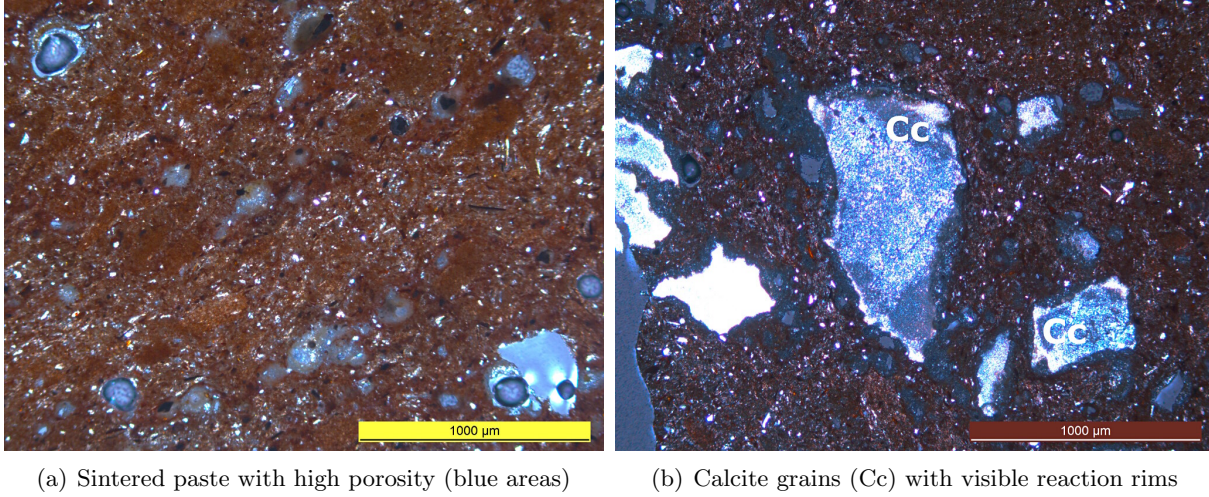


Figure 5.72: Paste and calcite grain with visible reaction rims in the sample fired at 1100°C, 9 h

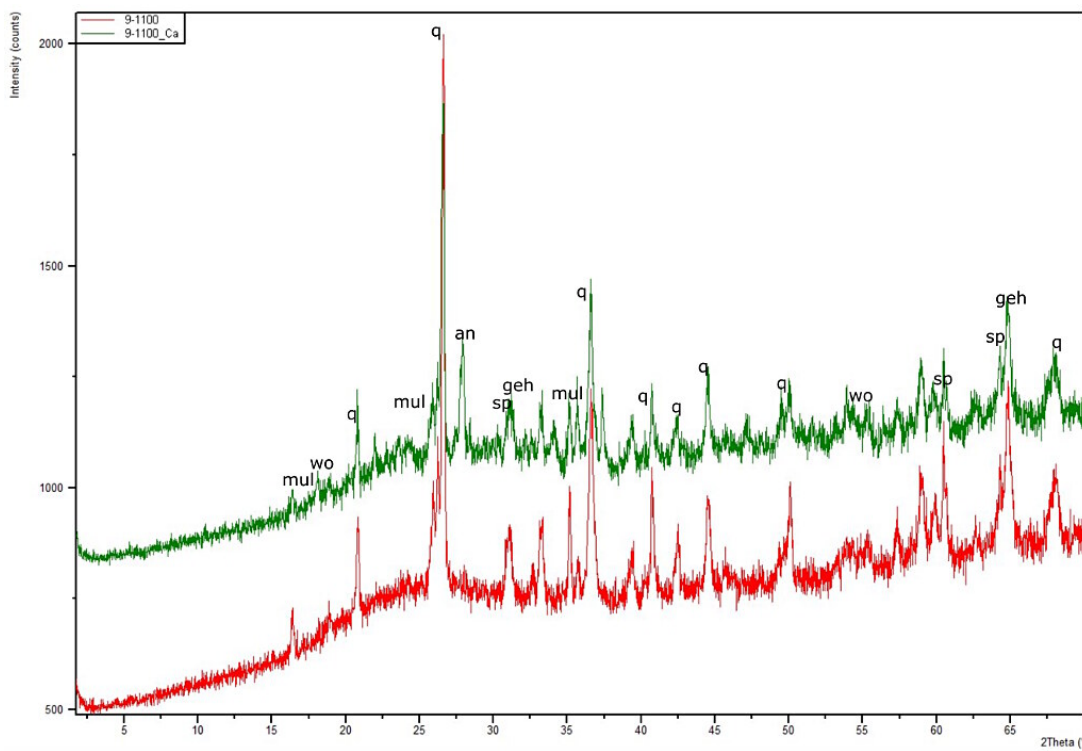
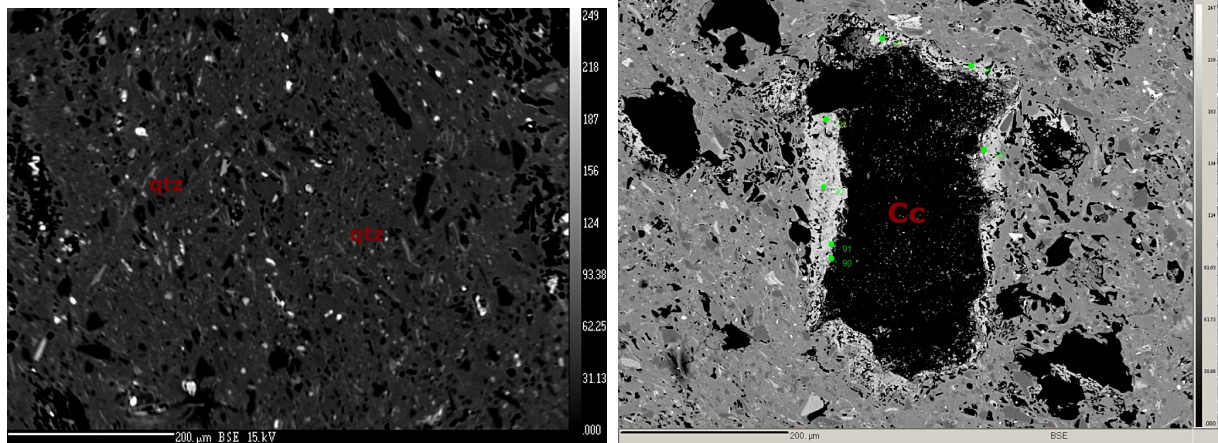
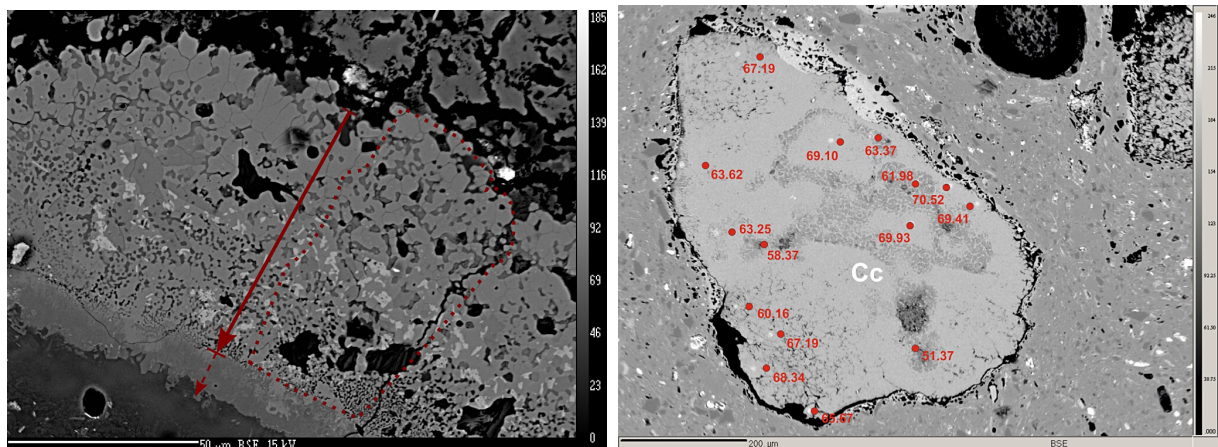


Figure 5.73: Combined XRD-diagrams of specimen soaked for 9 hours at 1100°C with CaCO_3 (green) and without CaCO_3 (red); q: quartz, mul: mullite, an: anorthite, geh: gehlenite, wo: (pseudo)wollastonite



(a) Sintered paste flowing around quartz grains, quartz grains can still be identified, but have continued to get smaller with increasing soaking time; qtz: quartz

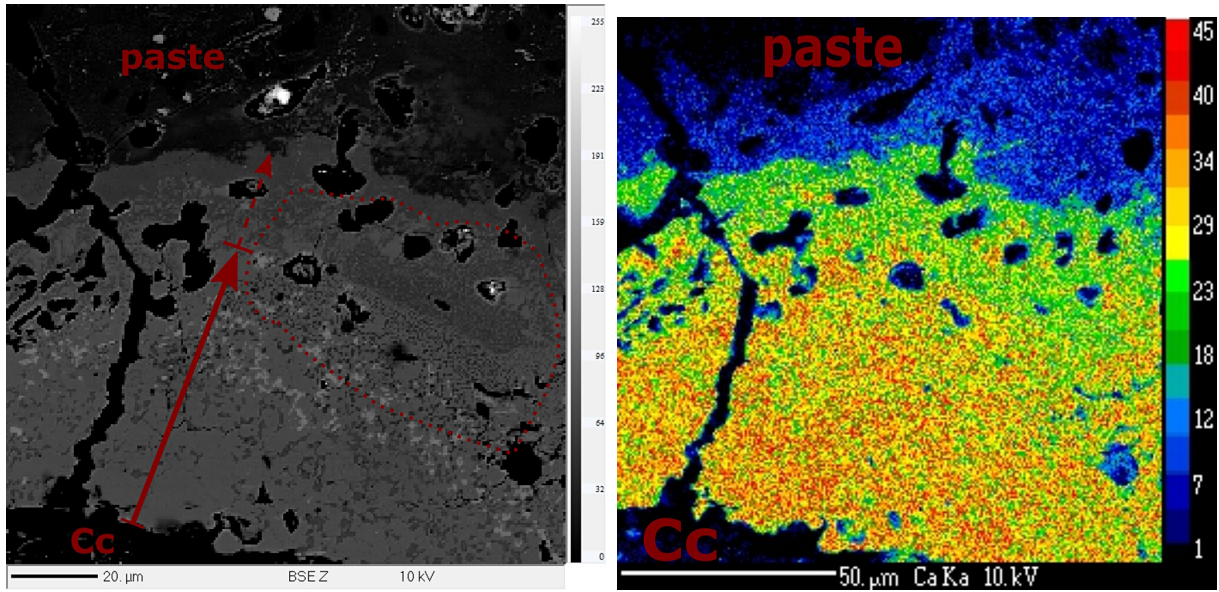
(b) Completely decomposed calcite grain (Cc), leaving only the reaction rim surrounding a hole; high porosity in the paste (black)



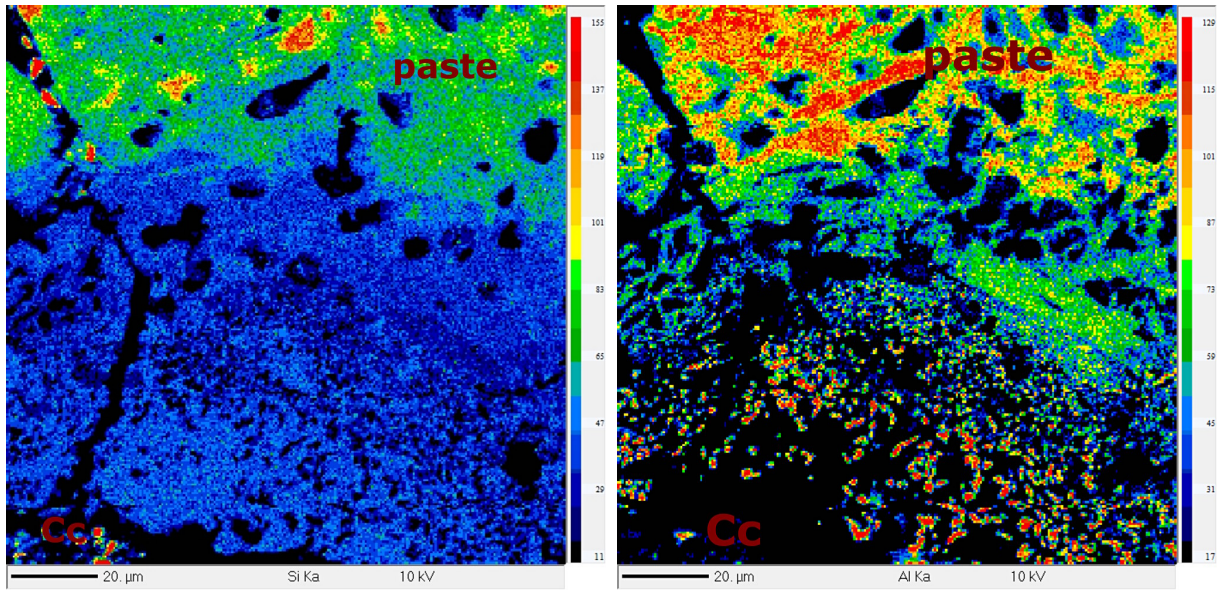
(c) Close-up into one reaction rim, showing zones and a spongy area; relict of calcite in the upper right corner; the former grain boundaries cannot be determined anymore; the red arrow indicates the zone with higher Ca content, the dashed arrow indicates the zones with lower Ca content; the dotted line highlights the spongy area, showing the inhomogeneous Ca distribution within the zone containing more Ca

(d) Coarse calcite with signs of shrinking and a reaction rim, no sign of decomposition; CaO distribution in wt% showing no trend from the core of the grain to the rim; numbers indicate EPMA point analyses

Figure 5.74: Paste and different calcite grains with reaction rims; 1100°C, 9 hours



(a) Elemental mapping BSE; close-up into the rim; red arrow: zone with higher Ca (closer to the decomposed calcite grain (Cc)), dashed arrow: zone with lower Ca (closer to the paste), dotted line highlights the spongy area
 (b) Elemental mapping for Ca, showing a diffusion of Ca into the paste in zones; yellow/red zone and green zone represent the rim, the blue zone show the diffusion further into the paste



(c) Elemental mapping for Si, diffusion of Si moving much slower than Ca into the grain
 (d) Elemental mapping for Al, spongy area closer to the calcite grain shows increased Al; Al diffuses is less homogeneous than Ca or Si

Figure 5.75: Elemental mapping of a reaction rim, indicated by the red and dashed arrow; the calcite grain (Cc) is completely decomposed

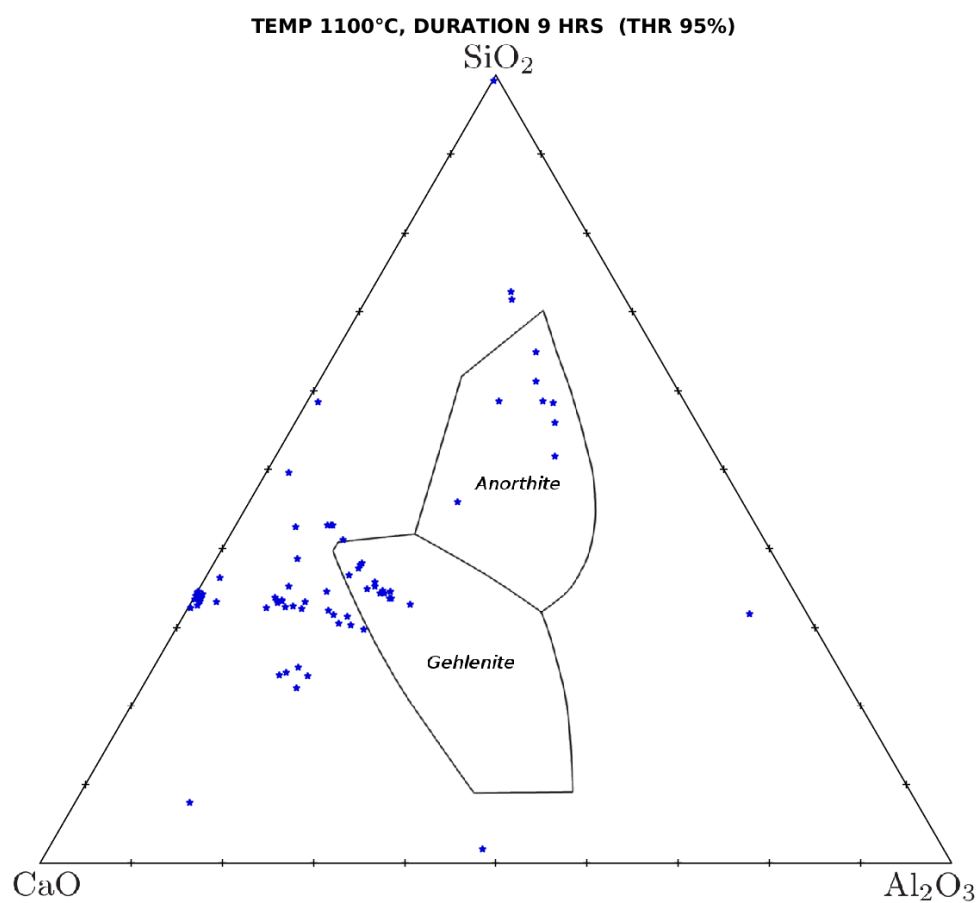


Figure 5.76: Ternary diagram with point analyses from the reaction rims that have a total higher than 95 % at 1100° C and a soaking time of 9 h; plotting into the stability fields of gehlenite (13 points) and anorthite (eight points)

— EPMA raw sample data, 1100°C, 9 hours —

Set/Pt	1/1.	1/1.	2/1.	3/1.	4/1.	5/1.	6/1.	7/1.	8/1.	9/1.
SiO₂	1.64	37.98	33.73	34.33	33.86	33.71	4.33	33.63	32.99	31.80
TiO₂	bdl	0.20	0.30	0.20	0.04	0.13	4.19	0.10	0.08	bdl
Al₂O₃	44.61	8.94	14.30	14.82	0.74	0.18	7.12	0.30	0.88	10.41
Cr₂O₃	bdl	bdl	bdl	bdl	bdl	bdl	bdl	bdl	bdl	bdl
FeO	2.10	3.48	3.61	3.21	0.25	0.19	33.08	0.19	0.12	0.34
CaO	47.36	41.53	40.82	42.35	64.48	64.59	45.00	64.84	65.04	55.49
MgO	1.21	6.88	5.65	3.97	0.15	0.05	1.28	0.03	0.02	1.47
MnO	0.02	0.03	0.02	bdl	bdl	bdl	0.74	bdl	bdl	bdl
NiO	bdl	bdl	bdl	bdl	bdl	bdl	bdl	bdl	bdl	bdl
K₂O	bdl	0.04	0.03	0.03	bdl	bdl	bdl	bdl	bdl	bdl
Na₂O	bdl	0.03	0.07	bdl	0.13	0.10	0.06	0.04	0.04	0.05
SO₂	bdl	bdl	bdl	bdl	0.02	0.04	0.06	0.05	0.18	bdl
Total	96.97	99.11	98.53	98.93	99.69	99.01	95.87	99.18	99.36	99.58

Set/Pt	10/1.	11/1.	12/1.	13/1.	14/1.	15/1.	16/1.	17/1.	18/1.	19/1.
SiO₂	32.51	59.68	55.44	62.69	54.23	33.67	65.07	32.47	33.84	33.62
TiO₂	0.03	0.37	0.71	0.99	0.48	0.08	0.72	0.21	0.08	0.14
Al₂O₃	9.60	20.25	21.62	14.03	23.88	0.35	13.82	18.97	0.03	0.16
Cr₂O₃	bdl	bdl	bdl	bdl	bdl	bdl	bdl	bdl	bdl	bdl
FeO	0.31	1.44	2.56	3.08	2.75	0.11	2.36	2.85	0.30	0.28
CaO	55.21	12.08	13.60	10.90	14.40	65.07	10.80	42.24	64.40	64.67
MgO	1.91	0.45	0.75	0.75	0.59	bdl	0.66	2.04	0.09	0.09
MnO	bdl	0.04	0.03	0.03	bdl	bdl	0.04	bdl	0.03	bdl
NiO	bdl	bdl	bdl	bdl	bdl	bdl	bdl	bdl	bdl	bdl
K₂O	bdl	3.15	2.48	4.15	1.94	bdl	4.18	0.04	0.03	0.02
Na₂O	0.09	1.29	1.21	0.96	1.22	0.04	0.80	0.09	bdl	0.03
SO₂	bdl	bdl	bdl	bdl	0.02	0.08	bdl	bdl	0.03	bdl
Total	99.69	98.75	98.42	97.58	99.51	99.42	98.45	98.93	98.82	99.01

Set/Pt	20/1.	21/1.	22/1.	23/1.	24/1.	25/1.	26/1.	27/1.	28/1.	29/1.
SiO₂	40.34	34.20	31.65	51.71	40.48	48.09	32.87	39.52	31.40	32.03
TiO₂	0.17	0.02	0.22	0.33	0.21	0.18	0.12	0.10	0.03	0.08
Al₂O₃	9.92	0.07	18.99	26.37	9.85	2.42	17.40	12.26	11.82	2.61
Cr₂O₃	bdl	bdl	bdl	bdl	bdl	bdl	bdl	bdl	bdl	bdl
FeO	1.84	0.13	2.57	2.46	1.70	0.48	2.78	1.02	1.49	1.40
CaO	43.61	64.70	41.53	14.33	43.95	46.34	41.78	44.49	51.30	61.82
MgO	2.91	0.08	3.41	0.55	2.48	1.39	3.48	1.78	2.82	0.18
MnO	0.05	bdl	0.04	bdl	0.06	0.04	0.05	bdl	bdl	0.06
NiO	bdl	bdl	bdl	bdl	bdl	bdl	bdl	bdl	bdl	bdl
K₂O	0.03	0.02	0.05	1.49	bdl	0.04	0.03	bdl	0.02	bdl
Na₂O	0.04	bdl	0.03	1.58	0.11	bdl	0.10	0.14	0.04	bdl
SO₂	bdl	bdl	bdl	bdl	bdl	bdl	bdl	bdl	0.03	0.09
Total	98.92	99.25	98.50	98.85	98.86	98.98	98.61	99.32	98.94	98.28

continued on next page...

— EPMA raw sample data, 1100°C, 9 hours —

Set/Pt	30/1.	1/1.	2/1.	3/1.	4/1.	5/1.	6/1.	7/1.	92/1.	95/1.
SiO₂	32.63	30.24	21.84	33.69	33.42	31.84	51.52	50.01	30.09	29.49
TiO₂	0.16	0.21	0.16	0.03	0.10	0.08	bdl	1.43	0.12	0.10
Al₂O₃	0.78	14.67	16.63	0.04	0.38	0.27	bdl	7.48	15.66	17.02
Cr₂O₃	bdl	bdl	bdl	bdl	bdl	0.05	bdl	bdl	bdl	bdl
FeO	1.08	2.64	1.01	0.10	0.06	0.14	bdl	8.27	1.21	1.75
CaO	63.62	49.31	59.38	65.37	65.13	66.01	48.37	17.44	49.59	47.60
MgO	0.19	2.78	0.04	0.09	bdl	0.08	0.06	12.38	2.61	2.03
MnO	0.04	bdl	bdl	bdl	bdl	bdl	bdl	0.14	bdl	bdl
NiO	bdl	bdl	bdl	bdl	bdl	0.02	bdl	bdl	bdl	bdl
K₂O	bdl	bdl	bdl	0.02	bdl	bdl	bdl	bdl	0.03	0.10
Na₂O	0.03	bdl	bdl	bdl	bdl	bdl	bdl	2.43	0.08	bdl
SO₂	0.02	bdl	bdl	bdl	bdl	bdl	bdl	bdl	bdl	bdl
Total	98.55	99.86	99.07	99.37	99.14	98.50	99.99	99.60	99.40	98.09

Set/Pt	96/1.	98/1.	99/1.	103/1.	104/1.	105/1.	106/1.	107/1.	108/1.	110/1.
SiO₂	28.40	21.12	32.32	32.89	31.76	31.26	99.03	31.44	31.76	30.84
TiO₂	0.16	0.04	bdl	0.09	0.04	0.26	0.03	0.06	0.26	0.13
Al₂O₃	19.71	41.30	9.27	13.48	8.44	19.87	0.08	10.93	18.61	12.02
Cr₂O₃	bdl	bdl	bdl	bdl	bdl	bdl	bdl	bdl	bdl	bdl
FeO	1.10	24.84	0.26	1.56	0.40	1.81	0.08	1.68	3.30	1.67
CaO	47.36	4.25	56.16	48.84	57.77	41.58	0.60	53.68	42.08	52.61
MgO	2.05	3.00	1.11	2.72	0.96	2.10	0.04	1.83	2.75	1.52
MnO	bdl	bdl	bdl	bdl	bdl	bdl	bdl	bdl	bdl	bdl
NiO	bdl	bdl	bdl	bdl	bdl	bdl	bdl	bdl	bdl	bdl
K₂O	0.05	1.18	0.06	0.05	bdl	0.06	bdl	bdl	0.03	0.04
Na₂O	0.03	0.72	bdl	bdl	bdl	0.03	bdl	bdl	0.03	bdl
SO₂	bdl	bdl	bdl	bdl	bdl	bdl	bdl	bdl	bdl	bdl
Total	98.86	96.45	99.19	99.63	99.37	96.96	99.87	99.63	98.81	98.85

Set/Pt	111/1.	112/1.	113/1.	114/1.	115/1.	116/1.	117/1.	118/1.	119/1.	120/1.
SiO₂	32.34	42.93	33.93	32.56	31.76	32.51	22.45	31.84	23.62	29.62
TiO₂	0.27	0.21	bdl	0.05	0.10	0.27	0.11	0.20	0.06	0.07
Al₂O₃	13.80	21.42	9.35	9.13	0.88	19.91	16.39	23.34	15.05	17.05
Cr₂O₃	bdl	bdl	bdl	bdl	bdl	bdl	bdl	bdl	bdl	bdl
FeO	3.88	2.19	0.95	0.19	0.14	2.32	1.10	1.10	1.06	0.84
CaO	42.26	29.28	53.26	55.93	64.33	41.70	55.29	41.51	56.20	50.53
MgO	6.32	2.35	2.68	1.59	bdl	2.44	0.09	1.25	0.10	1.77
MnO	bdl	bdl	bdl	bdl	bdl	bdl	bdl	bdl	bdl	bdl
NiO	bdl	bdl	bdl	bdl	bdl	bdl	bdl	bdl	bdl	bdl
K₂O	0.05	0.76	0.03	0.03	bdl	0.07	0.04	0.06	bdl	bdl
Na₂O	bdl	0.33	bdl	0.02	0.04	0.09	bdl	0.11	bdl	0.06
SO₂	bdl	bdl	bdl	bdl	bdl	bdl	bdl	bdl	bdl	bdl
Total	98.93	99.47	100.22	99.52	97.27	99.31	95.48	99.41	96.09	99.95

continued on next page...

— EPMA raw sample data, 1100°C, 9 hours —

Set/Pt	122/1.	123/1.	124/1.	125/1.	126/1.	127/1.	128/1.	129/1.	22/1.	23/1.
SiO₂	29.06	32.68	22.55	32.39	23.09	32.35	34.52	32.50	33.22	33.06
TiO₂	0.02	0.11	0.11	0.02	0.07	0.05	0.11	0.12	0.16	0.11
Al₂O₃	18.17	17.34	13.41	8.52	14.11	9.53	7.94	17.67	0.38	0.19
Cr₂O₃	bdl	bdl	bdl	bdl	bdl	bdl	bdl	bdl	bdl	bdl
FeO	1.42	2.02	0.93	0.83	1.04	0.48	2.25	2.94	0.13	0.13
CaO	48.64	43.82	58.06	55.02	57.99	55.15	46.69	42.23	64.96	65.18
MgO	2.17	2.43	bdl	2.14	bdl	1.95	4.28	3.10	0.03	0.03
MnO	bdl	bdl	bdl	bdl	bdl	bdl	bdl	bdl	bdl	bdl
NiO	bdl	bdl	bdl	bdl	bdl	bdl	bdl	bdl	bdl	bdl
K₂O	0.02	bdl	bdl	0.03	bdl	0.02	0.06	0.08	bdl	bdl
Na₂O	0.08	0.09	bdl	0.04	bdl	0.11	0.09	0.03	bdl	bdl
SO₂	bdl	bdl	bdl	bdl	bdl	bdl	bdl	bdl	bdl	bdl
Total	99.59	98.50	95.10	99.00	96.32	99.64	95.94	98.66	98.86	98.71

Set/Pt	24/1.	25/1.	26/1.	27/1.	28/1.	29/1.	30/1.	31/1.
SiO₂	36.71	51.32	52.93	33.66	36.56	48.44	31.33	54.96
TiO₂	0.18	1.11	0.37	0.20	0.21	0.25	0.17	bdl
Al₂O₃	5.73	18.39	24.51	1.47	15.57	28.73	20.21	1.13
Cr₂O₃	bdl	bdl	bdl	bdl	bdl	bdl	bdl	bdl
FeO	4.35	3.73	2.39	0.94	1.65	2.57	4.15	0.16
CaO	43.39	17.81	13.04	57.65	43.71	16.64	41.47	37.85
MgO	8.47	1.11	0.58	4.91	1.88	0.38	2.56	0.55
MnO	0.09	0.04	bdl	0.02	0.04	bdl	0.04	0.02
NiO	bdl	bdl	bdl	bdl	bdl	bdl	bdl	bdl
K₂O	0.06	1.20	1.97	0.03	bdl	0.67	bdl	0.28
Na₂O	0.07	0.99	1.13	0.03	0.02	1.17	0.03	0.06
SO₂	bdl	bdl	bdl	bdl	bdl	bdl	bdl	bdl
Total	99.03	95.70	96.94	98.90	99.65	98.83	99.96	95.03

Table 5.13: EPMA raw sample data in wt%, firing temperature 1100°C, soaking time 9 hours. (bdl = below detection limit.)

5.4 Archaeological samples

Archaeological samples were provided by the ÖAI. In order to maximize the possibility of finding gehlenite and apply the results of this thesis' experiments, sherds were requested to fulfill two requirements. First, they must contain calcite, and second, according to archaeological interpretation, they should have been fired at temperatures of 900° C or more. All sherds we received are from Velia, Italy, and were supposedly pre-analyzed by ÖAI with XRF and OM, even though results of those analysis were not provided.

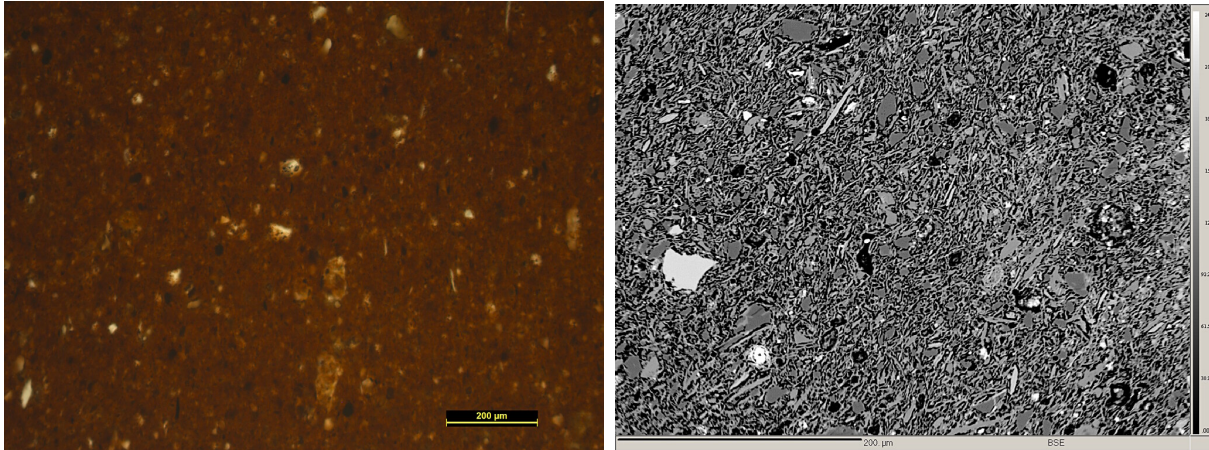
Polished and carbon-coated thin section were produced water-free and studied by OM and EMPA. The specimen were too small to provide enough material for XRD analysis, instead they were analysed with INAA, see the table in Tab. 5.14, showing low amount of Sr, indicating no carbonates are included in those samples; see Fig. 6.4.

	M2/104	M2/127	M2/138	M2/157	M2/161
Na₂O	3.25	0.85	1.61	0.96	1.44
K₂O	4.31	3.64	5.08	3.03	2.92
Sc	25.2	21.3	18.0	15.4	13.6
Cr	546	147	104	110	105
FeO	8.38	7.16	5.02	5.57	5.45
Co	41.2	26.9	16.9	18.3	17.0
Ni	384	67.3	42.0	66.9	59.4
Zn	160	142	122	150	117
As	40.8	20.2	11.0	3.299	7.25
Rb	178	173	228	172	169
Sr	311	186	202	182	383
Zr	140	180	201	198	258
Sb	1.821	1.121	0.793	0.547	0.927
Cs	15.1	9.55	13.0	9.77	18.0
Ba	570	679	711	611	656
La	79.7	48.8	64.4	45.1	62.7
Ce	83.5	96.5	96.2	86.4	117
Nd	28.3	41.8	38.0	26.3	49.3
Sm	14.0	8.18	9.09	7.22	8.91
Eu	1.523	1.739	1.462	1.361	1.683
Tb	0.861	0.867	0.956	0.761	0.825
Yb	2.968	3.252	3.592	2.725	2.837
Lu	0.912	0.519	0.674	0.456	0.414
Hf	3.824	5.68	6.18	5.06	6.09
Ta	0.983	1.439	1.742	1.321	1.427
W	3.031	bdl	3.299	1.416	2.190
Th	13.1	15.3	19.7	14.9	26.8
U	3.924	4.317	5.32	3.356	4.501

Table 5.14: INAA results for all archaeological samples; bdl = below detection limit; oxides in wt%, all others ppm.

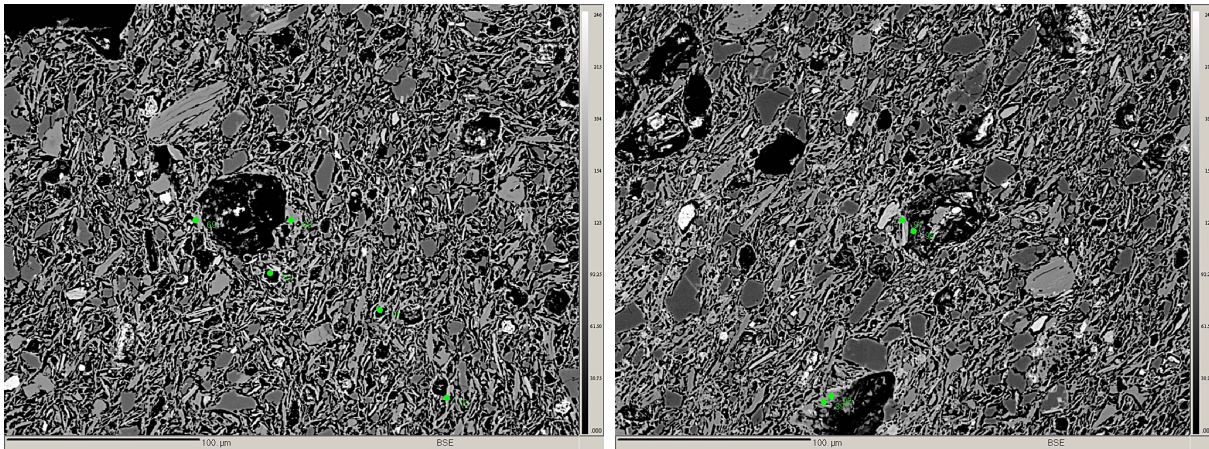
5.4.1 M2/104

M2/104 shows a finely grain paste with beginning of sintering and high porosity (Fig. 5.77(a)). The grain size of the minerals reaches up to $50\text{ }\mu\text{m}$. Quartz and feldspar can be identified, as well as possibly some relict mica (see Fig. 5.77(b)). Even though holes with relicts of a decomposed mineral surrounded by a reaction rim could be found, only little CaO could be detected, Fig. 5.77(c) and (d), and in a composition that fits neither calcite, gehlenite, anorthite nor wollastonite. All point analyses have been listed in table 5.15.



(a) Thin section of samples M2/104, showing finely grained paste and minerals with distinct grain boundaries

(b) Fine grained minerals and sintering effects within the paste



(c) Reaction rim around a decomposed mineral

(d) Another reaction rim with very little CaO

Figure 5.77: Archaeological sherd M2/104

Set/Pt	68/1.	69/1.	70/1.	71/1.	72/1.	73/1.	74/1.	75/1.	76/1.	77/1.
SiO₂	47.08	51.38	30.36	45.18	48.34	31.10	49.04	39.35	45.34	42.00
TiO₂	0.08	0.47	0.31	0.18	0.37	0.23	0.20	0.64	0.13	0.69
Al₂O₃	32.47	32.37	16.85	19.79	26.82	20.30	14.85	16.56	23.35	23.95
FeO	2.21	2.31	12.52	6.17	2.46	16.82	4.07	6.41	14.85	4.76
CaO	1.42	0.31	15.41	8.13	11.19	8.60	19.37	22.18	1.49	18.90
MgO	2.02	2.17	6.60	5.45	1.67	16.99	1.73	2.77	10.74	2.91
K₂O	9.24	11.25	0.30	3.06	3.71	0.76	0.57	0.57	3.30	0.66
Na₂O	0.35	0.17	0.08	0.92	0.82	bdl	0.13	0.13	0.31	0.10
Total	94.88	100.42	82.43	88.89	95.36	94.82	89.96	88.61	99.51	93.95

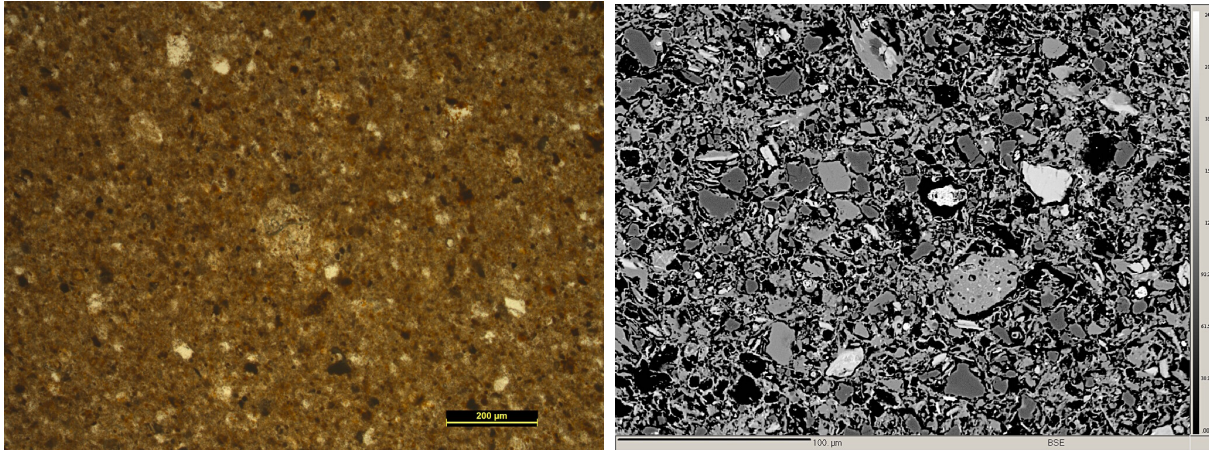
Set/Pt	78/1.	79/1.	80/1.	81/1.	82/1.	83/1.	84/1.	85/1.	86/1.	87/1.
SiO₂	44.95	50.78	32.63	32.99	41.92	39.13	43.90	38.34	41.67	38.69
TiO₂	0.20	0.67	0.22	0.24	0.23	0.30	0.59	0.40	0.10	1.06
Al₂O₃	24.12	28.57	18.57	22.08	24.61	25.54	15.51	20.50	17.56	15.84
FeO	12.46	2.84	3.19	2.59	6.11	4.57	10.74	5.06	13.56	7.43
CaO	3.10	1.17	23.68	31.48	15.92	16.43	15.99	25.03	4.99	19.14
MgO	9.93	3.99	2.58	2.21	3.75	2.39	4.21	5.63	16.87	5.30
K₂O	4.08	10.09	0.93	0.93	1.97	0.99	0.52	0.34	1.54	0.60
Na₂O	0.30	0.34	0.09	0.17	0.16	0.19	0.12	0.21	0.09	0.10
Total	99.14	98.44	81.89	92.69	94.68	89.53	91.58	95.53	96.38	88.16

Set/Pt	88/1.	89/1.	90/1.
SiO₂	37.52	50.94	46.50
TiO₂	0.37	0.14	0.61
Al₂O₃	16.74	20.17	26.95
FeO	10.32	10.46	4.91
CaO	14.41	1.91	4.41
MgO	4.99	11.73	3.53
K₂O	0.54	3.73	5.53
Na₂O	0.06	0.36	0.81
Total	84.94	99.42	93.24

Table 5.15: EPMA raw sample data in wt%, archaeological sample M2/104. (bdl = below detection limit.)

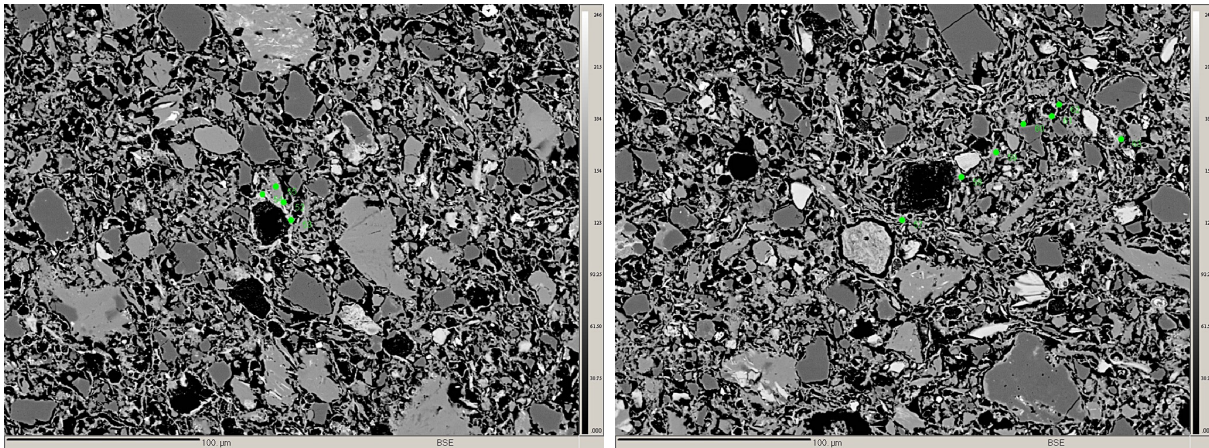
5.4.2 M2/127

Sample M2/127 (Fig. 5.78(a)) is finely grained with a maximum grain size of $50\text{ }\mu\text{m}$. Quartz and feldspar have well defined grain boundaries. The paste shows high porosity and partial sintering, Fig. 5.78(b). Relicts of decomposed minerals with small reactions can be found (see Fig. 5.78(c) and (d)), but as in M2/104, the small amount of CaO detected is never sufficient for calcite or a Ca-alumino-silicate. All point analyses have been listed in table 5.16.



(a) Thin section of samples M2/127, showing finely grained paste and minerals with distinct grain boundaries

(b) Finely grained, partially sintered paste with high porosity



(c) Decomposed mineral with narrow reaction rim

(d) Big calcite with a reaction rim and a crack beginning at the grain and moving into the paste

Figure 5.78: Archaeological sherd M2/127

Set/Pt	44/1.	45/1.	46/1.	47/1.	48/1.	49/1.	50/1.	51/1.	52/1.	53/1.
SiO₂	35.01	29.60	30.18	39.82	43.68	35.37	29.03	41.04	39.35	40.35
TiO₂	0.20	0.03	0.49	0.70	1.23	0.83	0.13	7.23	0.17	0.59
Al₂O₃	20.79	25.99	6.40	21.00	7.51	19.74	23.31	22.42	25.38	22.20
FeO	13.30	26.75	26.60	6.11	9.31	5.50	27.38	6.76	1.88	6.54
CaO	17.92	0.67	15.04	17.28	21.71	10.43	1.64	7.47	28.73	20.12
MgO	5.28	9.32	3.26	2.81	10.07	2.43	13.38	2.20	1.75	2.11
K₂O	0.29	2.99	0.30	0.34	0.10	1.08	1.03	3.03	0.39	0.40
Na₂O	0.09	0.38	0.05	0.51	0.32	0.62	0.06	0.91	0.24	0.11
Total	92.89	95.74	82.30	88.58	93.92	76.00	95.95	91.05	97.89	92.43

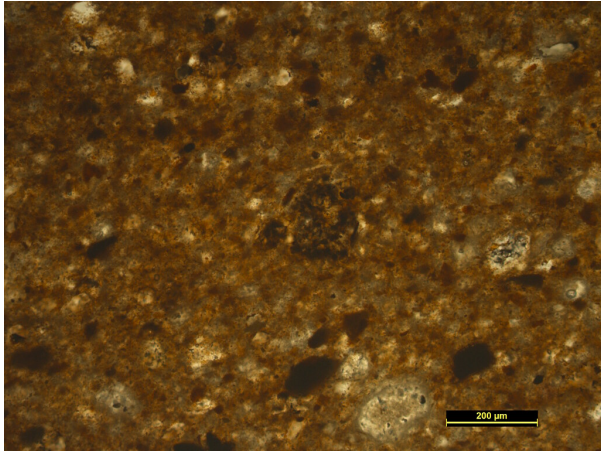
Set/Pt	54/1.	55/1.	56/1.	57/1.	58/1.	59/1.	60/1.	61/1.	62/1.	63/1.
SiO₂	28.61	46.88	44.88	40.48	44.28	44.23	46.50	40.49	42.85	30.21
TiO₂	0.35	4.90	0.31	0.57	0.28	1.63	0.96	0.62	0.27	19.73
Al₂O₃	18.55	29.86	27.86	21.04	21.88	24.57	24.99	17.93	18.73	19.38
FeO	20.06	2.38	2.43	5.53	5.37	4.48	11.03	5.84	6.70	8.01
CaO	9.15	3.88	6.00	9.69	15.30	14.35	4.61	14.90	16.16	5.47
MgO	7.70	1.91	2.09	2.63	2.10	1.89	4.67	2.39	2.74	3.13
K₂O	0.42	6.03	4.20	1.86	0.88	1.11	3.61	0.52	0.47	1.59
Na₂O	0.15	0.93	1.39	1.08	0.38	1.00	0.96	0.64	0.65	0.90
Total	84.99	96.77	89.18	82.88	90.46	93.25	97.32	83.32	88.57	88.42

Set/Pt	64/1.	65/1.	66/1.	67/1.
SiO₂	45.10	42.89	32.54	50.12
TiO₂	0.31	0.57	0.08	2.69
Al₂O₃	22.16	21.13	17.81	19.07
FeO	6.23	5.98	20.67	5.92
CaO	17.39	17.74	16.40	7.80
MgO	2.12	2.07	6.65	1.96
K₂O	0.65	0.25	0.24	3.24
Na₂O	0.28	0.22	0.06	1.02
Total	94.25	90.85	94.45	91.82

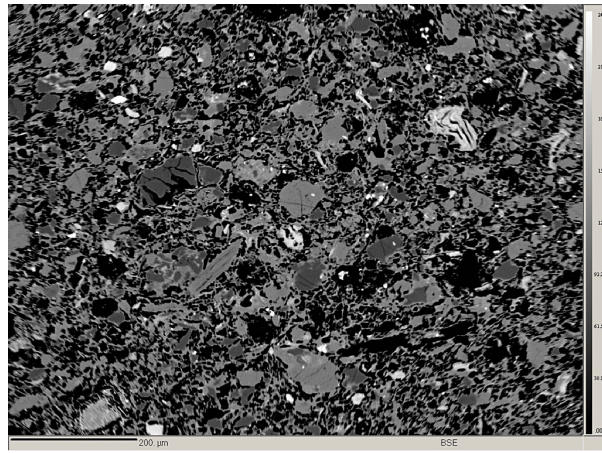
Table 5.16: EPMA raw sample data in wt%, archaeological sample M2/127. (bdl = below detection limit.)

5.4.3 M2/138

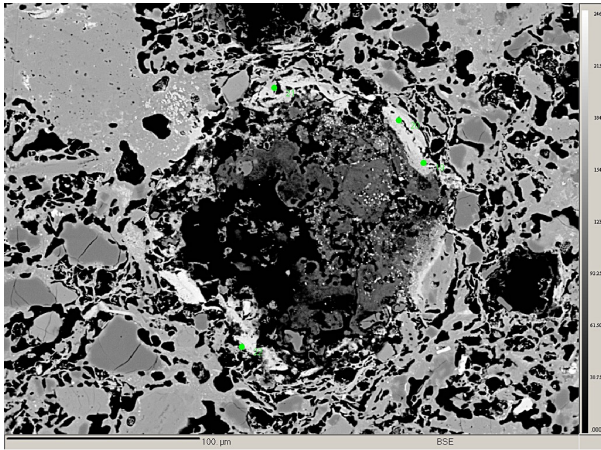
Sherd M2/138 presents slightly bigger grain sizes with grains of $150\text{ }\mu\text{m}$, which can be seen without any microscope (Fig. 5.79(a)). The paste is very well sintered (Fig. 5.79(b)), only quartz still maintains its boundaries. The boundaries are blurry and reaction with the paste can be found at some points, Fig. 5.79(c). As in M2/104 and M2/127, decomposed minerals with reaction rims can be found (Fig. 5.79(d)), but again measurements do not fit calcite, gehlenite or the higher temperature phases. All point analyses have been listed in table 5.17.



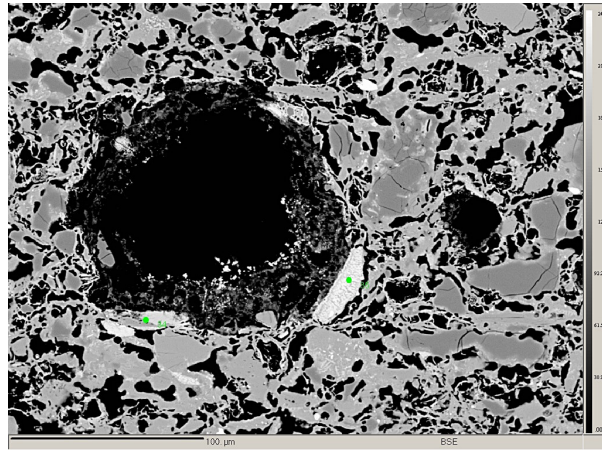
(a) Grains visible within the sample, displaying a coarser grain size than samples M2/104 and M2/127



(b) Well sintered paste with blurry grain boundaries



(c) Decomposed mineral with clearly visible reaction rim



(d) Reaction rim formed partially around decomposed mineral

Figure 5.79: Archaeological sherd M2/138

Set/Pt	1/1.	2/1.	3/1.	4/1.	5/1.	6/1.	7/1.	8/1.	9/1.	10/1.
SiO₂	27.36	28.74	37.73	31.63	37.88	26.70	27.25	23.22	34.10	35.42
TiO₂	0.09	0.20	1.05	1.30	1.22	0.15	0.17	0.22	0.15	0.29
Al₂O₃	22.47	20.05	16.53	14.74	18.66	22.14	24.44	18.75	21.70	21.85
FeO	33.33	29.90	21.59	21.47	22.87	31.16	27.79	29.92	21.79	11.88
CaO	0.57	0.56	0.79	0.58	2.21	1.82	1.27	1.34	0.92	23.32
MgO	7.93	10.73	9.92	9.65	9.52	9.47	12.23	14.99	11.58	5.54
K₂O	2.77	3.71	4.18	3.49	3.45	2.81	2.91	2.11	4.42	0.20
Na₂O	0.31	0.72	0.73	0.55	0.89	0.69	0.57	0.44	0.73	0.15
Total	94.83	94.60	92.51	83.41	96.69	94.95	96.64	90.98	95.40	98.65

Set/Pt	11/1.	12/1.	13/1.	14/1.	15/1.	16/1.	17/1.	18/1.	19/1.	20/1.
SiO₂	41.38	33.49	33.64	33.94	34.07	36.28	31.12	30.36	31.59	32.08
TiO₂	0.37	0.17	3.20	0.71	0.24	0.85	0.14	0.08	0.12	0.15
Al₂O₃	16.75	20.59	12.62	16.08	18.29	17.63	19.93	12.40	26.04	20.14
FeO	3.94	5.41	13.71	9.63	4.77	5.17	6.36	10.89	1.51	3.87
CaO	29.69	33.20	0.62	26.45	30.06	27.36	34.01	36.86	35.62	37.46
MgO	2.06	2.52	4.80	4.41	3.15	1.32	2.50	6.61	1.85	3.63
K₂O	0.14	0.18	2.95	0.12	0.14	0.23	0.23	0.06	0.16	0.21
Na₂O	0.05	0.14	0.29	bdl	0.11	bdl	bdl	0.06	0.04	0.04
Total	94.39	95.69	71.82	91.34	90.85	88.85	94.30	97.31	96.92	97.56

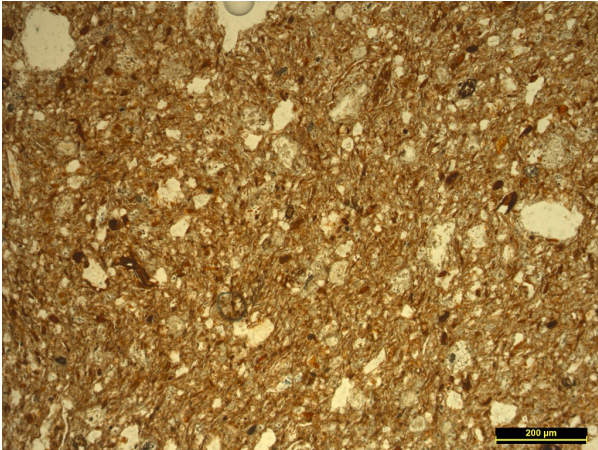
Set/Pt	21/1.	22/1.	23/1.	24/1.	25/1.	26/1.	27/1.	28/1.	29/1.	30/1.
SiO₂	32.95	25.91	50.22	47.24	43.00	41.70	44.42	29.24	34.72	31.34
TiO₂	0.09	0.23	0.17	0.23	0.35	2.42	0.89	1.87	0.17	0.09
Al₂O₃	23.51	15.16	27.20	20.96	21.93	17.36	20.40	15.20	16.64	16.68
FeO	2.90	6.69	2.40	5.10	5.10	9.10	8.15	8.66	4.01	18.07
CaO	37.64	31.21	15.16	18.40	26.80	20.78	20.73	38.34	39.55	21.29
MgO	0.98	3.31	1.83	5.69	2.20	5.51	3.90	4.13	2.46	4.39
K₂O	0.34	0.10	0.87	0.50	0.13	0.16	0.14	0.06	0.12	0.28
Na₂O	0.06	bdl	2.02	0.79	0.06	0.28	0.38	0.04	bdl	0.12
Total	98.47	82.61	99.86	98.92	99.57	97.31	99.01	97.53	97.67	92.25

Set/Pt	31/1.	32/1.	33/1.	34/1.	35/1.
SiO₂	35.39	50.43	40.16	31.50	37.34
TiO₂	0.15	0.31	0.32	bdl	0.04
Al₂O₃	18.64	25.37	21.52	26.78	20.83
FeO	5.13	4.65	5.85	0.41	22.25
CaO	35.01	7.24	20.61	39.79	5.62
MgO	2.21	2.94	4.75	0.08	5.81
K₂O	0.13	3.58	0.24	0.41	1.85
Na₂O	0.11	2.40	0.20	0.21	1.11
Total	96.79	96.91	93.66	99.18	94.84

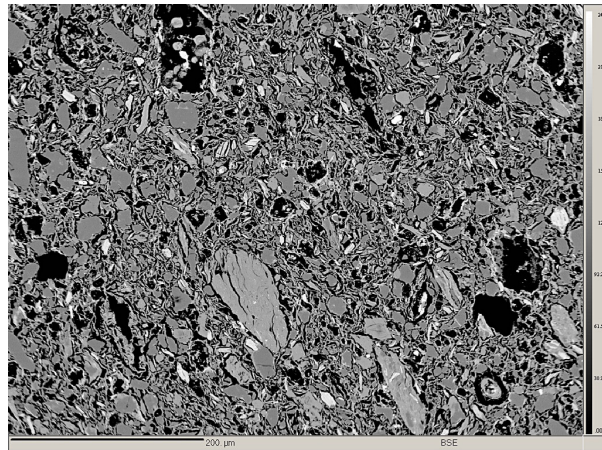
Table 5.17: EPMA raw sample data in wt%, archaeological sample M2/138. (bdl = below detection limit.)

5.4.4 M2/157

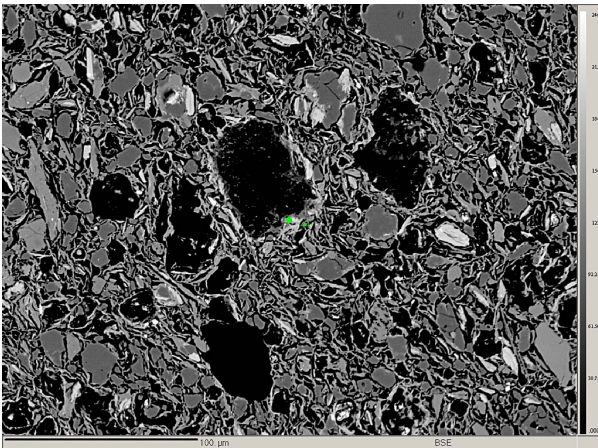
Sample M2/157 is finely grained with grain sizes up to $100\text{ }\mu\text{m}$ (Fig. 5.80(a)). The paste shows few signs of sintering and grain boundaries of quartz and feldspar are distinct, see Fig. 5.80(b). Relicts of decomposed minerals with narrow reaction rims can be found (Fig. 5.80(c)), some of which contain P_2O_5 . CaO has not been found in ratios to fit either calcite or the Ca-alumosilicates wanted. Local reactions involving the paste resulted in local sintering, see Fig. 5.80(d). All point analyses have been listed in table 5.18.



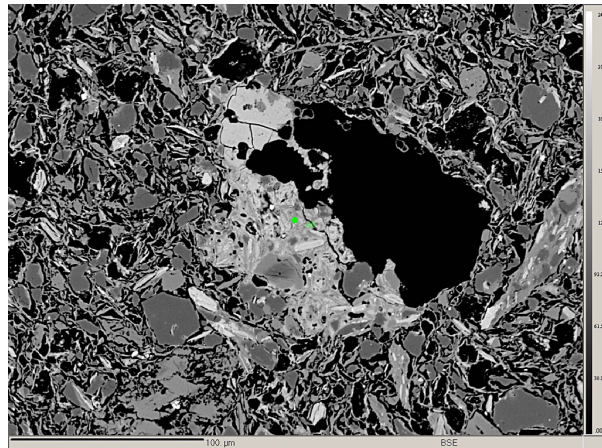
(a) Visible mineral grains within fine grained paste



(b) Paste with embedded minerals with distinct boundaries



(c) Relict of decomposed mineral with reaction rim



(d) Local sintering within the paste

Figure 5.80: Archaeological sherd M2/157

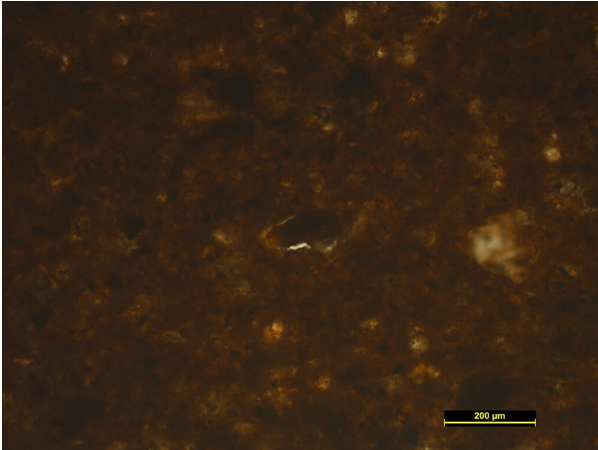
Set/Pt	35/1.	36/1.	37/1.	38/1.	39/1.	40/1.	41/1.	42/1.	43/1.	44/1.
SiO₂	82.81	70.21	38.32	0.04	35.10	40.52	32.63	34.08	23.28	29.03
TiO₂	0.38	0.64	0.37	bdl	0.79	0.02	0.04	bdl	0.60	0.39
Al₂O₃	8.02	14.58	25.07	bdl	16.99	22.82	24.74	23.35	13.14	20.19
FeO	0.54	5.54	2.54	0.08	6.94	2.58	22.04	2.49	2.31	10.01
CaO	2.56	2.03	24.44	45.68	14.08	24.39	6.98	33.62	35.52	22.39
MgO	0.36	1.09	1.00	0.64	2.67	1.34	10.05	1.63	1.31	2.88
MnO	0.03	0.03	0.10	0.26	0.10	bdl	0.41	0.21	0.16	0.11
K₂O	0.86	2.95	0.72	0.05	3.46	0.30	1.36	0.20	0.19	0.33
Na₂O	0.69	0.90	0.17	0.10	0.87	0.16	0.37	0.03	bdl	0.07
P₂O₅	0.05	bdl	2.10	27.84	10.41	0.05	0.09	0.53	18.52	3.34
Total	96.31	97.98	94.83	74.70	91.42	92.19	98.70	96.14	95.04	88.74

Set/Pt	45/1.	46/1.	47/1.	48/1.	49/1.	50/1.	51/1.	52/1.	53/1.
SiO₂	49.05	48.48	25.20	48.38	37.24	32.65	35.97	36.59	32.03
TiO₂	0.48	0.35	0.21	0.23	0.54	0.68	0.20	0.17	0.52
Al₂O₃	30.13	32.78	17.66	26.08	23.23	17.60	23.06	22.29	22.46
FeO	8.01	6.61	3.07	5.58	4.75	7.15	6.86	2.55	3.58
CaO	1.24	1.59	28.31	5.97	15.16	21.61	16.87	31.67	31.80
MgO	1.90	1.62	1.59	3.78	1.86	2.05	4.73	1.80	2.29
MnO	bdl	0.09	0.10	0.06	0.04	0.05	0.07	0.05	bdl
K₂O	4.42	5.05	0.21	3.69	3.10	0.43	0.65	0.39	0.34
Na₂O	1.17	0.88	0.03	1.00	1.10	0.04	0.32	bdl	0.13
P₂O₅	0.12	0.09	1.82	0.06	8.09	4.27	1.03	0.14	0.52
Total	96.53	97.54	78.20	94.83	95.12	86.52	89.76	95.66	93.69

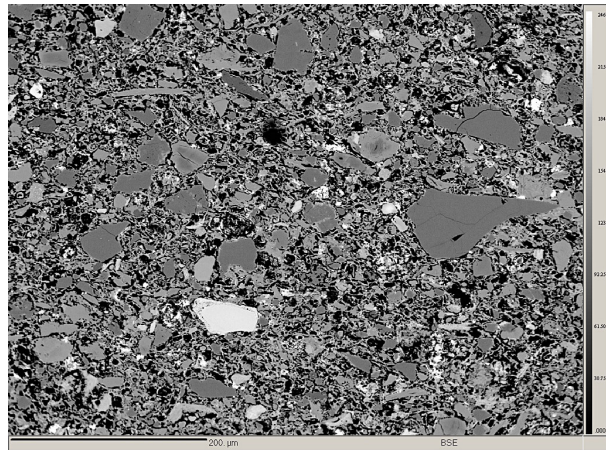
Table 5.18: EPMA raw sample data in wt%, archaeological sample M2/157. (bdl = below detection limit.)

5.4.5 M2/161

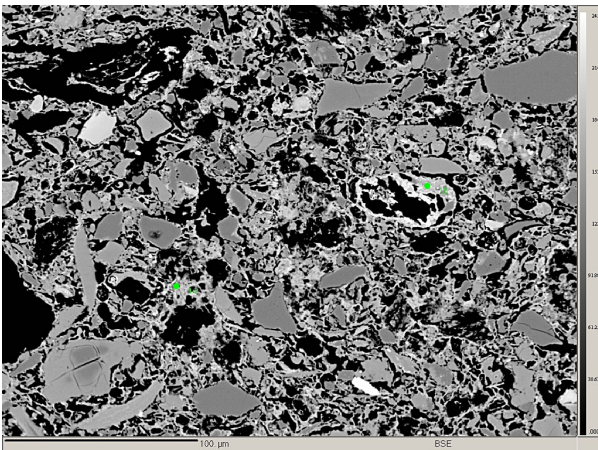
M2/161 shows a fine grained paste with temper grain size of $120\text{ }\mu\text{m}$ (Fig. 5.81(a)). The paste is intermediately sintered, with quartz grains still mostly maintaining their boundaries, see Fig. 5.81(b). While relicts of decomposed minerals can be found, reaction rims are sparse, Fig. 5.81(c) and (d). Measurements within the rims don't detect CaO in quantities needed for calcite, gehlenite, anorthite or wollastonite. All point analyses have been listed in table 5.19.



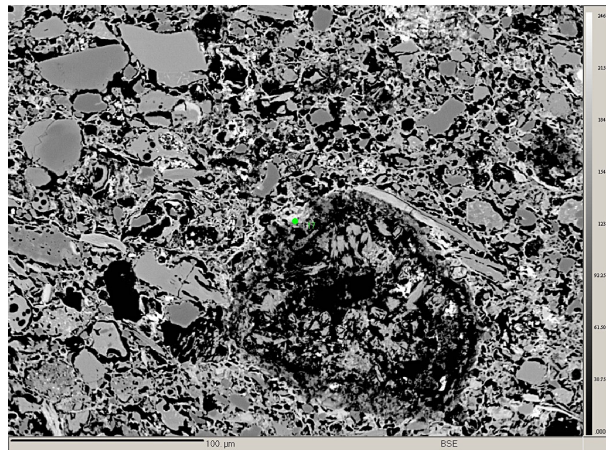
(a) A finely grained paste, with sintering visible



(b) Sintered paste with minerals still maintaining their grain boundaries



(c) Relicts of decomposed minerals, one with reaction rim



(d) Decomposed mineral with partial reaction rim

Figure 5.81: Archaeological sherd M2/161

Set/Pt	1/1.	2/1.	3/1.	4/1.	5/1.	6/1.	7/1.	8/1.	9/1.	10/1.
SiO₂	48.99	34.33	38.62	33.21	35.60	46.52	52.20	41.09	46.87	6.00
TiO₂	0.47	0.13	0.60	0.99	0.12	0.28	0.27	0.35	0.41	0.10
Al₂O₃	15.72	24.92	18.86	14.57	25.17	30.19	16.59	15.68	20.48	2.80
FeO	6.29	2.94	4.69	17.64	19.12	2.32	5.05	3.12	9.77	1.07
CaO	16.07	32.45	22.23	6.18	2.12	5.50	5.16	25.77	9.73	46.90
MgO	2.56	1.26	2.12	2.35	6.29	1.25	1.18	2.48	2.66	4.36
MnO	0.11	0.06	0.06	0.47	0.40	0.07	0.09	bdl	0.46	0.05
K₂O	0.55	0.42	0.24	1.72	4.19	6.18	2.60	0.16	1.42	0.14
Na₂O	0.37	0.08	0.08	1.66	1.19	1.06	2.01	0.04	2.09	0.12
P₂O₅	0.77	0.07	0.50	1.45	bdl	0.04	0.17	0.46	0.55	0.84
Total	91.90	96.68	88.01	80.24	94.19	93.41	85.30	89.16	94.44	62.37

Set/Pt	11/1.	12/1.	13/1.	14/1.	15/1.	16/1.	17/1.	18/1.	19/1.	20/1.
SiO₂	42.78	35.26	65.41	32.49	45.19	32.51	33.69	36.15	35.49	43.21
TiO₂	0.48	0.24	0.21	0.34	0.55	0.33	1.82	0.35	0.52	0.34
Al₂O₃	24.37	7.27	10.27	19.01	23.45	23.53	8.71	15.98	17.70	28.18
FeO	5.50	3.48	2.42	3.52	14.04	4.24	14.90	6.96	5.24	2.53
CaO	6.72	27.71	11.31	28.78	1.66	24.52	12.21	22.26	25.72	14.41
MgO	2.87	1.60	1.23	3.00	4.02	2.71	4.37	3.03	1.94	1.23
MnO	0.19	0.11	0.05	0.05	0.36	bdl	0.18	0.13	0.12	0.03
K₂O	3.02	0.20	0.46	0.21	5.18	0.28	0.27	0.23	0.37	3.31
Na₂O	1.81	bdl	0.02	0.04	1.43	0.03	0.03	0.03	0.20	0.36
P₂O₅	0.07	0.41	0.45	0.64	0.25	0.67	1.04	0.73	0.37	0.10
Total	87.82	76.30	91.83	88.08	96.14	88.81	77.24	85.84	87.68	93.70

Set/Pt	21/1.	22/1.	23/1.	24/1.	25/1.	26/1.	27/1.	28/1.	29/1.	30/1.
SiO₂	35.16	39.04	40.43	35.45	33.49	54.94	37.76	49.29	36.57	38.64
TiO₂	1.15	0.25	0.42	1.20	0.14	bdl	1.73	1.32	0.34	0.91
Al₂O₃	17.54	19.75	15.35	15.19	13.50	23.13	20.46	15.24	15.74	20.72
FeO	10.90	4.86	10.95	10.72	5.18	1.48	17.69	5.42	11.08	11.69
CaO	25.32	28.14	17.83	3.17	23.89	7.72	7.48	14.90	13.59	9.40
MgO	7.22	4.35	3.54	5.69	1.24	0.34	6.43	1.52	4.81	5.47
MnO	0.22	0.10	0.23	0.20	0.14	0.09	0.35	0.09	0.24	0.18
K₂O	0.20	0.49	0.16	2.26	0.49	4.05	1.24	0.35	0.40	1.42
Na₂O	0.18	0.13	0.34	1.23	1.23	3.15	1.90	0.18	0.91	1.91
P₂O₅	0.28	0.12	0.20	0.06	0.26	bdl	0.10	0.58	0.20	1.88
Total	98.17	97.23	89.45	75.18	79.56	94.89	95.13	88.88	83.88	92.22

Set/Pt	31/1.	32/1.	33/1.	34/1.
SiO₂	54.67	48.86	48.81	43.31
TiO₂	0.36	1.11	0.65	0.31
Al₂O₃	18.31	7.62	23.49	21.91
FeO	8.28	8.02	6.70	6.92
CaO	3.95	22.69	4.72	20.36
MgO	3.71	12.48	2.81	2.32
MnO	0.20	0.11	0.13	0.13
K₂O	3.72	0.04	4.06	0.53
Na₂O	1.61	0.13	2.65	0.90
P₂O₅	0.52	0.22	0.09	0.30
Total	95.34	101.26	94.10	96.99

Table 5.19: EPMA raw sample data in wt%, archaeological sample M2/161. (bdl = below detection limit.)

6

Discussion

"Somewhere, something incredible is waiting to be known."
– Carl Sagan

6.1 Experimental samples

A multi-analytical approach was chosen to analyze the effects of the soaking time on temperature dependent clay-calcite reactions. XRF was used to assess the elemental composition of the raw material mix, while Optical Microscopy, XRD and electron probe microanalysis were applied on the fired samples.

Optical microscopy has proven to be an unreliable choice as the differences within samples fired at a certain temperature are too small to be seen. XRD and microprobe analysis on the other hand are very useful.

XRD allows for a direct comparison of the separate samples, highlighting the continuous breakdown and/or formation of mineral phases within a temperature set, see Fig. 6.1. Specifically, the XRD pattern for samples fired at 800°C, Fig. 6.1(a), shows the breakdown of feldspar at $27,89^{\circ} 2\Theta$ as well as the formation of a new phase at $21,21^{\circ} 2\Theta$, possible wollastonite. The changes in these patterns are still small, implying a slow reaction. More obvious is the breakdown of all mineral phases in samples fired at 900°C that – even though progressing continuously through all samples – rapidly increases speed between seven and nine hours soaking time; Fig. 6.1(b). The soaking time is still too short to allow for the formation of enough gehlenite or other Ca-alumo-silicates to be detected by XRD.

Gehlenite, anorthite and wollastonite are detected by XRD in samples fired at 1100°C, Fig. 6.1(c). The XRD patterns for those samples widely differ from the patterns of the samples fired at lower temperature, showing a strong increase of background noise that represents a high amount of amorphous phases (Cultrone et al., 2001) as well as mineral phases that have not been present at lower temperatures, including spinel. The increased soaking time is less visible in XRD diagrams at 1100°C than in the ones for the other two temperatures, 800°C and 900°C, although the beginning breakdown of newly formed phases can also be observed. It can therefore be concluded, that XRD is very helpful in observing the soaking time when more than one sample is available.

Microprobe analysis proved to be very useful as it provided both BSE images and point analyses

within the reaction rims. While rim thickness can be and was measured in all samples, it is not to be relied upon. The reaction in and around calcite grains depends strongly on local disequilibria (Heimann and Maggetti, 2014), making an assumption of either soaking time or firing temperature based on calcite decomposition and rim diameter highly unreliable. Furthermore, the dependence on grain size, stated by Maggetti and Küpfer (1978), could not be confirmed. Large calcite grains could be found decomposing and forming reaction rims, while the neighboring small calcite grain was still intact, and vice versa. Large calcite grains of 400 μm and more diameter can resist decomposition throughout all temperatures and soaking times, despite e.g. Riccardi et al. (1999), Rathossi et al. (2004), Tschegg et al. (2009) amongst others, stating calcite decomposition to be complete latest at 900°C. While this can be a result of the specific clay used for this study (see below), it clearly shows that absolute statements and temperature thresholds that link calcite breakdown and temperature can be incorrect. While this is certainly correlation, there is no causal relation that links calcite breakdown only to temperature, as can be seen from this work's results (see discussion in this chapter and Results chapter starting at page 33).

Point analyses taken within the rims can prove useful, but also have to be treated with caution. The rims are not homogeneous, but show both zoning and spongy areas; see section 5.3. Therefore all measurements exceeding a total of 95 wt% have been plotted in $\text{CaO} - \text{SiO}_2 - \text{Al}_2\text{O}_3$ phase diagrams. This, unfortunately, tends to get confusing, when too many points group too closely together as can be seen in Fig. 6.2. However, they show an increase of points successfully measured with both increased soaking time and increasing firing temperature, indirectly confirming the increasing rim thickness. Furthermore, gehlenite is a metastable phase that will form and shortly coexist with anorthite and wollastonite at high temperatures, given a sufficient saturation of Ca and Si (Heimann and Maggetti, 2014). This can be seen in Fig. 6.2(c), where gehlenite, (pseudo-)wollastonite and anorthite are plotted. To really identify tendencies, the measurements were also plotted in a statistic graphic. As can be seen in Fig. 6.3, the trend for all temperatures show an increasing amount of gehlenite with increasing soaking time for all temperatures. Of course, this has to be treated with caution, as the analyses vary from sample to sample and gehlenite measurements depend not only on the position of the measurement within the rim, but also on the rim which should be thicker than the defocused electron beam used for the analyses. Nonetheless, throughout all methods, a progressive mineralogical change can be seen with increasing soaking time.

As mentioned before, firing temperatures were chosen specifically according to temperature thresholds defined in previous studies (see chapter 5). This was done to ensure the full focus of this thesis on the main question – the impact of increased soaking time on ceramic firing. The chosen soaking times do not necessarily reflect archaeologically realistic soaking times, but were chosen instead to clearly show trends in mineral decomposition. For the 800°C samples, in particular, soaking times of 20 hours and 25 hours can be considered unlikely for actual field-fired ceramics. However, especially those longer soaking times produced very interesting results for 800°C samples for longer firing durations show trends that clearly indicate the influence of the soaking time. Nonetheless, neither calcite breakdown nor gehlenite formation followed the behaviour described in literature. This might be explained through three factors.

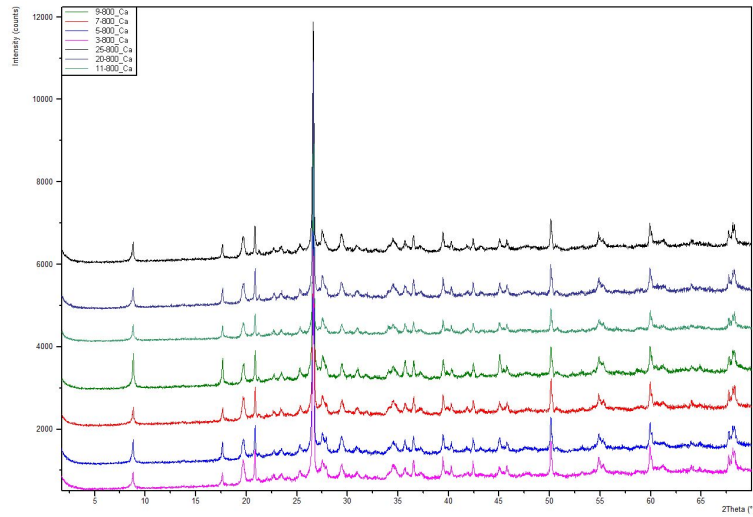
First, Stoob clay starts sintering at approximately 1000°C (Schönlaub, 2000), therefore no sintering would be expected at lower temperatures like the ones chosen for the experiments. Without clay sintering local conditions to form gehlenite might be harder to achieve, especially, when calcite breakdown has not been completed. The formation of new mineral phases without melt, depends solely on elemental diffusion (Heller-Kallai and Miloslavski, 1992). The long soaking times at low temperatures in combination with locally decomposing calcite provided the necessary conditions, explaining the formation of gehlenite in such locations.

Secondly, the clay-calcite mix produced as raw material for the experimental samples can still

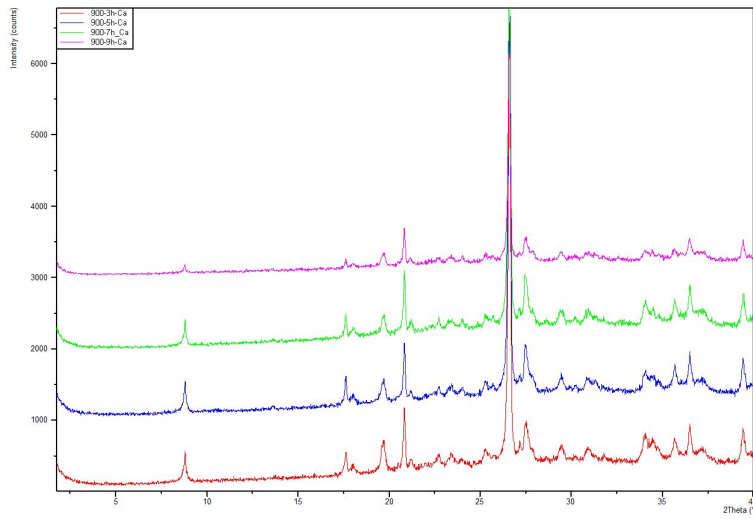
be considered Ca-poor. As the XRF analysis (table 3.2) shows, 5,4 wt% of the raw material are CaO. This amount lies between the Ca-rich and Ca-poor clay used by Duminuco et al. (1998), who described Ca-poor clay as not showing "*[...]the same variability of firing phases as displayed by Ca-rich ones[...]*". In other words, the Ca-amount in the raw material could be too low to allow the formation of appreciable gehlenite, despite the presence of calcite grains of variable size.

Finally, while the samples experienced a slow heating rate and varying soaking times, the usual cooling in the kiln was not applied. Although no study investigating this specific question could be found, the sudden and massive drop in temperature may also have influenced the formation of gehlenite, especially at low temperatures. The absence of an adequate cooling time in the kiln could favore the incipient gehlenite stages rather than fully crystallized gehlenite.

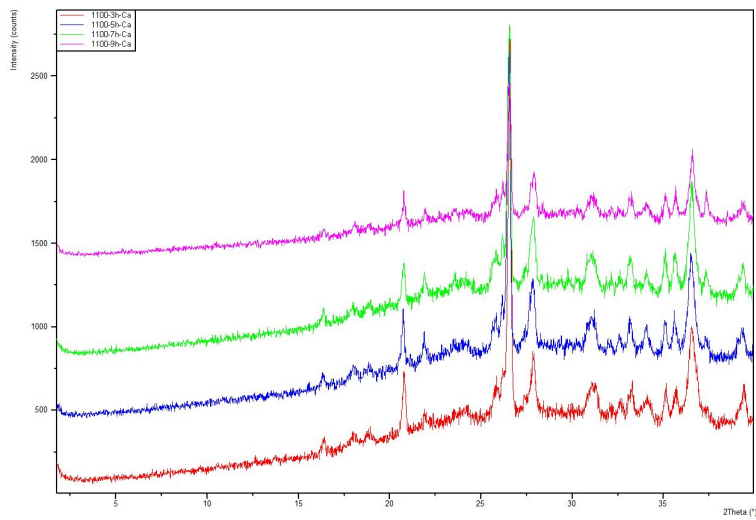
Further studies are needed to answer those questions and verify the results of this thesis.



(a) XRD of all samples containing calcite; fired at 800° C

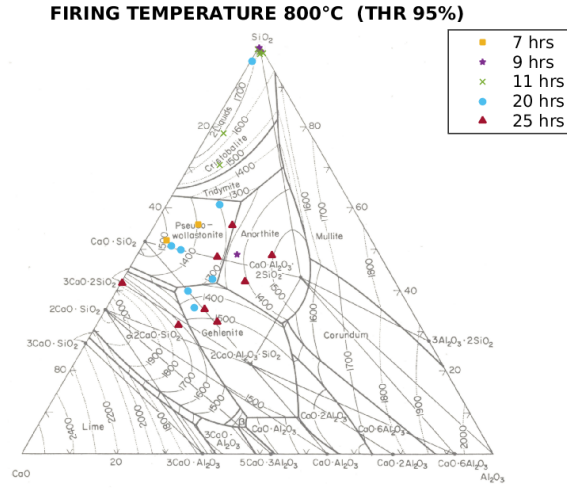


(b) XRD of all samples containing calcite; fired at 900° C

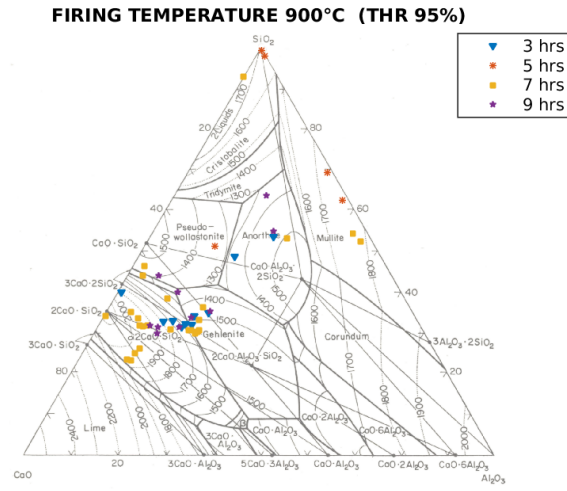


(c) XRD of all samples containing calcite; fired at 1100° C

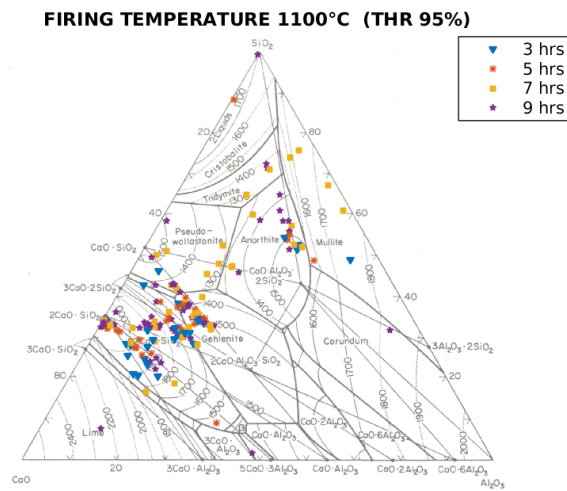
Figure 6.1: XRD diagram of samples containing calcite



(a) Point analyses at 800°C



(b) Point analyses at 900°C



(c) Point analyses at 1100°C

Figure 6.2: Microprobe point analyses exceeding 95 % total

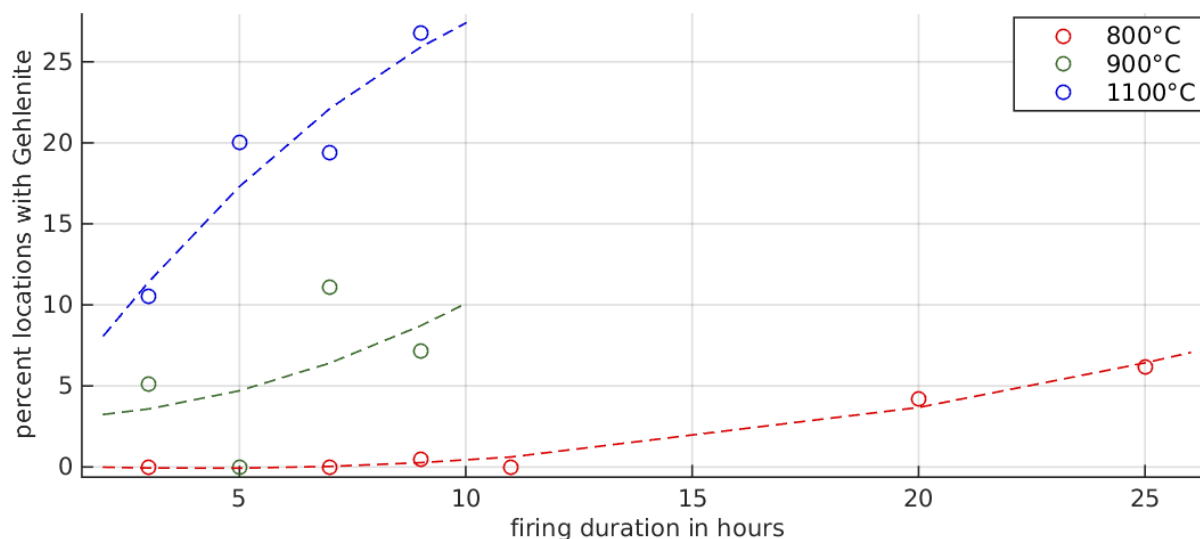


Figure 6.3: Statistical interpretation of all point analyses exceeding 95 % for all temperatures; circles stand for analysis, curves represent trends (2nd order polynomials, least-squares fitting). While this shows an increasing trends for gehlenite for all temperatures, it must not be forgotten, that those analyses depend heavily on specifically selected points within each sample. This also explains why no gehlenite was detected in the sample fired for 5 h at 900 °C

6.2 Archaeological samples

The archaeological samples analyzed for this thesis are a prime example why a multi-analytical approach for ceramics is required and that surface analysis with OM and (Handheld-) XRF tend to be unreliable. As the results of the archaeological samples clearly show, none of them contained any calcite as evidenced by the low amount of Sr in all samples, see Fig. 6.4. After thorough analysis with both OM and BSE images reaction rims around holes or mineral relicts can be found, but those rims have different elemental compositions than gehlenite, anorthite or wollastonite would require. In fact, the composition of most rims was as such as does not permit the assumption of what kind of mineral decomposed and formed the rim in this spot. The only point measurement – in sample M2157 – allowing for any conclusions on the decomposed mineral, has a relatively high amount of P_2O_5 (27,842%) as well as a CaO amount of 45,667%, indicating the possible decomposition of apatite. While this could speak for a tempering of the clay raw material with bone dust, the data in this sample is not sufficient.

While disappointing for this thesis in as much as the main question of the possible appliances of the experimental results to ancient ceramics could not be investigated, those samples nonetheless emphasize the importance of a multi-analytical approach to ceramic analysis.

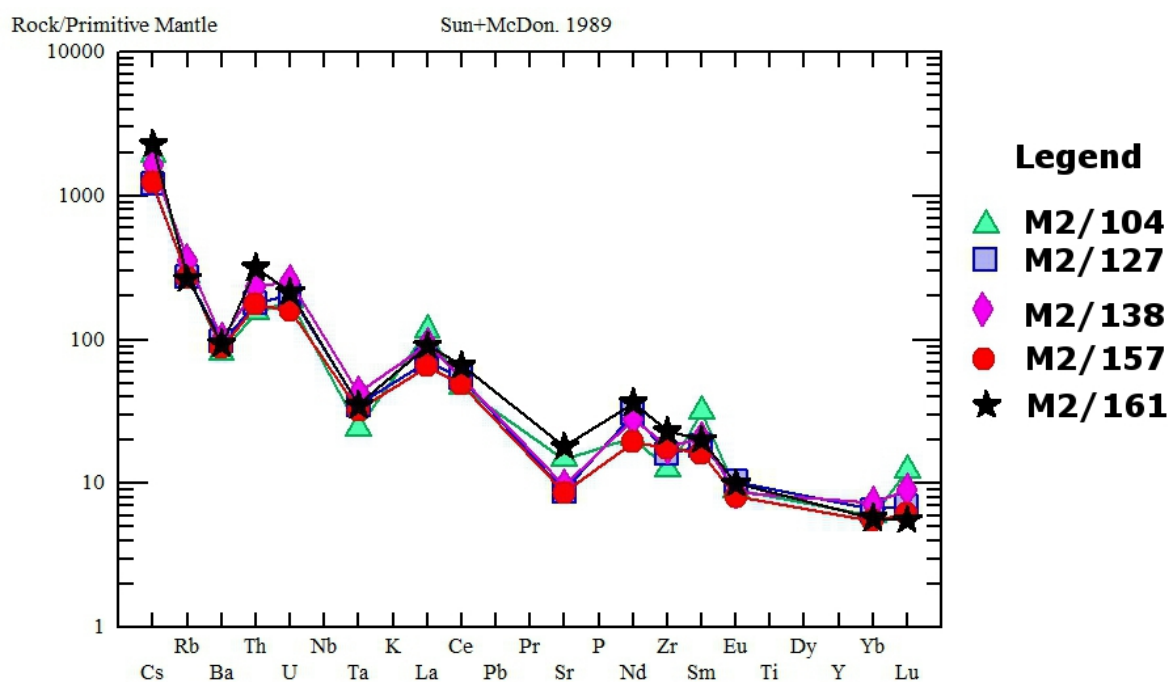


Figure 6.4: INAA analysis of all archaeological samples, plotted in against the primary mantle. The low Sr amount clearly shows the samples contain no calcite

7

Conclusio

"Study the past if you would define the future."
– Confucius

This thesis investigated the influence of the soaking time on the firing of ceramics with special focus on gehlenite. To study those effects, experimental samples were prepared using a raw material mix of calcite-free Stoob clay and pure Hierlatz calcite. The specimen were fired at 800° C, 900° C and 1100° C for soaking times of three, five, seven and nine hours, with additional samples fired at 800° C for eleven, 20 and 25 hours. All samples have been analyzed by Optical Microscopy (OM), X-ray Diffraction (XRD) and Electron Probe Microanalysis (EPMA). Furthermore, five archaeological sherds were analyzed with OM, EPMA and Instrumental Neutron Activation Analysis (INAA).

Results can be best observed by comparing all samples fired at a specific temperature with each other. The XRD comparison clearly showed that the soaking time indeed has an impact on the formation and development of gehlenite. The reaction is still slow for low temperatures, but distinct changes can be seen by comparing the XRD diagrams. Plotting the results of microprobe point analyses in $\text{CaO} - \text{SiO}_2 - \text{Al}_2\text{O}_3$ phase diagrams also showed an increasing amount of gehlenite for both longer soaking time and higher firing temperature.

Calcite decomposition in the analyzed samples was found not to follow the expected patterns. It withstood decomposition much longer than predicted by previous research. Gehlenite also did not develop as expected. Especially the results for 800° C and 900° C were so misleading that analysis with XRD or OM alone would have identified an archaeological sherd with those specific results as having been fired at much lower temperatures. The archaeological sherds analyzed to apply the results of the experimental analyses unfortunately do not contain any calcite and can therefore not be used to answer this specific question. This emphasizes the importance of a multi-analytical and especially in-situ analysis for samples to determine the firing temperature. After the thorough analysis of all experimental and archaeological samples, it can be concluded, that the firing process of ceramics is a complex process that depends on many variables. Conclusions regarding individual process parameter such as the firing temperature based on single observations like calcite decomposition or gehlenite formation have to be considered unreliable. This is compounded by the fact, that some analytical methods, e.g. Handheld XRF, have large measurement uncertainties that cannot be ignored for the analysis.

Bibliography

- A. Aras. The change of phase composition in kaolinite-and illite-rich clay-based ceramic bodies. *Applied Clay Science*, 24(3):257–269, 2004.
- E. Cantisani, M. Cavalieri, C. Lofrumento, E. Pecchioni, and M. Ricci. Ceramic findings from the archaeological site at aiano-torraccia di chiusi (siena, italy): a multi-analytical approach. *Archaeological and Anthropological Sciences*, 4(1):29–46, 2012.
- M. Carretero, M. Dondi, B. Fabbri, and M. Raimondo. The influence of shaping and firing technology on ceramic properties of calcareous and non-calcareous illitic-chloritic clays. *Applied Clay Science*, 20(6):301–306, 2002.
- J. Cogswell, H. Neff, and M. Glascock. The effect of firing temperature on the elemental characterization of pottery. *Journal of Archaeological Science*, 23(2):283–287, 1996.
- G. Cultrone, C. Rodriguez-Navarro, E. Sebastian, O. Cazalla, and M. J. De La Torre. Carbonate and silicate phase reactions during ceramic firing. *European Journal of Mineralogy*, 13(3):621–634, 2001.
- W. Deer, R. Howie, and J. Zussman. Rock-forming minerals: Disilicates and ring silicates, v. 1b, 1986.
- P. Duminuco, B. Messiga, and M. P. Riccardi. Firing process of natural clays. some microtextures and related phase compositions. *Thermochimica Acta*, 321(1):185–190, 1998.
- P. Faupl. *Historische Geologie*. Facultas Universitätsverlag, 2003.
- H. W. Flügel and F. Neubauer. *Steiermark: Erläuterungen zur geologischen Karte der Steiermark, 1: 200.000*. Geologische Bundesanstalt, 1984.
- M. A. Götzinger, I. Altenburger, and L. Burgenland. Die tone von stoob im mittleren burgenland. In *Die Mineralien des Burgenlandes: Geologie, Mineralogie und mineralische Rohstoffe*, volume 26, page 101. Amt der Burgenländischen Landesregierung, Abt. 7-Kultur, Wiss. und Archiv, Landesmuseum Burgenland, 2009.
- R. B. Heimann and M. Maggetti. *Ancient and Historical Ceramics*. Schweizerbart’sche Verlagsbuchhandlung, 2014.
- L. Heller-Kallai and I. Miloslavski. Reactions between clay volatiles and calcite reinvestigated. *Clays and Clay Minerals*, 40:522–522, 1992.
- G. Hoeschek. Gehlenite stability in the system $\text{cao-al}_2\text{o}_3\text{-sio}_2\text{-h}_2\text{o-co}_2$. *Contributions to Mineralogy and Petrology*, 47(4):245–254, 1974.
- E. M. Levin and C. Robbins. Hf mcmurdie phase diagrams for ceramists. *The American Ceramic Society, Columbus, OH*, page 122, 1964.
- M. Maggetti and T. Küpfer. Composition of the terra sigillata from la péniche (vidy/lausanne, switzerland). *Archaeometry*, 20(2):183–188, 1978.

- M. Maggetti, H. Westley, and J. S. Olin. Provenance and technical studies of mexican majolica using elemental and phase analysis. In *Archaeological chemistry-III*, pages 151–191. American chemical society, 1984.
- M. Maggetti, C. Neururer, and D. Ramseyer. Temperature evolution inside a pot during experimental surface (bonfire) firing. *Applied Clay Science*, 53(3):500–508, 2011.
- L. Maritan, L. Nodari, C. Mazzoli, A. Milano, and U. Russo. Influence of firing conditions on ceramic products: experimental study on clay rich in organic matter. *Applied Clay Science*, 31(1):1–15, 2006.
- L. Plan, C. Tschegg, J. De Waele, and C. Spötl. Corrosion morphology and cave wall alteration in an alpine sulfuric acid cave (kraushöhle, austria). *Geomorphology*, 169:45–54, 2012.
- C. Rathossi, P. Tsolis-Katagas, and C. Katagas. Technology and composition of roman pottery in northwestern peloponnese, greece. *Applied Clay Science*, 24(3):313–326, 2004.
- M. P. Riccardi, B. Messiga, and P. Duminuco. An approach to the dynamics of clay firing. *Applied Clay Science*, 15(3):393–409, 1999.
- H. Schönlaub. Geologie der österreichischen bundesländer – burgenland. *Wien: Geologische Bundesanstalt*, 2000.
- S. Shoval. Mineralogical changes upon heating calcitic and dolomitic marl rocks. *Thermochimica acta*, 135:243–252, 1988.
- S. Shoval, M. Gaft, P. Beck, and Y. Kirsh. Thermal behaviour of limestone and monocrystalline calcite tempers during firing and their use in ancient vessels. *Journal of Thermal Analysis and Calorimetry*, 40(1):263–273, 1993.
- K. Traoré, T. S. Kabré, and P. Blanchart. Low temperature sintering of a pottery clay from burkina faso. *Applied Clay Science*, 17(5):279–292, 2000.
- M. Trindade, M. Dias, J. Coroado, and F. Rocha. Mineralogical transformations of calcareous rich clays with firing: a comparative study between calcite and dolomite rich clays from algarve, portugal. *Applied Clay Science*, 42(3):345–355, 2009.
- C. Tschegg, T. Ntaflos, and I. Hein. Thermally triggered two-stage reaction of carbonates and clay during ceramic firing – a case study on bronze age cypriot ceramics. *Applied Clay Science*, 43(1):69–78, 2009.
- M. Vizenz. Erforschung Stoober Tone. In: *8. Arbeitstag Bund-Bundesländerkoop. Rohstoff- und Energieforsch. (9. & 10. Okt. 1985)*, 1985. Umwelt Burgenland: 4, 122–130, Eisenstadt.
- A. Vörös. Hierlatzkalk – a peculiar austro-hungarian jurassic facies. *Jubiläumsschrift*, 20:145–154, 1991.

